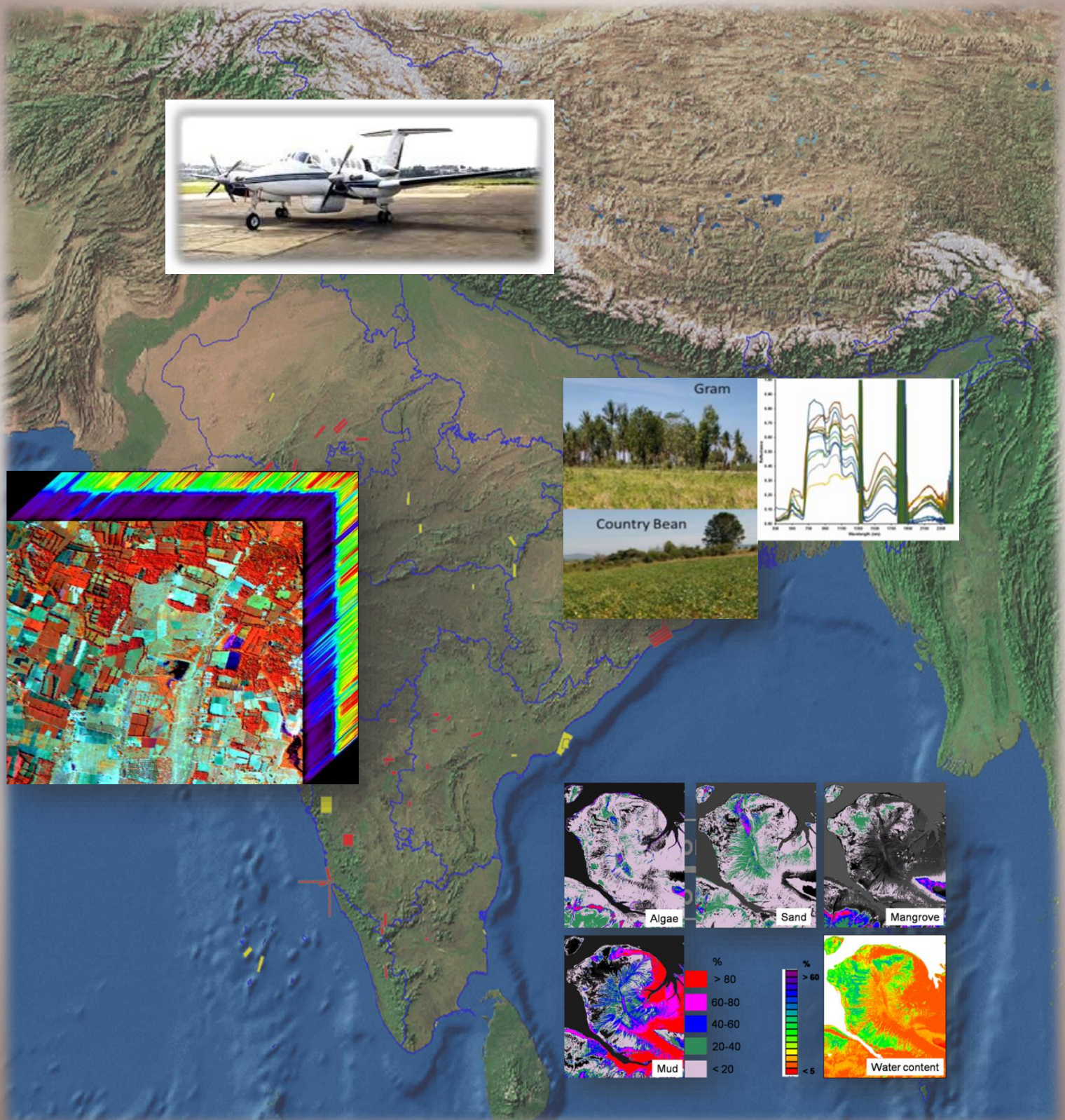




# Science Results from Phase – 1 Airborne Hyperspectral Campaign with AVIRIS-NG over India



July 2017

Indian Space Research Organization

## Document control and Datasheet

---

<b>1</b>	<b>Report No.</b>	:	ISRO-JPL/AVIRIS-NG/SR01
<b>2</b>	<b>Publication Date</b>	:	July 2017
<b>3.</b>	<b>Title and Subtitle</b>	:	Science Results from Phase – 1 Airborne Hyperspectral Campaign with AVIRIS-NG over India
<b>4</b>	<b>Type of Report</b>	:	Scientific Report
<b>5</b>	<b>No. of Pages</b>	:	Three hundred twenty two (322)
<b>6</b>	<b>No. of sections</b>	:	Four (4)
<b>7</b>	<b>No. of sub-sections</b>	:	Seven (7)
<b>8</b>	<b>No. of research articles</b>	:	Fourty (40)
<b>8</b>	<b>Authors</b>	:	Science team members of AVIRIS-NG Airborne Hyperspectral Campaign from ISRO and JPL
<b>9</b>	<b>Originating Unit</b>	:	Space Applications Centre (ISRO), Ahmedabad
<b>10</b>	<b>Abstract</b>	:	This contains a synthesis of initial scientific results generated by ISRO science community using AVIRIS-NG Airborne hyperspectral data collected during first phase of campaign over 57 sites in India.
<b>11</b>	<b>Keywords</b>	:	Hyperspectral Imaging, Land- Water- Atmosphere, Airborne
<b>12</b>	<b>Security Classification</b>	:	Unrestricted
<b>13</b>	<b>Distribution statement</b>	:	General

---

भारतीय अन्तरिक्ष अनुसंधान संगठन  
अन्तरिक्ष विभाग  
भारत सरकार  
अन्तरिक्ष भवन  
न्यू बी ई एल रोड, बेंगलूर – 560 231, भारत  
दूरभाष : +91-80-2341 5241 / 2217 2333  
फैक्स : +91-80-2341 5328



Indian Space Research Organisation  
Department of Space  
Government of India  
Antariksh Bhavan  
New BEL Road, Bangalore - 560 231, India  
Telephone: +91-80-2341 5241 / 2217 2333  
Fax : +91-80-2341 5328  
e-mail : chairman@isro.gov.in

आ. सी. किरण कुमार / A. S. Kiran Kumar  
अध्यक्ष / Chairman

## MESSAGE

Indian Earth Observation satellite missions play a pivotal role in generating valuable information required for natural resources management by employing sensors on board in different electro-magnetic wavelengths. Over the years, advances in sensor technology have led to development of hyperspectral imagers which collect data in large number of contiguous narrow bands spanning a vast region of the electromagnetic spectrum.



The requirements of users on space-based products and services put forward a unique challenge for ISRO to develop advanced imaging sensors. In this context, the collaborative program between ISRO and JPL, NASA on hyper-spectral remote sensing and imaging spectroscopy is one such endeavour towards achieving the precision in sensor technology and advanced application requirements.

AVIRIS-NG developed by JPL is being used by ISRO to acquire Hyperspectral data over India covering diverse ecosystems. In Phase-1 of this campaign Hyperspectral data was collected over 57 sites in India. Various academic institute and scientific organizations have participated during the airborne campaign (December 2015 to March 2016) and large amount of hyperspectral data over the multiple natural targets was collected. The campaign provided unique opportunity to scientific community to develop spectral libraries, algorithms and models which are precursor to the India's future hyperspectral missions.

It is heartening to note that an excellent compilation has been brought out through contributions of ISRO scientists on various themes using data from the phase-1 airborne campaign with AVIRIS-NG. I appreciate the sincere efforts to bring out this scientific compilation.

आ सी किरण कुमार  
(आ सी किरण कुमार) 13/7/17  
(A. S. Kiran Kumar)



**तपन मिश्रा**  
निदेशक  
**Tapan Misra**  
Director



भारत सरकार GOVERNMENT OF INDIA  
अंतरिक्ष विभाग DEPARTMENT OF SPACE  
अंतरिक्ष उपयोग केंद्र  
SPACE APPLICATIONS CENTRE

अहमदाबाद AHMEDABAD - 380 015

(भारत) (INDIA)

दूरभाष PHONE : +91-79-26913344, 26928401

फैक्स /FAX : +91-79-26915843

ई-मेल E-mail : [director@sac.isro.gov.in](mailto:director@sac.isro.gov.in)



## P R E F A C E

Space Applications Centre (ISRO), Ahmedabad is involved in designing and developing imaging, non-imaging payloads and is engaged in the development of advanced techniques, value-added products using satellite data for societal benefits. In the space age, significant progress has been made to strengthen the remotely sensed observations through electro-optical sensors and microwave radar-radiometer systems onboard ISRO's satellites. The development of space-borne hyperspectral sensors is a challenging task and is in the process of realization. The airborne hyperspectral data from AVIRIS-NG sensor system provides unique opportunity in understanding the three-dimensional data cube, its calibration and validation. The utilization of such valuable data calls for the newer development of the algorithms, data processing and customized solutions for societal benefits. The coordinated effort by campaign and science teams facilitated the acquisitions of hyperspectral airborne data and ground-truth over 57 sites in India. This Centre has archived these data and is engaged in disseminating the same to scientific community of India through a geoportal called VEDAS. Different trainings are being organized to develop the skill of using hyperspectral data which would help in practical applications of hyperspectral data from ISRO's future satellite-based hyperspectral missions. Research support has also been extended to academia especially to doctoral students through Announcement of Opportunity (AO) programme.

The present compilation of research articles contains the initial science results using the hyperspectral data from phase-1 airborne campaign with AVIRIS-NG. I hope this would help the students and initial learners to develop deeper insight on the data and their practical utility.

Place: Ahmedabad

Date: 10 July 2017

*तपन मिश्रा*

(तपन मिश्रा) / (Tapan Misra)

निदेशक / Director

भारतीय अंतरिक्ष अनुसंधान संगठन



INDIAN SPACE RESEARCH ORGANISATION

भारत सरकार  
अन्तरिक्ष विभाग  
**राष्ट्रीय सुदूर संवेदन केन्द्र**  
बालानगर, हैदराबाद-500 037, तेलंगाना, भारत  
टेलिफोन : +91 40 23878360  
+91 40 23884000-04  
फैक्स : +91 40 23877210



Government of India  
Department of Space  
**National Remote Sensing Centre**  
Balanagar, Hyderabad-500 037, Telangana, India  
Telephone : +91 40 23878360  
+91 40 23884000-04  
Fax : +91 40 23877210

**Dr. Y.V.N. Krishna Murthy**  
Director



**FOREWORD**

AVIRIS –NG is one of the important aerial missions undertaken for Hyperspectral mapping in the country under the Indo –US cooperation in Science mission. The flights over Indian sub-continent were conducted during Dec,2015 to March,2016 period where in hypespectral data was collected for diverse terrain covering themes like Agriculture , Forestry, Geology and Water . This is one of the unique missions wherein scientific team from ISRO and NASA-JPL collaborated for providing Science data to the country. Various researchers were benefited by this programme and they had opportunity to work with one of the best science data in the area of hyper spectral domain. The present Science meet on the phase-1 of the activity is an important milestone wherein the team will be discussing the data processing results for the benefit of the academic community of the country and also to interact with the science team member of AVIRIS programme to understand data products and their related use to create larger user base of the these scientific data products. NRSC has also contributed significantly in conducting flight operations effectively to ensure maximum data have been collected for this mission in shortest period of time. I understand many important results would be discussed covering various themes which will play a significant role in planning future applications on space platform. I wish this meet a grand success.

**(Y.V.N.Krishna Murthy)**

July 08, 2017

**भारतीय अन्तरिक्ष अनुसंधान संगठन Indian Space Research Organisation**

भारत सरकार  
अंतरिक्ष विभाग  
अंतरिक्ष उपयोग केन्द्र  
आंबावाडी विस्तार डाक घर,  
अहमदाबाद-380 015. (भारत)  
दूरभाष : +91-79-26912000, 26915000  
फैक्स :



Government of India  
Department of Space  
SPACE APPLICATIONS CENTRE  
Ambawadi Vistar P.O.  
Ahmedabad - 380 015. (INDIA)  
Telephone : +91-79-26912000, 26915000  
Fax

**डॉ. राज कुमार / Dr. Raj Kumar**

उप निदेशक / Dy. Director  
ईपीएसए / EPSA

दूरभाष Phone: +91 79-26914024

फैक्स Fax: +91 79-26915862

ई-मेल E-mail: rksharma@sac.isro.gov.in  
ddepsa@sac.isro.gov.in



## PRELUDE

Several Hyper-Spectral Spectrometer (HSS) instruments are available for hyperspectral imaging to provide data with high spatial resolution from airborne and ground-based platforms. The satellite-based HSS missions are able to provide data over the globe however suffers with low SNR problem. Several application studies have also been demonstrated by Indian scientists using ground based and spaceborne sensors. Keeping the future potential in tandem with the development of advanced technology, to provide the required ground truth data, science understanding, techniques development and applications demonstrations for present and future ISRO space imaging spectrometer missions, ISRO and NASA have designed joint airborne hyperspectral science campaign over India in 2015. In the first phase, data over 57 sites, covering various themes, such as agriculture, forest, geology, water, urban, coastal etc. have been acquired. The initial results of the research performed with the data has been compiled and presented here with combined effort of scientists and engineering team of ISRO centres and researchers from various institutes as well as academia. It has been a great experience for science team members of AVIRIS-NG Airborne Hyperspectral Campaign, working with an excellent hyperspectral payload data. The team is grateful to the support extended by Shri A. S. Kirankumar, Chairman, ISRO. The constant encouragement and review on the progress of airborne campaign and scientific data archival, dissemination, analysis by Shri Tapan Misra, Director, SAC, Ahmedabad is gratefully acknowledged. The cooperation extended by Dr. V. K. Dadhwal, Ex-Director and Dr. Y.V.N. Krishnamurthy, present Director, NRSC, Hyderabad for the aircraft operations in a time-scheduled manner is acknowledged. The entire team is highly benefitted by the support provided by JPL, NASA for their AVIRIS-NG payload for hyperspectral airborne campaign for the first time in India and basic data products of imaging spectroscopy for scientific analysis. We hope to develop much more scientific understanding and various application potential with the present dataset and future acquisitions.

  
(डॉ. राज कुमार)  
(Dr. Raj Kumar)

## Contents

<b>Sr. No.</b>	<b>SECTIONS</b>	<b>Page No.</b>
1.0	An Overview of First Phase of AVIRIS-NG Hyperspectral Science Campaign	1
2.0	Calibration and Validation	15
3.0	Parameter Retrieval & Technique Development	25
4.0	Thematic Applications	
4.1	<i>Agriculture</i>	79
4.2	<i>Forestry</i>	151
4.3	<i>Geology</i>	179
4.4	<i>Coastal-Ocean</i>	223
4.5	<i>Water quality</i>	248
4.6	<i>Land use and Urban</i>	270
4.7	<i>Snow and Glacier</i>	296

## List of Chapters

1. Overview of First Phase of AVIRIS-NG Airborne Hyperspectral Science Campaign over India.....	1
<b>Calibration and Validation</b> .....	15
2. Calibration of AVIRIS-NG hyperspectral imager over natural targets .....	16
3. AVIRIS-NG Calibration and Validation procedure and results .....	21
<b>Parameter Retrieval and Technique Development</b> .....	25
4. Retrieval of atmospheric parameters for atmospheric correction of AVIRIS-NG L1 data .....	27
5. Retrieval of integrated water vapor from AVIRIS-NG using two band ratio techniques .....	33
6. Air quality study using AVIRIS-NG and ground data .....	38
7. Estimation of columnar molecular methane concentration using AVIRIS-NG data .....	44
8. Study of Cloud Microphysical Parameters (CMP) using AVIRIS-NG Hyperspectral data .....	49
9. Development of Atmospheric Correction Scheme over Soil-Vegetation Complex .....	54
10. Atmospheric Correction Algorithm for Ocean Colour Remote Sensing .....	59
11. SPECSOFT for Creating, Visualization of Spectral Library and Hyperspectral Image Analysis ..	67
12. Absorption Peak Decomposition Technique for Forest Species Identification .....	73
<b>Agricultural Applications</b> .....	79
13. Crop discrimination over homogeneous and heterogeneous agriculture area .....	81
14. Fine Level Classification of Mango Orchards Using AVIRIS-NG Hyperspectral Data .....	89
15. Comparison of Crop discrimination from AVIRIS-NG and LISS-IV over agricultural area .....	95
16. Identification and discrimination of sugarcane fresh v/s ratoon using AVIRIS-NG data .....	104
17. Specific crop/Soil discrimination form AVIRIS Hyperspectral data .....	110
18. Hyperspectral modeling for soil texture prediction in semi-arid tropical region of India .....	115
19. Crop bio-physical-chemical parameter retrieval over agriculture area.....	121
20. Exploring AVIRIS-NG Data for Crop and Soil Studies.....	129
21. Hyper Spectral Sensing of Crops under Varying Conditions of Soil Wetness .....	135
22. Wheat yellow rust identification through AVIRIS-NG data.....	143

<b>Forestry Applications</b> .....	151
23. Mapping Forest Diversity using Airborne Hyperspectral Data .....	153
24. Mangrove Species Discrimination using Hyperspectral data .....	158
25. Mangrove ecosystem analysis – A perspective of hyperspectral remote sensing .....	163
26. Mapping vegetation parameters for fuel load estimation in Shoolpaneshwar forests.....	171
<b>Geological Applications</b> .....	179
27. A mineralogical appraisal of Jahazpur and adjoining areas of Rajasthan.....	181
28. Analysis of AVIRIS data for mineralogical mapping in parts of Ambaji, Gujarat.....	192
29. AVIRIS-NG data for mineral exploration studies.....	210
30. Identification of Terrestrial analogues of Noachian period of Mars using AVIRIS-NG data ...	219
<b>Coastal-Ocean Applications</b> .....	223
31. Application of hyperspectral data in Coastal Zone Studies .....	225
32. Study of Coral Reef Environment based on Airborne Hyperspectral Imaging.....	234
33. Simultaneous Validation Programme for Hyper-Spectral Data from AVIRIS Flights .....	239
<b>Water Quality Applications</b> .....	248
34. Assessment of Water Quality in River Ganga using AVIRIS NG Hyperspectral Data .....	250
35. Water Quality Studies in Chilika Lake .....	254
36. Assessment of Water Quality by inversion of bio-optical models in inland waters .....	263
<b>Land Use Land Cover and Urban Applications</b> .....	270
37. AVIRIS - NG Data Utilization for Land Use/ Land Cover Applications .....	272
38. Hyper-spectral Remote Sensing of Urban and Peri-Urban Areas .....	279
39. Hyper-spectral Remote Sensing of Urban Areas.....	288
<b>Snow &amp; Glacier Applications</b> .....	296
40. Snowpack Characterization using Hyperspectral airborne data.....	298

## List of Figures

Figure 1.1. Geographical distribution of AVIRIS-NG science campaign sites.....	4
Figure 1.2. Examples of sites and flight paths.....	4
Figure 1.3. Airborne campaign team and science field campaign team with B200 aircraft.....	5
Figure 1.4. Flight paths of Phase-1 AVIRIS-NG airborne campaign.....	7
Figure 1.5. Field photographs of Ground-truth campaigns .....	7
Figure 1.6. Examples of field-based hyperspectral signatures over different thematic targets .....	8
Figure 1.7. Examples of 3D data cubes from AVIRIS-NG.....	9
Figure 1.8. Examples NCC images from AVIRIS-NG.....	9
Figure 1.9. AVIRIS-NG data archival facility and data flow mechanism.....	11
Figure 2.1. Desalpar site as viewed by AVIRIS-NG and the field photograph.....	17
Figure 2.2. The flow chart of TOA spectral radiance simulation.....	18
Figure 2.3. At sensor TOA radiance (a). over Desalpar (b). SAC-Bopal (c). GMDC-Ahmedabad.....	19
Figure 3.1. Comparison of in-situ and remote reflectance measurements.....	22
Figure 3.2. Comparison of in-situ and remote reflectance measurements.....	23
Figure 4.1. Block diagram for atmospheric correction of AVIRIS-NG data to generate L2 data.....	27
Figure 4.2. (a) AOD retrieval. (b) TOA reflectance spectrum. (c) Flowchart for spectral polishing. ....	29
Figure 4.3. True colour image, AOD map and histogram for Ambaji (a) and Bhukia (b), region. ....	31
Figure 4.4. (a) WV map derived by SAC and JPL (b) Effect of spectral polishing on L2 spectra. (c) Comparison between sensor level apparent reflectance & derived surface reflectance. ....	32
Figure 5.1. Flow chart representing the entire APDA process.....	34
Figure 5.2. (a) RGB image (Howrah), WV retrieved using (b) APDA & (c) CIBR technique .....	35
Figure 5.3. (a) RGB image (Hyderabad), WV retrieved using (b) APDA & (c) CIBR technique .....	35
Figure 5.4. Scatter diagram of WV retrieval using Wyoming and APDA (a) and CIBR (b).....	36
Figure 6.1. Flowchart of the study .....	40
Figure 6.2. Spatial variability in PM <sub>2.5</sub> , PM <sub>10</sub> and Black Carbon distribution at Ahmedabad.....	40

Figure 6.3. (a). CO <sub>2</sub> retrieval over Kota (b). CO <sub>2</sub> retrieval over Ahmedabad and validation with in-situ observations (CO <sub>2</sub> retrievals draped over AVIRIS-NG NCC .....	41
Figure 7.1. Flow chart of columnar methane (XCH <sub>4</sub> ) retrieval from AVIRIS-NG radiance.....	45
Figure 7.2. Retrieved atmospheric CH <sub>4</sub> molecular column density map from (a) AVIRIS-NG using 3-channels ratio (b) from ground based FTIR spectrometer at 2.29 μm absorption band.....	46
Figure 8.1. Flow chart for the determination of cloud microphysical properties. ....	50
Figure 8.2. (a) Spectra of model simulated and AVIRIS-NG measured radiances for different cloud types and (b) Spectra obtained for the best match of radiances .....	51
Figure 8.3. (a) RGB image (b) retrieved CER and retrieved COT (c) retrieved COT for Chilika .....	52
Figure 8.4. (a) RGB image (b) retrieved CER and (c) Muddur .....	52
Figure 8.5. 3D Map of cloud microphysical parameters where height represents COD and colors represent CER .....	53
Figure 8.6. Scatter plot of MODIS and AVIRIS cloud effective radius .....	53
Figure 9.1. Flow of the data in atmospheric correction .....	56
Figure 9.2. Sample of comparison of level-2 products from SAC & JPL over various targets .....	57
Figure 9.3. Uncorrected Vs corrected FCC.....	58
Figure 10.1. AVIRIS-NG Natural Colour Composite Image with in-situ station locations (red dots) ....	60
Figure 10.2. Image in upper left part, shows the radiance and right side reflectance data over Chilika. lower left side, shows radiance and in right side, reflectance spectra acquired over Chilika.....	63
Figure 10.3. Comparison of AVIRIS-NG reflectance spectra with in-situ at twenty different locations (dotted curve-AVIRIS-NG and solid curve in-situ spectra).....	64
Figure 11.1. Spectral library main menu (top left), vegetation spectral library (top middle), plant general info (bottom left), observation details (bottom middle) and vegetation analysis (top right). 70	
Figure 11.2. Hyperspectral image analyzer main menu and indices calculator window (bottom left). On choosing ROI option in indices calculation, window opens with FCC image to draw the ROI.....	71
Figure 12.1. False Color Composite (FCC) of AVIRIS-NG image (R: Band-82; G: Band-58; B: Band-36) over the Shimoga forest area (Karnataka).....	74
Figure 12.2. Flow chart of classification & selection of peak parameters of end-members from ASD	75
Figure 12.3. <b>(a)</b> Vegetation spectrum of a sample target, peak shoulders, continuum and normalised spectrum. <b>(b)</b> Normalised spectra decomposed to maximum possible Gaussian peaks .....	76

Figure 12.4. (a) FCC image of the part of the study site and (b) Classified image of three dominant species (Red: <i>Tectona grandis</i> , Green: <i>Dalbergia latifolia</i> and Blue: <i>Lagerstroemia lanceolata</i> ).....	77
Figure 13.1. Flow of methodology for classification.....	84
Figure 13.2. Spatial crop classified map using AVIRIS-NG data and validation with independent ground dataset over Jhagadia site 1. ....	85
Figure 13.3. Spatial crop classified map using AVIRIS-NG data and validation with independent ground dataset over Jhagadia site 2.....	85
Figure 13.4. Spatial crop classified map using AVIRIS-NG data and validation with independent ground dataset over Kota site 1.....	86
Figure 14.1. Figure showing the study site of Talala (up) and AVIRIS-NG image over the same (down). .....	91
Figure 14.2. Flowchart showing the methodology adopted for the classification. ....	91
Figure 14.3. Figure showing FCC of a.) AVIRIS-NG image over Talala (left), b.) SAM classified image (middle) and c.) wrapper based classified output (right). ....	93
Figure 15.1. Flow of methodology for classification.....	98
Figure 15.2. Principal components analysis using AVIRIS-NG and LISS-IV data.....	99
Figure 15.3. Crop classification using AVIRIS-NG data using spectral angle mapper algorithm.....	99
Figure 15.4. Crop classification using LISS-IV equivalent spectral data using SAM algorithm.....	100
Figure 15.5. Crop classification using AVIRIS-NG data using maximum likelihood classification .....	100
Figure 15.6. Crop classification using LISS-IV equivalent spectral data using MXL classification.....	101
Figure 16.1. Methodology.....	105
Figure 16.2. a.) SAM Classified, b.) Hierarchical Decision rule.....	106
Figure 16.3. (a) AD (661.93-702.0nm), (b) AD (947.43-997.52nm) .....	107
Figure 16.4. a.) AD (661.93-702.0nm), b.) AD (947.43-997.52nm).....	107
Figure 17.1. Ground Spectra for Different Crops/Soils .....	112
Figure 17.2. Image Spectra for Different Crops/Soils .....	112
Figure 18.1. Study Area False Color Composite .....	116
Figure 18.2. Overall methodology .....	117
Figure 18.3. Particle size distribution of soil samples.....	117

Figure 18.4. Spectral library of soil samples .....	118
Figure 18.5. Various Spectral Reflectance transformations .....	119
Figure 18.6. Soil textural prediction using different reflectance transformations: PLSR technique. .	119
Figure 19.1. Study area .....	122
Figure 19.2. Flow of methodology for retrieval of B-P-C canopy parameters using RT model. ....	123
Figure 19.3. Forward simulation of calibrated CRT model over various LAI ranges .....	124
Figure 19.4. Retrieval of agricultural LAI using RT method (Site: Kota).....	125
Figure 19.5. (a) Histogram of LAI and (b) validation of retrieved LAI from CRT model .....	125
Figure 19.6. Leaf Chlorophyll content from AVIRIS NG using forward and inversion of Canopy Radiative Transfer Model (Site: Jhagdia, (Gujarat) AVIRIS Flight date 9th Feb 2016) .....	126
Figure 19.7. (a) Histogram of Chlorophyll and (b) validation of retrieved Chlorophyll: CRT model...	126
Figure 20.1. Flow chart for estimating biochemical and biophysical properties of crop and soil .....	131
Figure 20.2. Models developed for (a)Plant N, (b) plant water content, (c) plant Chl and (d) LAI.....	132
Figure 20.3. Plant N content map over AVIRIS-NG scene. ....	132
Figure 20.4. LAI map over AVIRIS-NG scene along with validation result with ground.....	133
Figure 21.1. Overview of the methodology .....	137
Figure 21.2. Spectral profile of various features observed during ground truth.....	138
Figure 21.3. FCC image and Water Indices of the Nagarjuna Sagar command area .....	139
Figure 21.4. Scatter plots of NDVI vs NDWI, NDII, LSWI and WI.....	140
Figure 21.5. Plot of the Standardize Water Condition Index of NDWI, NDII, LSWI and WI .....	140
Figure 22.1. Flowchart for complete work.....	144
Figure 22.2. Band range selection for wheat disease identification.....	144
Figure 22.3. SAM classified image.....	146
Figure 22.4. Index based classified image.....	147
Figure 22.5. Band range selection for wheat disease identification.....	148
Figure 22.6. Absorption depth based classified image .....	148
Figure 23.1. (a) Hyperspectral Data; (b)Shannon Diversity Index.....	155

Figure 23.2. SAM based species classified map for study area .....	156
Figure 24.1. (a) Study area; (b) Total Mangrove Coverage in AVIRIS-NG; (c) Classified Mangrove....	159
Figure 24.2. Methodology.....	159
Figure 24.3. Hyperspectral signature of various mangrove species .....	160
Figure 24.4. Comparison of classified Multispectral and Hyperspectral data .....	160
Figure 24.5. Capability to discriminate fresh and marine water .....	161
Figure 25.1. Flowchart showing detail methodology .....	165
Figure 25.2. Mangrove forest discrimination based on SAM .....	166
Figure 25.3. Comparison of classification using Resourcesat 2 LISS 4 and AVIRIS data.. ..	167
Figure 25.4. Mangrove forest health assessment.....	168
Figure 25.5. Spectra from hyperspectral imager for dominant mangrove species .....	168
Figure 26.1. Study area map showing AVIRIS data over part of Shoolpaneshwar forest.....	172
Figure 26.2. Vegetation indices (MRENDVI, MSI, PSRI) for fuel load estimation .....	175
Figure 26.3. Forest fuel load map of Shoolpaneshwar forest using AVIRIS based indices .....	175
Figure 26.4. Vicarious validation of fuel load using active fire points .....	176
Figure 27.1. Lithological map of Hindoli-Jahazpur Group.....	184
Figure 27.2. Stringers of chalcopyrite ( $CuFeS_2$ ) within dolomitic marble .....	185
Figure 27.3. Integrated Band Depth (IBD) based FCC of Jahazpur and adjoining regions .....	186
Figure 27.4. Spectral endmembers derived from the IBD-based FCC mosaic of Jahazpur.....	186
Figure 27.5. Spectral plot of mineral endmembers obtained after known vs. unknown analysis .....	187
Figure 27.6. SFF-based FCC of the Jahazpur mosaic highlighting Mg-carbonate-bearing lithologies, talc and kaolinite/montmorillonite-bearing regions .....	187
Figure 27.7. Zoomed-in portion marked by red rectangular box in Figure 27.6 .....	188
Figure 28.1. AVIRIS colour infrared image of the study area.....	193
Figure 28.2. Mask of pixels containing vegetation and water is prepared using NDVI and NDSI. ....	197
Figure 28.3. Map depicting spatial variations of deepest absorption feature in SWIR .....	198

Figure 28.4. Field photographs of marble quarry exposed at location 1 (Figure 28.1) and pink granite at location 2 (Figure 28.1).	199
Figure 28.5. Inter-comparison of dolomite spectra of AVIRIS-NG and field.	200
Figure 28.6. Inter-comparison of field reflectance spectra of kaolinite.	200
Figure 28.7. Inter-comparison of image spectra with library spectra of mineral dolomite in 0.4-2.5 $\mu\text{m}$ and 2.0 – 2.5 $\mu\text{m}$ wavelength range	201
Figure 28.8. Inter-comparison of image spectra with library spectra of mineral Kaolinite in 0.4-2.5 $\mu\text{m}$ and 2.0 – 2.5 $\mu\text{m}$ wavelength range.	201
Figure 28.9. Mapping of subtle differences in carbonate mineralogy.	202
Figure 28.10. Integrated band depth at 2.30 $\mu\text{m}$ showing spatial distribution of carbonate.	203
Figure 28.11. Integrated band depth at 2.20 $\mu\text{m}$ showing spatial distribution of clay.	204
Figure 28.12. Map showing regions having occurrence of relatively pure carbonate minerals.	205
Figure 28.13. Map depicting regions having dominant presence of clay minerals obtained by applying threshold ( $> 0.35$ ) on 2.20 $\mu\text{m}$ IBD image.	205
Figure 29.1. Flow chart of methodology.	212
Figure 29.2. Geological map of Sittampundi Layered complex. b. 2D map ground magnetic anomaly. C. Enhanced portion of magnetic anomaly.	214
Figure 29.3. Field exposures of granodiorite gneiss(a), anorthosite(b) meta gabbro(c) and chromitite(d). e. Spectral profiles of major rocks of the study area.	214
Figure 29.4. MNF composite of AVIRIS Level 1B data delineating major rocks of the area. Enhanced part of the image composite (b) of different rocks shown with field photograph of rocks.	215
Figure 29.5. MNF composite of AVIRIS Level 1B data delineating major rocks of the area. Enhanced part of the image composite (b) of different rocks with field photograph.	215
Figure 29.6. AVIRIS based dolomite map prepared using image spectra of dolomite (from mine area). b. ASTER based dolomite map derived from broad band ASTER image spectra of dolomite.	216
Figure 30.1. Flow chart shows the detail methodology of the study	220
Figure 30.2. Hydrothermally altered minerals around Ambaji and Dungarpur.	221
Figure 30.3. Hydrothermally altered minerals at Nili Fossae region of Mars.	221
Figure 31.1. Conceptual Methodology.	226
Figure 31.2. Abundance map of submerged aquatic vegetation in Chilika Lagoon	228

Figure 31.3. Water Column height estimation using spectral inversion technique .....	228
Figure 31.4. Coastal classification map .....	229
Figure 31.5. Mapping of different ecological parameters within Chilika Lagoon.....	230
Figure 31.6. Abundance map of coastal features and moisture content at Gulf of Kachchh.....	231
Figure 32.1. Flow chart showing the methodology .....	235
Figure 32.2. Species level distribution map of Sargassaceae Family in Pirotan reef .....	236
Figure 33.1. The scan lines of AVIRIS-NG flight: Hooghly and Saga Island .....	239
Figure 32.1. Flow chart showing the methodology to retrieve the Geophysical products .....	240
Figure 33.3. Remote sensing reflectance spectra collected on 28th February 2016, at Howrah .....	240
Figure 33.3. Comparison of ENVI (a) Flaash and (b) QUAACK atmospheric correction.....	241
Figure 33.3. Validation of in-situ and AVIRIS-NG reflectances and chlorophyll .....	241
Figure 33.3. Retrieval of chlorophyll concentration and TSM in the Hooghly estuary.....	242
Figure 33.3. Representation of (a) bottom albedo (b) Depth and (c) error estimation .....	242
Figure 33.1. Index Map of Study Area. ....	251
Figure 33.2. a.) Turbidity map of Ganga River near Buxar, b.) Turbidity map of Hooghly River. ....	253
Figure 34.1. Chilika Lake as seen in Landsat 8 OLI along with location of sampling points.....	255
Figure 34.2. Flow chart of methodology adapted .....	257
Figure 34.3. Instruments used to collect ground data, a) field spectro-radiometer, b) portable eco-sounder, c) hand held GPS, d) turbidity meter, e) sun-photometer.....	257
Figure 34.4. Field spectra of points fall in each turbidity concentration class and its comparison with Ritchie et al. (1976) spectra along with field photo of different water.....	258
Figure 34.5. (a) FCC of AVIRIS-NG image of December 27, 2015 with location of sample collection sites (b) SAM classified image of the part of Chilika Lake.....	259
Figure 34.6. Field and AVIRIS-NG image spectra matching (continuum-removed spectra of selected locations for each class of turbidity).....	260
Figure 35.1. Study Area along with AVIRIS strips & locations of in-situ sampling.....	264
Figure 35.2. Flow chart of the methodology .....	265
Figure 35.3. Simulated RS reflectance for varying water optical properties and various depth.....	266

Figure 35.4. Water quality maps over Ganga River, Buxar .....	267
Figure 35.5. Turbidity and bathymetry maps over Chilika Lagoon .....	267
Figure 36.1. Flow chart of the methodology .....	273
Figure 36.2. Comparison of ground, ATREM and FLAASH .....	274
Figure 36.3. Classified land use map.....	276
Figure 37.1. Study Area - Part of Ahmedabad city.....	280
Figure 37.2. Field Spectra Collection in Ahmedabad City .....	282
Figure 37.3. Comparison of Field Spectra with Image Spectra .....	283
Figure 37.4. Plot-level Estimation of Fraction of Impervious Surface .....	284
Figure 37.5. Spectral End Members for SAM.....	285
Figure 37.6. Urban Land Cover Classification using SAM.....	285
Figure 38.1. GPS location showing different locations for field spectra collection/LISS III .....	289
Figure 38.2. Spectra averaged using conventional method and spectral similarity analysis .....	290
Figure 38.3. Comparison of TAR spectra.....	291
Figure 38.4. Comparison of Soil spectra .....	291
Figure 38.5. Comparison of Concretespectra .....	292
Figure 38.6. Comparison of Water spectra.....	292
Figure 38.7. (a) Hyperion image; (b) classified image using spectra developed precisely; (c) classified image using spectra developed conventionally.....	292
Figure 39.1. Location map of Patsio region and ground measurement at Dhundi Observatory .....	299
Figure 39.2. Continuum removed spectra of model derived and field derived snow reflectance .....	300
Figure 39.3. Snow grain size variability over AVIRIS-NG data in Patsio region.....	301

## List of Tables

Table 1.1. Science themes and study sites for Phase-1 campaign.....	3
Table 1.2. AVIRIS-NG Airborne hyperspectral Phase-1 Campaign diary.....	6
Table 1.3. Product type, definition and correction levels.....	10
Table 2.1. The Desalpar site AVIRIS-NG calibration exercise details .....	17
Table 2.2. The Ahmedabad (SAC-Bopal, GMDC) site AVIRIS-NG calibration exercise details .....	17
Table 4.1. Shows the in-situ (Sun-photometer) and retrieved AOD values in region covered by AVIRIS data over Muddur (Karnataka) on 10-01-2016.....	31
Table 6.1. Data used in the study.....	39
Table 10.1. Percentage (%) Error between retrieved Rrs and in-situ of 20 stations in Chilika lagoon.	64
Table 11.1. Table showing the format of data required to create spectral library .....	69
Table 16.1. Percentage (%) error between retrieved Rrs and in-situ observations .....	108
Table 22.1. Absorption features analysis of ASD data of the site Roper, Punjab.....	145
Table 23.1. Area under different Species dominance.....	156
Table 25.1. Spectral separability analysis using D-matrix. Species with higher difference in the values are better separable in spectral domain.....	166
Table 26.1. Records of VIIRS detected fire during 10 Feb 2016 to 7 June 2016) on underlying fuel condition as detected by AVIRIS-NG on 08 Feb 2016.....	176
Table 27.1. The stratigraphic succession as given by G.S.I. ....	183
Table 29.1. Details of the study .....	211
Table 34.1. AVIRIS-NG Imaging Schedule .....	256
Table 34.2. Details of AVIRIS-NG Data Collected .....	256
Table 37.1. List of Data Used .....	280
Table 38.2. CBD analysis for Concrete .....	291
Table 38.3. Accuracy assesment of image classified using conventionally developed spectra.....	293
Table 38.4. Accuracy assesment of image classified using precisely developed spectra.....	293

## EXECUTIVE SUMMARY

The first phase of airborne hyperspectral campaign has been organized with AVIRIS-NG payload over 22840 km<sup>2</sup> area in 57 sites in India for 84 days during December 16, 2015 to March 6, 2016 under the ambit of ISRO-NASA joint initiative for **HYperSpectral Imaging (HYSI)** programme. Collocated science field campaigns were also conducted. The sites represent agriculture, horticulture, forest, geology, coastal, ocean, river water, snow etc. The spatial resolution of airborne data varies from 4 to 8 m with flight altitude varying from 4 to 8 km. Researchers from different ISRO centres at Ahmedabad, Hyderabad, Dehradun, Indian Institute of Technology, Universities have participated in this campaign and collected in situ data. Laboratory-based bio-geochemical analysis has also been carried out with the leaves, soils, water and rock samples. On-board data processing has been carried out to produce Level-0 (L0) and Level-1(L1) radiance data. The L1 data have been used subsequently to generate Level-2 (L2) surface reflectance in 425 bands at 5 nm interval. Both AVIRIS-NG L1 and L2 data as well as the ground-truth data have been archived in VEDAS ([vedas.sac.gov.in](http://vedas.sac.gov.in)) geoportal. The primary data have been disseminated to ISRO as well as other Indian researchers including those participating as part of ISRO's Announcement of Opportunity (AO) programme. The initial results of the hyperspectral data analysis for the phase – 1 campaign are consolidated in this report. It has four broad sections: (1) Overview of AVIRIS-NG first phase campaign, (2) Calibration and validation, (3) Data processing and retrieval algorithms, (4) Thematic applications. The section 4 is divided into seven (7) sub-sections such as: Agriculture, Forestry, Geology, Coastal-Ocean, River water, Land use and Urban, Snow and Glacier applications. About 100 researchers have contributed to 37 research articles.

The results showed that airborne hyperspectral data are able to discriminate crops in mixed agriculture, horticultural orchards, forest species and to assess their abundance and health. The retrieval of crop biochemical parameters, major nutrients, soil physical and chemical parameters could be used for precision farming, crop insurance and carbon foot printing. These are only possible using band continuum of sensitive band regions in VNIR and SWIR such as 400-900 nm, 1000-1700 nm and 1900-2200 nm. New rock and mineral types were identified using the spectra mostly beyond 2000 nm. Inversion schemes have been implemented to retrieve different water quality parameters using band continuum of 400-800 nm and bio-optical model. Medicinally important coral macrophytes (e.g. Sargassaceae sp.) have been identified and mapped using triple peaks around 646 nm. Quantification of some important atmospheric GHG gas constituents such as CO<sub>2</sub>, CH<sub>4</sub>, water vapour, aerosol loading and cloud microphysical parameters was possible using characteristic sensitive bands at 1900-2100nm, 2290nm, 867, 940, 1009, 470, 650, 1240 and 2100nm. Snow grain-size variability has been quantified using narrow band continuum in NIR region. Second phase of airborne campaign would facilitate the validation of models/techniques, building up of spectral library with spectro-chemical characterization, development of automated tools for general users, definition of future space-based hyperspectral mission and creation of skilled human resources in the country.

# Overview of First Phase of AVIRIS-NG Airborne Hyperspectral Science Campaign over India

Bimal K Bhattacharya<sup>1</sup>, Manish Saxena<sup>1</sup>, Robert O. Green<sup>3</sup>, Sadasiva Rao<sup>2</sup>, G. Srinivasulu<sup>2</sup>,  
Shashikant Sharma<sup>1</sup>, Debojyoti Dhar<sup>1</sup> and Arundhati Misra<sup>1</sup>

<sup>1</sup>Space Applications Centre, ISRO, Ahmedabad, India

<sup>2</sup>National Remote Sensing Centre, ISRO, Hyderabad, India

<sup>3</sup>Jet Propulsion Laboratory, California Institute of Technology, Pasadena, California, USA

## ***1. Scientific Rationale***

Imaging Spectroscopy or Hyperspectral sensing (HSS) of Earth's land and ocean environments is based on the principles of spectroscopy, either reflectance or emission spectroscopy, over shortwave (0.3 to 3  $\mu\text{m}$ ) and longwave (5 to 50  $\mu\text{m}$ ) spectrum. Interaction of energy with the molecular and structure of surface materials results into characteristic or diagnostic absorption or emission features in the reflectance or emittance spectra. These diagnostic features occur due to changes in energy state of molecules as a function of electronic or vibrational transitions. The former occurs predominantly at shorter wavelengths due to changes in energy state of electrons bound to atoms or molecules or lattices. The latter occurs generally in longer wavelength due to stretches and bendings where overtones occur at sums or multiples of the fundamental vibration frequencies. HSS refers to 100 - 200 spectral bands, generally in continuum with relatively narrow band interval (5 – 10 nm), in contrast to Multi-Spectral Sensing (MSS) that refers usually to 5-10 discrete wide bands with bandwidths about 50-400 nm. The advantages of reflectance HSS over MSS are: (i) the former can detect more materials or surface types such as minerals, rocks, vegetation, snow, (ii) relates directly to surface chemistry and (iii) can estimate the abundance of material present. This greater information content enables new methods for detection, characterization and quantification in a broad range of Earth system environments. The ability to develop HSS instrument is only recently enabled by technologies of the 21<sup>st</sup> Century. For high uniformity spectroscopy, the grating-based spectral dispersion approach has distinct advantages in comparison to the wedge-filter technological approach. Handheld field spectrometers are generally useful for ground-based survey. However, they provide only point target spectra and not the continuous spatial coverage over large areas required for many local, regional research and applications.

Several imaging HSS instruments such as micro-hyperspec, nano-hyperspec and snapshot are available for hyperspectral imaging to provide data with centimeter spatial resolution from airborne (e.g. Aeroplane, Robotic UAV, Drones etc.) and ground-based platforms. The satellite-based HSS mission such as EO-1 Hyperion of NASA provided reasonably good datasets sampled around the globe, including India, but Hyperion suffers from low Signal-to-Noise Ratio (SNR). Nevertheless, potential applicability of HSS data from EO-1 Hyperion over India have been demonstrated for agriculture (e.g. mustard crop disease), geology (e.g. Dungargarh, Rajasthan) by Bhattacharya and Chattopadhyay (2013), Dutta et al. (2006), Bhattacharya et al. (2012). In addition, several ground-based studies in India by Ramakrishnan and Bharti (2015), Sahoo et al. (2015), Das et al. (2015) using ground-based field spectrometers proved the potential advantages of using HSS data for crops, soils, geology etc. The applicability of HSS has already been shown for coastal-ocean chemistry, snow and glacier, coral reef and cloud microphysical characterization. The hyperspectral science initiative is also included in the “Big Data Initiatives” of Department of Science and Technology (DST), Govt. of India. Keeping the future applicability potential in tandem with the development of advanced technology, the ISRO-NASA joint airborne hyperspectral science campaign over India was begun in 2015.

## **2. Objectives**

The broad objectives of ISRO-NASA hyperspectral programme are:

- To harness the benefits of unique and advanced remote sensing measurements for society by bringing together important talents and expertise in instrumentation, science and applications of both ISRO and NASA.
- To jointly develop advanced science understanding, models, algorithms and techniques through knowledge sharing and to open up new avenues of collaboration.
- To provide the required precursor ground truth data and science and application research demonstrations for present and future ISRO space imaging spectrometer missions.

### 3. Airborne Hyperspectral Instrument and Study sites

The Airborne Visible and InfraRed Imaging Spectrometer – Next Generation (AVIRIS-NG), of JPL (Jet Propulsion Laboratory), NASA, has been used for the ISRO-NASA airborne campaign on-board an ISRO B200 aircraft. There are about 430 narrow continuous spectral bands in VNIR and SWIR regions in the range of 380-2510 nm at 5 nm interval with high SNR (>2000 @ 600 nm and >1000 @ 2200 nm) with accuracy of 95% having FOV of 34 deg and IFOV of 1 mrad. Ground Sampling Distance (GSD) vis-à-vis pixel resolution varies from 4-8m for flight altitude of 4-8 km for a swath of 4-6 km. The science themes are spread over eight broad areas with a total 57 sites in Priority 1 and 25 sites in Priority 2 scheduled for imaging by AVIRIS-NG based on proposals by scientists from ISRO centres, universities and IITs. The science themes and number of Phase-1 campaign sites are given in table 1.1.

Table 1.1. Science themes and study sites for Phase-1 campaign

<b>Sr. no.</b>	<b>Broad science themes</b>	<b>Sub-themes</b>	<b>No. of study sites</b>
1.	Agriculture and Ecosystem	Crop, Soil, Mangrove, Wetland	21
2.	Geology		11
3.	Ocean & coastal	Coastal zone, biological oceanography, coral reef	11
4.	Rivers and water quality		5
5.	Urban		2
6.	Snow and ice		2
7.	Atmosphere	Air quality, cloud microphysics	3
8.	Calibration and validation		2

The geographical distribution of sites and False Color Composites (FCC) of few sites as acquired by IRS (Indian Remote Sensing) satellite sensors are shown in figure 1.1 and figure 1.2, respectively.

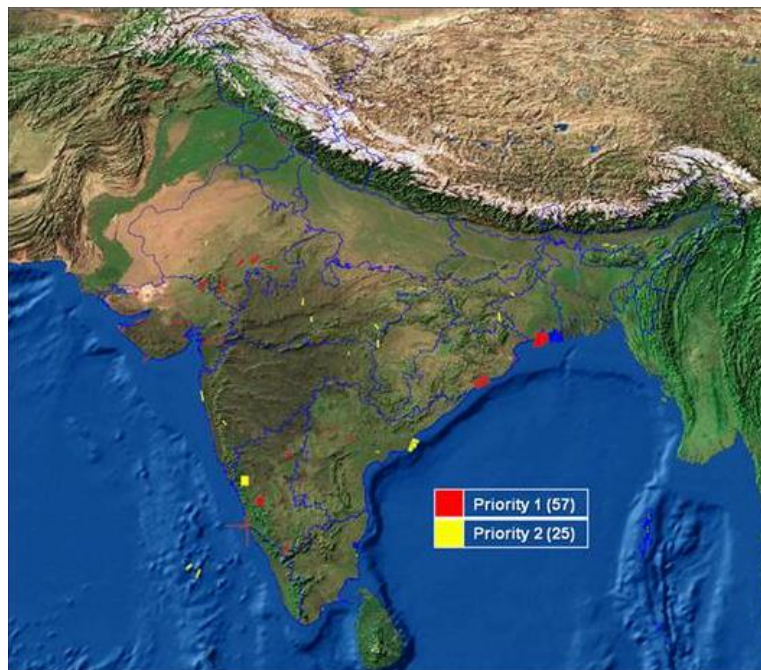


Figure 1.1. Geographical distribution of AVIRIS-NG science campaign sites

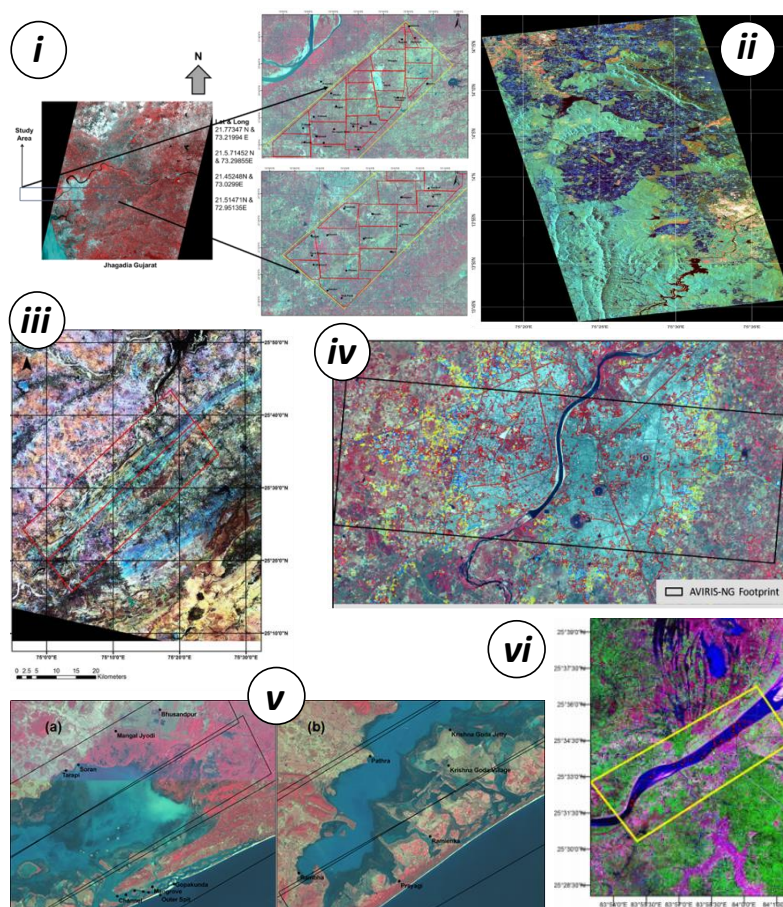


Figure 1.2. Examples of sites and flight paths for (i) agriculture (ii) forest (iii) geology (iv) urban and air quality (v) coastal and ocean and (vi) river and water quality

The photographs of airborne campaign teams with B200 aircraft and AVIRIS-NG instrument are shown in figure 1.3.



Figure 1.3. Airborne campaign team and science field campaign team with B200 aircraft and AVIRIS-NG instrument

#### ***4. Campaign Coordination, Execution and Ground-Truth Data Collection***

First pre-campaign science meeting took place on September 30, 2015 at Space Applications Centre, Ahmedabad among the interested researchers to organize theme-wise field sampling plans, sampling points, time of samplings, availability of field spectrometers, sun photometers for atmospheric measurements, and other field instruments. The types and protocols of biochemical, geochemical analysis, laboratory-based spectroscopy of field samples have been planned. Site-wise teams were formed for each theme by pooling the participating researchers from SAC, NRSC, IIRS, RRSCs, IIT, ICAR, Universities keeping in view of smooth transition of field instruments from one team to another. Two rounds of cross-calibration of different sets of field instruments and hands-on were arranged at SAC. The IRS RS-2, LISS IV and RISAT-1 FRS-1 data have been arranged near coincident to date of flights for highly dynamic sites (e.g. agriculture). The airborne acquisition campaign with AVIRIS-NG started on

19 December 2015 and continued through 8 March 2016. First data sets were acquired with a brief CAL-VAL campaign at Begumpet airport, Hyderabad to evaluate performance of AVIRIS-NG with respect to ground measured spectra. The final data set were acquired over the Gulf of Kutch in Gujarat. The flight campaign was organized from nine airport bases (table 1.2) Ahmedabad, Udaipur, Bhubaneswar, Hyderabad, Mangalore, Coimbatore, Chandigarh, Patna, Kolkata. More than 200 people participated in the field campaigns corresponding to date of flight and flight path. An internet-based ‘What’s App’ group was made for better on-site coordination for mobility of field teams to accommodate last-minute changes due to change in flight schedule depending on Air Traffic Control (ATC) clearances. High-resolution short-range weather forecast on cloud fraction from MOSDAC was provided to campaign coordination teams and field campaign teams for effective and efficient flight planning and field data collection.

Table 1.2. AVIRIS-NG Airborne hyperspectral Phase-1 Campaign diary

<b>Serial No.</b>	<b>Airports (In chronological order as per flight schedule)</b>	<b>Duration</b>	<b>No. of sites</b>	<b>Area Imaged (km<sup>2</sup>)</b>
1.	Begumpet	16 to 21 December 2015 25 to 29 January 2016	12	2650
2.	Bhubaneswar	22 to 28 December 2015	6	3780
3.	Mangalore	29 December 2015 to 2 January 2016	5	3491
4.	Coimbatore	3 to 8 January 2016	5	1416
Phase inspection of aircraft				
5.	Udaipur	31 January to 5 February 2016	8	3697
6.	Ahmedabad	6 to 16 February 2016 6 to 9 March 2016	10	2788
7.	Chandigarh	17 to 21 February 2016	4	835
8.	Patna	22 to 24 February 2016	3	396
9.	Kolkata	24 February to 6 March 2016	4	3787
Total no. days = 84, Total area imaged = 22840 km <sup>2</sup> over 57 sites				

Exceptional volumes of high quality field spectra and associated field data were collected coincident with airborne measurements. Examples of flight paths, field photographs, field-based spectroscopic measurement over different targets are shown in figure 1.4, figure 1.5 and figure 1.6, respectively.

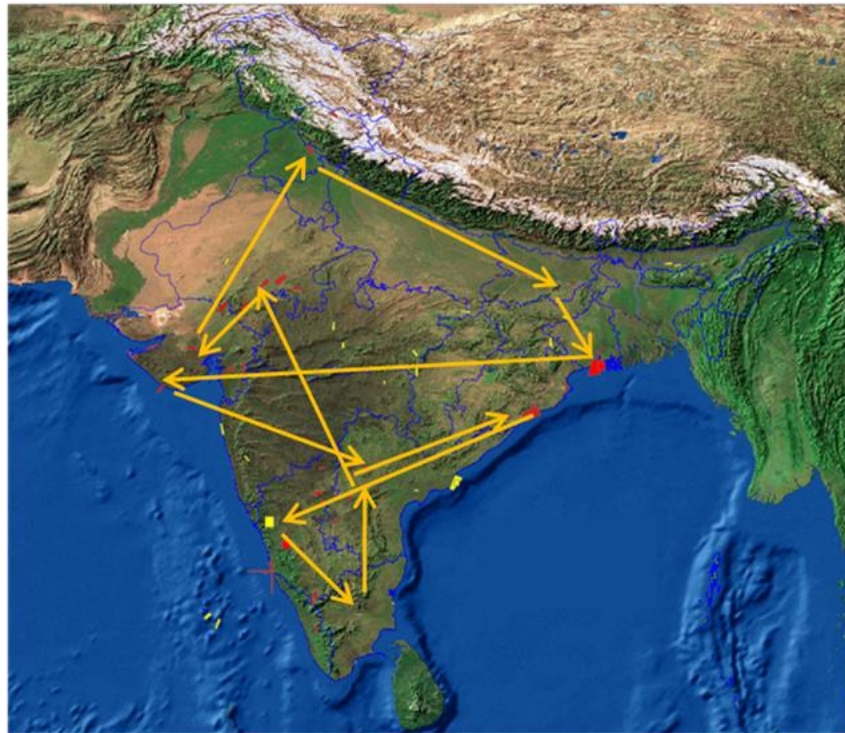


Figure 1.4. Flight paths of Phase-1 AVIRIS-NG airborne campaign



Figure 1.5. Field photographs of Ground-truth campaigns

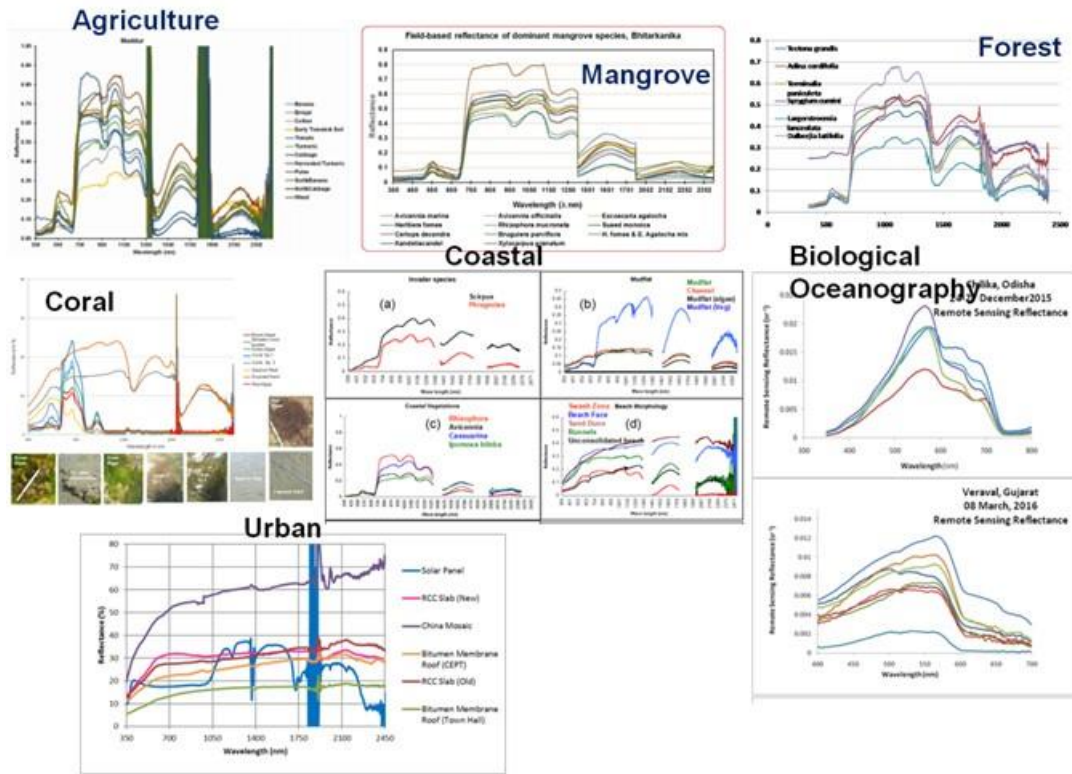


Figure 1.6. Examples of field-based hyperspectral signatures over different thematic targets

Laboratory-based chemical analysis were also carried out on soil, vegetation, rock and water samples collected during field campaigns. These have been used along with AVIRIS-NG data to demonstrate the utility of imaging spectroscopy measurements, to test and develop new algorithms, tools, techniques, enhanced science understanding and also to define future space-based satellite mission.

### 5. Product levels

Examples of imaging spectroscopy data sets acquired by AVIRIS-NG are shown as 3D data cubes in the figure 1.7.

The sample natural color composites in 2D frame are shown in figure 1.8.

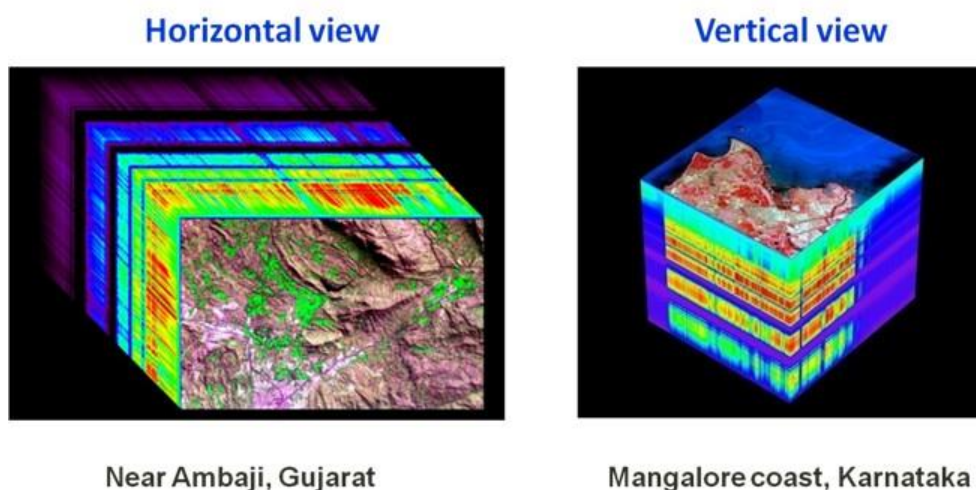


Figure 1.7. Examples of 3D data cubes from AVIRIS-NG

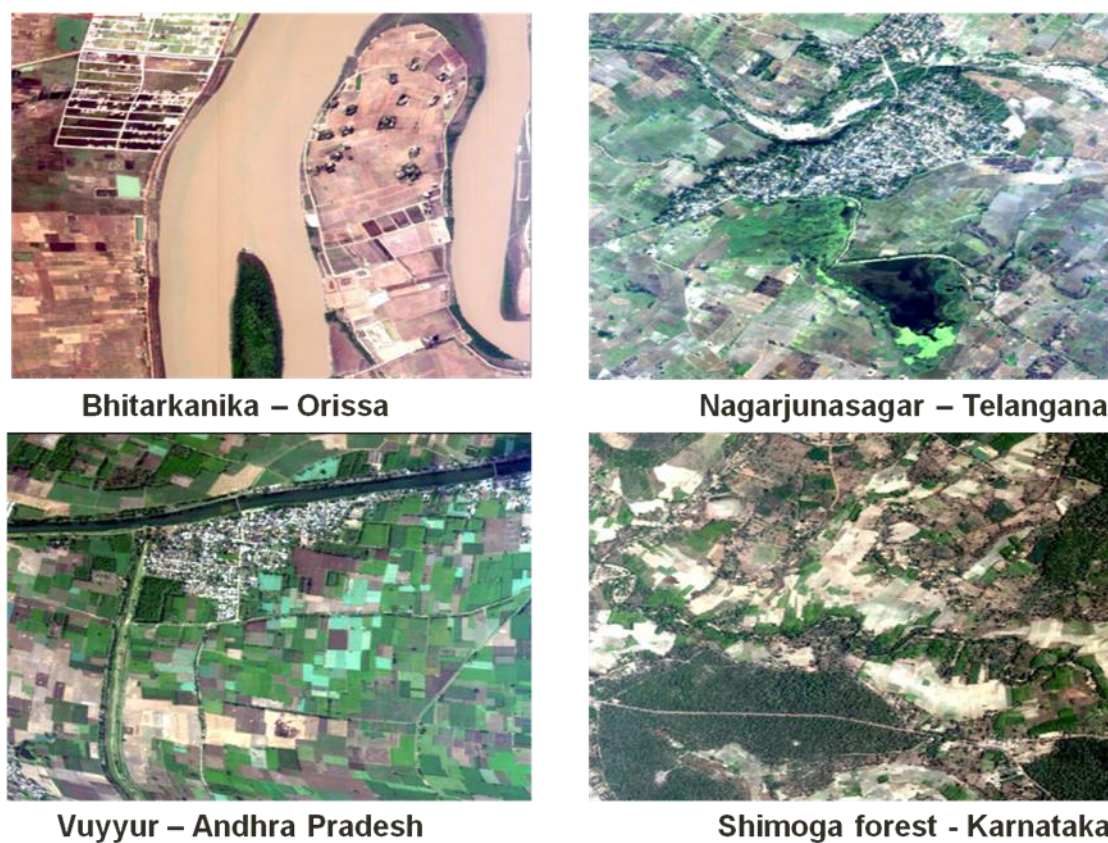


Figure 1.8. Examples NCC images from AVIRIS-NG

Three levels of products, viz. L0, L1 and L2 have been targeted to be obtained from AVIRIS-NG data (table 1.3). The L0 and L1 data represent raw data, calibrated and ortho-rectified top-of-radiance (TOA), respectively which were generated on-board the aircraft. The L2 data represent surface reflectance products in all the bands after atmospheric correction. Two

types of prototype models viz. point-based and pixel-based, have been developed. The former is useful for a sub-scene where atmosphere is assumed spatially invariant and point-measured aerosol optical depth and water vapour can be used for generating surface reflectance. Pixel-based approach first derives atmospheric water vapour and aerosol optical depth at pixel-level from TOA radiance itself, which serve as input to atmospheric correction models.

Table 1.3. Product type, definition and correction levels

<b>Product type</b>	<b>Product definition</b>	<b>Data content</b>
Level - 0	Raw	Raw data as captured by the sensor + GLT, IGM & LOC Files
Level - 1	Calibrated Radiances	Radiance Image Cube + GLT, IGM & LOC Files
Level - 2	Atmospherically-corrected surface reflectance	Surface Reflectance Image Cube + GLT, IGM & LOC Files

## **6. Data archival and dissemination**

The AVIRIS-NG data have been archived in VEDAS web portal ([vedas.gov.in](http://vedas.gov.in)) of SAC after obtaining due clearances of collected data from Ministry of Defence (MoD), Govt. of India and further processing by JPL and SAC. The different facilities of VEDAS portal and data flow mechanism are shown in figure 1.9. About 230 AVIRIS-NG scenes with data storage of 1.5 TB collected over 57 sites in the 1<sup>st</sup> Phase of campaign have been archived in VEDAS. In addition to that, ground-truth data and field campaign reports are also archived in VEDAS. Data are being disseminated to interested researchers of different Indian Academia based on certain guidelines.



Figure 1.9. AVIRIS-NG data archival facility and data flow mechanism

## 7. Capacity Building: Announcement of Opportunity (AO)

Human resources will be developed among different research agencies and academia to develop the expertise on the use of imaging spectroscopy measurements. To that end, an Announcement of Opportunity (AO) for proposals has been released to Indian research agencies. About thirty-five (35) such proposals have been short-listed based on the technical merits and innovativeness. PhD work is being encouraged through these proposals. First course of training has been given to AO Principal Investigators (PIs) and students involved in the research. The AVIRIS-NG data have been shared to all Indian AO PIs through VEDAS. NASA has also announced AO for US researchers and the received proposals are in the process of selection.

## 8. Major Achievements

The highlights of major achievements are given below:

- Prototype ATCORR algorithms for land & water have been developed and evaluated.

- Processing module has been developed for pixel-based Integrated Band Depth (IBD), First-order derivative, to determine hidden or children peaks of pigment absorption through spectral deconvolution.
- Processing module developed for field spectroscopy data (Savitzky-Golay filtering, absorption band centre, FWHM & depth).
- Prototype of creating, visualization of spectral library and improved classification through genetic algorithm.
- Cal-Val experiments have been carried out for AVIRIS-NG TOA radiance and surface reflectances at Desalpar, Gujarat and GMDC ground, Ahmedabad.
- Different sensitive band regions identified for improved discrimination of forest species, crop types, disease detection, canopy and soil water stresses, soil types, land uses, coral reef, macro-algae, mineral, coastal vegetation, urban roof types.
- Retrieval schemes have been developed for determination of crop chlorophylls, ocean chlorophyll, CDOM concentration, suspended sediments and coastal bathymetry, water turbidity parameters and validated.
- Retrieval schemes of different atmospheric parameters such as aerosol optical depth, water vapour, atmospheric CO<sub>2</sub>, cloud-microphysical parameters have been developed and validated.
- Snow-grain size characterization and lichen presence in alpine areas in Western Himalayan region have been ascertained with AVIRIS-NG spectra.

Theme-wise achievements are elaborated in various subsequent sections of this document. The future plans include (i) conducting a second phase of airborne campaign with AVIRIS-NG data with repeat observations over 57 sites and imaging over additional sites to develop sound spectral library and digital spectroscopy catalogue (ii) to carry out exhaustive validation (iii) holding international workshops. The experience with AVIRIS-NG data will be useful to generate operational products from future space imaging spectrometer payloads.

## ***9. Linkage to Key Societal benefit areas***

The end-use applications of thematic investigations would support important key societal benefit areas such as:

- Food security: Precision farming, crop insurance, soil health assessment, fertilizer prospecting;
- Mineral exploration: Identifying new mining areas, mineral abundance mapping, hydrothermal alteration;
- Water and air quality assessment for river, lakes, ponds, canals and industrial plume dispersal;
- Mapping medicinally important coral macrophytes, medicinally important plants and commercially important forest tree species;
- Urban development and planning for climate change mitigation;
- Improved scientific understanding of bio-geochemical cycles for climate change.

## **Acknowledgements**

Authors are grateful to Director, Space Applications Centre, ISRO, Ahmedabad and Director, National Remote Sensing Centre, ISRO, Hyderabad for their constant support and encouragement to carry out this airborne campaign in a time-bound manner. The AVIRIS-NG contribution has been supported by NASA and the Jet Propulsion Laboratory, California Institute of Technology.

## **References**

Bhattacharya, B. K. and Chattopadhyay, C., 2013. A multi-stage tracking for mustard rot disease combining surface meteorology and satellite remote sensing. *Computers and Electronics in Agriculture*, 90, 35 – 44.

Bhattacharya, S., Majumdar, T.J., Rajawat, A.S., Panigrahy, M.K., Das, P.R., 2012. Utilization of Hyperion data over Dongargarh, India, for mapping altered/weathered and clay minerals

along with field spectral measurements. *International Journal of Remote Sensing*, 33(17), 5438–5450.

Das, B. S., Sarathjith, M. C., Santra, P., Sahoo, R. N., Srivastava, R., Routray, A., Ray, S. S., 2015. Hyperspectral remote sensing: opportunities, status and challenges for rapid soil assessment in India. *Current Sci.*, 108(5), 860-868.

Dutta, S., Bhattacharya, B. K., Rajak, D. R., Chattopadhyay, C., Patel, N.K. and Parihar, J.S., 2006. Disease detection in mustard crop using EO-1 Hyperion satellite data. *Journal of the Indian Society of Remote Sensing*, 34(3), 311 – 316.

Mozumdar, C, Reddy, K.V and Pratap, D. (2012). Air pollution modeling from remotely sensed data using regression techniques. *J Indian Soc. Remote Sens.* DOI 10.1007/s12524-012-0235-2.

Ramakrishnan, D. and Bharti, R., 2015. Hyperspectral remote sensing and geological applications. *Current Sci.*, 108(5), 879-891

Sarangi, R. K., Singh, S., Dwivedi, R. S. and Matondkar, S.G.P. (2008). Hyperspectral Radiometric Observation of the Northeast Arabians Sea during April 2006. *J. Indian Soc. Remote Sens.*, 36:13–25

Sahoo, R. N., Ray, S. S., Manjunath, K. R., 2015. Hyperspectral remote sensing of agriculture. *Current Sci.*, 108(5), 848-859.



## Calibration and Validation

# Calibration of AVIRIS-NG hyperspectral imager over natural targets

K. N. Babu, R. P. Prajapati, P. N. Patel and A. K. Mathur

*Calibration and Validation Division,  
Space Applications Centre, ISRO, Ahmedabad, Gujarat, India*

## **1. Scientific rationale and Objectives**

Sensor radiometric calibration, the most fundamental part of the calibration–validation process, is a broad and complex field that imposes the greatest limitations on quantitative applications of remote sensing (Teillet, Horler, & O’Neill 1997). The methods and instrumentation involved can be grouped into three domains: on the ground prior to launch, onboard the spacecraft post launch, and vicarious or indirect approaches using Earth scenes imaged in-flight. Whereas preflight methods encompass a vast array of painstaking sensor characterizations in the laboratory and occasionally outdoors, onboard and vicarious calibrations are devoted primarily to the monitoring of the radiometric responsivities or gain coefficients of sensor spectral bands over time. In all cases, the objective is traceability of data calibration accuracies to the International System of Units (SI) for science users and data products with consistent quality for the broader user community.

The objective of this document is to report the initial measurements and calibration results obtained during the calibration campaigns of AVIRIS-NG aerial mission over Desalpar, SAC-Bopal and GMDC-Ahmedabad Calibration and Validation site of SAC-ISRO.

## **2. Study area and data used**

The vicarious calibration method relies on in-situ characteristics of the surface and atmosphere during the aerial survey. Several important environmental conditions are necessary, such as surface characterizations without cloud cover and a flat homogeneous surface with less aerosol loading. For the AVIRIS-NG mission the calibration campaign was conducted over Desalpar (little Rann of Kuchchh) on February 9-10, 2016, SAC-Bopal and GMDC-Ahmedabad on February 11, 2016 (figure 2.1 shows the AVIRIS-NG image and the

actual field photograph) and the experimental parameter along with instruments used are given in table 2.1 and table 2.2.



Figure 2.1. Desalpar site as viewed by AVIRIS-NG and the field photograph

Table 2.1. The Desalpar site AVIRIS-NG calibration exercise details

<b>Site name/ID</b>	<b>Desalpar/72</b>
Ground sampling area (m <sup>2</sup> )	2880 (120x24)
Total spectrum	674
Instruments	ASD, spectro radiometer, MicroTOPSII (sunphotometer, Ozonometer), CIMEL sunphotometer, Labsphere Spectrolon reflectance panel
Dates	9,10 Feb. 2016

Table 2.2. The Ahmedabad (SAC-Bopal, GMDC) site AVIRIS-NG calibration exercise details

<b>Site name/ID</b>	<b>SAC-Bopal, GMDC-Ahmedabad/69</b>
Ground sampling area (m <sup>2</sup> )	1584 (66x24), 1200 (30x40)
Total spectrum	153, 37
Instruments	ASD, spectro radiometer, MicroTOPSII (sunphotometer, Ozonometer), CIMEL sunphotometer, Labsphere Spectrolon reflectance panel
Dates	11 Feb. 2016

### **3. Methodology**

The improved 6SV radiative model used to compute the at sensor TOA radiance using ground measurements. 6Sv2 RT model predicts the sensor TOA radiance using ground reflectance measurements along with atmospheric parameters (aerosol optical thickness, total ozone and integrated water vapor content). The brief methodology is shown in figure 2.2.

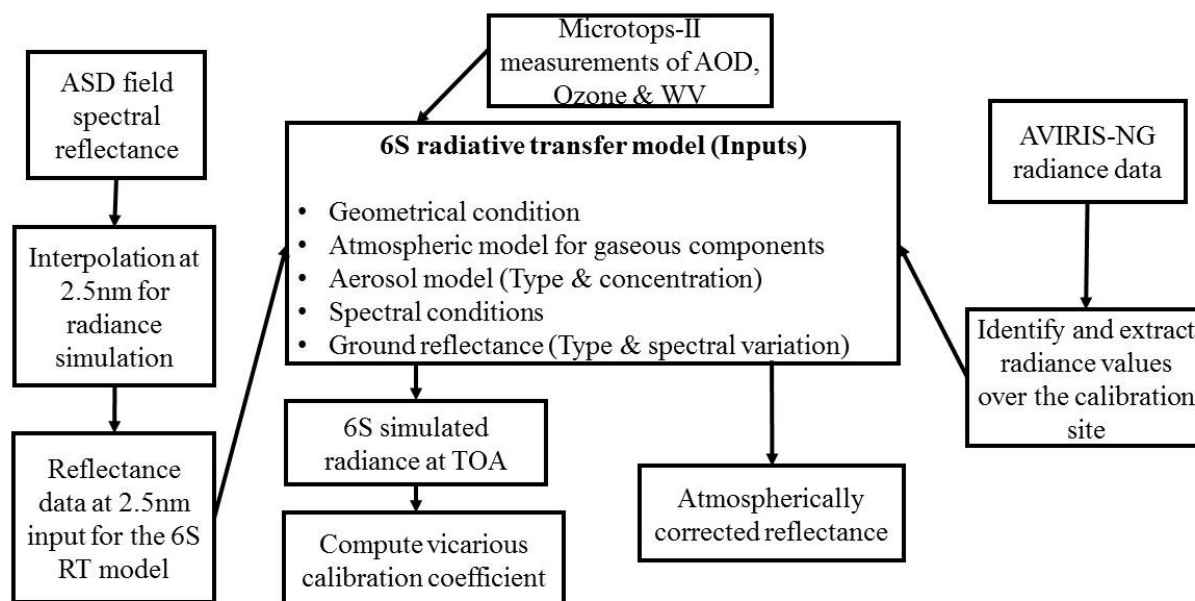


Figure 2.2. The flow chart of TOA spectral radiance simulation

## 4. Outcome

### 4.1 Salient findings

The AVIRIS-NG sensor radiance (level 1B) over Desalpar, SAC-Bopal, GMDC-Ahmedabad sites and the predicted radiance on February 10-11, 2016 is shown in figure 2.3. The sensor geometry values are taken from the header file and the solar geometry is calculated for the particular time of imaging. The model was run for each 5 nm spectral interval along with other input parameters. The computed spectral vicarious calibration gains are within 5% with respect to model simulation over the site.

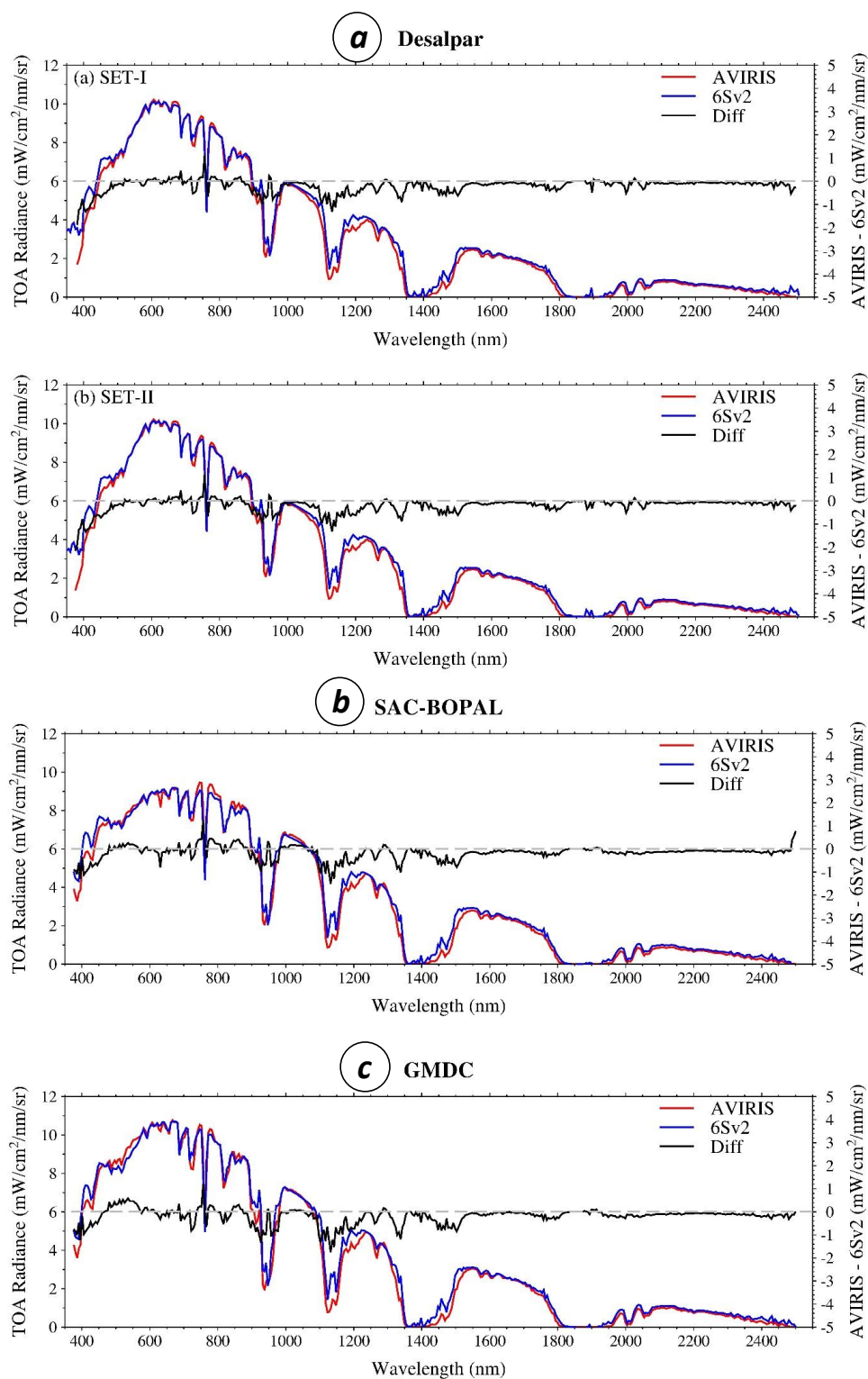


Figure 2.3. (a). At sensor TOA radiance over Desalpar site; measured by AVIRIS-NG (red solid line), 6Sv2 RT model simulation (blue solid line); (b). At sensor TOA radiance over SAC-Bopal site; measured by AVIRIS-NG (red solid line), 6Sv2 RT model simulation (blue solid line); (c). At sensor TOA radiance over GMDC-Ahmedabad site; measured by AVIRIS-NG (red solid line), 6Sv2 RT model simulation (blue solid line)

## 4.2 Target vs. Achievement

Vicarious calibration exercise for the airborne hyper-spectral imager over Desalpar, SAC-Bopal and GMDC-Ahmedabad sites results are consistent with each other by more than 95%. The further investigation along with JPL team is needed for understanding/improvement and with other radiative transfer model comparison.

## 4.3 Linkage to societal benefits

Calibration of AVIRIS-NG spectral radiances with respect to ground measurements is essential as well as crucial to improve the quality of all the derived products. Therefore, it impacts the quality of each geophysical product and in turn the interpretation of spectral signature of AVIRIS-NG measurements.

## 5. Conclusions

- The spectral vicarious calibration gains are within 5% with respect to model simulation.
- The 3-4% total RMSE is found for the full range at Desalpar, SAC-Bopal and GMDC-Ahmedabad.
- The site is dominated by absorbing aerosol in general during winter season.

## Acknowledgements

The authors gratefully express their sincere gratitude to Shri Tapan Misra, Director, Space Applications Centre (SAC) for encouragement to carry out this study. The valuable suggestions and guidance received from Dr. Raj Kumar, Deputy Director, EPSA are gratefully acknowledged. Thanks are due to AVIRIS – NG team and others who supported directly and indirectly.

## References

Teillet, P.M., Horler, D., O'Neill, N.T., 1997. Calibration, validation, and quality assurance in remote sensing: a new paradigm. *Can. J. Remote Sens.* 23 (4), 401–414.

# AVIRIS-NG Calibration and Validation procedure and results

David R. Thompson, Robert O. Green, Michael L. Eastwood

*Space Jet Propulsion Laboratory, California Institute of Technology,  
Oak Grove Dr., Pasadena, USA*

## ***1. Scientific Rationale and Objectives***

In situ measurements at the Desalpar site on 10 February 2016 enabled National Aeronautics and Space Administration (NASA) investigators to validate remote data from the Next Generation Airborne Visible Infrared Imaging Spectrometer (AVIRIS-NG). The in situ measurements, conducted by Indian Space Research Organization (ISRO) investigators, provided coincident data on atmospheric conditions and ground reflectance while the airborne instrument was flying overhead. This enabled a complete end-to-end test of the AVIRIS-NG radiometric and spectral calibration. It also indicated the accuracy of the default atmospheric correction used in science data products by investigators at ISRO and NASA. This section describes the comparison, which sought to address two questions. First, using the best available atmospheric model and best-fitting atmospheric parameters, what was the accuracy of the AVIRIS-NG radiometric calibration and radiance products? Second, using the default atmospheric model from the standard AVIRIS-NG atmospheric correction, what was the typical accuracy of the surface reflectance products?

## ***2. Methodology and results***

To address the first question, investigators selected a coincident overflight scene (ang20160210t061239) containing the in situ data. They analyzed the overflight using the latest AVIRIS-NG radiometric solution incorporating new advances such as correction for spectral stray response functions (Thompson et al., 2017) and calibration data from hangar calibrations during the India campaign. They then applied the standard atmospheric correction strategy detailed by Thompson et al., (2015). The result was a map of surface reflectance at the Desalpar site. The ground team acquired ground reference reflectance data

from a rectangular region on the surface of a large open area covered by soil. Since the site was mostly uniform, the NASA team took an area average in the remote image to form a single aggregate reflectance estimate. The in-situ spectrometer had higher noise in shortwave channels longer than 2300 nm, so they used the median of these spectra to better insulate the surface reflectance from any outliers. A direct comparison of the radiance and reflectance data (figure 3.1) suggested that the two overlay within the standard deviations of the region. Reflectance estimates aligned to within 1-2% across most of the spectral range. This shows the typical accuracy of the AVIRIS-NG reflectance products provided to ISRO investigators.

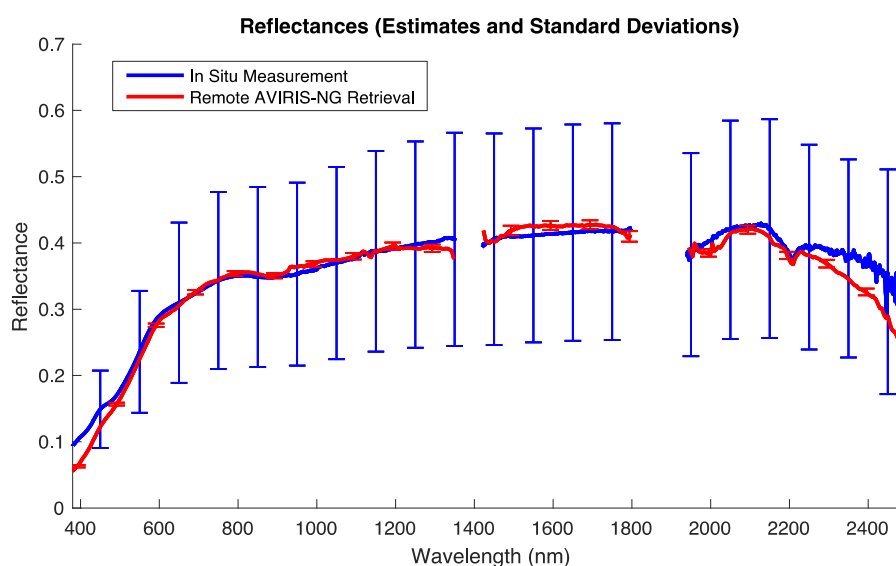


Figure 3.1. Comparison of in-situ and remote reflectance measurements

To address the second question, we constructed a model atmosphere using the MODTRAN 6.0 Radiative Transfer Model (RTM). Investigators projected the in situ reflectance measurement to the sensor altitude and compared the result directly to measured radiances. They determined RTM parameters from multiple sources. They used atmospheric vertical profiles and concentrations based on tropical standards, which produced the best match to the remote measurement. They used a water column of 1.11 cm precipitable water vapor, consistent with spectra as well as the in situ data. Aerosol Optical Depths were measured at multiple wavelengths from an in-situ sunphotometer, and were adopted directly into the RTM. Investigators posited aerosol Single Scattering Albedos (SSAs) from 0.5 at 300 nm to 1.0 at 870 nm, possibly most consistent with strongly absorbing dust aerosols. This selection

provided the best agreement between spectra, though overall match was generally insensitive to the choice of SSA. Atmospheric ozone was set at 300 Dobson Units, consistent with local climatology, remote orbital observations, and in situ data. Figure 3.2 shows the agreement between radiances. A slight departure at wavelengths shorter than 500 nm could be related to uncertainties in atmospheric parameters (including aerosol optical properties and ozone), or calibration of either in situ or remote instruments. The match across atmospheric features including deep water absorption features was generally good, consistent with an instrument providing science quality calibrated data.

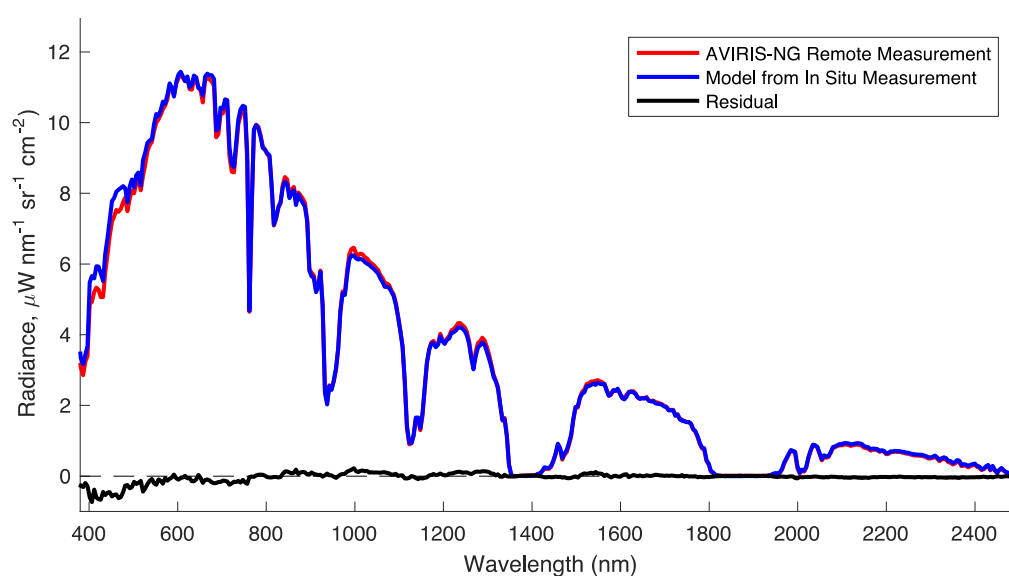


Figure 3.2. Comparison of in-situ and remote reflectance measurements

### 3. Outcome

The comparison led the NASA team to conclude that the quality of AVIRIS-NG data at the Desalpar site was science quality and that the instrument was well-calibrated. There was (as always) potential to improve the agreement further, refining the calibration and atmospheric correction in later versions of the data products. Despite the comprehensiveness and high quality of the dataset provided by ISRO investigators, such refinements would lie within uncertainties in atmospheric knowledge. Consequently, a rigorous treatment of these uncertainties might be needed to appropriately attribute error and help achieve to the next level of precision.

The match between remote and in situ spectra is good relative to other experiments in the literature. It was encouraging that atmospheric correction performed well despite some aerosol loading. Regardless, investigators should be careful when analyzing other data from particularly hazy conditions – particularly in the presence of a “wet” atmosphere – where scattering and absorption coupling could impact results in ways not revealed by these tests. Regardless, the Desalpar experiment was a positive step toward validating the AVIRIS-NG data and laying a foundation for further improvements in the future. It also demonstrated the ability of NASA and ISRO investigators to perform meaningful experiments together leveraging the diverse expertise and resources of both communities.

### **Acknowledgements**

Portion of this research was carried out at the Jet Propulsion Laboratory, California Institute of Technology. The AVIRIS-NG instrument is funded by the NASA Earth Sciences Division. US Government Support is acknowledged. Copyright 2017; All Rights Reserved.

### **References**

Berk, A., Conforti, P., Kennett, R., Perkins, T., Hawes, F. and van den Bosch, J. (2014). MODTRAN6: a major upgrade of the MODTRAN radiative transfer code. In SPIE Defense+ Security (pp. 90880H-90880H). International Society for Optics and Photonics.

Thompson, D. R., B. C. Gao, R. O. Green, P. E. Dennison, D. A. Roberts and S. Lundeen (2015). Atmospheric Correction for Global Mapping Spectroscopy: Advances for the HypsIRI Preparatory Campaign. *Remote Sensing of Environment*, 167, 64–77, 2015. ISSN 0034-4257,

Thompson, D. R., J. W. Boardman, M. L. Eastwood, R. O. Green, J. M. Haag and B. Van Gorp (2017). “Imaging Spectrometer Stray Spectral Response: In-Flight Characterization, Correction, and Validation.” Manuscript in review.



**Parameter Retrieval and  
Technique Development**

## Summary

The AVIRIS-NG airborne campaign has provided an excellent opportunity to carry out atmospheric applications using shortwave hyperspectral observations. In this theme, the main areas of focus are the retrieval of atmospheric constituents such as water vapour (WV), Greenhouse (GHG) and trace gases, air pollutants, aerosol etc. and the characterization of clouds at the micro-scale. Moreover, it also deals with atmospheric correction (ATCORR) schemes developed for land surface and turbid / inland water bodies to convert top-of-atmosphere (TOA) radiance (L1) data into surface reflectance (L2) data. Some of the parameters such as WV and aerosol optical depth (AOD) are, in particular, crucial for atmospheric correction to generate surface reflectance product. The hyperspectral and high spatial resolution of the AVIRIS-NG data are used for characterization and quantification of major air pollutant such as AOD. Detection and retrieval of GHG such as atmospheric CO<sub>2</sub> and mapping of plume density and dispersion from a point source has also been demonstrated in synchronization with *in-situ* measurements. Atmospheric columnar methane (CH<sub>4</sub>) has been quantified using CH<sub>4</sub> absorbing channel and non-absorbing channels to compute atmospheric transmittance spectrum using line-by-line radiative transfer algorithm and validated with *in-situ* measurements. Cloud studies focusing on the micro-physical parameters is yet another interesting application of AVIRIS-NG data. A RT simulated spectral library of clouds has been developed particularly for this mission to retrieve cloud microphysical parameters such as optical depth, effective radius using spectral matching techniques.

A software 'Specsoft' has been developed which provides a platform for user to easily create and visualize the spectral library as well as analyze hyperspectral images. This currently provides visualization of different species of plants with general information, observational details along with data records from other instruments and bio-physical and chemical parameters, vegetation analysis etc. The hyperspectral 'image analyzer' module enables user to display hyperspectral images along with other facilities such as index calculation, wrapper based classification methods, etc. There are some wavelength zones in vegetation spectra where multiple absorption peaks are present. Peaks with low intensities are not prominently visible and remain as hidden due to the presence of very dominant pigment absorption. These cumulative absorption peaks are decomposed into number of possible peaks associated with certain pigments or biochemical constituents. The collected pure spectra of 19 tree species of Shimoga forest region, Karnataka were analyzed and species-wise absorption peaks (Gaussian) with central wavelength, peak amplitude and dispersion are used as the endmember for classification. An automated end-to-end processor has been developed for decomposition of absorption peaks into associated hidden peaks using least square minimum error approach applied over continuum removed normalized spectral data.

# Retrieval of atmospheric parameters required for atmospheric correction of AVIRIS-NG L1 data

Manoj K Mishra

MHTD/GHCAG/EP  
Space Applications Centre, ISRO, Ahmedabad, Gujarat, India

## 1. Scientific rationale and Objectives

AVIRIS-NG provides measurement in the wavelength range from 0.38  $\mu\text{m}$  to 2.5  $\mu\text{m}$  with  $\sim 5\text{nm}$  sampling and with 3.0 to 4.0 m spatial sampling. AVIRIS-NG and other hyperspectral imaging sensors acquire data in many contiguous spectral channels such that for each pixel a complete reflectance spectrum can be derived from the wavelength region covered. The solar radiation incident on the surface and scattered from the surface to sensor is subject to absorption and scattering by the atmosphere. Almost half of the 0.4-2.5  $\mu\text{m}$  spectral region is affected by atmospheric gas absorptions and the shorter wavelength region below 1  $\mu\text{m}$  is significantly affected by molecular and aerosol scattering. There is now growing interest in hyperspectral remote sensing for research and applications in a variety of fields, including geology, agriculture, forestry, coastal and inland water studies, environment hazards assessment, and urban studies. In order to study surface properties using AVIRIS-NG data, accurate removal of atmospheric effects is first requirement. In this report algorithm for retrieval of, (a) aerosol optical depth, (b) water vapour, and (c) spectral smoothing, is described. Finally, the effect of atmospheric correction on reflectance spectrum is discussed.

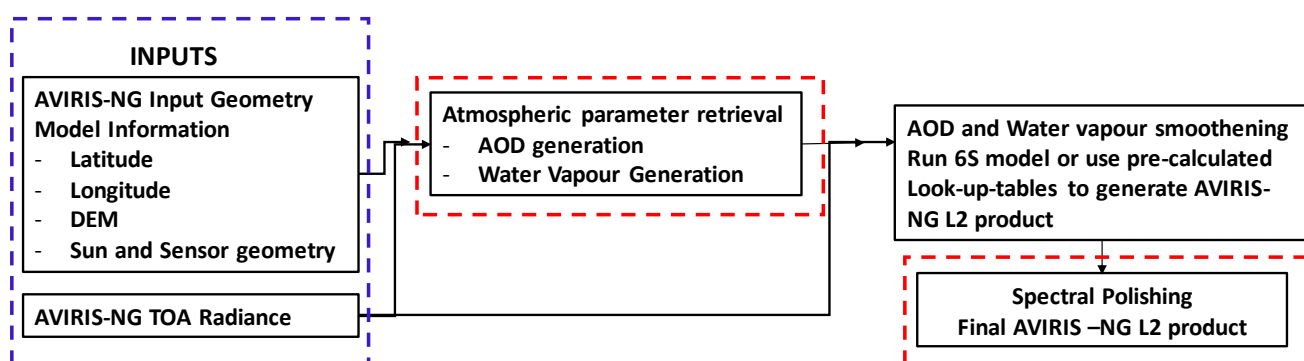


Figure 4.1. Block diagram for atmospheric correction of AVIRIS-NG data to generate L2 data.

## **2. Study area and data used**

The AVIRIS-NG L1 data acquired over India in regions namely Muddur, Ambaji and Bhukia on dates January 10, February 2, and February 3, 2016, respectively, is used in the present work. AVIRIS L1 data consists of at-sensor radiance in 425-432 spectral channels, sun-sensor geometry, elevation and geo-location data.

## **3. Methodology**

**Aerosol optical depth (AOD) retrieval:** AOD retrieval algorithm relies on the correlation between the surface reflectance in the visible and shortwave-infrared ( $2.1 \mu\text{m}$ ) spectral domains. For retrieval of AOD at visible wavelength around  $0.55 \mu\text{m}$  from AVIRIS-NG data, the assumption made are: (a) Aerosols are transparent in the  $2.12 \mu\text{m}$  channel, (b) The surface reflectance in the visible channels  $0.47$  or  $0.66 \mu\text{m}$  is a function of the surface reflectance at  $2.1 \mu\text{m}$ , the scattering angle and the “greenness” of the surface in the SWIR spectrum (NDVI based on  $1.24$  and  $2.1 \mu\text{m}$ ). The at-sensor reflectance at  $0.47$ ,  $0.65$ ,  $1.24$  and  $2.1 \mu\text{m}$  will be used for retrieval of AOD at  $0.55 \mu\text{m}$  based on look-up table (LUT) approach, i.e., radiative transfer calculations are pre-computed for a set of aerosol and surface parameters and compared with the observed radiation field. Spectral reflectance from the LUT is compared with sensor measurements to find the best match. This best fit is the solution to the inversion. Stepwise AOD retrieval is shown in figure 4.2 (a).

**Water Vapor retrieval:** Water vapour retrieval is performed by using CIBR (Continuum Interpolated Band Ratio) method. The assumptions made in CIBR method are: (i) the atmospheric transmittance at  $0.94 \mu\text{m}$  and  $1.14 \mu\text{m}$  water vapour band is highly sensitive to the column water vapour amount (figure 4.2(b)), and (ii) the surface reflectance commonly varies linearly with wavelength in two water vapour bands. The ratio of apparent reflectance in  $0.94$  ( $1.14$ )  $\mu\text{m}$  with respect to the weighted average reflectance at two shoulder channels gives pseudo water vapour transmittance, which is then matched with modeled transmittance for different values of water vapour. The best match obtained by interpolation gives the water vapour amount for the particular pixel.

**Spectral polishing:** Due to high variability in water vapour and AOD with altitude, it is not possible to remove completely the effect of scattering and absorption in atmosphere,

therefore, atmospherically corrected spectrum contains frequent spikes. In general, any smoothing method like moving-window averaging or Savitzky-Golay filtering removes the noise (spikes), but along with that it also removes the fine absorption lines thereby decreasing the information content of the spectra. However, the method used here (Figure 4.2(c)) first identifies the reference soil spectra within the scene from which the spectral polishing factor for each band is computed and then applies the same over whole scene. Since soil spectra are inherently smoother in nature therefore polishing factors computed from these spectra will not affect the fine absorption lines.

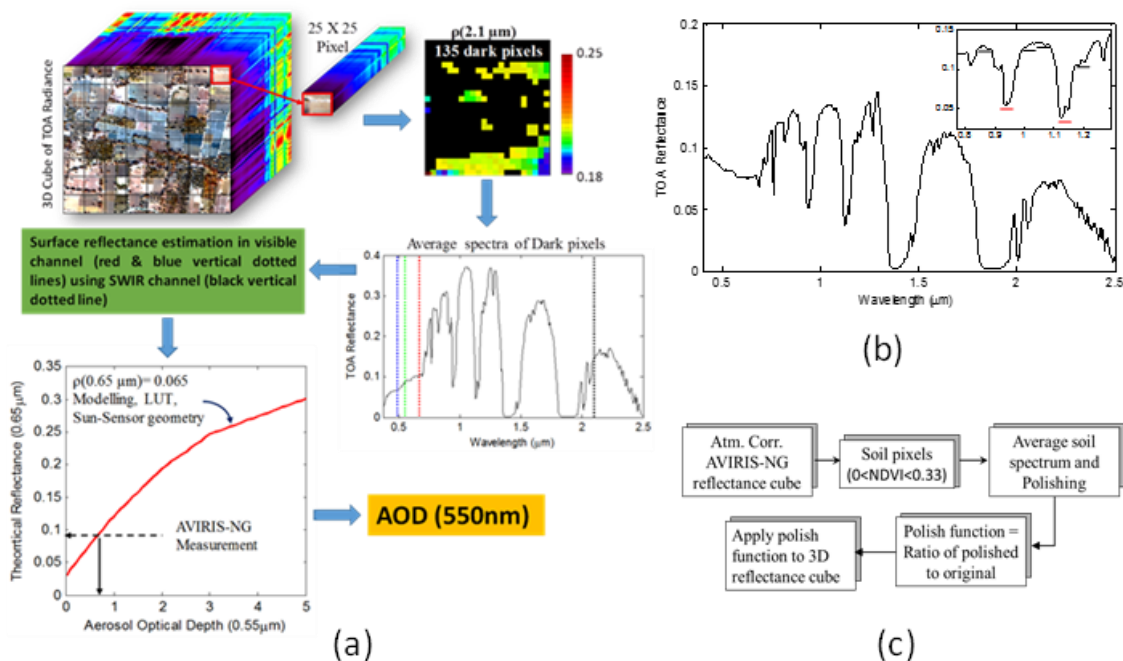


Figure 4.2. (a) Example of AOD retrieval using AVIRIS-NG Hyperspectral cube. (b) Example of an AVIRIS-NG TOA reflectance spectrum. Inset shows the two water vapour absorption band and the shoulder bands used in CIBR method. (c) Flowchart for spectral polishing.

## 4. Outcome

### 4.1 Salient findings

Figure 4.3 (a) and (b) shows the true color, AOD mosaic and normalized histogram of derived AOD over Ambaji and Bhukia regions, respectively. The mean AOD found in the Ambaji region is 0.35. In Ambaji region AOD varies from 0.25 to 0.45, therefore, use of mean AOD value in whole scene for correction can introduce significant error in derived surface reflectance. In Bhukia region mean AOD is around 0.19 and most of the AOD values lies (except for the region

represented by red dotted oval) in the range of 0.1-0.2. Thus most of region shows clear atmospheric condition with an exceptionally high AOD plume in lower part. After investigation it is found that the region represented by red dotted oval encompasses a cement factory (MAHI cement factory) which is responsible for continuous suspension of fine aerosol particles into the atmosphere. Table 4.1 shows the in-situ and derived AOD at 13 locations in Muddur (Karnataka) region. The linear correlation coefficient and root mean square error is equal to 0.71 and 0.024, respectively. From figure 4.4 (a) it is clear that the water vapour derived by us and JPL shows good agreement with linear correlation coefficient equal to 0.96-0.98 and RMSE of around 0.028. Figure 4.4 (b) shows that spectral polishing algorithm is capable of removing the frequent spikes from the surface reflectance spectra without affecting the absorption lines. Figure 4.4 (c) shows comparison between sensor level reflectance and derived surface reflectance spectrum.

#### **4.2 Linkage to societal benefits**

The AOD maps derived from high spatial resolution data (e.g., AVIRIS-NG data) can be used to identify sources and hot spots of air pollution. Such information can play important role in mitigation of air pollution. Per pixel aerosol correction is first requirement to derive surface reflectance with accuracy required in variety of fields such as precise mapping, agriculture and change detection of Earth's surface.

### **5. Conclusions**

- Method for deriving critical atmospheric parameters for atmospheric correction of AVIRIS-NG L1 data are described.
- Derived AOD shows good correlation with in-situ AOD measurements.
- AOD retrieval software described here is operational in DP chain to generate AVIRIS-NG L2 product.

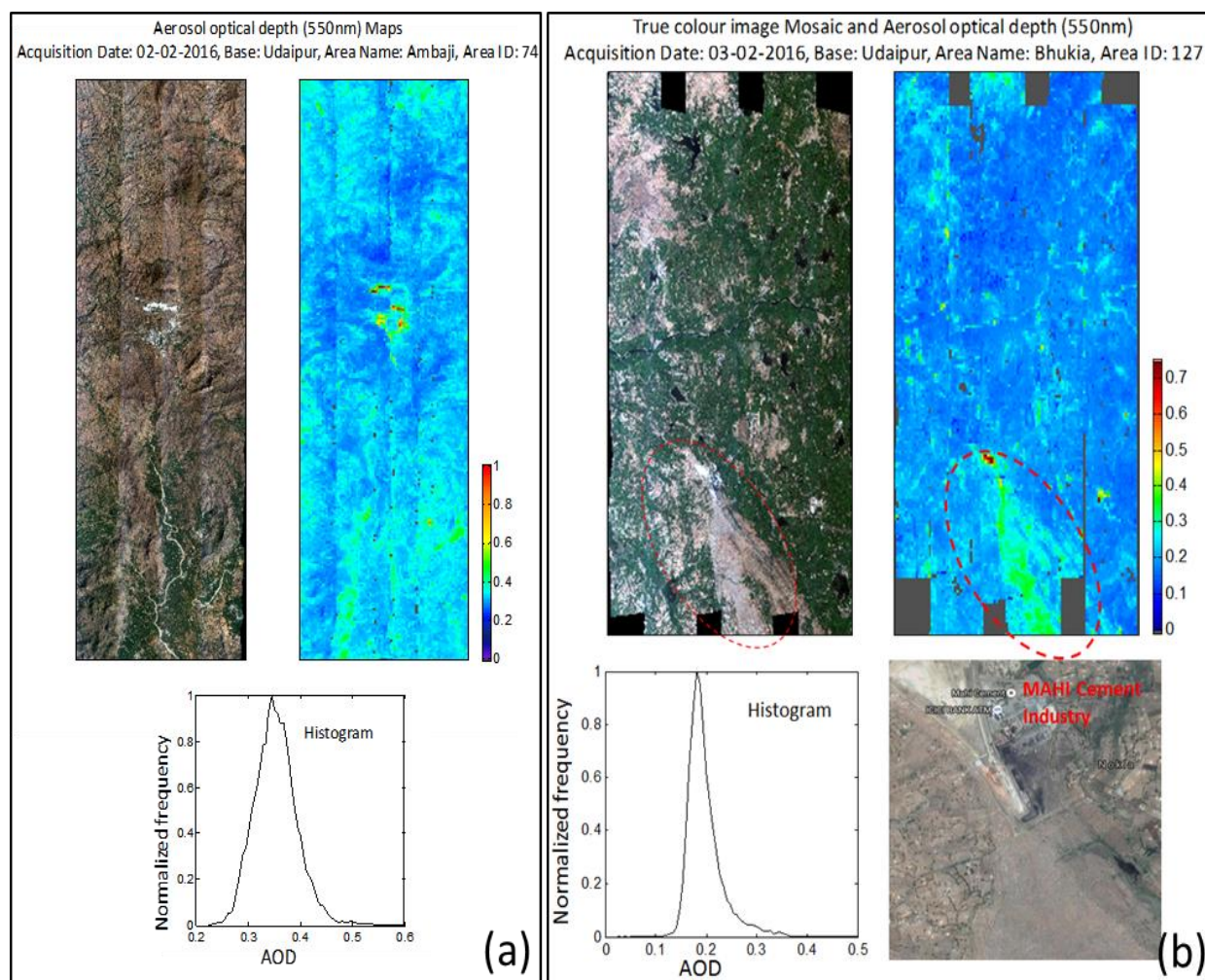


Figure 4.3. True colour image, AOD map and histogram for Ambaji (a) and Bhukia (b), region.

Table 4.1. Shows the in-situ (Sun-photometer) and retrieved AOD values in region covered by AVIRIS data over Muddur (Karnataka) on 10-01-2016.

Station Number	Latitude (N)	Longitude (E)	AVIRIS AOD 550nm	Sun photometer AOD 550nm	Angstrom Exponent
1	11.762	76.578	0.27	0.282	1.07
2	11.761	76.586	0.24	0.314	1.08
3	11.761	76.586	0.26	0.316	1.10
4	11.756	76.605	0.31	0.369	1.03
5	11.778	76.627	0.29	0.360	1.03
6	11.796	76.63	0.30	0.365	1.07
7	11.793	76.643	0.36	0.366	1.06
8	11.858	76.666	0.30	0.316	1.09
9	11.884	76.66	0.29	0.329	1.06
10	11.944	76.652	0.29	0.286	1.13
11	11.966	76.666	0.26	0.308	1.09
12	11.774	76.568	0.32	0.390	1.11
13	11.761	76.586	0.33	0.410	1.08

Root mean square error = 0.024

Linear correlation coefficient=0.71

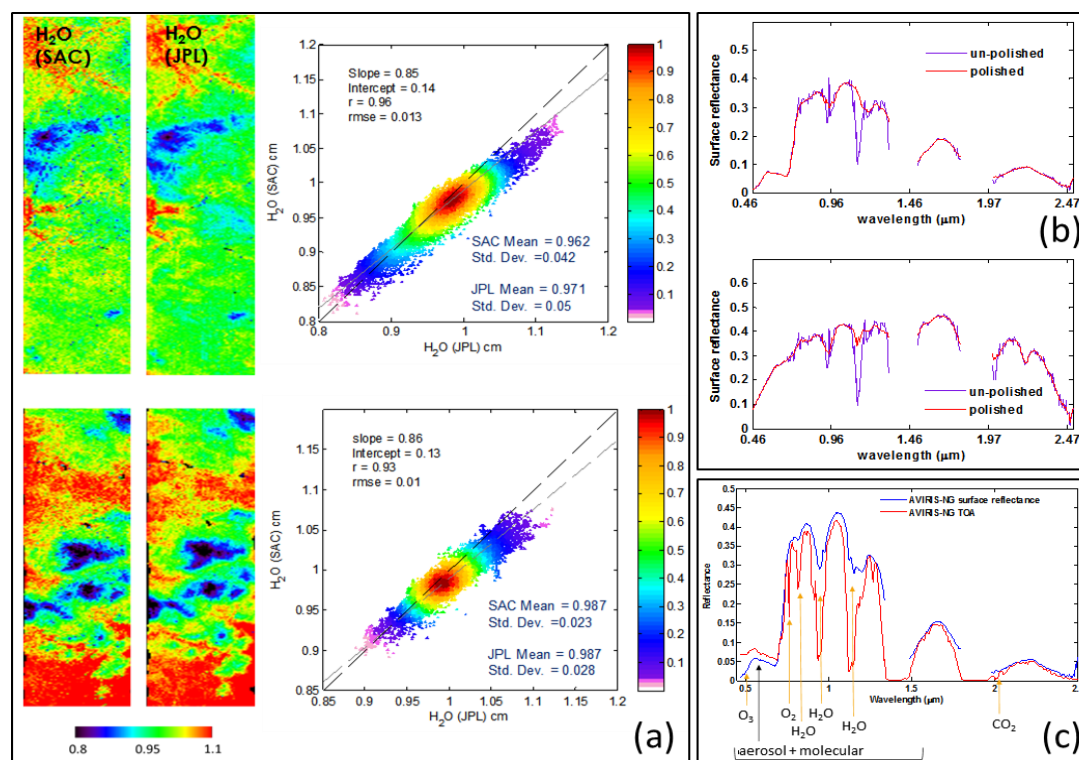


Figure 4.4. (a) Shows water vapour map derived by SAC and JPL, with scatter plots over Ambaji region. (b) Effect of spectral polishing on L2 spectra. (c) Comparison between sensor level apparent reflectance (TOA) and derived surface reflectance.

## Acknowledgements

We are very thankful to the Head, MHTD, Arundhati Misra and the Director, SAC, Shri Tapan Misra for his keen interest and for providing strong motivation to do this work. We are also thankful to B.K. Bhattacharya and Rahul Nigam for providing in-situ surface reflectance and AOD data.

# Retrieval of integrated water vapor from AVIRIS-NG using two band ratio techniques

Bipasha Paul Shukla and Jinya John

Atmospheric Science Division, Space Applications Centre (ISRO)

## ***1. Scientific rationale and Objectives***

Water vapor is one of the important constituents of Earth's atmosphere covering about 4% of the total atmospheric gases and plays an important role in the hydrological cycle and is also a major driving force for the weather and climate system of the Earth. The estimation of water vapor is possible due to the presence of several absorption bands in the near infrared portion of the electromagnetic spectrum. In this regard, the aircraft campaign AVIRIS-NG over Indian region provides us an excellent opportunity to compare and fine tune different algorithms for integrated water vapour retrieval. The main objectives of the study are:

1. To retrieve integrated water vapour using band ratio technique
2. To compare different techniques and fine tune models as a preparatory for integrated water vapour retrieval for GISAT mission.

## ***2. Study area and data used***

**Sites:** Indian region (Ahmedabad, Howrah, Hyderabad and Cochin)

AVIRIS-NG (Airborne Visible and Infrared Imaging Spectrometer-Next generation) data is used to derive the precipitable water vapor contents. We have also used upper air sounding data from Wyoming weather web for validating on point to point basis. Wyoming weather web provides the vertical distribution of various atmospheric physical properties.

## ***3. Methodology***

We have considered two band ratioing techniques i.e. CIBR (Continuum Interpolated Band Ratio) and APDA (Atmospheric Pre-Corrected Differential Absorption) to determine precipitable water vapor from AVIRIS-NG measurements. CIBR is simply a ratio of the radiances in the measurement channels and reference channels while APDA is an augmented

one including the atmospheric path radiances. The measurement channel includes the 940 nm (m) water vapor absorption band and the reference channels are located outside the water vapor absorption feature centered on 867nm (r1) and 1009 nm (r2). While both the techniques are equally good, APDA is a better one for the determination of water vapor especially over dark targets since it corrects for the atmospheric path radiances.

The figure (figure 5.1) represents the flow chart describing the overall procedure for the retrieval of precipitable water vapor using APDA.

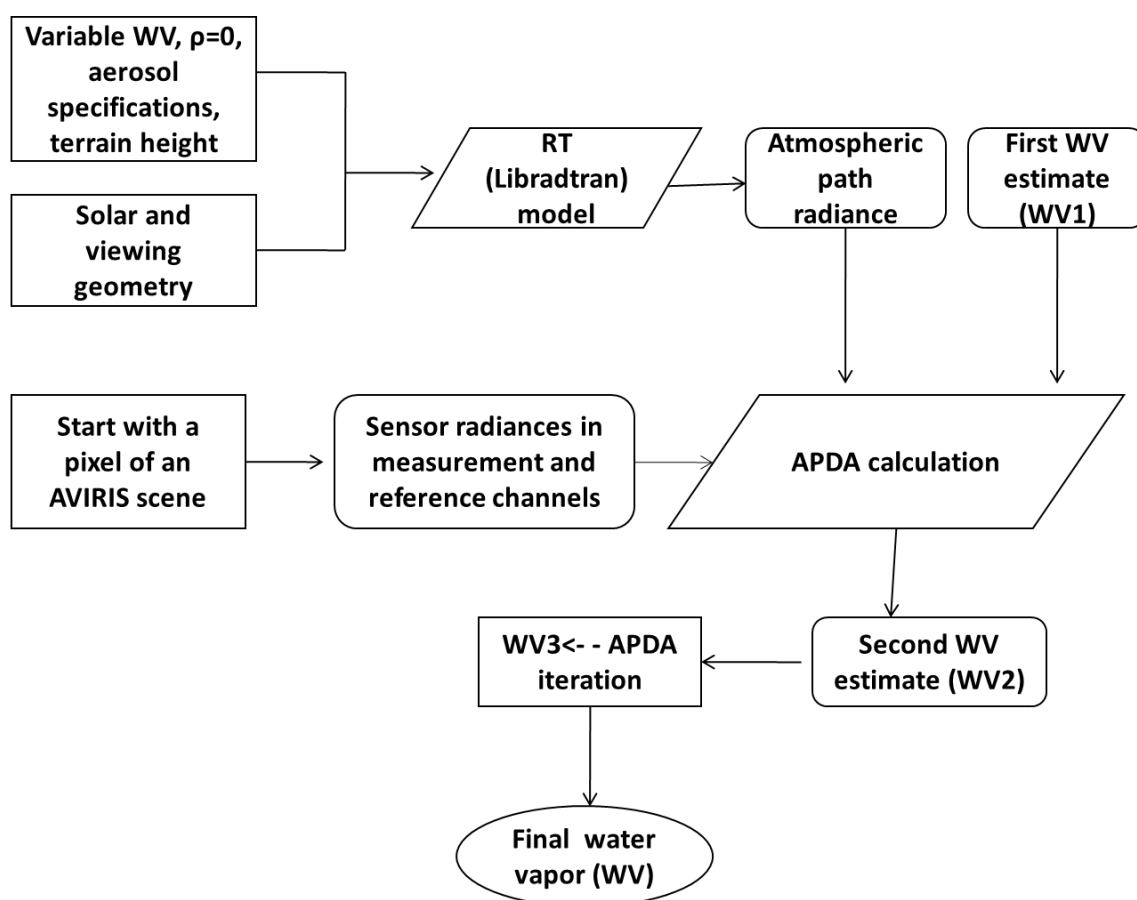


Figure 5.1. Flow chart representing the entire APDA process

#### 4. Outcome

Here we demonstrate the retrieval of water vapor content for two scenes using APDA and CIBR techniques.

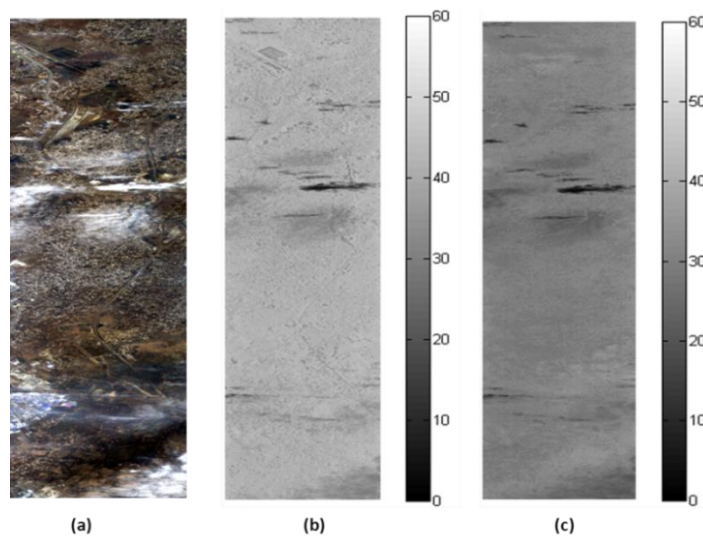


Figure 5.2. (a) RGB image of a scene (Howrah), water vapor retrieved using (b) APDA and (c) CIBR technique

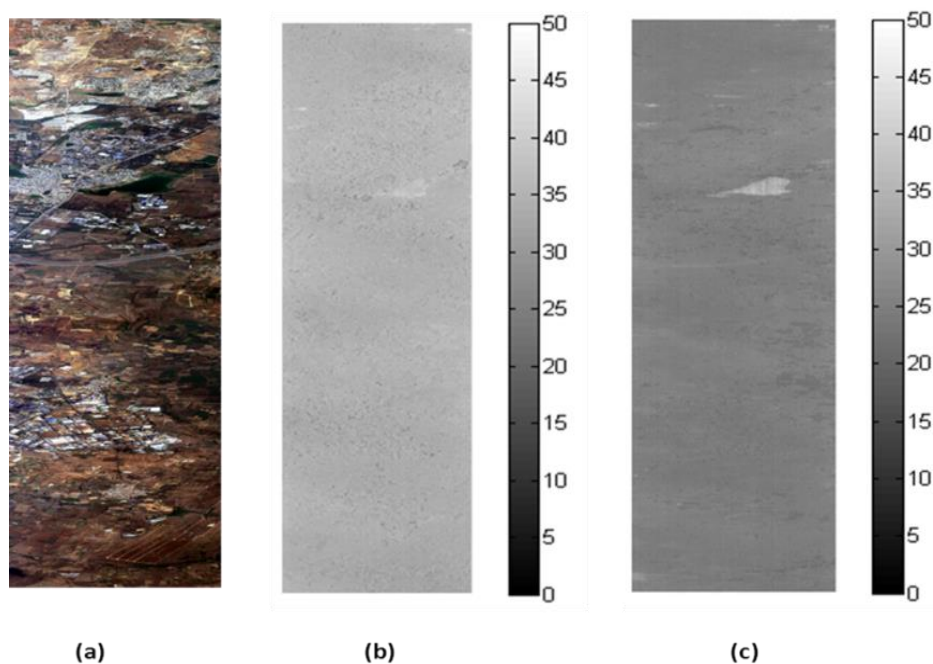


Figure 5.3. (a) RGB image of a scene (Hyderabad), water vapor retrieved using (b) APDA and (c) CIBR technique

Figure 5.2 depicts the scene for air-campaign over Howrah (ang20151219t081738) on 19 December 2015. Figure 5.2 (a), (b) and (c) represents true colour composite (RGB), APDA PWV and CIBR PWV respectively. It can be observed that the derived water vapor values are higher for APDA as compared to CIBR. Similarly, Figure 5.3 describes the scene over Ahmedabad (ang20160227t063144) on 27 February, 2016.

The integrated water vapor is determined using both the techniques and compared to in-situ Wyoming measurements on point-to-point basis. The figures represent the scatter diagram of water vapor retrieved using Wyoming and APDA (Figure 5.4 (a)) and CIBR (Figure 5.4(b)).

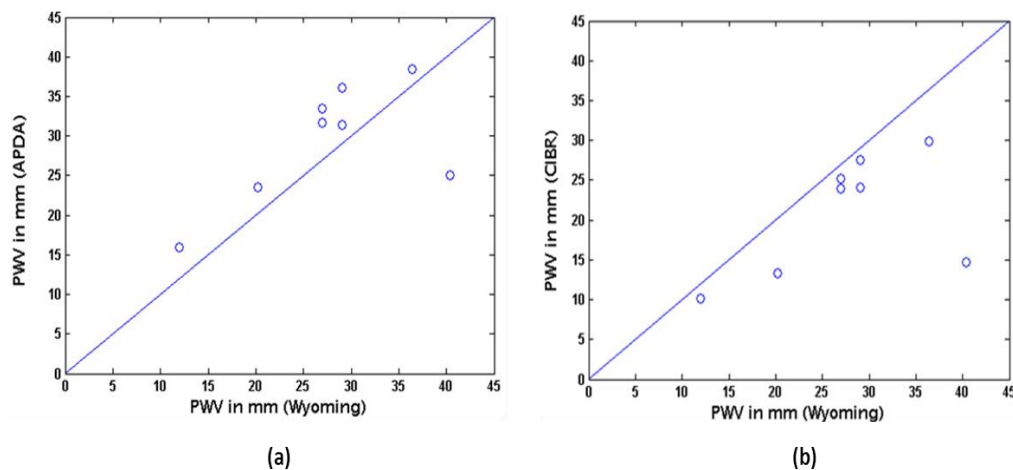


Figure 5.4. Scatter diagram of WV retrieval using Wyoming and APDA (a) and CIBR (b)

#### 4.1 Salient findings

We find that both the algorithms i.e. CIBR and APDA perform equally well. This is not surprising, since CIBR for high reflectance targets approaches the transmission estimate for APDA. It is found that there is underestimation of water vapor retrieved through CIBR technique as compared to APDA technique which is quite expected due to the atmospheric correction included in the latter. The mean percentage error for sites within 3 km radius of Wyoming measurements is 14.72% and 16.52% for CIBR and APDA respectively.

#### 4.2 Target vs. Achievement

As planned, water vapour retrieval techniques were successfully implemented on AVIRIS-NG scenes. The module for water vapour estimation was also integrated with the software for atmospheric correction. Some fine tuning will be carried out with the availability of data for diverse humidity conditions.

#### 4.3 Linkage to societal benefits

Since the concentration of water vapor at any specific location determines the weather at that place, the determination of water vapor from high resolution measurements would be

very important. The methodology developed here, will also be very useful for water vapor retrieval for upcoming GISAT mission.

## **5. Conclusions**

- We find that in the present campaign which was carried during winter-spring season, both band ratio techniques perform equally well.
- However, with different humidity conditions, the experiments may yield different result. It would be interesting to process the data for campaign during summer-rainy season.

## **Acknowledgements**

The authors are extremely grateful to Director, Space Applications Centre, Shree Tapan Mishra for his encouragement and motivation. The authors are sincerely thankful to Dr. Rajkumar, Dr. C. M. Kishtawal and R. M. Gairola for their guidance. The authors especially express their sincere gratitude to Dr. Bimal K. Bhattacharya and Dr. Shailendra Srivastava for providing valuable suggestions and help for the study, and the entire AVIRIS-NG campaign team for their support.

## **References**

<https://aviris-ng.jpl.nasa.gov>

Schlapfer D., Christoph C. B., Keller J. and Klaus I. I., 1998, Atmospheric Precorrected Differential Absorption Technique to retrieve columnar water vapor, *Remote. Sens. Environ.* 65,353-366.

## Air quality study using AVIRIS-NG and ground data

Abha Chhabra<sup>1</sup>, Mehul Pandya<sup>1</sup>, Prakash Chauhan<sup>1</sup>, Rekha Kashyap<sup>2</sup>, K.V. George<sup>3</sup>

<sup>1</sup>BPSG/EPISA, Space Applications Centre, ISRO, Ahmedabad, Gujarat, India

<sup>2</sup>National Institute of Occupational Health, ICMR, Ahmedabad Gujarat, India

<sup>3</sup>National Environmental Engineering Research Institute, CSIR, Nagpur, Maharashtra, India

### **1. Scientific rationale and Objectives**

During the recent period, air quality has become a subject of great research interest owing to its serious impacts on climate, human health, hydrological cycle, radiation budget etc. Besides CO<sub>2</sub>, CH<sub>4</sub> and N<sub>2</sub>O are also potent “Green House Gases” (GHGs). Consequently, one of the major challenges is to assess and quantify the impact of pollutants on the air quality from local to global scales (IPCC, 2013). Hyperspectral remote sensing can be used for direct and indirect identification or detection of atmospheric trace/green-house gases, measurement of their relative concentrations, derivation of their spatial distribution (e.g. mapping), and their evolution over time (Tuominen and Lipping, 2011). Ground in-situ observations are essential for proper reflection of the actual air quality and understanding pollution dispersion as well as validation of remote sensing derived information.

NASA’s JPL Next Generation ‘Airborne Visible/Infrared Imaging Spectrometer’ (AVIRIS-NG) is one of the most advanced hyperspectral instruments capable of taking observations over a continuous electromagnetic spectrum spread over 380-2510 nm at 5 nm band interval. Spinetti et al., 2008, Dennison et al., 2013, Thompson et al., 2015 have demonstrated the potential of airborne imaging spectroscopy using AVIRIS-NG high spatial resolution mapping of elevated atmospheric CO<sub>2</sub> and CH<sub>4</sub> concentrations from volcanic plumes, power plant plumes or anthropogenic sources like oil and natural gas infrastructure. However, such studies are not available in Indian context.

The present research study was undertaken as an opportunity under the first ever ISRO-JPL-AVIRIS-NG airborne mission in India conducted during November 2015-March 2016. The main objectives of the study included:

- Field experiments involving in-situ measurements of gaseous and particulate matter air pollutants, AOD, Water Vapour and Surface Reflectance at selected study sites.
- Exploring the potential of AVIRIS-NG data for detection and quantification of major GHGs and other air pollutants and validation with in-situ observations.

## 2. Study area and data used

The study was carried out for two sites- Kota city, Rajasthan (Site Id 94) and Ahmedabad city, Gujarat (Site Id 69). Data used are listed in table 6.1.

Table 6.1. Data used in the study

<b>Data used</b>	<b>Measurements/ Observations</b>
Field Data	Air Pollutants Dust, Particulate Matter (size range 0.25 $\mu$ -32 $\mu$ m), Black Carbon, CO, CO <sub>2</sub> CH <sub>4</sub> , O <sub>3</sub> , SO <sub>2</sub> , NO <sub>2</sub> , NH <sub>3</sub> , Volatile Organic Compounds (VOCs), Poly Aromatic Hydrocarbons (PAHs).
	Remote Sensing measurements Location Lat/long coordinates, Reflectance spectra of various targets, Aerosol Optical Depth (AOD), Columnar water vapour(WV), and Columnar Ozone content
Hyperspectral Data	AVIRIS-NG L1 data
Ancillary Data	Point Source Inventory Data Point source inventory data of Kota Super Thermal Power Station, DCM IndustrialComplex at Kota
	Human Health Data* Secondary data on human respiratory disorders and morbidities due to air pollutants during January-February 2015, 2016 at Kota.

## 3. Methodology

The flow chart of methodology of the study is shown in figure 6.1.

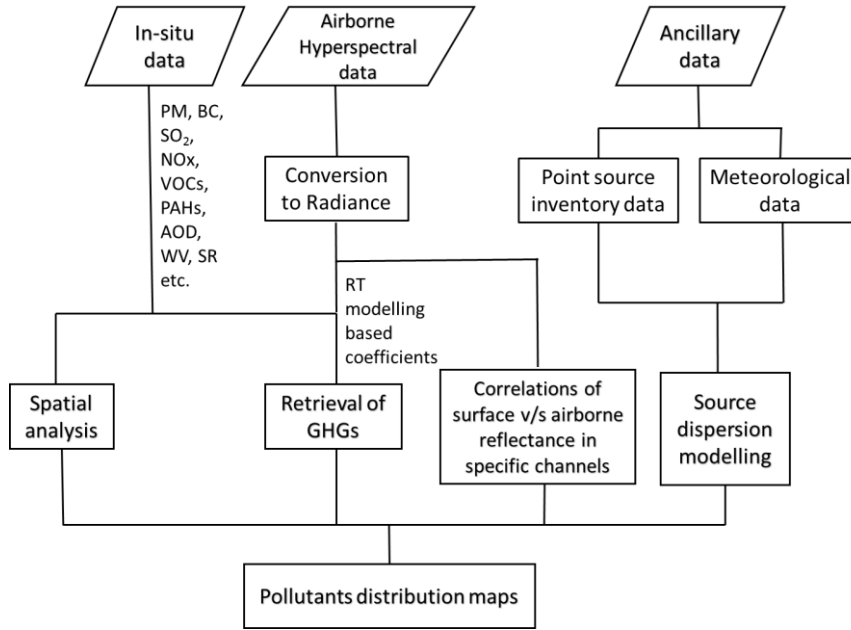


Figure 6.1. Flowchart of the study

## 4. Outcome

### 4.1 Salient findings

- ‘Hotspots’ of high PM<sub>1</sub>, PM<sub>2.5</sub> and PM<sub>10</sub>, Black Carbon pollutants identified (figure 6.2)

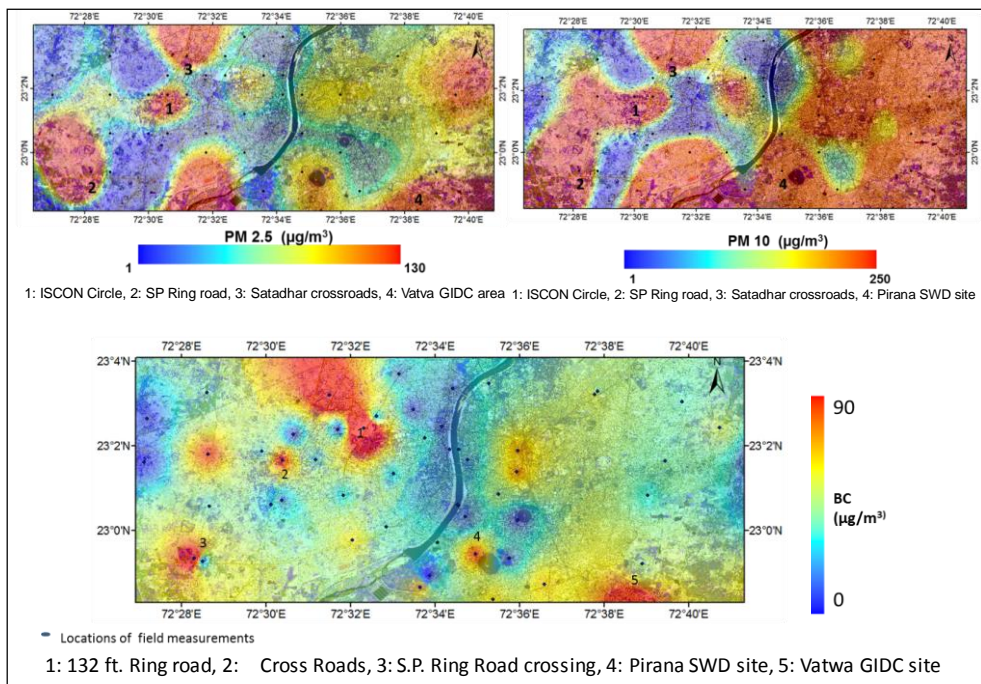


Figure 6.2. Spatial variability in PM<sub>2.5</sub>, PM<sub>10</sub> and Black Carbon distribution at Ahmedabad

- **Detection of Thermal Power Plant Plume and retrieval of CO<sub>2</sub> at Kota using AVIRIS-NG Hyperspectral data**

A method was developed to retrieve atmospheric CO<sub>2</sub> concentration from Kota Super Thermal Power Station (KSTPS) using MODTRAN Radiative Transfer simulations and AVIRIS-NG L1 radiance data of February 4, 2016 over Kota. In-situ observations of AOD and WV were used to generate site-specific coefficients and a Continuum Interpolated Band Ratio (CIBR) algorithm was used for CO<sub>2</sub> retrieval. Power plant plume density and dispersal could also be mapped using AVIRIS-NG data. The results are shown in figure 6.3 (a).

- **CO<sub>2</sub> distribution map of Ahmedabad using AVIRIS-NG Hyperspectral data and validation with in-situ observations**

CO<sub>2</sub> retrieval was attempted over Ahmedabad site using AVIRIS-NG L1 radiance data of 11 February, 2016 and RT simulation model coefficients. AVIRIS-NG derived XCO<sub>2</sub> retrievals were validated against surface ambient CO<sub>2</sub> measurements within ±1 hour of aerial flight. The results are shown in figure 6.3 (b).

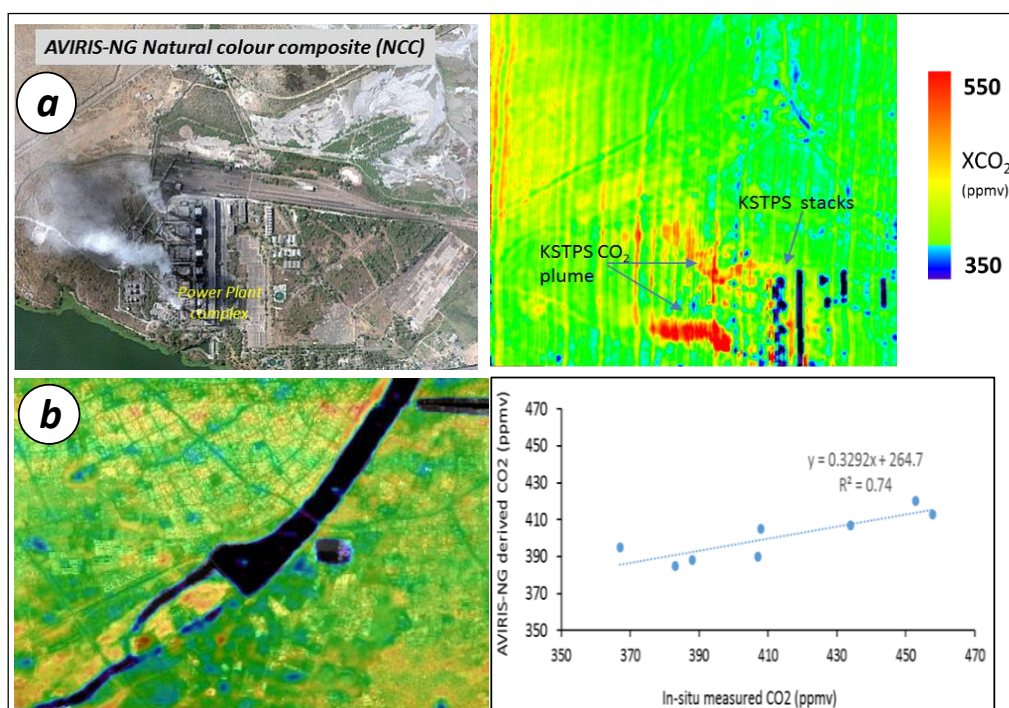


Figure 6.3. (a). CO<sub>2</sub> retrieval over Kota using AVIRIS-NG data, (b). CO<sub>2</sub> retrieval over Ahmedabad using AVIRIS-NG data and validation with in-situ observations (CO<sub>2</sub> retrievals draped over AVIRIS-NG NCC based on data acquired on Feb. 11, 2016)

- **Chemical characterization of VOCs samples collected during ground campaign indicated presence of several human carcinogens.**

## 4.2 Target vs. Achievement

Target	Achievement
In-situ measurements	90% (except CO <sub>2</sub> , CH <sub>4</sub> measurements at Kota)
Retrieval of GHGs using AVIRIS-NG data	CO <sub>2</sub> retrieval (may be improved with variable WV)

## 4.3 Linkage to societal benefits

AVIRIS-NG derived results are being used to correlate with source dispersion model run and ancillary data of human health ailments to study impacts of air pollutants on human health. Direct linkage with human health and society.

## 5. Conclusions

- Detection of CO<sub>2</sub> plume from point source could be demonstrated using AVIRIS-NG high spectral resolution data in SWIR channels (1900-2100 nm).
- In future, for CH<sub>4</sub> retrievals, point source study sites would be useful in 2<sup>nd</sup> phase.
- Higher spectral resolution and range including UV channels are required for detection of SO<sub>2</sub>, NO<sub>x</sub>, CO, VOCs pollutants in ambient air quality.

## Acknowledgements

Sincere thanks to Shri Tapan Misra, Director, SAC for providing an opportunity to participate in first of its kind ISRO-JPL-AVRIS-NG Hyperspectral airborne mission. The encouragement, support and guidance from DD, EPSA, Dr. Bimal Kumar Bhattacharya, Project Science Team Leader and Dr. R. P. Singh Head LHD/EPSA is sincerely acknowledged. The support from SEDA team, JRFs, student /field assistants of collaborating institutes, govt. and industry officials is thankfully acknowledged.

## References

Dennison, P.E., Thorpe, A.K., Pardyjak, E.R., Roberts, D.A., Qi, Y., Green, R.O., Bradley, E.S., Christopher C.F., 2013. High spatial resolution mapping of elevated atmospheric carbon dioxide using airborne imaging spectroscopy: Radiative transfer modeling and power plant plume detection. *Remote Sensing of Environment* 139, pp. 116–129.

IPCC, Climate Change 2013: The Physical Science Basis. Contribution of Working Group I to the Fifth Assessment Report of the Intergovernmental Panel on Climate Change [Stocker, T.F., D. Qin, G.-K. Plattner, M. Tignor, S.K. Allen, J. Boschung, A. Nauels, Y. Xia, V. Bex and P.M. Midgley (eds.)]. Cambridge University Press, Cambridge, United Kingdom and New York, NY, USA, 1535 pp.

Spinetti, C., Carrère, V., Buongiorno, M.F., Sutton, A.J., Elias, T., 2008. Carbon dioxide of Pu`u`O`o volcanic plume at Kilauea retrieved by AVIRIS hyperspectral data. *RSE*, 112, pp. 3192–3199.

Thompson, D.R., Bovensmann, L.H., Eastwood, M., Fladland, M., Frankenberg, C., Gerilowski, K., Green, R.O., Kratwurst, S., Krings, T., Luna, B., Thorpe, A.K., 2015. Real-time remote detection and measurement for airborne imaging spectroscopy: a case study with methane. *Atmos. Meas. Tech.*, 8, 4383–4397, 2015.

Tuominen, J. and Lipping, T., 2011. Detection of environmental change using Hyperspectral Remote Sensing at Olkiluoto Repository Site. Working Report, 2011-26, Tampere University of Technology, 56p.

# Estimation of columnar molecular methane concentration using AVIRIS-NG data

Mahesh P<sup>1</sup>, Biswadip.G<sup>1</sup>, Rao P.V.N.<sup>1,2</sup>, Sreenivas. G<sup>1</sup>,  
Mallikarjun.K<sup>1</sup>, Subin Jose <sup>1,3</sup>, Sesa Sai M.V.R.<sup>1</sup>

<sup>1</sup>Atmospheric Chemistry and Processes Studies Division (AC&PSD),  
Earth and Climate Science Area (ECSA)

<sup>2</sup>Remote Sensing Applications Area (RSAA), National Remote  
Sensing Centre (NRSC)-Hyderabad

<sup>3</sup>Andhra University, Visakhapatnam

## 1. Scientific rationale and Objectives

Atmospheric methane (CH<sub>4</sub>) is a long-lived greenhouse gas, which absorbs long-wave infrared radiation that causes global warming (Bradley et al., 2011). The concentration of CH<sub>4</sub> in the atmosphere has increased by 150% since pre-industrial times, mainly from fossil fuel and secondarily from net land use change emissions (Huang et al., 2015). Although, Kirschke et al. (2013) reported that in India major sources include agricultural and waste constitute, their ratio of contribution to CH<sub>4</sub> is remain uncertain. High spatial columnar measurements can reduce the vertical transport induced variability compared to point data. Thus, remote sensing has been established as a powerful tool in the atmospheric science to address the spatial and temporal variability of greenhouse gases (GHGs).

The total columnar measurements provided by ground-based Fourier Transform InfraRed (Make: FTIR-IFS 125M, Bruker Optik, Germany) spectrometer can be used for the validation of satellite and other airborne measurements (Xiong et al., 2016). Therefore, high spatial and moderate spectral resolution airborne imaging spectrometers namely AVIRIS and AVIRIS-NG are well suited for mapping and quantification of CH<sub>4</sub> source and sink regions in a given LULC. In the present study, we attempted to estimate molecular columnar CH<sub>4</sub> (XCH<sub>4</sub>) concentration from AVIRIS-NG over sub-urban region and compared against ground based FTIR spectrometer.

## 2. Study area and data used

The present study utilized one AVIRIS-NG image data acquired over Shadnagar area covering the Atmospheric Science Laboratory (ASL) of NRSC on 19 December, 2015.

### 3. Methodology

The present study utilized AVIRIS-NG image data acquired over Shadnagar. During the AVIRIS-NG campaign, ground based FTIR spectrometer collected solar spectra in 0.90 to 8.30 $\mu$ m spectral range using Indium antimonide (InSb) detector and Calcium fluoride (CaF<sub>2</sub>) beam splitter with spectral resolution of 0.01cm<sup>-1</sup>. Based on water vapor retrieval technique proposed by Gao et al., 1990, attempts have been made in the present study to retrieve column averaged concentration of CH<sub>4</sub> over Shadnagar in 2.20 to 2.35  $\mu$ m spectral band as shown in figure 7.1.

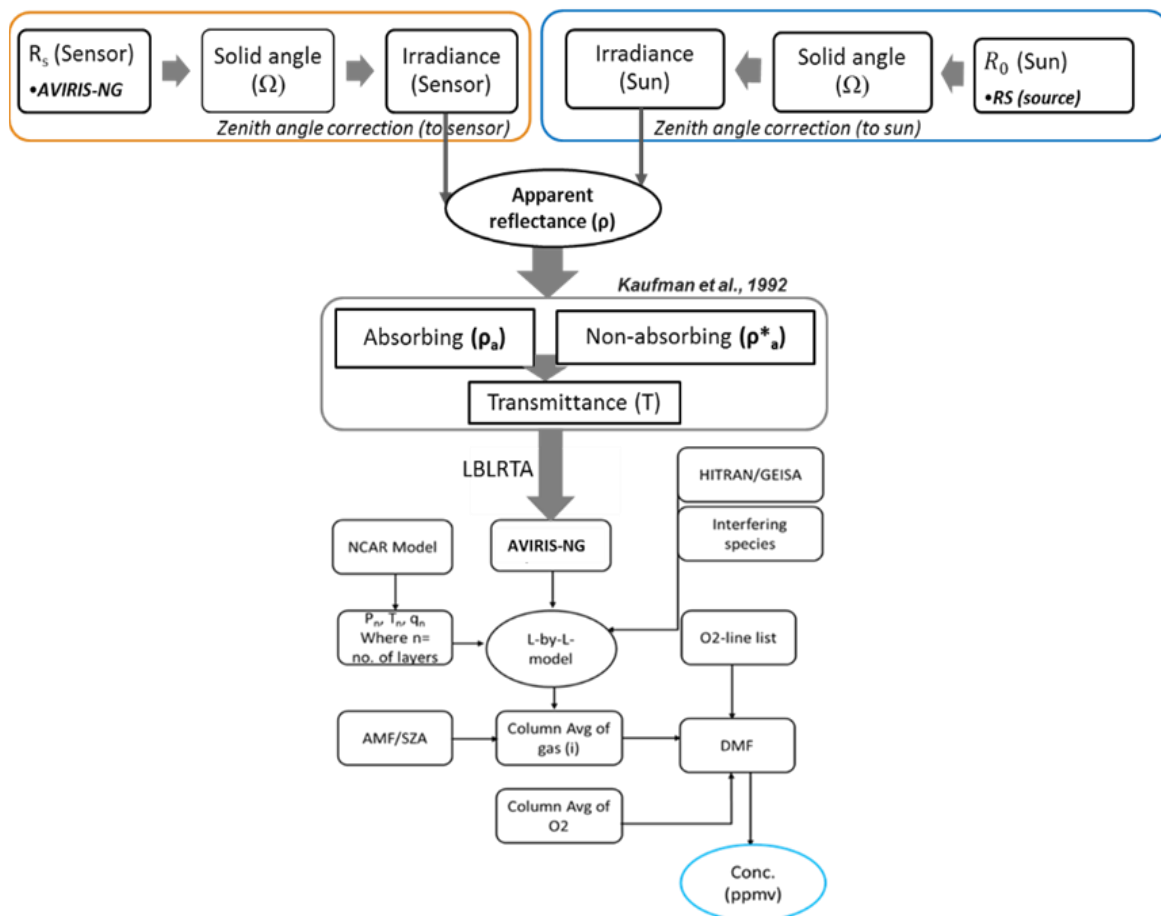


Figure 7.1. Flow chart of columnar methane (XCH<sub>4</sub>) retrieval from AVIRIS-NG radiance

### 4. Outcome

#### 4.1 Salient findings

In this study, we used FASCODE3 radiative transfer model to compare the radiance simulated at the sensor height (5 km) and measured radiance obtained by the AVIRIS-NG sensor.

Though, the spectral resolution of the applied radiative transfer model ( $0.01\text{cm}^{-1}$ ) and AVIRIS-NG sensor (5 nm) are different, comparison shows good agreement. LBLRTA has been implemented to retrieve the molecular column density of methane ( $\text{XCH}_4$ ) from AVIRIS-NG radiance and ground based FTIR spectrometer data over the study site at spectral window of 2.20 to 2.35  $\mu\text{m}$  as shown respectively, in Figure 7.2 (a) and (b). Figure 7.2(a) shows a little to moderate variation with probable source regions of  $\text{CH}_4$  over the agricultural area. Therefore, band ratio technique is proved to be a suitable method to detect relative amount of  $\text{CH}_4$  concentration in the atmosphere from imaging spectrometer. Retrieved  $\text{XCH}_4$  from AVIRIS-NG compared against ground based FTIR spectrometer as shown in figure 7.2 (b), which holds a very good validation to the AVIRIS-NG retrievals. Yellow regions in figure 7.2 (a) represent potential  $\text{CH}_4$  hotspots from paddy fields.

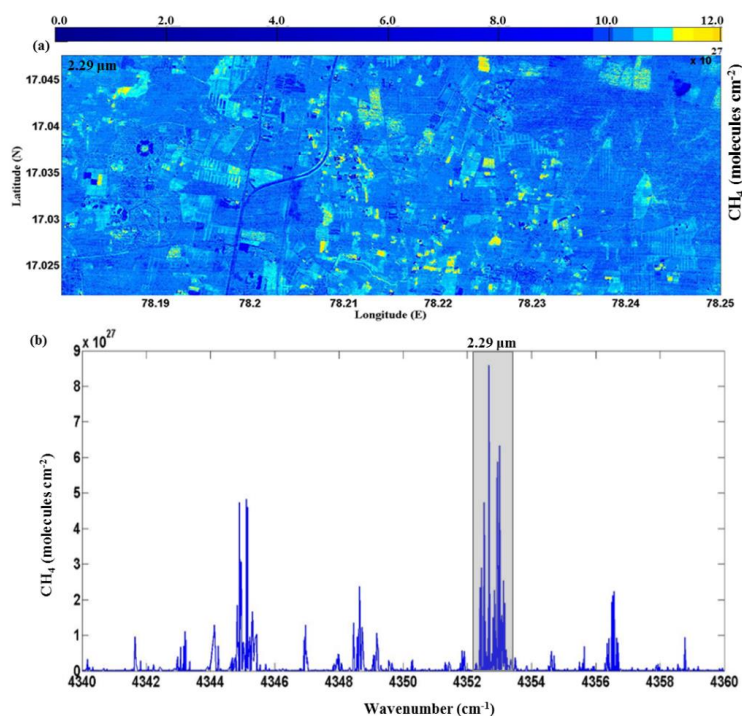


Figure 7.2. Retrieved atmospheric  $\text{CH}_4$  molecular column density map from (a) AVIRIS-NG imaging spectrometer using 3-channels ratio technique, (b) from ground based FTIR spectrometer at 2.29  $\mu\text{m}$  absorption band.

## 4.2 Target vs. Achievement

Target	Achievement
100%	100%

### 4.3 Linkage to societal benefits

- Emission of high CH<sub>4</sub> directly indicates the active phase of agriculture and presence of livestock. This information may also be used as an indicator of the agricultural growth of a given area.
- CH<sub>4</sub> is a greenhouse gas and it contributes to the global warming. Hence, high levels need to be closely monitored and the collected information may be used to manage the emission levels.
- Results from the AVIRIS-NG (XCH<sub>4</sub>) helps to identify the source and sinks of different Land Use Land cover (LULC) system. Thus, one can take policy decisions depending upon their levels at respective LULCs.

## 5. Conclusions

- Detected and validated relative amount of CH<sub>4</sub> concentration retrieved from AVIRIS-NG against ground-based FTIR spectrometer.
- Future campaigns with AVIRIS-NG will enable to identify and detect the change in atmospheric CH<sub>4</sub> concentration over paddy fields.
- With the acquired experience, repeat campaign will provide the opportunity to extend the retrievals of other trace gases like CO<sub>2</sub>, N<sub>2</sub>O etc. besides present retrievals of CH<sub>4</sub>. It also provides the opportunity to validate retrieved trace gases concentration from AVIRIS-NG using present algorithm and comparison against *in-situ* data.
- From the present study, we conclude that AVIRIS-NG has the potentiality to develop atmospheric application apart from its known applications in vegetation and land surface processes.

## Acknowledgements

We acknowledge and thank the AVIRIS-NG team from Jet Propulsion Laboratory (JPL) for their great campaign on collecting the data over Indian region. We also thank Dr. Y.V.N. Krishna Murthy, Director NRSC for his support to do this work.

## References

Bradley, E. S., I. Leifer, D. A. Roberts, P. E. Dennison, and L. Washburn (2011), Detection of marine methane emissions with AVIRIS band ratios, *Geophys. Res. Lett.*, 38, L10702, doi:10.1029/2011GL046729.

Huang, J., Yu, H., Guan, X., Wang, G., and Guo, R.: Accelerated dryland expansion under climate change, *Nature Climate Change*, 6, 166–171, 2015

Kirschke, S., et al.: Three decades of global methane sources and sinks, *Nature Geosci.*, 6, 813–823, 2013

Gao, B. C., & Goetz, A. F. (1990). Column atmospheric water vapor and vegetation liquid water retrievals from airborne imaging spectrometer data. *Journal of Geophysical Research: Atmospheres*, 95(D4), 3549-3564.

Kaufman, Y. J., and Gao, B. C. (1992). Remote sensing of water vapor in the near IR from EOS/MODIS. *IEEE Transactions on Geoscience and Remote Sensing*, 30(5), 871-884.

# Study of Cloud Microphysical Parameters (CMP) using AVIRIS-NG Hyperspectral data

Bipasha Paul Shukla and Jinya John

Atmospheric Science Division,  
Space Applications Centre (ISRO)

## 1. Scientific rationale and Objectives

Clouds are the modulators of earth radiation budget and are also the drivers of the hydrological cycle. The observations of cloud properties, particularly microphysical ones like cloud effective radius (CER), thermodynamic phase, cloud optical thickness (COT) is of extreme importance both for short term weather processes and climate scale studies. High spatial and spectral resolution of AVIRIS-NG provides us an opportunity to observe and study these micro-scale parameters and interactions. The main objectives of the study are:

- To gain an insight to the sensitivity of shortwave hyperspectral observations to cloud microphysical parameters (CMP);
- To develop methodology for retrieval of CMP using AVIRIS-NG observations.

## 2. Study area and data used

The following table gives the details of the data and the sites for which cloudy scenes were identified and are used for retrieving cloud microphysical properties.

<i>S. No.</i>	<i>AVIRIS flight no.</i>	<i>Site name</i>	<i>Site ID</i>
1	ang20160125t083343	Kurnool	116
2	ang20151225t090536	Chilika lagoon	110
3	ang20160128t063030	HuttiMuski	62
4	ang20160110t075851	Muddur	99
5	ang20151225t071437	Chilika	53

### 3. Methodology

The clouds were classified based on the ISCCP cloud classification and nine input datasets were created. Based on this classification, a simulated cloud spectral library for nine different cloud types has been generated using the high resolution radiative transfer model (libRadtran). Thereafter, a spectral matching technique namely the spectral angle mapper (SAM) was used to select the spectrum closest to the AVIRIS-NG cloud spectrum. This cloud spectrum is assigned the cloud microphysical parameters corresponding to the simulated spectrum. The figure 8.1 shows the flow diagram indicating the entire procedure for the determination of cloud microphysical properties.

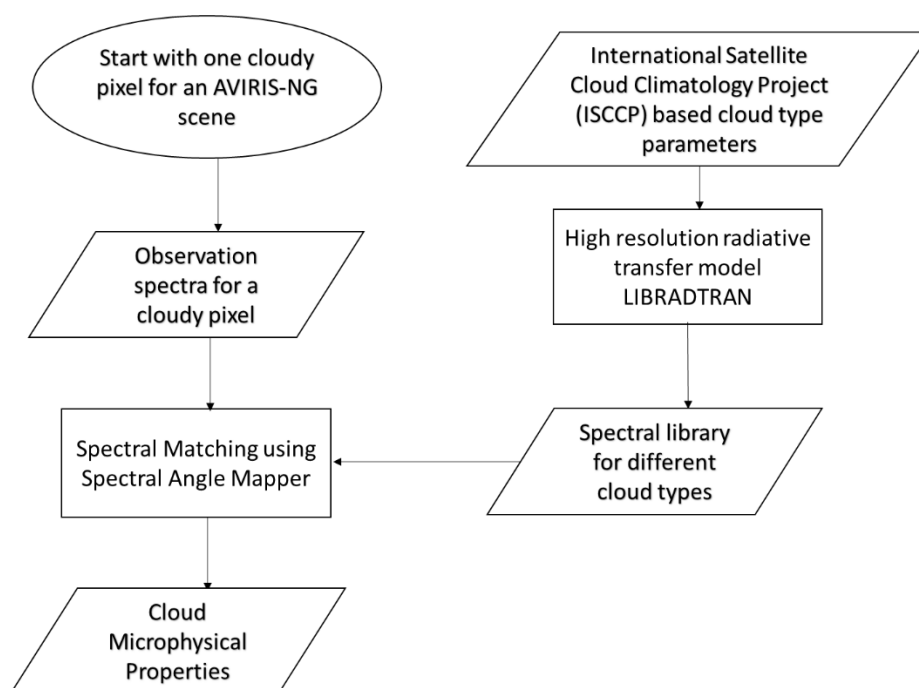


Figure 8.1. Flow chart for the determination of cloud microphysical properties from AVIRIS-NG radiances.

## 4. Outcome

### 4.1 Salient findings

The simulations using libRadtran were carried out for different cloud types. A typical sample spectra for each cloud type is plotted in figure 8.2 (a). A sample observed spectra from AVIRIS-NG cloudy pixel is plotted in figure 8.2 (b) with its closest match from the simulated spectral library. It can be seen that the spectral signatures are closely matching and for this particular

case, the best match was associated with low clouds having medium opacity with a cloud optical depth (COD) of 3.6 and cloud effective radius (CER) of 4 microns.

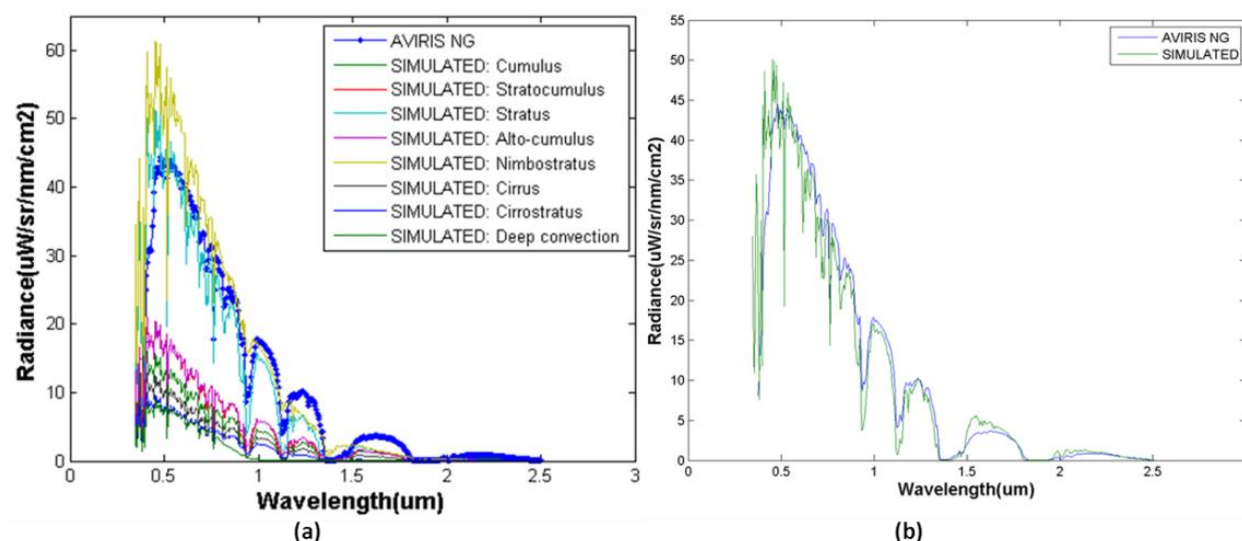


Figure 8.2. (a) Spectra of model simulated and AVIRIS-NG measured radiances for different cloud types and (b) Spectra obtained for the best match of radiances

The same procedure was then extended for full AVIRIS-NG scenes and corresponding CMP maps were generated. The results for 2 sites: Chilika lagoon and Muddur are presented in the following figures (Figure 8.3 & Figure 8.4). It is observed that the clouds are low optically medium clouds with effective radius ranging from 4-18 microns in both the cases.

Also, in Figure 8.5, we have plotted 3D cloud map using cloud optical depth and cloud effective radius for Kurnool region. These 3-D maps are possible due to very high resolution spatial and hyper-spectral measurements and are very useful to pick fast developing cloud cells. In order to validate the retrieval, we have used Moderate Resolution Imaging spectro-radiometer (MODIS) cloud microphysical parameters. Only very few points could be obtained for comparison with AVIRIS cloud parameters. We have compared cloud effective radius of both the sensors and the same is plotted in the scatter diagram (Figure 8.6).

## 4.2 Target vs. Achievement

An end to end retrieval scheme was demonstrated for cloud microphysical parameters from hyperspectral observations. The exercise was the first of its kind in Indian scenario. More advanced inversion techniques are being explored for better accuracy.

### 4.3 Linkage to societal benefits

The determination of cloud microphysical parameters is important to understand the evolution of different types of cloud systems. This would be especially useful during extreme weather events which affect the social life directly. The methodology developed here, will be very useful for cloud property retrieval for upcoming GISAT mission as well.

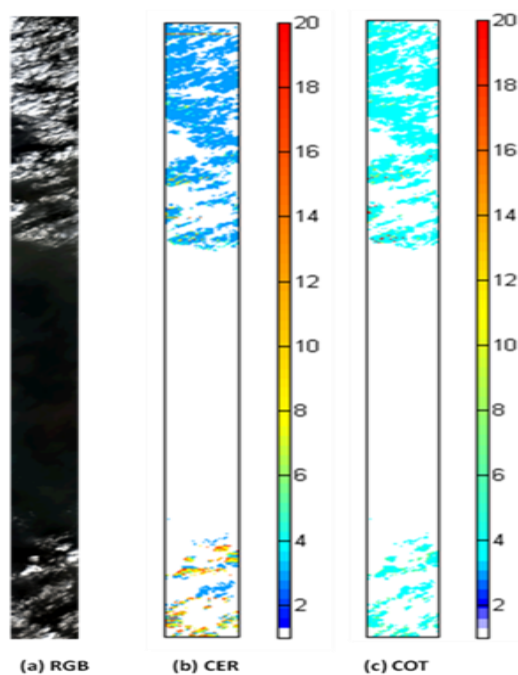


Figure 8.3. (a) RGB image (b) retrieved CER and retrieved COT for (c) retrieved COT for Chilika lagoon

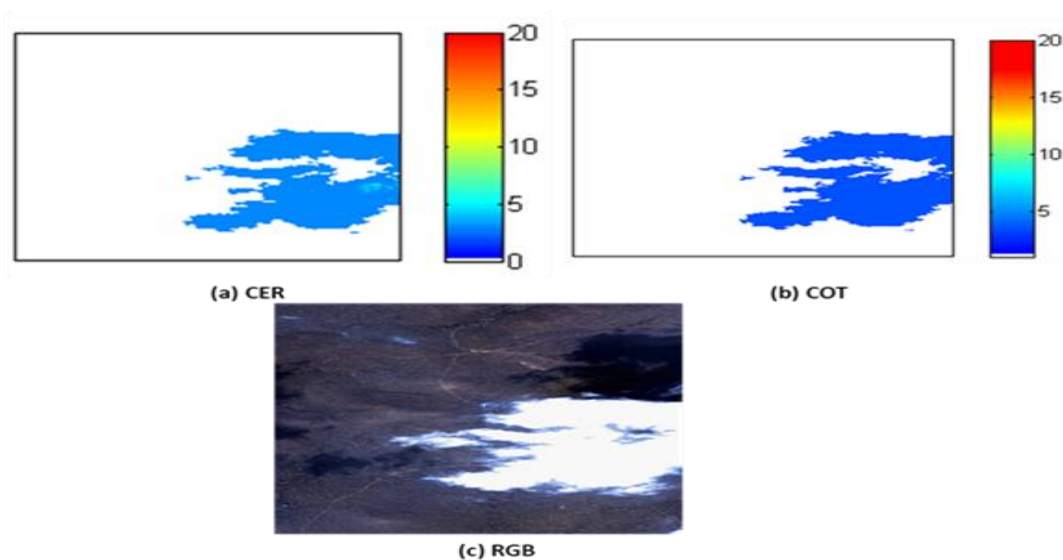


Figure 8.4. (a) RGB image (b) retrieved CER and (c) Muddur

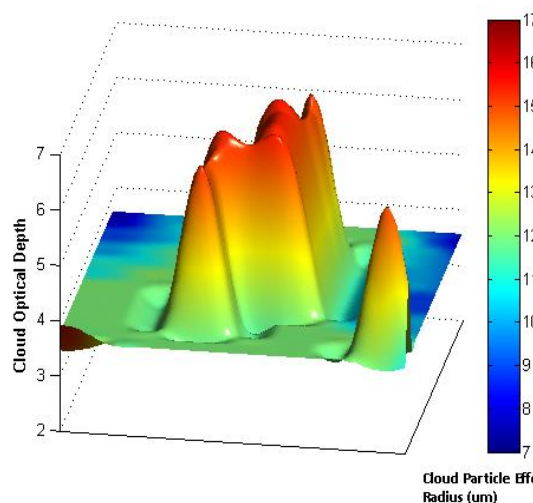


Figure 8.5. 3D Map of cloud microphysical parameters where height represents COD and colors represent CER

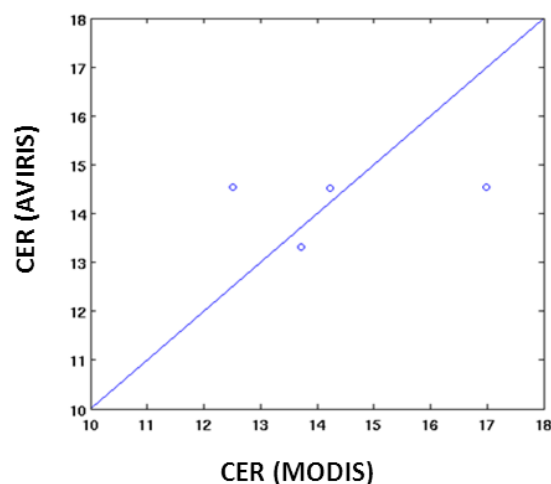


Figure 8.6. Scatter plot of MODIS and AVIRIS cloud effective radius

## 5. Conclusions

To sample different cloud kinds, it is proposed that observations be carried for convective cloud systems for the next campaign phase.

## Acknowledgements

The authors are extremely grateful to Director, Space Applications Centre, Shree Tapan Mishra for his encouragement and motivation. The authors are sincerely thankful to Dr. Rajkumar, Dr. C. M. Kishtawal and Dr. R. M. Gairola for their guidance. The authors especially express their sincere gratitude to Dr. Bimal K. Bhattacharya for providing valuable suggestions and help for the study, and the entire AVIRIS-NG campaign team for their support.

## References

- Kindel, B. C., P. Pilewskie, K. S. Schmidt, O. Coddington, and M. D. King (2011), Solar spectral absorption by marine stratus clouds: Measurements and modeling, *J. Geophys. Res.*, 116, D10203, doi:10.1029/2010JD015071
- Vukicevic, T., O. Coddington, and P. Pilewskie (2010), Characterizing the retrieval of cloud properties from optical remote sensing, *J. Geophys. Res.*, 115, D20211, doi:10.1029/2009JD012830.

# Development of Atmospheric Correction Scheme over Soil-Vegetation Complex for Generating Level-2 Hyperspectral Surface Reflectance product using AVIRIS-NG Level-1 data

Shailendra S. Srivastava, Nitesh Kaushik and Meenakshi Sarkar

ODPD/SIPG, Space Applications Centre, ISRO, Ahmedabad, Gujarat, India

## ***1. Scientific rationale and objectives***

Hyperspectral surface reflectance studies for a broad area is only possible through airborne or space-borne imaging, and it can be very helpful to understand the changing ecosystem and land use. The main objective here was to generate the accurate surface reflectance from the AVIRIS-NG Level-1 radiance datasets.

## ***2. Study area and data used***

AVIRIS-NG provides very high spatial resolution data (depending on the flying altitude and optics) in 432 contiguous spectral bands in the range 0.4-2.5  $\mu\text{m}$ . There are three main levels of processing: level-0 (raw data), level-1 (calibrated radiances) and level-2 (atmospherically-corrected surface reflectances). Only, the first two levels of processing are available on site, while level 2 is produced at the JPL Science Data System (SDS). Radiances are provided in the units of  $\text{W}\cdot\text{sr}^{-1}\text{nm}^{-1}\text{cm}^{-2}$ . Values are stored in an IEEE little-endian floating point format (32-bit single precision) with 598 cross-track samples and 432 channels per line, with BIL interleave.

Airborne AVIRIS-NG flights, which lasted for about four months captured data over variety of sites (~57 sites) across the Indian sub-continent. This model is successfully applied to the entire available datasets. Though, improvements in the algorithms are in progress.

## ***3. Methodology***

Aerosol optical depth and water vapor retrievals are presented elsewhere. Here, we briefly present the methodology of the surface reflectance retrieval. Atmospheric correction requires accurate absolute calibration for each spectral band. AVIRIS-NG is well calibrated instrument. This method corrects for the aerosol scattering, and absorption/scattering

primarily from the atmospheric trace gases O<sub>2</sub>; O<sub>3</sub>; H<sub>2</sub>O, CO<sub>2</sub>, CH<sub>4</sub> and N<sub>2</sub>O. Rayleigh scattering is handled empirically, utilizing the height of the location. It assumes a single aerosol model: Continental. It solves the equation of transfer for a lambertian homogeneous target of reflectance ( $\rho_s$ ) at an altitude  $z$  with  $\Theta_v$  (zenith angle of view) and  $\Phi_v$  (azimuth angle of view) and illuminated by sun at angles  $\Theta_s$  and  $\Phi_s$  (solar zenith and azimuth angles respectively). Top of the atmosphere reflectance ( $\rho^*$ ) can be computed from the following equation [Vermote et al., 1997].

$$\rho^*(\theta_s, \theta_v, \phi_s - \phi_v) = T_g(\theta_s, \theta_v) \left[ \rho_{Ray+Aero} + T^\downarrow(\theta_s) T^\uparrow(\theta_v, z) \frac{\rho_s}{1 - S\rho_s} \right]$$

Where  $\rho^*$  is apparent reflectance measured at the top of the atmosphere (TOA),  $T^\downarrow$  is total transmission from the sun to the surface,  $T^\uparrow$  is total transmission from the surface to the sensor,  $T_g$  is total gas transmission,  $\rho_{Ray+Aero}$  is the Intrinsic reflectance of the molecules and aerosols, and  $S$  is the Spherical Albedo of the atmosphere.

Instrument characteristics (spectral bands) have several features, which can be utilized to retrieve the state of the atmosphere from the scene data itself. Its narrow bands also add to its ability to avoid the overlapping of the absorption features. The quantities (refer above equation)  $T$ ,  $S$ ,  $T_g$ ,  $\rho_{Ray+Aero}$  are the functions of aerosol optical depth, single scattering albedo, and phase function of the scatterers and absorbers in the atmosphere. It would be impractical to make computations for every value of the given atmosphere. Thus, we precomputed look-up-tables with various combinations of solar/view zenith angles, azimuth angles, water vapor, ozone, aerosol optical depth, and height values. It is done with keeping the size of the table tractable.

### 3.1 Implementation: Open MP

Atmospheric correction process computes reflectance for each pixel by using geometric information (latitude, longitude and satellite/sun azimuth/elevation) along with Aerosol Optical Depth (AOD), Water Vapor and DEM for each pixel. The computation process for each pixel is independent of each other and can be carried out in parallel. Current CPU (central processing unit) architecture consist of processor having multiple cores on them which significantly increase computational resources. To achieve high throughput and reduced

turnaround time (TAT) user has to achieve high degree of parallelism using available programming APIs. OpenMP is one of the best solution to achieve high degree of parallelism with the help of pragma notations. Pragas are compiler directives which can make a portion of program to execute in parallel. Pragas to execute for loop in parallel were used in Atmospheric Correction process. Let us assume that we have to correct an image of dimension 598 lines and 9904 columns using only four threads:

```
pragma omp parallel for (int i=0; i<598*9904; i++)
```

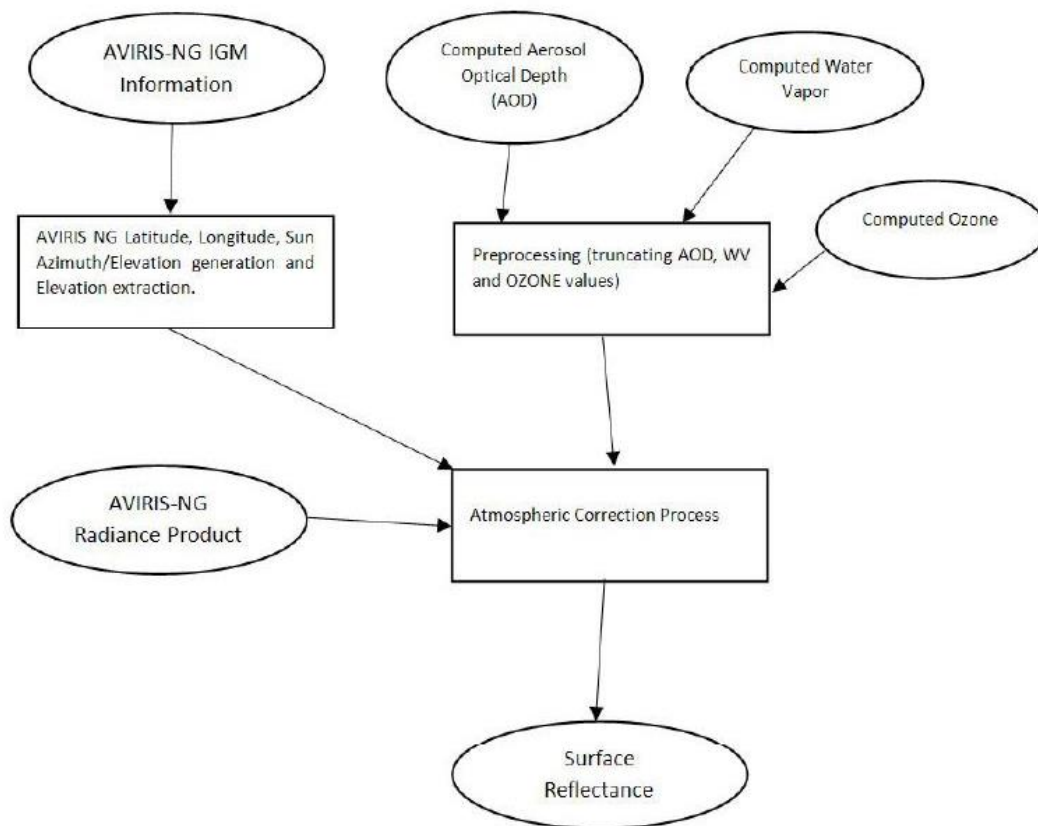


Figure 9.1. Flow of the data in atmospheric correction

At this point the master thread creates some additional threads (three in this example), and together with these additional threads (often referred to as slave threads) forms a team of four parallel threads. These four threads divide the iterations of the do loop among themselves, with each thread executing a subset of the total number of iterations. There is an implicit barrier at the end of the parallel do construct. Therefore, after finishing its portions of the iterations, each thread waits for the remaining threads to finish their iterations. Once

all the threads have finished and all iterations have been executed, the barrier condition is complete and all threads are released from the barrier. At this point, the slave threads disappear and the master thread resumes execution of the code past the for loop of the parallel for construct. Following block diagram (figure 9.1) shows the data flow in the atmospheric correction.

## 4. Outcome

### 4.1 Salient Findings

Level-2 product could be generated successfully, and comparison with the level-2 product generated by JPL team shows a good agreement (figure 9.2 and figure 9.3).

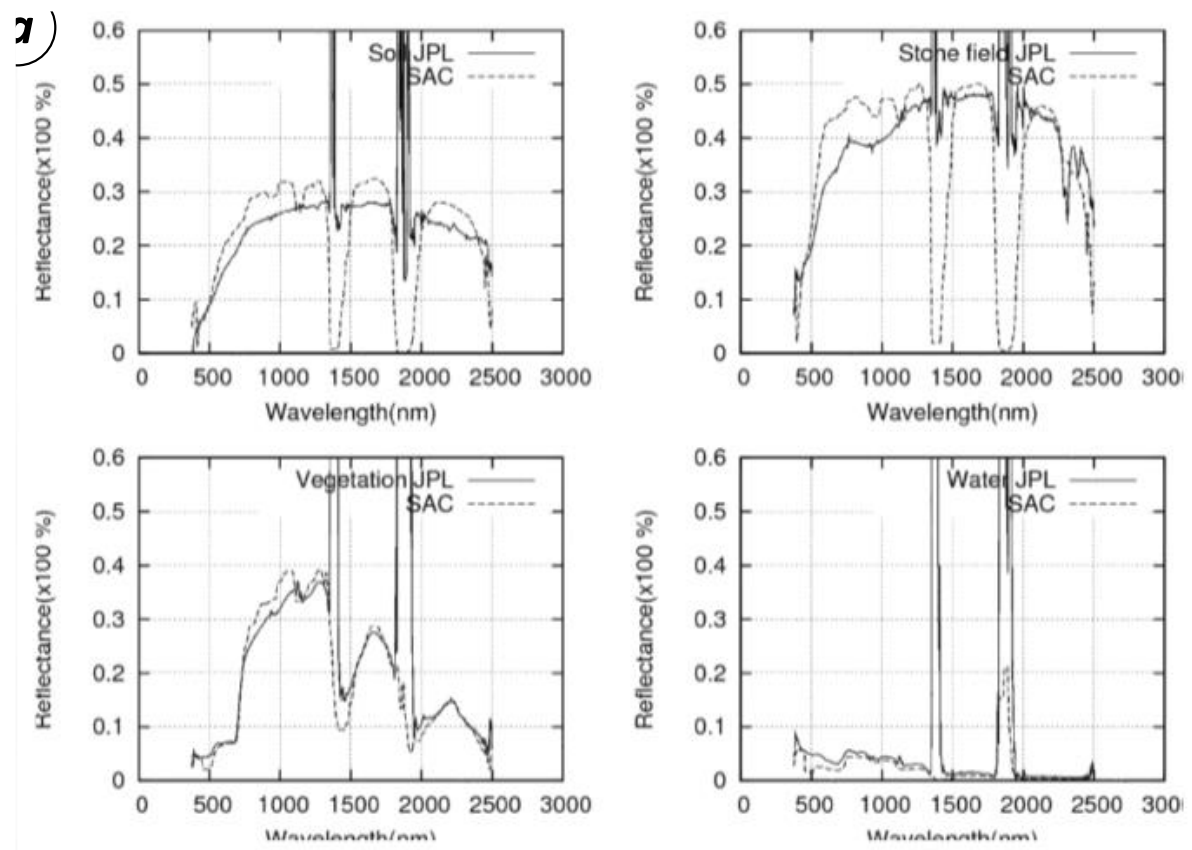


Figure 9.2. Sample of comparison of level-2 products from SAC & JPL over various targets (dataset: ang20160204t073848 and ang20160107t054711)

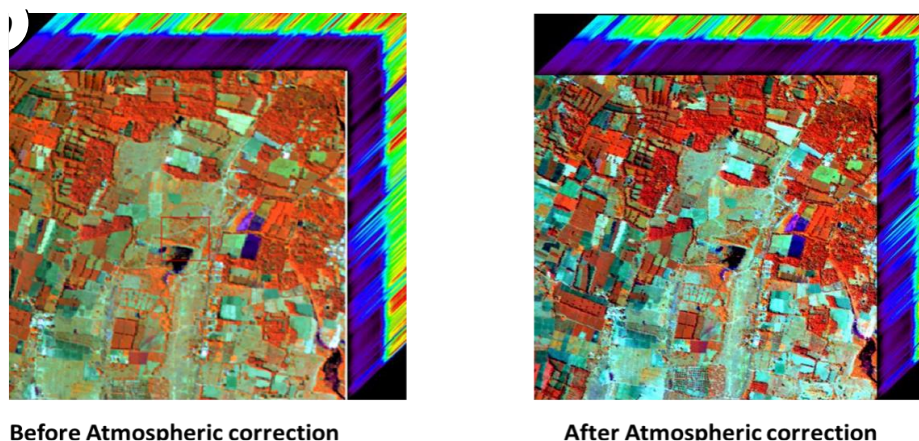


Figure 9.3. Uncorrected Vs corrected FCC

## 4.2 Target Vs Achievement

Though, there are still differences in the spectral signatures, which require further refinements on the atmospheric correction scheme.

## 4.3 Linkage to societal benefits

Enhancement of our capabilities in the field of hyperspectral remote sensing would help us to design better systems and models, which in turn would benefit the society.

## 5. Conclusions

The comparison of surface reflectance signatures from SAC and JPL over various representative targets was carried out, and results are presented. It is apparent that the patterns of TOA and surface reflectances from SAC are matching well, except in the lower wavelength regions (below 400 nm). The JPL surface reflectance showed very smooth transition across the wavelength. Further validation and improvement in the retrieval algorithms are definitely desired.

## Acknowledgements

Authors wish to thank Sri Anurag Pushpakar, ODPD for his help in analyzing data.

## References

Vermote, E. F., Tanre, D., LucDeuze, J., Herman, M., and Morcrette, J.-J. Second simulation of the satellite signal in the solar spectrum, 6s: An overview. *IEEE Transactions on Geoscience and Remote Sensing* (1997).

# Atmospheric Correction Algorithm for Hyperspectral Data of AVIRIS-NG for Ocean Colour Remote Sensing in Turbid and Inland Waters

Anurag Gupta, Arvind Sahay and Syed Moosa Ali

Space Applications Centre, ISRO, Ahmedabad, Gujarat, India

## ***1. Scientific rationale and Objectives***

The airborne visible/infrared imaging spectrometer (AVIRIS) development was begun in 1984 and the imager first flew aboard a NASA ER-2 aircraft at 20 km altitude in 1987. Since then major development has come in the field of hyperspectral mission. Atmospheric correction of hyperspectral data for the remote sensing of ocean color requires very accurate modelling of scattering and absorption effects in the atmosphere. Gordon and Wang (1994a) developed a detailed atmospheric correction algorithm for multispectral sensors with higher radiometric sensitivity such as SeaWiFS/MODIS which included accurate calculations of Rayleigh scattering and the multiple scattering effects of aerosol and gas molecules. This work was extended to hyperspectral sensor by Gao et al. (2000) where he calculated scattering from atmospheric aerosols and molecules using 5S computer code. Here, the approach is little different i.e. instead of aerosol modeling using computer code, aerosols are retrieved using two bands viz. 1.0075 and 1.5535  $\mu\text{m}$  from TOA radiance.

Another important source of error in retrieving water leaving radiance in highly turbid coastal region is because of aerosol optical depth over the ocean is derived from Near Infrared (NIR) channels, since the oceanic signal is assumed to be zero in this part of the spectrum (black pixel approximation). This assumption yields good result in Case I open ocean waters, but when applied to turbid Case II waters the algorithm frequently results in negative values of water leaving radiance. This is due to the fact that constituents in case II waters are mainly dominated by suspended sediments, which can contribute significantly to water leaving radiance in NIR bands (Hu et al. 2000). The advantage of hyperspectral over multispectral is that it (AVIRIS) gives continuous spectra (0.3764-2.5 $\mu\text{m}$ ) and two bands in the SWIR region

i.e. 1.0075 and 1.5535  $\mu\text{m}$  were chosen to overcome the above said problem to get the improved Rrs in shorter wavelengths.

## Objectives

- Development and validation of atmospheric correction algorithm in ocean waters and inland waters for hyper spectral remote sensing data of ocean using hyper-spectral measurements of the light field.
- To validate normalized water leaving radiance or remote sensing reflectance from *insituda*ta.

## 2. Study area and data used

Chilika is the largest brackish water lagoon in the Asian continent and is a very good site for studying optically complex waters from space-borne platform. Chilika being connected by sea through a mouth in the northern sector and by many tributaries in the northern central and south sector provides a suitable site to study such optically complex water. AVIRIS-NG, a hyperspectral sensor (375-2400  $\mu\text{m}$ ) was flown over Chilika lagoon (Odisha, India) on 27 December, 2015 to study the bio-optical properties from hyperspectral space-borne platform.

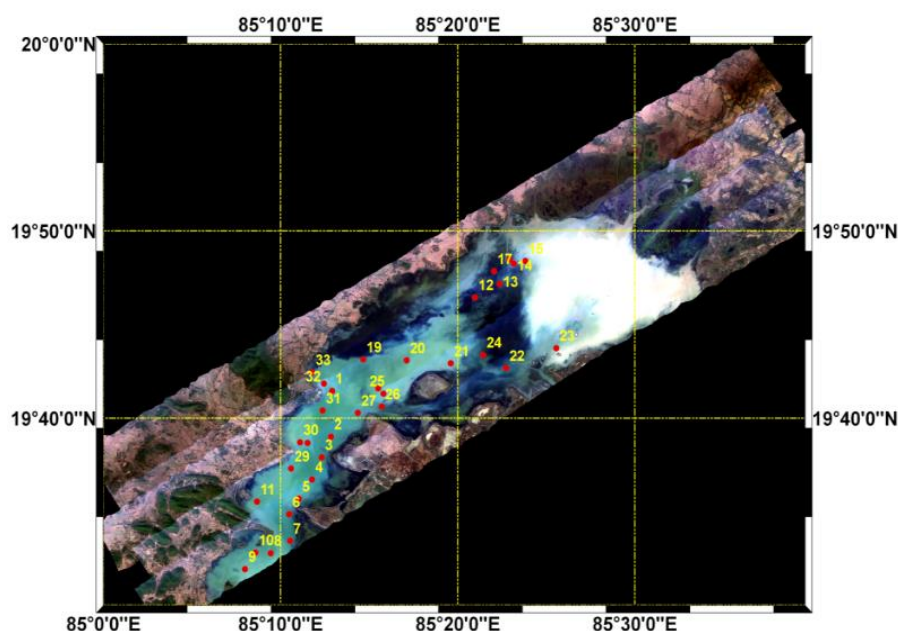


Figure 10.1. AVIRIS-NG Natural Colour Composite Image with in-situ station locations (red dots)

Figure 10.1 shows the coverage by AVIRIS-NG over Chilika lagoon (A mosaic of 12 scenes of AVIRIS-NG flight) for this study. The station locations for collecting in-situ bio-optical data with longitude and latitude are given by red dots.

### 3. Methodology

Radiance at the sensor level can be modelled using molecular scattering and particle scattering based on existing mathematical models and gaseous absorption in the atmosphere, provided solar and satellite viewing geometry are known. Path radiance due to Rayleigh scattering ( $L_r$ ) computed for single scattering approximation can be expressed as (Gordon et al. 1988)

$$L_r = \tau_r(\lambda) F'_o(\lambda) p_r(\theta_s, \theta_v, \lambda) \quad \dots (1)$$

where,

$$p_r(\theta_s, \theta_v, \lambda) = \{P_r(\gamma^-, \lambda) + [r(\theta_v) + r(\theta_s)] P_r(\gamma^+, \lambda)\} / \cos(\theta_v) \quad \dots (2)$$

$$\cos(\gamma^\pm) = \pm \cos(\theta_s) \cos(\theta_v) - \sin(\theta_s) \sin(\theta_v) \cos(\phi_v - \phi_s) \quad \dots (3)$$

$\theta_s$  and  $\theta_v$  are solar and viewing zenith angle respectively,  $\phi_s$  and  $\phi_v$  are solar and viewing azimuth angle respectively,  $r(\theta)$  is the Fresnel reflectance at the air-water boundary for a light incident at an angle  $\theta$ ,  $\tau_r(\lambda)$  is the Rayleigh scattering optical depth and  $P_r(\gamma)$  is the Rayleigh scattering phase function, which is calculated as

$$P_r(\gamma) = (3/4) [1 + \cos^2(\gamma)] \quad \dots (4)$$

$F'_o(\lambda)$  is the extraterrestrial solar irradiance ( $F_o(\lambda)$ ) corrected for its absorption at the ozone layer, and is written as

$$F'_o(\lambda) = F_o(\lambda) \exp[-\tau_{oz}(1/\cos(\theta_v) + 1/\cos(\theta_s))] \quad \dots (5)$$

Secondly, different types of aerosol, indicating the aerosol optical depth  $T_a$  to be wavelength dependent can be modelled by power law as

$$L_a(\lambda) / F'_o(\lambda) = A' T_a = A (\lambda)^{-\alpha} \quad \dots (6)$$

where,  $\alpha$  is Angstrom exponent and  $L_a$  path radiance,  $A$  and  $A'$  are constants. The above equation can be solved to retrieve the aerosol optical thickness  $\tau_a$  using two bands say, 1.0075 and 1.5535  $\mu\text{m}$ . In this way, aerosol from data itself was retrieved on pixel to pixel basis. Atmospheric transmittance  $T_a$  (Sun to sea surface to sensor) can be estimated using following equation:

$$T_a = \exp [ - (\tau_a + \tau_r)(1/\cos(\theta_v) + 1/\cos(\theta_s))] \quad \dots (7)$$

Radiance measured  $L_t$  at the sensor level is nothing but the linear combination of atmospheric path radiance and diffuse transmittance of radiation to the top of atmosphere  $t_u$  times water leaving radiance  $L_w$ , can be expressed as (Gordon et al. 1997).

$$L_t = L_a + L_r + t_u L_w \quad \dots (8)$$

where,  $L_a$  and  $L_r$  represents radiance reaching the sensor due to aerosol and Rayleigh scattering, respectively. So using equation (1) to (7) in (8), water leaving radiance can be retrieved. Since the effects of water vapor absorption and gaseous absorption are negligible in visible region of electromagnetic spectrum, so they were avoided in retrieving water leaving reflectance.

## **4. Outcome**

### **4.1 Salient findings**

Aerosol Optical Depth (AOD) from pixel to pixel basis is retrieved and hyperspectral image of AVIRIS-NG is corrected for turbid and inland water bodies. Figure 10.2 represents the uncorrected radiance and corrected reflectance data over acquired over Chilika lagoon, Odisha, India on 27 December 2015 (Flight stripe No-61133). Atmospheric spectra of radiance and reflectance collected at seven different locations are shown in Figure 10.2 respectively. Reflectance from Figure 10.2 at seven different locations show a peak around 0.55  $\mu\text{m}$ . The peak shows that the water is green may be due to high phytoplankton concentration.

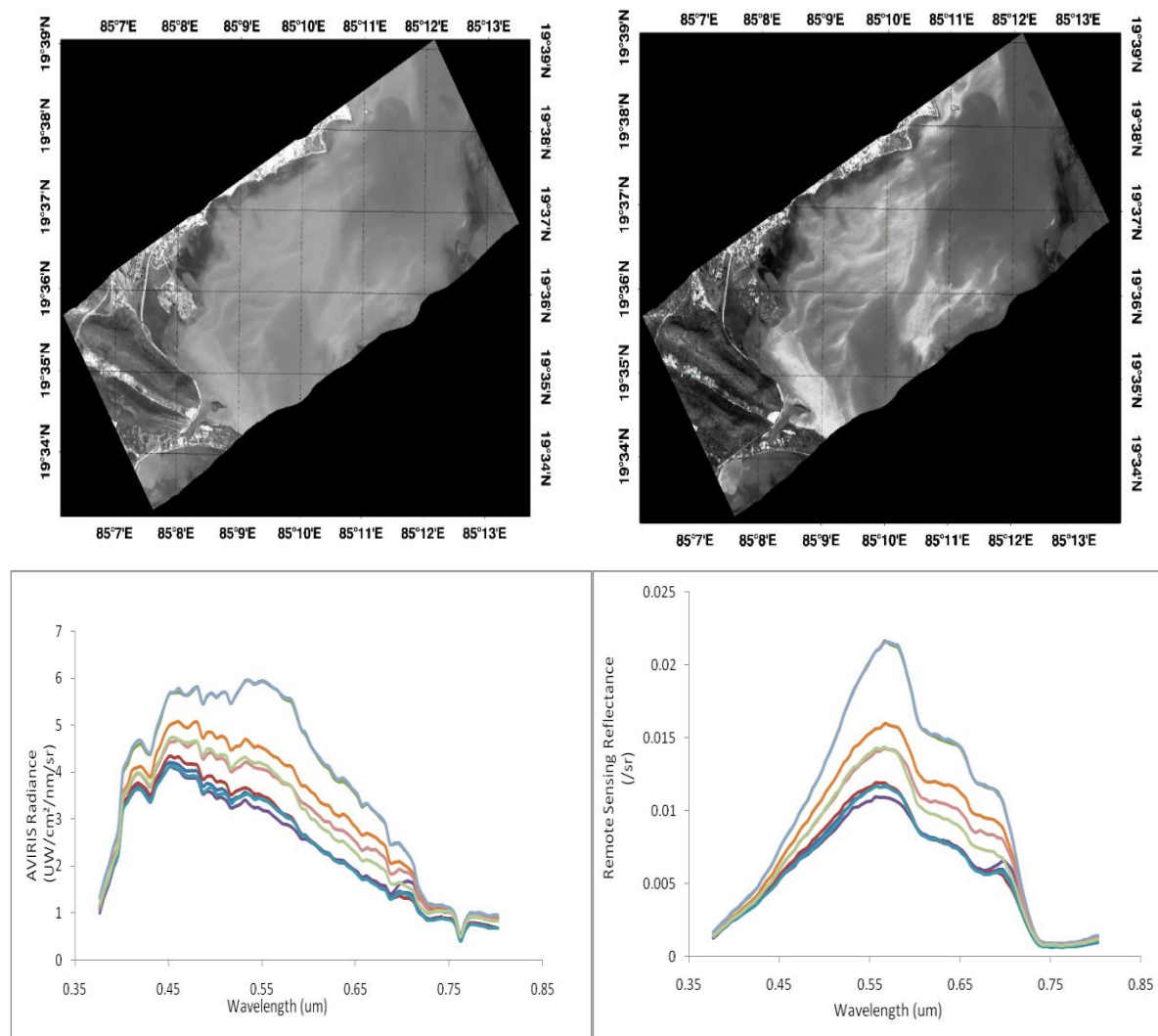


Figure 10.2. Image in upper left part, shows the AVIRIS-NG radiance and in right side reflectance data acquired over Chilika lagoon, Odisha, India on 27December-2015. Image in lower left side, shows the AVIRIS-NG radiance and in right side, reflectance spectra acquired over Chilika lagoon, Odisha, India on 27December-2015.

### Error Estimation

Error estimation has been done based on Carder’s approach (Carder et al., 2004) which is as follows:

$$rmse = [(\sum_{n=1}^n (\log O - \log E)^2)/n]^{1/2} \quad \dots (9)$$

$$error = 0.5 [(10^{rmse}-1) + (1-10^{-rmse})] \quad \dots (10)$$

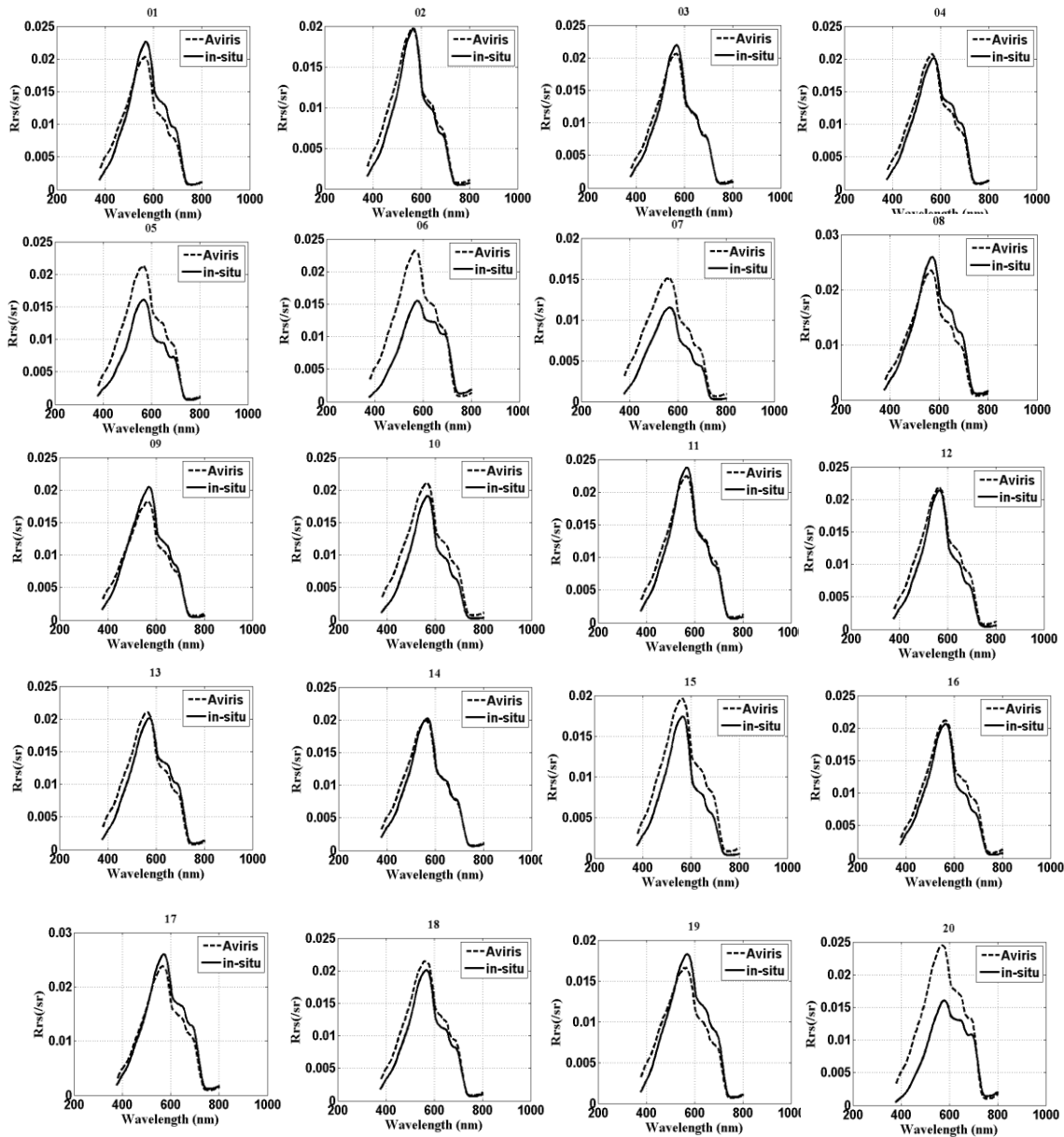


Figure 10.3. Comparison of AVIRIS-NG reflectance spectra with in-situ at twenty different locations (dotted curve-AVIRIS-NG and solid curve in-situ spectra)

Table 10.1. Percentage (%) Error between retrieved Rrs and in-situ of 20 stations in Chilika lagoon

<b>Sr No.</b>	<b>Latitude</b>	<b>Longitude</b>	<b>% error</b>
1	19.65043	85.2141	21.9
2	19.63206	85.20562	25.9
3	19.61239	85.19638	16.5
4	19.59511	85.18411	17.4
5	19.59252	85.14459	38.4
6	19.68882	85.26347	23.7
7	19.67716	85.26204	22.9

<b><i>Sr No.</i></b>	<b><i>Latitude</i></b>	<b><i>Longitude</i></b>	<b><i>% error</i></b>
8	19.64474	85.19214	20.3
9	19.6219	85.17666	35.2
10	19.59511	85.18411	24.5
11	19.5813	85.17477	14.9
12	19.54673	85.15763	27.2
13	19.5325	85.13333	15.6
14	19.54726	85.14314	20.8
15	19.71154	85.37883	22.7
16	19.69111	85.21522	27.4
17	19.71824	85.28537	33.9
18	19.64544	85.185	15.4
19	19.67371	85.20633	17.0
20	19.69756	85.20774	28.1

## 4.2 Target vs. Achievement

60% of the objectives has been completed.

## 4.3 Linkage to societal benefits

The atmospheric correction to generate RRS is a precursor for extracting the optical properties of water bodies and their pollution content and health.

## 5. Conclusions

- An algorithm is developed for atmospheric correction of hyperspectral radiance data of AVIRIS-NG over complex turbid water.
- The algorithm uses two SWIR bands (1.0025  $\mu\text{m}$  (band-127) and 1.5535  $\mu\text{m}$  (band-236) for computing angstrom exponent and aerosol optical depth (AOD).
- The atmospherically corrected reflectance data of AVIRIS-NG is compared with in-situ data of twenty stations. A fairly good match is obtained between in-situ and AVIRIS-NG reflectance.
- The maximum error is 38.4% and minimum error is 14.9%. This research demonstrates the atmospheric correction technique in complex water environment of Chilika lagoon, Odisha, India and determines that the technique may be used for other similar complex water environment for atmospheric correction of hyperspectral images.

## Acknowledgements

The authors are thankful to Director SAC for his kind support and valuable guidance during the AVIRIS-NG campaign and to AVIRIS-NG team (ISRO and JPL/NASA) both at ground and space segment, without which this work wouldn't have been possible at all. The authors express their thanks to DD EPSA and GD BPSG for their valuable guidance during the multiple review of the work. We are also thankful to NIO Goa and Chilika Development Authority (CDA) for their support during the campaign.

## References

Chuanmin Hu, Kendall L. Carder, and Frank E. Muller-Karger, "Atmospheric correction of SeaWiFS Imagery over Turbid coastal waters: A practical method", *Remote Sens. Environ.* 74:195-206(2000).

H. R. Gordon, "Removal of atmospheric effects from satellite imagery of the oceans," *Appl. Opt.* 17, 1631–1636 ~1978.

H. R. Gordon and M. Wang, "Retrieval of water leaving radiance and aerosol optical thickness over the oceans with SeaWiFS: a preliminary algorithm," *Appl. Opt.* 33, 443–452~1994.

Gordon, H. R., Atmospheric correction of ocean color imagery in the Earth Observing system era, *J. Geophys. Res.*, 102, 17081-17106, 1997.

H.R. Gordon, J.W. Brown, and R.H. Evans, "Exact Rayleigh scattering calculations for use with the Nimbus 7 coastal zone color scanner", *Appl. Opt.* 27, 862-871(1988).

Gao, B.-C., et al (2000), Atmospheric correction algorithm for hyperspectral remote sensing of ocean color from space, *Appl. Opt.*, 39, 887-896.

# SPECISOFT for Creating, Visualization of Spectral Library and Hyperspectral Image Analysis

Rohit Nagori

Space Applications Centre, ISRO, Ahmedabad, Gujarat, India

## ***1. Scientific rationale and Objectives***

Spectral libraries are collections of spectra that characterize the reflectance or emissivity spectral response of terrestrial surfaces and materials (Jiménez et al., 2015). AVIRIS-NG Airborne campaign held over selected sites of Indian region by joint efforts of NASA-JPL and ISRO provided an excellent opportunity to organize massive Ground Truth Campaign synchronously with flight. The Ground Campaign resulted in harboring a large amount of spectral observations from variety of materials under different themes. The existence of extensively documented metadata on spectral libraries enhances the suitability, long-term usability, and quality assurance of data from other researchers (Hueni et al., 2009). Currently widely used spectral libraries are the U.S. Geological Survey (USGS) ([http://speclab.cr.usgs.gov/spectral.lib04/spectral\\_lib.html](http://speclab.cr.usgs.gov/spectral.lib04/spectral_lib.html)) Spectral Library for minerals, and the ASTER Spectral Library available at the NASA Jet Propulsion Lab (JPL) for a collection of spectra from a range of materials including data from the USGS Spectral Library and the Johns Hopkins University (JHU) Spectral Library that specializes in minerals and meteorites with some snow and vegetation spectra (<http://speclib.jpl.nasa.gov/>). Manjunath et al. (2014) developed spectral library of major plant species of Western Himalayas using field observations. They developed a standardized technique for vegetation spectral library development and made data available to user for easy comparison. The objective of our study is to develop a software tool to create and visualize spectral library for hosting the ground spectra along with observation details and ancillary information collected under various theme during the AVIRIS-NG ground truth campaign. Additional to it, a software will be developed for analyzing hyperspectral images which will also act as a platform to facilitate various newer algorithms developed during scientific analysis of AVIRIS-NG datasets.

## **2. Study area and data used**

Currently, spectral library contains data of different varieties of mango, sapota, banana, etc. as collected during the ground campaign over Talala (Site Id 155). The spectra were collected using ASD (spectro-radiometer) FieldSpec version 3 (350-2500 nm).

## **3. Methodology**

The software 'Specsoft' developed has both spectral library component and hyper-spectral image analysis component. The spectral library provides option to create as well as visualize. The visualization of spectral library is facilitated under different themes of "vegetation", "minerals", "soil", "snow & ice" and "man-made structures". There are further sub-categories to each theme for ex: "vegetation" theme has different categories of "crops", "plantation", "ornamental plants", "mangroves", etc. The data input while creating the spectral library gets organized in the folders corresponding to these sub-categories under the parent folder of respective themes. At the time of visualization, the data is extracted accordingly and displayed. Easy access of the spectral data can be exploited in hyper-spectral image analysis part too. Table 11.1 shows some of the input parameters required for creation of spectral library under "vegetation" theme which is currently developed and usable. Data collected under AVIRIS-NG campaign over Site ID 155 (Talala) has been included. Along with spectra visualization and export, several other options of plant general info, observation details, vegetation analysis can be used. Plant general info provides the information about the plant species been observed whereas observation details give ancillary information about the time of observation, readings of other instruments taken along with spectral observation such as SPADmeter, Leaf Area Index, etc. Bio-physical parameters of chlorophyll, lignin, etc. as available from laboratory measurements are also provided in observation details. Vegetation indices give different types of indices i.e. structural indices, red-edge indices, pigment related indices, water related indices, etc. which have been calculated from the various regions of spectra affected by the bio-physical or bio-chemical properties of a plant. Furthermore, different types of spectra such as field spectra, pure spectra, AVIRIS-NG image spectra and adjacent soil spectra have been provided wherever possible.

Hyper-spectral image analyzer provides user opportunity to open and display hyper-spectral images and perform certain basic operations on it such as subsetting, region of interest

formation, etc. The software allows incorporating any module to the existing frame at ease. Three modules of index calculator, classification and unmixing have been added till now. Under index calculator, currently all or selective vegetation indices can be calculated at once for full image or a region of interest. Choosing of full image or rectangular 1 ROI creates indices' image whereas any other option leads to result in an ASCII format. Under classification module, wrapper based classification has been included which is based on the optimization problem of genetic algorithm. Currently, only linear unmixing has been developed under the unmixing module.

Table 11.1. Table showing the format of data required to create spectral library

1	parameters	data1	data2
2	library	veglib	veglib
3	category	plantation	plantation
4	local name	Mango Khatta Meetha	Mango Sinduria
5	data address	D:\soft_spec v1\input_libdata\data1.xlsx	D:\soft_spec v1\input_libdata\data2.xlsx
6	pic_veg address	D:\soft_spec v1\input_libdata\DSCN3464.JF	D:\soft_spec v1\input_libdata\DSCN3506.J
7	pic_leaf address	D:\soft_spec v1\input_libdata\khatta mitha	D:\soft_spec v1\input_libdata\Sinduriya.JPG
8	scientific name	-	-
9	division	-	-
10	class	-	-
11	order	-	-
12	family	-	-
13	genus	-	-
14	species	-	-
15	major national distribution	-	-
16	occurrence (endemic/common/occasional/rare)	-	-
17	habit (herb-annual/herb-perennial/climber/tree/shrub/liana)	Tree	Tree
18	name of observer	Rohit Nagori, Dr. Saroj Maity, Dipanwita H	Rohit Nagori, Dr. Saroj Maity, Dipanwita H
19	institution of observer	SAC, AAU	SAC, AAU
20	type of observation	GT AVIRIS NG	GT AVIRIS NG
21	date of observation	12-2-16	12-2-16
22	crop variety	Khatta Meetha	Sinduria
23	season of observation	winter	winter
24	longitude	70.6413	70.64197
25	latitude	21.0701	21.0705
26	altitude	-	-
27	location	Moruka, Talala	Moruka, Talala
28	block	-	-
29	district	Junagadh	Junagadh
30	state	Gujarat	Gujarat
31	country	India	India
32	vigour	-	-
33	crop stage	-	-
34	age	50-60	-
35	spad average	56.8, 40.7, 54.7	50.7, 45.7, 47.3
36	lai reading	0.765	1.16
37	plant height	-	-

## 4. Outcome

### 4.1 Salient findings

Figure 11.1 shows the spectral library Graphical User Interface (GUI) and the flow of all the information that can be visualized and exploited. Figure 11.2 shows the Hyperspectral image analyzer part of 'Specsoft' where shows how to display hyperspectral images using different sets of bands and indices calculation.

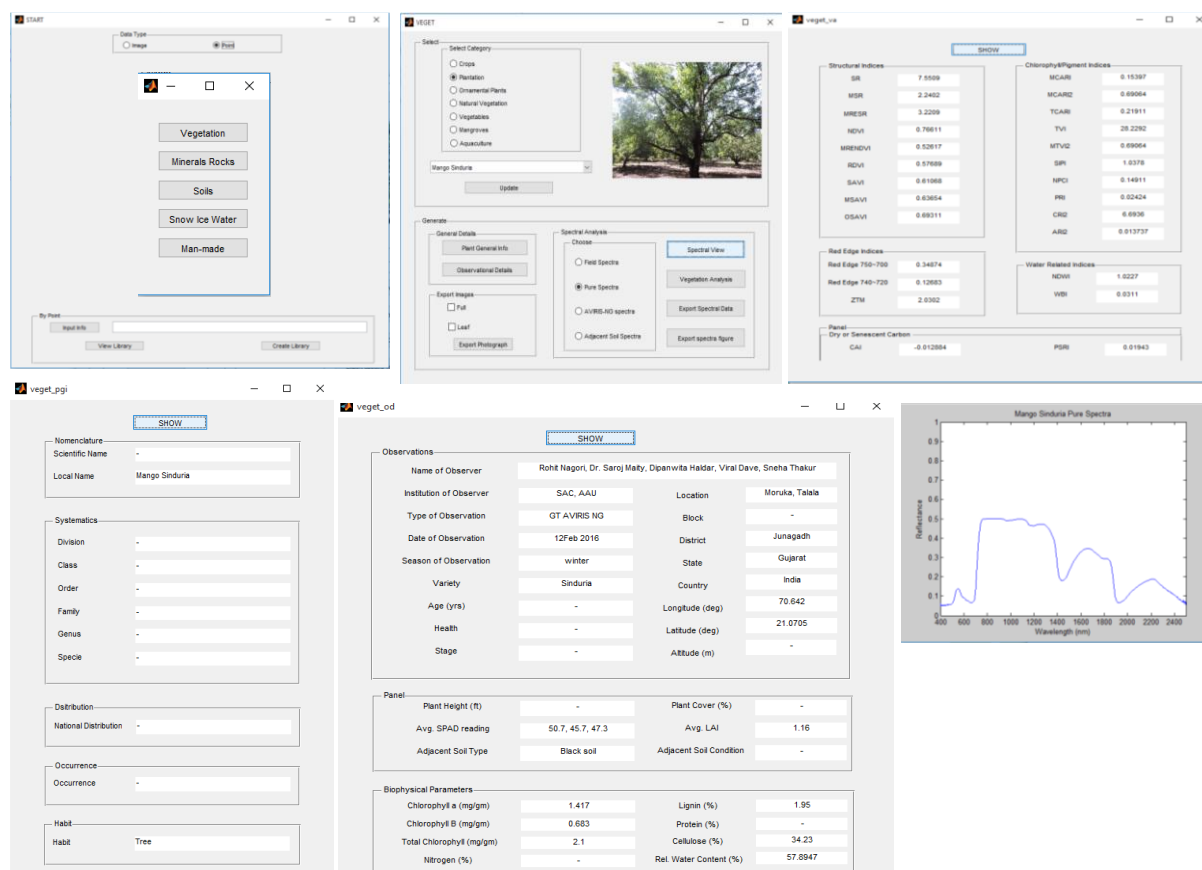


Figure 11.1. Figure showing the spectral library main menu (top left), vegetation spectral library (top middle), plant general info (bottom left) and observation details (bottom middle) and vegetation analysis (top right).

## 4.2 Target vs. Achievement

- Spectral Library has been completed for the vegetation theme. For the other themes, no inputs are available till now. As soon as the format of the inputs is provided, it will be completed.
- In the hyper-spectral image analyzer, some more basic functions need to be incorporated such as mapping information, etc. It will keep on evolving as the new modules get added to it.

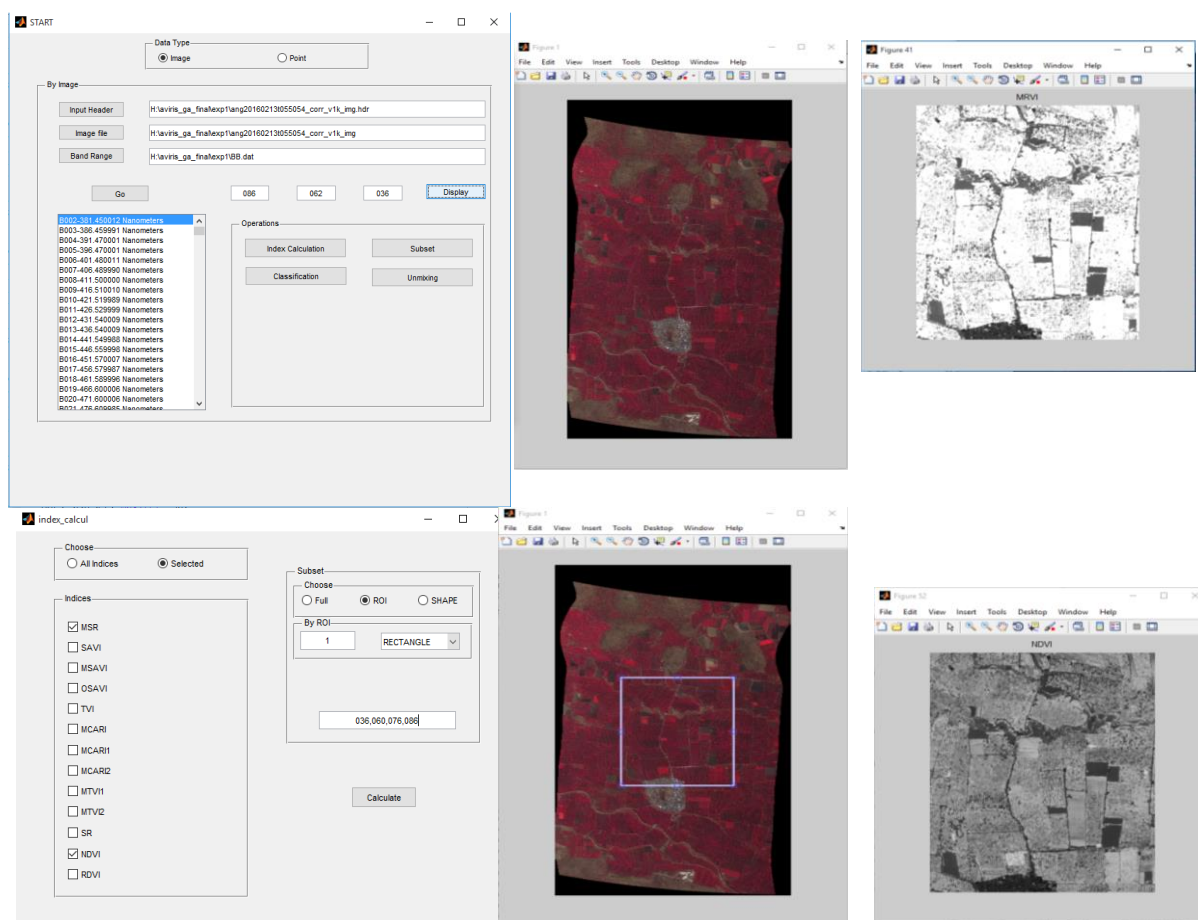


Figure 11.2. Figure showing the Hyperspectral image analyzer main menu (top left) and indices calculator window (bottom left). On choosing region of interest (ROI) option in indices calculation, window opens with FCC image to draw the ROI.

### 4.3 Linkage to societal benefits

Spectral library is very important component in any Hyper-spectral image analyses. Growth of database of spectra from various newer materials collected over various ground campaigns is always appreciated and a value addition to existing knowledge. The Hyperspectral image analyzer allows basic image processing and thus with further developments may be substituted for expensive commercial software. Also addition of newly developed and uncommon algorithms such as wrapper based classification, etc. makes it unique in comparison to other existing software.

## 5. Conclusions

- Newer spectra of different materials under various themes will be collected under the second phase of the AVIRIS-NG campaign inclusion of which will lead to growth of spectral library.
- Few basic and advanced modules are required to be incorporated in the Hyperspectral imager which is still in developmental stage.

## Acknowledgements

Author is grateful to Shri Tapan Mishra, Director SAC (ISRO), Ahmedabad, Dr. Bimal Bhattacharya, Dr. A. S. Arya for their support and encouragement to carry out this study. I also acknowledge JPL and ISRO AVIRIS-NG campaign team for providing data for analysis.

## References

- Hueni, A.; Nieke, J.; Schopfer, J.; Kneubühler, M. and Itten, K.I. The spectral database SPECCHIO for improved long-term usability and datasharing. *Comput. Geosci.* 2009, 35, 557–565.
- Jiménez, M. and Delgado, R. D. Towards a Standard Plant Species Spectral Library Protocol for Vegetation Mapping: A Case Study in the Shrubland of Doñana National Park. *ISPRS Int. J. Geo-Inf.* 2015, 4, 2472-2495.
- Manjunath, K. R.; Kumar, A.; Mehra, M.; Renu, R.; Uniyal, S. K.; Singh, R. D.; Ahuja, P. S.; Ray, S. S. and Panigrahy, S. Developing Spectral Library of Major Plant Species of Western Himalayas Using Ground Observations. *J Indian Soc Remote Sens* (March 2014) 42(1):201–216.

# Absorption Peak Decomposition Technique for Forest Species Identification from AVIRIS-NG Hyperspectral Data

Saroj Maity, C. Patnaik, Anup Das and Arundhati Misra

MHTD/GHCAG/EPISA

Space Applications Centre, ISRO, Ahmedabad, Gujarat, India

## ***1. Scientific rationale and Objectives***

Remote sensing has demonstrated its potential in mapping of forest's physical and structural features and plays a critical role in identifying the tree species. A variety of tree types and species are present in a forest and efforts are in place to develop a method to generate a map that can provide species-wise description. A number of studies were conducted in past to classify tree species from hyperspectral imaging data with varying degrees of success using various indices. In Indian scenario, species-wise forest map is non-existent and not tried before using hyper spectral data set.

Airborne hyper spectral sensor measures the reflectance of leaf and canopy of the tree and provides enormous amount of information about the abundance and distribution of different pigments present in the canopy constituents. As biochemical compositions of leaves among the various species differ, different absorption/emission spectra will be observed at different wavelengths. Spectral variations are due to different biochemical composition like water content, cellulose, leaf pigment etc. and pixel wise information of band center, band width and band intensity of forest can help in species wise classification of forest. In this study, absorption peak parameters based techniques has been used to identify the tree species with major objectives:

- Deriving species level forest characterization from hyper spectral data.
- Development of proper model for AVIRIS data for better forest stand classification and biomass estimation.

## 2. Study area and data used

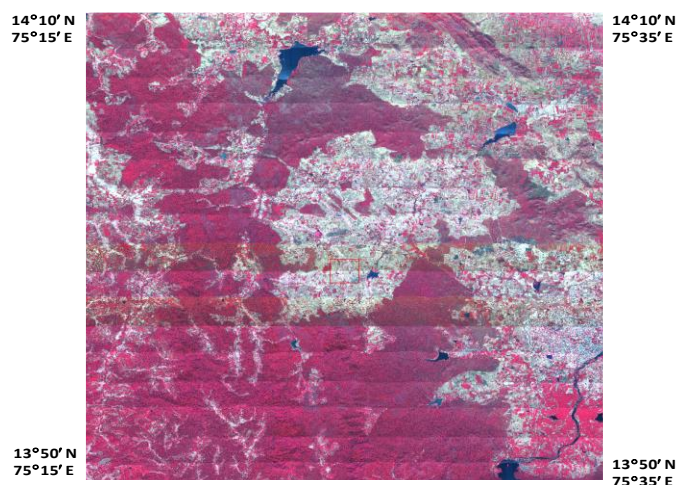


Figure 12.1. False Color Composite (FCC) of AVIRIS-NG image (R: Band-82; G: Band-58; B: Band-36) over the Shimoga forest area (Karnataka).

## 3. Methodology

A large number of field spectra are collected during ground campaign from individual species at different locations. Spectra of total nineteen tree species were collected in our study sites and for each species, at least 8-10 spectra are averaged for data analysis. Spectra are filtered, smoothed and shoulders of absorption peaks are estimated for hull (continuum) estimation. Normalized continuum removed spectra are generated as per following equation for further analysis:

$$C = \frac{R_C(\lambda) - R_T(\lambda)}{R_C(\lambda)} \quad \dots (1)$$

where,  $R_C(\lambda)$  is reflectance of the continuum;  $R_T(\lambda)$  is reflectance from target and C is the normalized continuum removed spectrum. In every absorption zone, broad and skewed peaks are observed in normalised spectrum (see figure 12.2). Reflectance from vegetation is dominated by absorption features of plant pigments like chlorophyll-a / b, carotenoids, lignin with nitrogen, cellulose, proteins and water. As different tree species have different amount of pigments present in their vegetation part, the peak centre, peak amplitude and peak width will also be different. Thus, each and every species owns a set of absorption peak parameters which are unique. Sometimes, few peak parameters may match with others, but there must be some peaks which are really not overlapping with others. Comparing all the peak

parameters estimated from ASD data, a unique set of peak parameters associated with particular species are identified and used as endmember for further classification. The flow chart for classification is shown in figure 12.2.

### 3a. Decomposition of normalised spectra

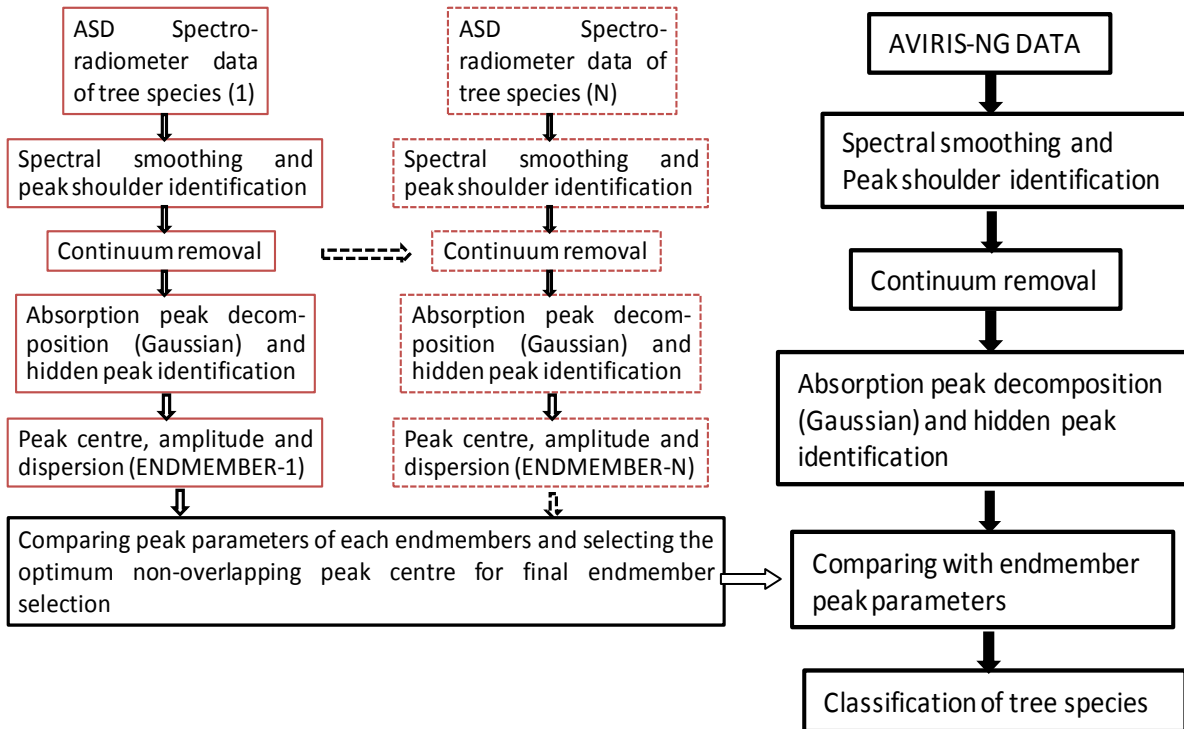


Figure 12.2. Flow chart of classification & selection of peak parameters of end-members from ASD

#### 3.1 Estimation of endmember parameters:

During ground truth data collection, we have collected large number of spectrum of nineteen pure species. As shown in the figure 12.2, individual spectrum is filtered and smoothed for peak shoulder detection and using these peak shoulders, continuum is estimated for normalised continuum removed spectrum generation. As observed in figure 12.3 (a), these normalised spectra are very broad and skewed to contain number of hidden children peaks. It is well documented in the field spectroscopy that these types of hidden peaks are in general Gaussian in nature. Normalised broad peaks are decomposed into number of hidden peaks using non-linear least square fitting approach. It is observed that each of these broad peak inherits two to three hidden peaks with varying peak parameters (peak amplitude, centre and std. deviation). In figure 12.3 (b), decomposed peaks are shown inside the broad normalised spectrum. These peak parameters pertaining to the species are considered for final

‘endmember parameters’ selection. Using the same procedure, a set of peak parameters for nineteen species are made and termed as endmember-1 to endmember-n (figure 12.2). Among the nineteen sets of peak parameters, it is observed that centre of absorption of some of the peaks are matching with others and some are totally different and unique. These unique and non-overlapping set of peak centers and its associated parameters like amplitude and dispersion, are finally assigned as ‘endmember parameters’.

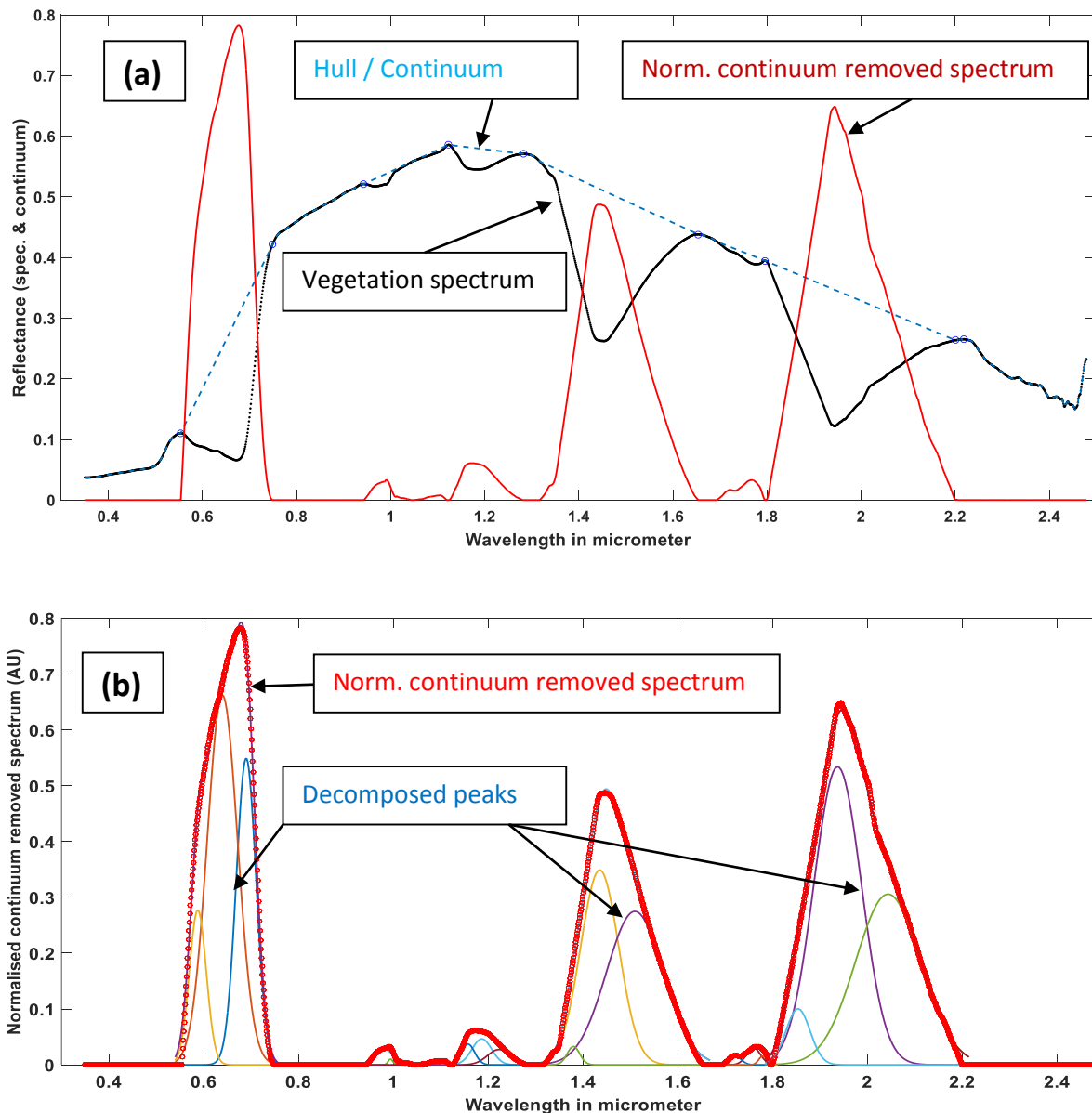


Figure 12.3. (a)Vegetation spectrum of a sample target,peak shoulders, continuum and normalised spectrum are shown in the graph.(b)Normalised spectra are decomposed to maximum possible Gaussian peaks which are hidden within the broad peak.

### 3.2 End member parameters for classification

AVIRIS image is filtered and then normalised continuum removed spectrum for every pixel is generated. As per the ‘endmember parameters’ of each species, calculated from ASD spectrum analysis, a lookup table is generated. Each pixel is assigned the class as per the lookup table if the band parameters, particularly the peak centre matches. The weightage of that pixel is given as per the peak amplitude. Here, in figure 12.4, FCC of NIR, Red and Green band is shown with the classified image of three major dominant species (*Tectona grandis*, *Dalbergia latifolia* and *Lagerstroemia lanceolata*).

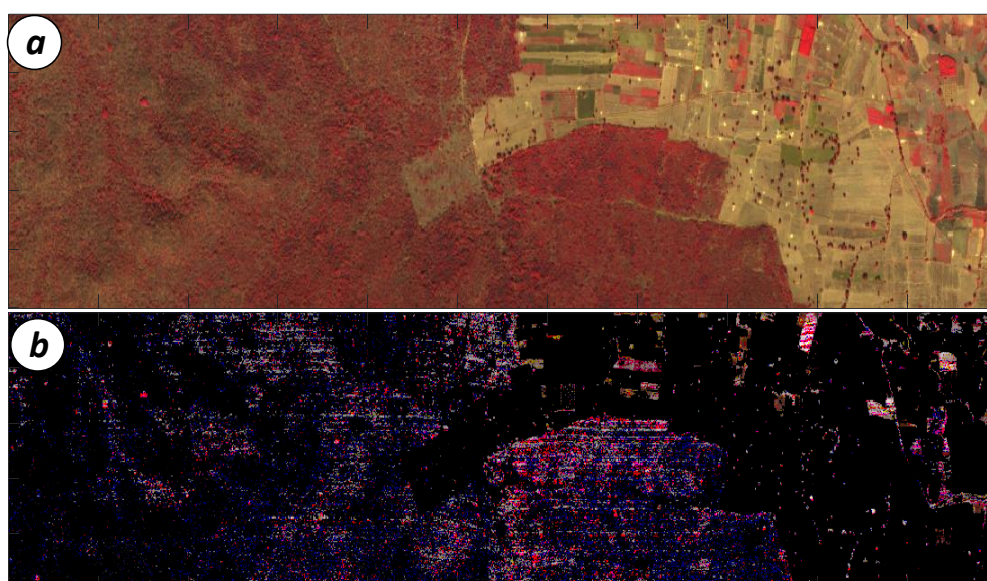


Figure 12.4. (a) FCC image (NIR, Red and Green) of the part of the study site is shown and (b) Classified image of three dominant species (Red: *Tectona grandis*, Green: *Dalbergia latifolia* and Blue: *Lagerstroemia lanceolata*). The weightage of each class is provided as per the amplitude of decomposed image.

## 4. Outcome

### 4.1 Salient findings

Preliminary analysis shows that the absorption peak decomposition method picks up the unique signature of nineteen species quite satisfactorily and can be used to map all nineteen species. This is the only method that can be used for species level discrimination as it uses the absorption peak parameters of different pigments level using all the AVIRIS-NG bands. Entire processing, i.e., from data ingestion, filtering, smoothing, peak shoulder determination, continuum removal, peak decomposition to classification, is written in Matlab.

## **4.2 Target vs. Achievement**

As AVIRIS data is very voluminous and processing of this data takes lot of computational time, we are lagging behind the target time. The concept of absorption peak decomposition technique is widely used in geological applications but for species level discrimination, we are modifying the existing concept in such a way that it can be applied in forestry / agricultural application too. The concept visualization, scripting, coding is taking some time and we hope to finish it within six months.

## **4.3 Linkage to societal benefits**

The exercise would be beneficial in deriving localised information of the forested area. Discriminating the various species of trees is a challenging task and needs to be done to identify the distribution and impact on the ecosystem. In addition to the species level discrimination, the vigour, age and type helps the policy planners to estimate potential timber quality and other commercial benefits from the forested areas. Secondly, from the analysis of spectra, a more scientific approach to plantation / forest management can be suggested by identifying potential phenotypic or morphological manifestations.

## **5. Conclusions**

The previous campaign for hyperspectral data collection was during the leaf fall season. The second air-borne campaign for hyperspectral data collection over the area during leaf-on season would help in the following ways:

- Assessing the temporal variations for both deciduous and semi-evergreen species.
- A feasibility study for assessing the vigour of species.
- Validation of the results carried out so far.
- Generation of a change matrix image to map the different forest types.

## **Acknowledgements**

Authors are thankful to Director, Space Applications Centre and Deputy Director, EPSA for their constant encouragement and critical suggestions. We are also thankful to AVIRIS-NG Science team leader for timely coordination of field campaigns and data availability.



**Agricultural Applications**

## Summary

Feeding world population through depleting natural resources has put a challenge among agricultural scientific community, not only to grow more but at the same time monitor in season crop growth and health at spatial and temporal scale. Advancement in remote sensing technology has opened new doors to explore innovative ways to map crop in terms of area and chemical constituents. In past, multispectral remote sensing technology has been harnessed to address in season agriculture monitoring for dominant crop at regional scale to generate crop specific statistics. Presently in India, approximately 60% of agricultural crop area statistics has been derived using multi-spectral data. But still approximately 40% area covering minor but economically valuable crops has no update from remote sensing techniques. Nevertheless, traditional multispectral broadband sensor data have known limitations of sensor saturation and absence of specific narrow bands to target and highlight crop health. Moreover, multispectral bands produce significant uncertainties in biophysical and biochemical retrieval which act a backbone for crop health monitoring. The specific narrow bands have a capability to reveal bio-physical-chemical properties of vegetation as molecular composition of the plant material reflects, absorbs, and emits electromagnetic energy at specific wavelengths and with distinct patterns. To study crop and soil classification at field scale along with crop health, an airborne AVIRIS-NG hyperspectral survey has been conducted in different parts of India. Crop classification with various available and developed algorithm has been done over homogenous and heterogeneous agriculture areas. Spectral Angle Mapper (SAM) showed accuracy of 86% for homogenous (Kota) and 81% for heterogeneous (Jhagdia) site, where as for similar resolution LISS IV spectral bands showed accuracy less than 40% for both sites. The genetic algorithm based classification developed scheme showed an accuracy of 87% for mapping of mango orchard. Mapping of fresh and ratoon sugarcane at Bharuch district showed accuracy of 84 to 87% for ratoon and 68 to 75% for fresh crop. The soil mapping at ICRISAT site has been done for red, black and mixed soil type and texture modelling showed RMSE of 6.67, 10.33 and 9.59 for clay, sand and silt respectively. The forward and inversion scheme has been developed using canopy radiative transfer model for retrieval of crop physical-chemical parameters such as LAI (451, 551, 686, 797,857, 882 nm) and chlorophyll (451, 551, 656, 686 nm) with AVIRIS-NG narrow bands reflectance. The retrieval showed a 15 and 21% deviation from measured mean for LAI and chlorophyll respectively. The crop parameters as well as plant nitrogen content also mapped with developed empirical models with hyperspectral indices. Biotic stress in the form wheat yellow rust is identified at field scale over part of Rupnagar district of Punjab using band absorption depth analysis at 662-702 nm and 2155-2175 nm. The dry and wet edge (NDVI vs NDWI, NDII, LSWI and WI) are used for computation of Standardized Water Content Index (SWCI) to discriminate abiotic stress in crops. In future, such missions give us better understanding of high economically valuable minor (pulses, oilseed, medicinal, cash crops) crops and cultivar type. Moreover, multi-year data will help us to generate spectral libraries for various crop type and soil. This will further help to understand the crop rotation at field scale and give insight of plant chemistry in terms of pigment mapping.

# Crop discrimination using AVIRIS-NG data over homogeneous and heterogeneous agriculture area

Rahul Nigam, Rajsi Kot\* and Bimal K Bhattacharya

Agriculture and Land Eco-System Division (AED), BPSG/EP  
Space Applications Centre (ISRO) Ahmedabad, INDIA

\*M. G. Science Institute, Ahmedabad, INDIA

## ***1. Scientific rationale and Objectives***

Sustainable management of the agricultural areas from field to regional scale is crucial for agricultural agencies and planners, since agriculture plays a vital role in Indian economy (Thenkabail, 2001). Crop mapping and discrimination provide an important basis for many agricultural applications such as acreage, biomass, yield, crop rotation and soil productivity (Mariotto et al., 2013). Remote sensing data, methods and approaches provide the best options for large area agricultural cropland characterization for precision agricultural management practices by accurately mapping of crop type and yield indicators. Traditional multispectral broadband sensor data have known limitations of sensor saturation and absence of specific narrow bands to target and highlight specific biophysical and biochemical characteristics according to crop type. These factors lead to significant uncertainties in the discrimination of crop type. Recent advances in hyperspectral remote sensing technology provides the opportunity to measure the response of different crop type in terms of morphological and physiological characteristics. The continuous availability of hyperspectral imagery, which records hundreds of image corresponding to different wavelength channels has opened new avenues in the field of classification. Hyperspectral observation offers an advance technique for improving the consistency of crop assessments (Ozdogan & Woodcock, 2006). This will further enhance the possibility to explore assessment of minor (pulses, oilseed, medicinal, cash crops etc.) economical valuable crops at field to landscape scale. Availability of such data in discrete narrowband provide an opportunity to study crop characteristics and possibility for better separation and classification of crop type as compared to limited bands of multispectral data. This motivate us to frame the objective to

study crop classification in homogeneous and heterogeneous agricultural environment using airborne AVIRIS-NG hyperspectral data.

## ***2. Study area and data used***

The study area is Jhagadia, Gujarat and Kota, Rajasthan. Jhagadia is a taluka in Bharuch district in the state of Gujarat. Jhagadia is located 3.2 km south of the southern bank of the Narmada river. Jhagadia has semi-arid climate with extreme temperatures, erratic rainfall and high evaporation. The average annual normal rainfall is 924.8 mm. Major crops in Jhagadia are banana, sugarcane, cotton, wheat, sorghum, arhar and onion. During the field campaign of AVIRIS-NG mission heterogeneous agricultural areas were observed with sugarcane, wheat, banana, arhar and onion. Kota is located in the southeast of northern Indian State of Rajasthan. It is located around 250 km south of the state capital Jaipur, situated on the banks of Chambal river. Kota has a semi-arid climate with high temperatures throughout the year. The average annual rainfall in Kota is 660.6 mm. During the field campaign most agricultural area was found irrigated with alsin, beans, chickpea, coriander, garlic, wheat, methi (fenugreek), mustard and peas. In this study for crop discrimination, ground based hyperspectral data collected during AVIRIS-NG field campaign and airborne hyperspectral imagery of AVIRIS-NG were used. During the field campaign, crop spectra for every crop was collected by ASD Spectroradiometer.

## ***3. Methodology***

### **3.1 Pre-processing of Ground data**

*In situ* crop spectra are collected for different crop type during the during the AVIRIS-NG flight time. Twenty spectra of each crop and soil type are used for generation of spectral library by computing their mean. *In situ* measured crop spectra and soil spectra measured from 390 nm to 2500 nm at 1 nm interval. These field spectra are extracted in the harmony with AVIRIS-NG hyperspectral bandwidth.

### **3.2 Crop Discrimination using AVIRIS-NG Hyperspectral Data**

Crop classification over AVIRIS-NG data is performed by supervised classification technique, spectral angle mapper algorithm (SAM). SAM defines the spectral similarity between two spectra by calculating the angle between the spectra, treating them as vectors in a space with

dimensionality equal to the number of bands. SAM compares the angle between the spectrum vector of known class and each pixel vector of unknown class in the n-dimension space where n is the number of spectral bands. In the classification, the class with the smallest angle is assigned to the corresponding image pixel. The angle  $\alpha$  between the test spectrum  $t$  and the reference  $r$  is calculated as

$$\alpha = \cos^{-1} \left( \frac{(\sum_{i=1}^{nb} t_i r_i)}{\sqrt{\sum_{i=1}^{nb} t_i^2} \sqrt{\sum_{i=1}^{nb} r_i^2}} \right) \quad \dots (1)$$

where,

$nb$ = Number of bands in the image

$t$ = Test Spectrum

$r$ = Reference Spectrum

$\alpha$ = Spectral Angle

In this study, spectral subset of AVIRIS-NG data is used to perform the SAM classification. Bands responsible for atmospheric noise such as 1351-1420; 1800-2020; 2370-2500 are removed during the analysis. Spectral library generated from ground based mean crop and soil spectra are applied as an input in classification algorithm as reference spectra. Single threshold value, 0.1 radian is given to all the classes. The maximum acceptable angle between the test spectrum vector and the pixel vector is 0.1 radian. The flow of overall methodology is given in figure 13.1.

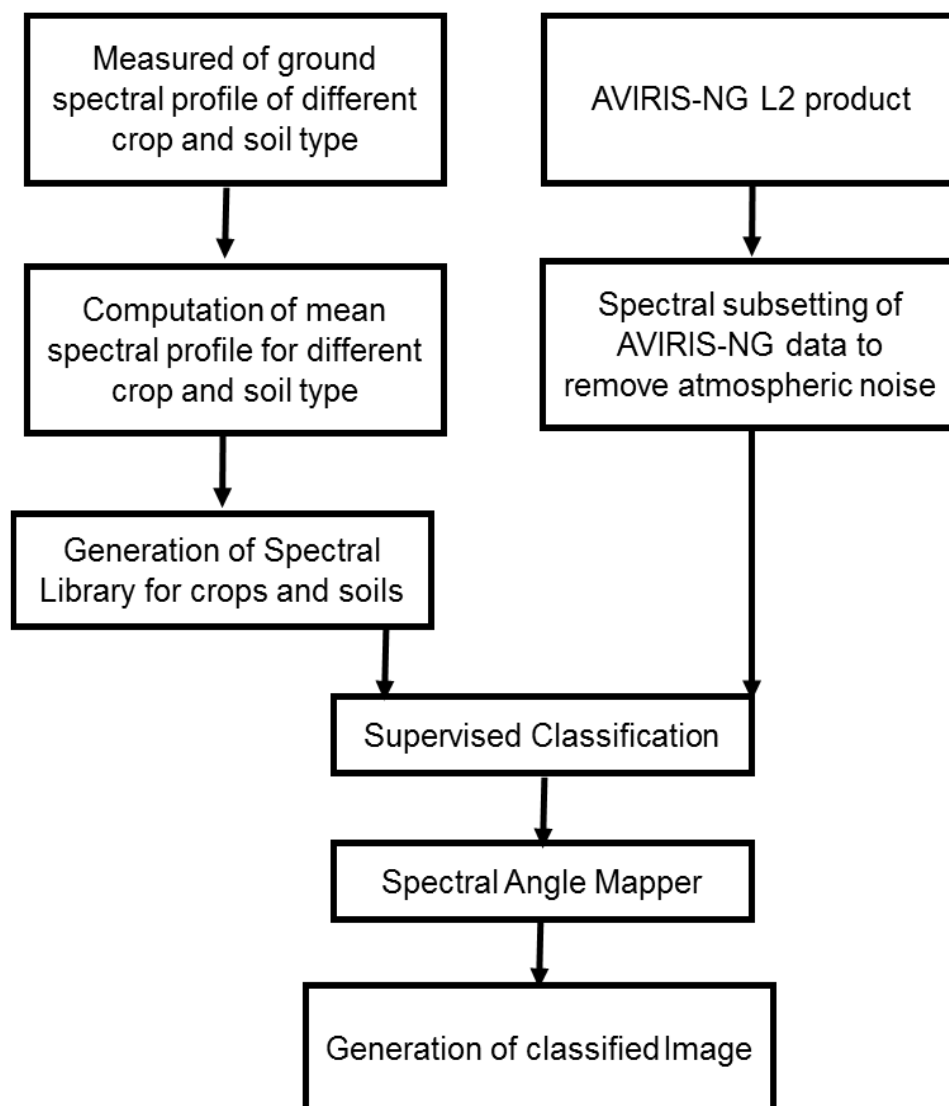


Figure 13.1. Flow of methodology for classification

### 3.3 Crop Discrimination using LISS-IV Multispectral Data

To estimate applicability of above stated methodology of crop discrimination similar steps are performed using LISS-IV data. AVIRIS-NG image and ground based crop and soil spectra are convoluted by applying relative response function of 3 bands of LISS-IV data. Spectral library is generated using crop and soil spectra equivalent to LISS-IV data. Spectral subset of AVIRIS-NG image data is created using 520-590; 620-680 and 770-860 nm bands equivalent to LISS-IV data. After generation of LISS-IV equivalent data from AVIRIS-NG image and ground data SAM algorithm is applied over the data. Single threshold value, 0.1 radian is given to all the classes. This classification scheme shows poor classification results and generated.

### 4. Outcome

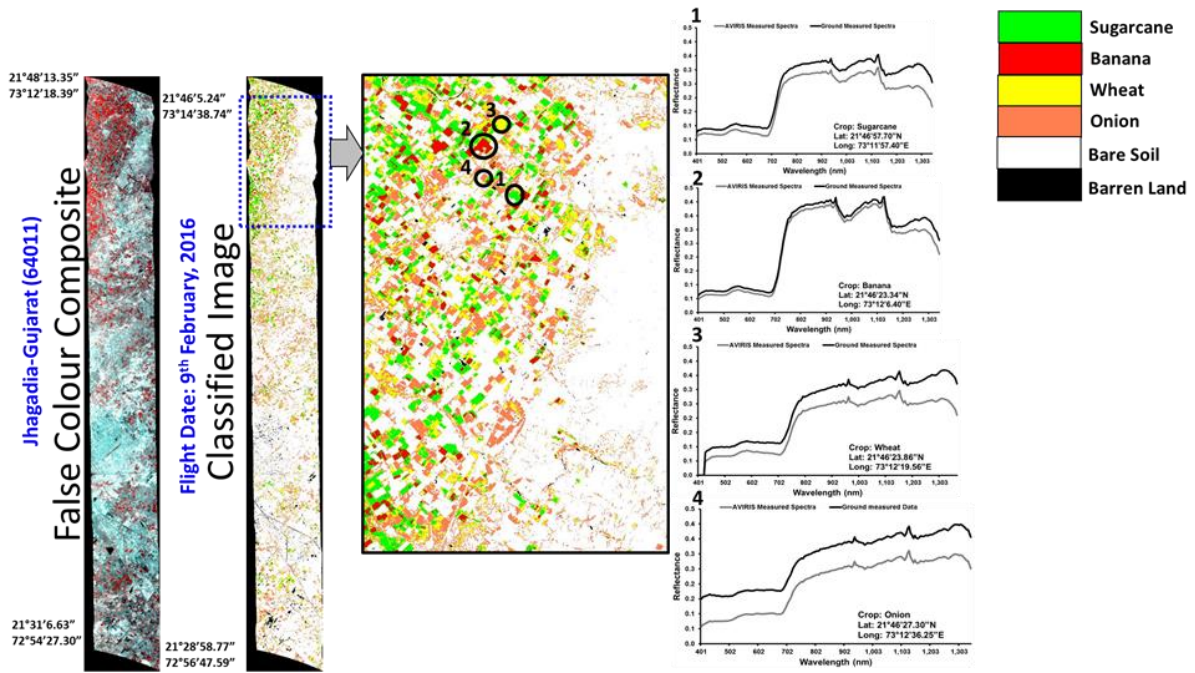


Figure 13.2. Spatial crop classified map using AVIRIS-NG data and validation with independent ground dataset over Jhagadia site 1.

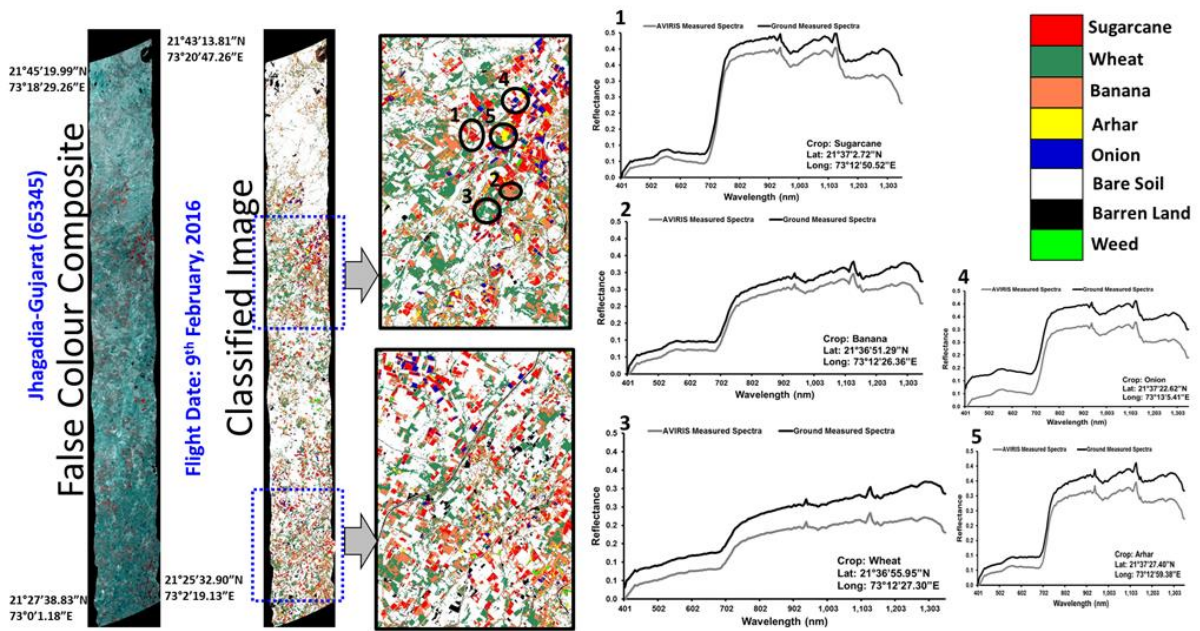


Figure 13.3. Spatial crop classified map using AVIRIS-NG data and validation with independent ground dataset over Jhagadia site 2.

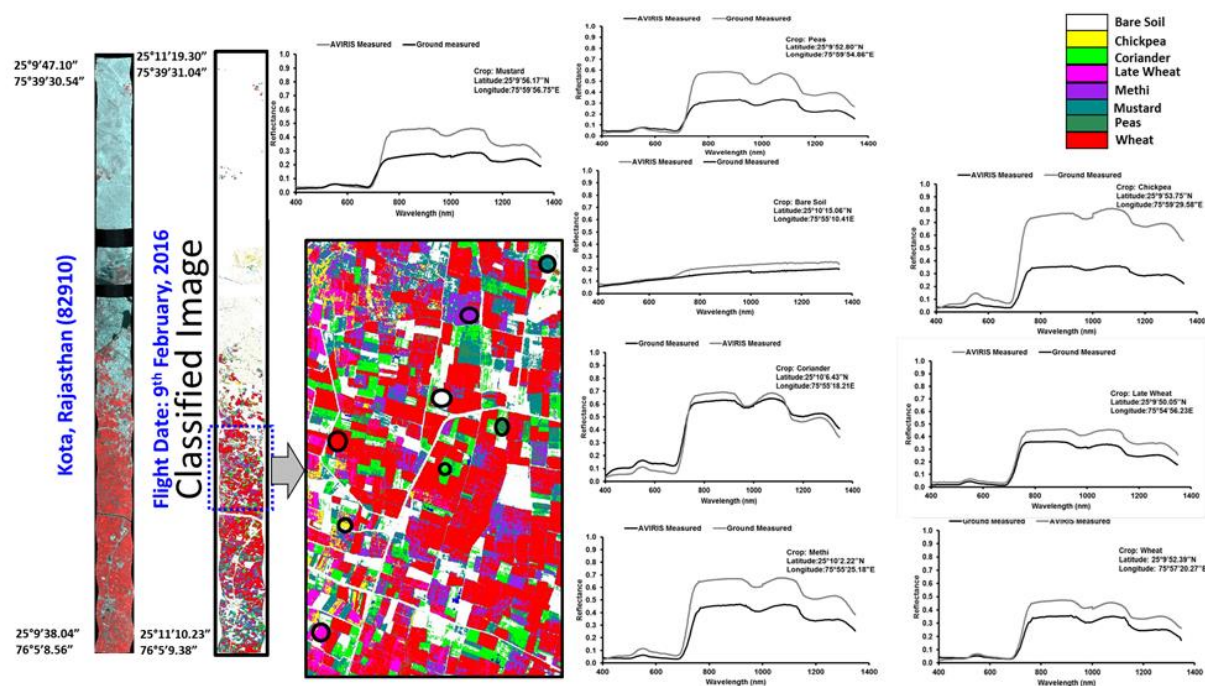


Figure 13.4. Spatial crop classified map using AVIRIS-NG data and validation with independent ground dataset over Kota site 1.

Crop discrimination is successfully achieved through spectral angle mapper over homogeneous and heterogeneous agricultural area using AVIRIS-NG hyperspectral data. SAM algorithm determines the spectral similarity between two spectra by calculating the angle between them as vectors in a space with dimensionality equal to the number of bands ( $n$ ). SAM compares the angle between the reference spectrum and test spectrum in  $n$ -dimension space. Smaller angle represents closer matches to the reference spectrum. Spectral angle mapper is used to classify the selected crop types in Jhagadia, Gujarat and Kota, Rajasthan. Successful application of ground based crop and soil spectra over AVIRIS-NG hyperspectral data for crop discrimination proved strength of ground data. Validation of crop discrimination is done with independent in situ dataset. The comparison between AVIRIS-NG and ground data reveals that difference between two spectra is observed in magnitude whereas spectral curvature remains the same. In other words, both the spectra show same slope values for all bands. Magnitude difference is observed due to (i) exposure of soil within plant canopy, (ii) two or more crops within a pixel, (iii) atmospheric perturbations. Crop discrimination is successfully achieved over homogeneous and heterogeneous agricultural areas. Major advantage of hyperspectral data is inferred that efficient crop discrimination is achieved over

homogeneous and heterogeneous agricultural areas. Classification accuracy is estimated by computing confusion matrix. For Kota, overall classification accuracy 86.4 % and kappa coefficient 0.84 and for Jhagadia overall classification accuracy 81.8% and kappa coefficient 0.77 is achieved.

#### 4.1 Target vs. Achievement

<i>Target</i>	<i>Achievement</i>	<i>% remaining</i>
Crop Classification using different classification algorithms over five study sites (Jhagadia, Kota, Maddur, Raichur, Sundarbans) using AVIRIS-NG hyperspectral data	Crop classification for all five sites is achieved applying supervised classification technique Spectral Angle Mapper.	50%

#### 4.2 Linkage to societal benefits

At present, Indian agriculture is dominated (80%) by small holding farmers. Hence, to map this heterogeneity effort has been made with various type of multispectral optical and microwave sensor data with limited accuracy at landscape to regional scale. This data has a major limitation to discriminate minor crops which are grown simultaneously with the dominant crop types contribute to agriculture production under the category of cereal, pulses, oilseed, cash crop, medicinal and vegetables. Hence, mapping of these minor crops will boost our planning for national and international commodity market. Through present study mapping of minor crops can be achieved more accurately using one date hyperspectral data over multispectral temporal data. This study also feed to design of ISRO's future hyperspectral sensors for agricultural applications.

### 5. Conclusions

- In this study, crop discrimination over homogeneous and heterogeneous agricultural areas is carried out successfully by application of SAM algorithm.
- Study also proved potential of AVIRIS-NG hyperspectral imagery to accurately discriminate and map different crop types.
- AVIRIS-NG data is up scaled to LISS-IV spectral bands with same spatial resolution and classification with similar scheme showed poor classification results.

- In future, such mission gives us better understanding of high economic value minor (pulses, oilseed, medicinal, cash crops) crops. Moreover, multi-year data will help us to generate spectral libraries for various crop type and soil. This will further help to understand the crop rotation at field scale.
- In future mission our target will be for discrimination of cultivar type for same crop with in a study site as well across the study sites.

## Acknowledgements

Authors would like to thank Shri A. S. Kiran Kumar, Chairman, ISRO, for his keen interest and support in the science activities of AVIRIS-NG Campaign. We would also like to thank Dr. Tapan Misra, Director, Space Applications Centre (ISRO), Ahmedabad for his kind support and encouragement to carry out this study. We would also like to extend our thanks to AVIRIS-NG Science Team for their continuous guidance and support.

## References

Mariotto, I., Thenkabail, P.S., Huete, A., Sloncker, E.T., Platonov, A. (2013) Hyperspectral versus Multispectral crop-productivity modeling and type discrimination for the HypsIRI mission, *Remote Sensing of Environment*, 139, 291-305.

Ozdogan, M., Woodlock, C.E., 2006. Resolution dependent errors in remote sensing of cultivated areas. *Remote Sens. Environ.* 103, 203-217. <http://dx.doi.org/10.1016/j.rse.2006.04.004>.

Thenkabail, P.S. (2001) Optimal hyperspectral narrowbands for discriminating agricultural crops. *Remote Sensing reviews*, 20:4, 257-291, DOI: 10.1080/02757250109532439.

# Fine Level Classification of Mango Orchards Using AVIRIS-NG Hyperspectral Data

Rohit Nagori

Space Applications Centre, Ahmedabad, Gujarat, India

## ***1. Scientific rationale and Objectives***

Mango is an important horticultural crop in India with large varieties of it and some are even possessing the Geographic Indicator (GI) tag. Optical data such as LISS IV (three bands of Green, Red and NIR; spatial resolution of 5.8 m) obtained from ResourceSat-2 satellite by India helps to discriminate it from other agricultural crops using textural properties. However, when orchards of different types are present or combination of different trees exists in the orchards such as mango and sapota, multispectral data consisting of 3 or 4 bands fails in further discrimination due to spectral inseparability. Hyperspectral data such as from AVIRIS-NG having higher spatial and spectral resolution are able to notice minute changes in spectral response of different species and thus discriminate to a much finer level. However, challenging problems of redundancy, intensive computation, etc. are posed by the hyperspectral data due to high dimensionality. So in order to reduce dimensions without losing the critical information, band selection method (selecting subset of original bands) is preferred over band extraction method (transforming the dataset to different space and then selecting bands) as physical meaning of data remains unchanged. Vaiphasa et al. (2007) in their study found that GA-based band selector was able to cope with spectral similarity at the species level. It meaningfully selected spectral bands that related to principal physio-chemical properties of plants, and, simultaneously, maintained the separability between species classes at a high level. Ullah et al. (2012) investigated the performance of genetic algorithms coupled with the spectral angle mapper (SAM) to identify a meaningful subset of wavebands sensitive enough to discriminate thirteen broadleaved vegetation species from the laboratory measured hyperspectral emissivities. For the multiple plant species, the targeted bands based on genetic algorithms resulted in a high overall classification accuracy (90%).

There are primarily two objectives of our study. The first objective is to develop a classification algorithm to perform fine level classification of mango orchards. The second objective is to find a few selective bands that can effectively classify without utilizing whole dataset and to study the importance of such bands if any.

## ***2. Study area and data used***

Talala taluka of Junagadh district, Gujarat is the hub of 'Gir Kesar' mangoes (*Mangifera Indica*) which also have GI (Geographical Indicator) tag. The region is largely occupied by Mango Kesar orchards with few orchards of sapota or orchards having intercropping of Mango Kesar with other plants such as banana, etc. The agricultural fields of wheat, coriander are also present in the region.

AVIRIS-NG airborne campaign over site id 155 imaged Talala on 13 February 2016 which has been utilized in our study. Ground truth data was collected synchronously with the imaging date by the team consisting of Dr. Saroj Maity, Dr. Dipanwita Haldar, Rohit Nagori, Viral A. Dave and Sneha Thakur. Various atmospheric parameters of aerosol, ozone concentration, water vapour amount were also collected. Figure 14.1 shows the study site.

## ***3. Methodology***

In supervised classification, a classification algorithm is trained using a training set and then used to classify a testing set. If this classification algorithm is placed inside an optimization problem such that the variable to be optimized is chosen as the bands and cost function is the classification accuracy, it can identify those bands which will ensure maximum classification accuracy and these bands may be indicative of some specific bio-physical or bio-chemical properties too which brings out the variation in the spectra of these species. As the classification algorithm is wrapped inside the feature selection algorithm, it is called as wrapper based classification. Figure 14.2 shows the whole methodology adopted.

In this study, the optimization problem of genetic algorithm has been selected. Genetic algorithms, introduced for the first time by Holland (1975), are a popular type of evolutionary optimization computation based on the concept of natural selection. Genetic algorithms (GA) is a general adaptive optimization search methodology based on a direct analogy to Darwinian natural selection and genetics in biological systems.

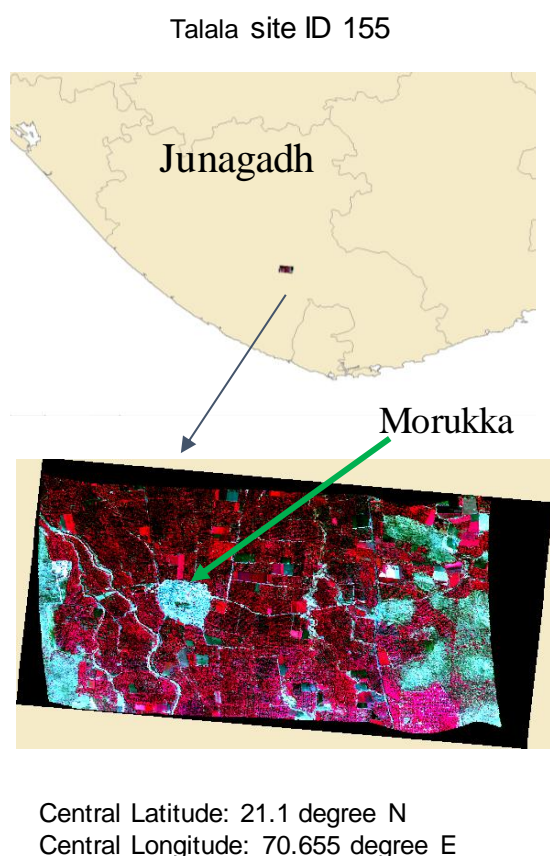


Figure 14.1. Figure showing the study site of Talala (up) and AVIRIS-NG image over the same (down).

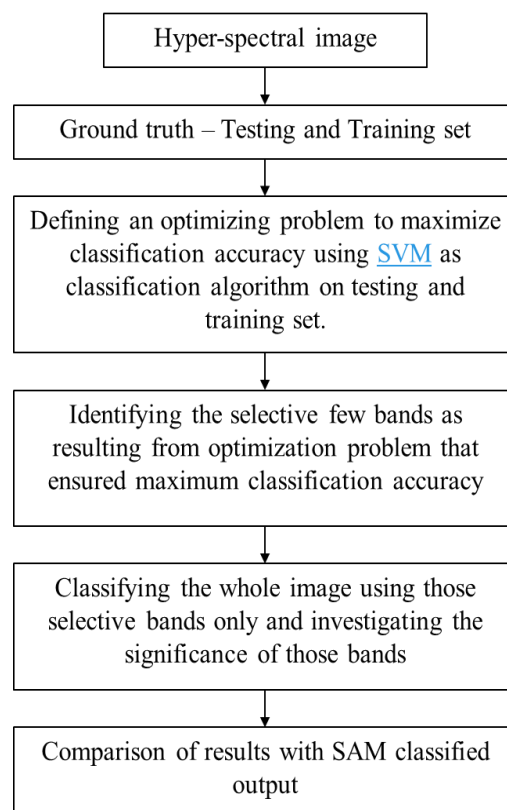


Figure 14.2. Flowchart showing the methodology adopted for the classification.

Based on the principle of ‘survival of the fittest’, GA works with a set of candidate solutions called a population and obtains the optimal solution after a series of iterative computations (Zhuo et al., 2008). The classification algorithm that has been chosen is Support Vector Machine. The SVM separates the classes with a decision surface that maximizes the margin between the classes. The surface is often called the optimal hyperplane, and the data points closest to the hyperplane are called support vectors. The support vectors are the critical elements of the training set. While SVM is a binary classifier in its simplest form, it can function as a multiclass classifier by combining several binary SVM classifiers (creating a binary classifier for each possible pair of classes) (Zhuo et al., 2008). In the developed algorithm, the optimization problem, i.e., genetic algorithm is supplied with an input of number of bands. It creates a variable of size of number of bands and generate a population in which different combination of bands are taken and passed into the cost/fitness function.

The bands which minimize the cost function the most are chosen as best parents. The cost function in our study is the negative of classification accuracy achieved while classifying a testing set using Support Vector machine trained over testing set. Then iteratively parents are chosen at random from the population and acted upon by the bio-operators of mutation and crossover in order to generate newer population which is passed to cost function. The process is repeated till an optimal solution is reached. The number of bands are repeatedly increased to a point where increase in number of bands doesn't lead to an appreciable increase in the classification accuracy. For that a function has been defined which is the weighting sum of classification accuracy and inverse of number of bands.

$$f(x) = (-wf_1 \times CA) - \left(\frac{wf_2}{n\_bands}\right) \quad \dots (1)$$

where 'CA' represents classification accuracy (as a fraction, ex: 0.8744) and 'n\_bands' represents number of bands utilized. The value of  $wf_1$  and  $wf_2$  is chosen as 0.95 and 0.05 respectively. The loop compares the function value of two previous consecutive runs and if value of function has increased, it stops.

## 4. Outcome

### 4.1 Salient findings

In this study, a comparison has been made between the potential of traditional Spectral Angle Mapper classifier and wrapper based classification algorithm in species level classification of orchards in hyper spectral images. In wrapper based classification algorithm, as the number of bands increased, initially the maximum classification accuracy that can be achieved with given number of bands rapidly increased afterwards becoming constant. A maximum classification accuracy of 87.44 % was achieved with 9 bands which are positioned at wavelengths of 386.4 nm, 551.74 nm, 717.03 nm, 917.38 nm, 1122.73 nm, 1333.10 nm, 2019.28 nm, 2399.94 nm and 2435.00 nm. With the same training and testing set, a classification accuracy of mere 67.44 % was achieved with Spectral Angle Mapper using whole dataset. A post flight validation supported the better classification achieved with wrapper based classification highlighting its effectiveness. As shown in figure 14.3 (b) and (c), region 1 shows mango with banana in SAM classified output but only mango in wrapper based

classified output. The ground truth validation just shows the presence of mango with no trace of any other species. In region 2, ground truth validation shows a highly dense sapota orchard as seen in wrapper based classified output in contrast to SAM classified output. However large areas in wrapper based classification were found as unclassified in comparison to SAM output.

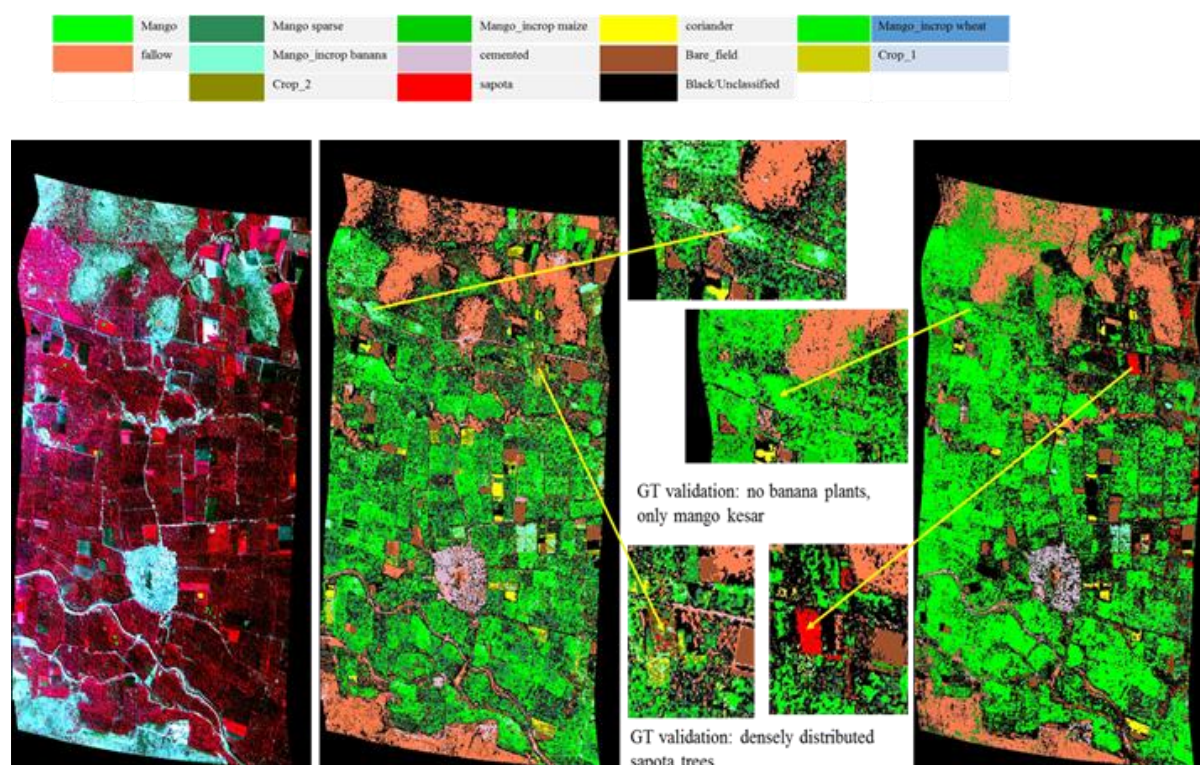


Figure 14.3. Figure showing FCC of a.) AVIRIS-NG image over Talala (left), b.) SAM classified image (middle) and c.) wrapper based classified output (right).

## 4.2 Target vs. Achievement

With the AVIRIS-NG data having ample amount of information in large number of narrow bands, it was possible to achieve the species level classification. The target to develop the classification algorithm that can ensure much better classification accuracy as compared to the traditional classifiers has been achieved. Furthermore, with the algorithm developed, we were able to find selective few bands that can effectively classify without the usage of whole dataset that contains a lot of redundant information.

## 4.3 Linkage to societal benefits

The study provided an improved classification for the mango orchards in the selected region using hyperspectral image. Usage of this algorithm may lead to more accurate inventory

development as required under the CHAMAN project. Furthermore, the importance of selected few bands identified and their relationship with bio-physical and bio-chemical parameters can be explored in several other images too such that those band regions can be used in future multispectral sensors.

## **5. Conclusions**

- Algorithm development completed and validated.

## **Acknowledgements**

Author is grateful to Shri Tapan Mishra, Director SAC (ISRO), Ahmedabad, Dr. Bimal Bhattacharya, Dr. A. S. Arya for their support and encouragement to carry out this study. I specially thank Ground Truth Team from SAC and Viral A. Dave from Anand Agricultural University for providing their support and contribution in the Ground Truth Data collection. I also acknowledge JPL and ISRO AVIRIS-NG campaign team for providing data for analysis.

## **References**

Holland, J. *Adaptation in Natural and Artificial Systems*; University of Michigan: Ann Arbor, MI, USA, 1975.

Ullah, S.; Groen, T. A.; Schlerf, M.; Skidmore, A. K.; Nieuwenhuis, W. and Vaiphasa, C. Using a Genetic Algorithm as an Optimal Band Selector in the Mid and Thermal Infrared (2.5–14  $\mu\text{m}$ ) to Discriminate Vegetation Species. *Sensors* 2012, 12, 8755-8769.

Vaiphasa, C.; Skidmore, A.K.; de Boer, W.F.; Vaiphasa, T. A hyperspectral band selector for plant species discrimination. *ISPRS J. Photogram. Remote Sens.* 2007, 62, 225–235.

Zhuo, L.; Zheng, J.; Wang, F.; Li, X.; Ai, B. and Qian, J. A Genetic Algorithm based Wrapper Feature Selection method for classification of hyperspectral images using Support Vector Machine. *The International Archives of the Photogrammetry, Remote Sensing and Spatial Information Sciences*. Vol. XXXVII. Part B7. Beijing 2008.

# Comparison of Crop discrimination from AVIRIS-NG and LISS-IV over agricultural area

Rahul Nigam, Rajsi Kot\* and Bimal K Bhattacharya

Agriculture and Land Eco-System Division (AED), BPSG/EP  
Space Applications Centre (ISRO) Ahmedabad 3800 15 INDIA.

\*M. G. Science Institute, Ahmedabad 380009 INDIA Centre, Ahmedabad, Gujarat, India

## ***1. Scientific rationale and Objectives***

Accurate and efficient crop discrimination is a key requirement for precision agricultural management. Cropland characterization in terms of crop type and health are very important in order to study cropping system, crop rotation and stresses (Richards and Jia, 1999). Technological growth in the field of remote sensing provides a path for precision agricultural practices by accurate mapping of crop type and health indicators. Multispectral satellite technologies have been commonly used for various mapping of agricultural area (Ferrato and Forsythe, 2013). In a single observation, multispectral sensors generate three to six spectral bands information that range from visible to near infrared (NIR) portion of the electromagnetic spectrum (Ferrato and Forsythe, 2013). These traditional multispectral broadband sensor data have known limitations of providing limited information about crop type and health. These factors lead to significant uncertainties in various agricultural applications. During the last decade, advances in imaging spectrometer have begun to fill the gap in multispectral sensor limitations. Hyperspectral sensors commonly collect more than 200 narrow contiguous spectral bands that range from the visible to shortwave infrared section of the electromagnetic spectrum (Ferrato and Forsythe, 2013). The continuous availability of hyperspectral imagery, which records hundreds of image corresponding to different wavelength channels has opened new avenues in the field of crop type discrimination, yield, biomass and area estimation and various biophysical and biochemical parameters estimation. Availability of AVIRIS-NG hyperspectral data in discrete narrowbands provide us an opportunity to study crop type discrimination. The primary objective of this

study is to compare discrimination of crop type using hyperspectral and multispectral remote sensing data using one date AVIRIS-NG data.

## ***2. Study area and data used***

The study area is Maddur, Chamarajanagar, Karnataka. Maddur village is located in Gundlupet tehsil of Chamarajanagar district in Karnataka, India. It is situated 16 km away from the sub-district headquarter Gundlupet and 52 km away from district headquarter Chamarajanagar. Chamarajanagar falls in the southern arid agro-climatic zone of Karnataka. The climate of Chamarajanagar district is quite moderate throughout the year with fairly hot summer and cold winter. The mean maximum temperature ranges from 32.6°C to 34°C in the summer. Overall, the mean maximum temperature in the district is 34°C and the mean minimum temperature is 16.4°C. Relative humidity ranges from 69 to 85% in the morning and 21% to 70% in the evening. Average rainfall of the district is 731.80 mm yearly. Major soil types are reddish brown forest soil, yellowish grey to greyish sandy loam soils and mixed soils. Major crops are paddy, ragi, sorghum, jowar, maize, gram, tur, other pulses, sunflower and other oilseeds and vegetables. During the field campaign of AVIRIS-NG cotton, field beans, Horsegram, tomato, turmeric, pulses, maize, beans, cabbage, carrot, banana, chili, brinjal, sugarcane, beetroot, garlic and potato was observed. In this study for crop discrimination, ground based hyperspectral data collected during AVIRIS-NG field campaign and airborne hyperspectral imagery of AVIRIS-NG are used. During the field campaign, locations of various crops were recorded using hand held GPS and spectral information from spectroradiometer data.

## ***3. Methodology***

### **Pre-processing of AVIRIS-NG data and image generation equivalent to LISS-IV**

In situ crop locations are collected for different crop type during the during the AVIRIS-NG field campaign in harmony with air borne data collection. Region of interest (ROI) are generated from the ground measured data. Relative response function of LISS IV is applied to AVIRIS-NG data in order to generate equivalent LISS-IV multispectral data. Three bands are retrieved after the application of relative response function of LISS-IV.

### **Principal Component Analysis, Spectral Angle Mapper and MXL classification**

Hyperspectral imaging provides the advantage in many applications that are often difficult with multispectral imaging. Although, hyperspectral remote sensing may cause new difficulties in data analysis and image processing due to its high data dimensionality and redundancy. These difficulties can lead to low classification accuracy. Therefore, hyperspectral data analysis involves crucial attention to data compression. Reducing dimensionality in a large dataset while maintaining the data and their complexity is the requirement for crop discrimination (Tsai et al., 2007). Principal components analysis (PCA) is a general tool used for reducing data dimensionality in remote sensing image processing. The process of PCA can be divided into three steps:

- Calculation of the covariance matrix of multi-band images.
- Extraction of the eigenvalues and eigenvectors of the matrix.
- Transformation of the feature space coordinates using these eigenvectors.

In this study, PCA was applied to AVIRIS-NG hyperspectral image data and LISS-IV equivalent image. First five principal components (PCs) from AVIRIS-NG image and first two PCs are selected to perform crop classification. Based on collected in situ crop information ROIs are generated for AVIRIS-NG data. The classification over AVIRIS-NG data is performed by supervised classification technique, spectral angle mapper algorithm (SAM). SAM defines the spectral similarity between two spectra by calculating the angle between the spectra, treating them as vectors in a space with dimensionality equal to the number of bands. SAM compares the angle between the spectrum vector of known class and each pixel vector of unknown class in the n-dimension space where n is the number of spectral bands. In the classification, the class with the smallest angle is assigned to the corresponding image pixel. The angle  $\alpha$  between the test spectrum  $t$  and the reference  $r$  is calculated as:

$$\alpha = \cos^{-1} \left( \frac{(\sum_{i=1}^{nb} t_i r_i)}{\sqrt{\sum_{i=1}^{nb} t_i^2} \sqrt{\sum_{i=1}^{nb} r_i^2}} \right) \quad \dots (1)$$

Where, nb = Number of bands in the image; t= Test Spectrum; r= Reference Spectrum;  $\alpha$ = Spectral Angle.

In this study, Single threshold value, 0.1 radian is given to all the classes. The maximum acceptable angle between the test spectrum vector and the pixel vector is 0.1 radian. The flow of overall methodology is given in figure 15.1. Maximum likelihood classification is commonly used for supervised classification technique based on the conditional probabilities of pixel vectors. In this classifier, training data is used to estimate the conditional probabilities and these conditional probabilities are used to develop the maximum likelihood decision rule. MLC can result in high classification accuracy if the data distribution is multivariate normal and adequate numbers of training samples. The accuracy of MLC depends upon the accuracy of the mean vector and covariance matrix estimated for the classes. If N features are used for classification, the training set for each class must contain a minimum of N+1 pixels in order to calculate the sample covariance matrix. In this study, MLC is also applied on PCs derived AVIRIS-NG hyperspectral and LISS-IV equivalent multispectral data.

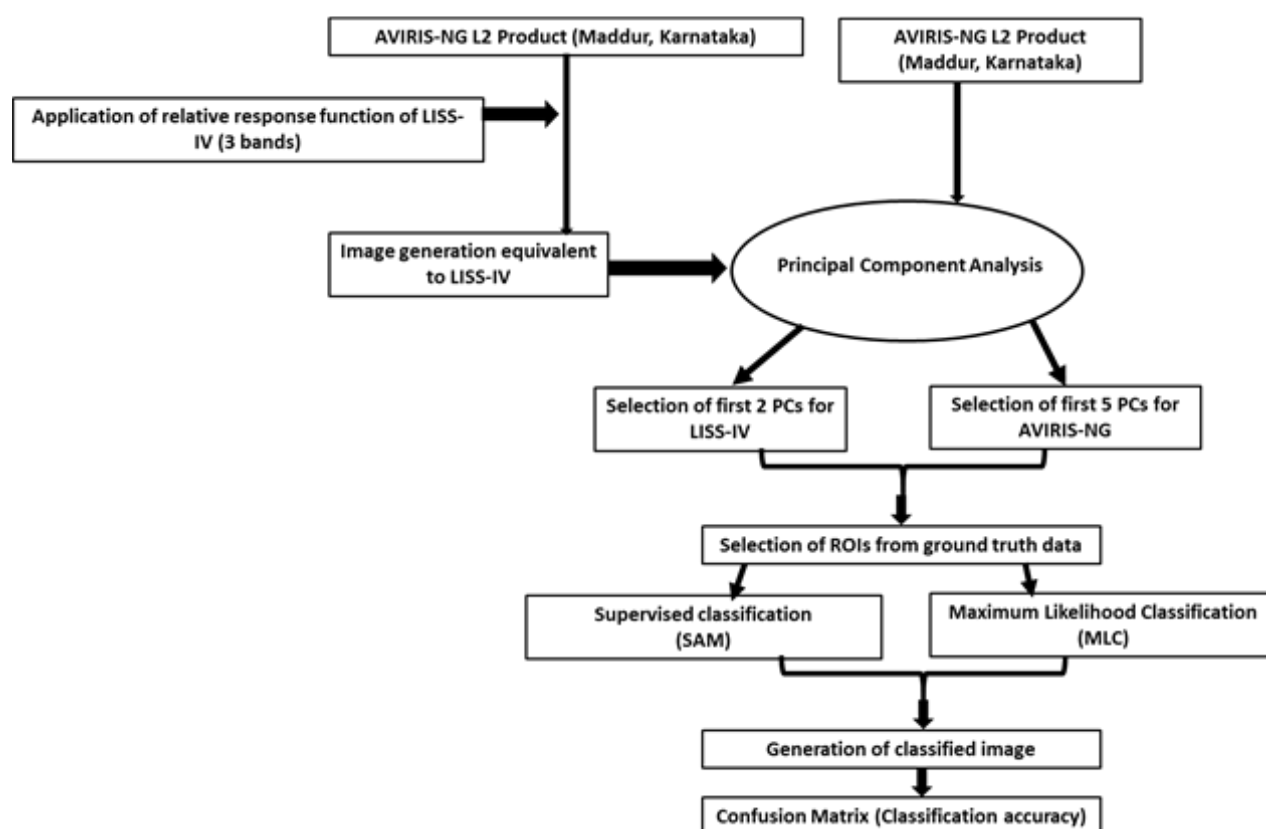


Figure 15.1. Flow of methodology for classification

## 4. Outcome

### 4.1 Salient findings

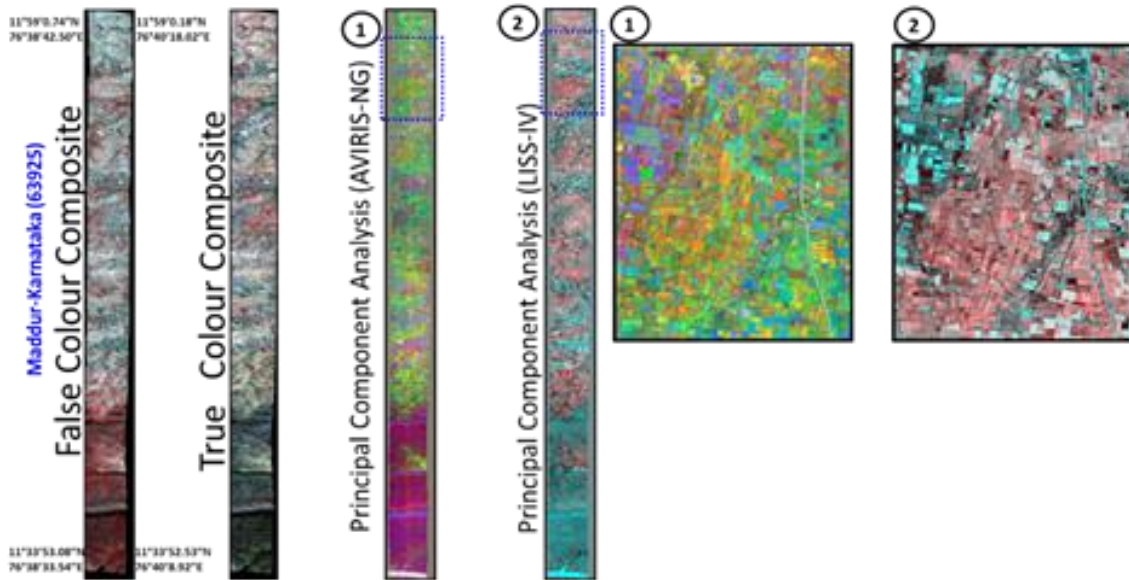


Figure 15.2. Principal components analysis using AVIRIS-NG and LISS-IV data

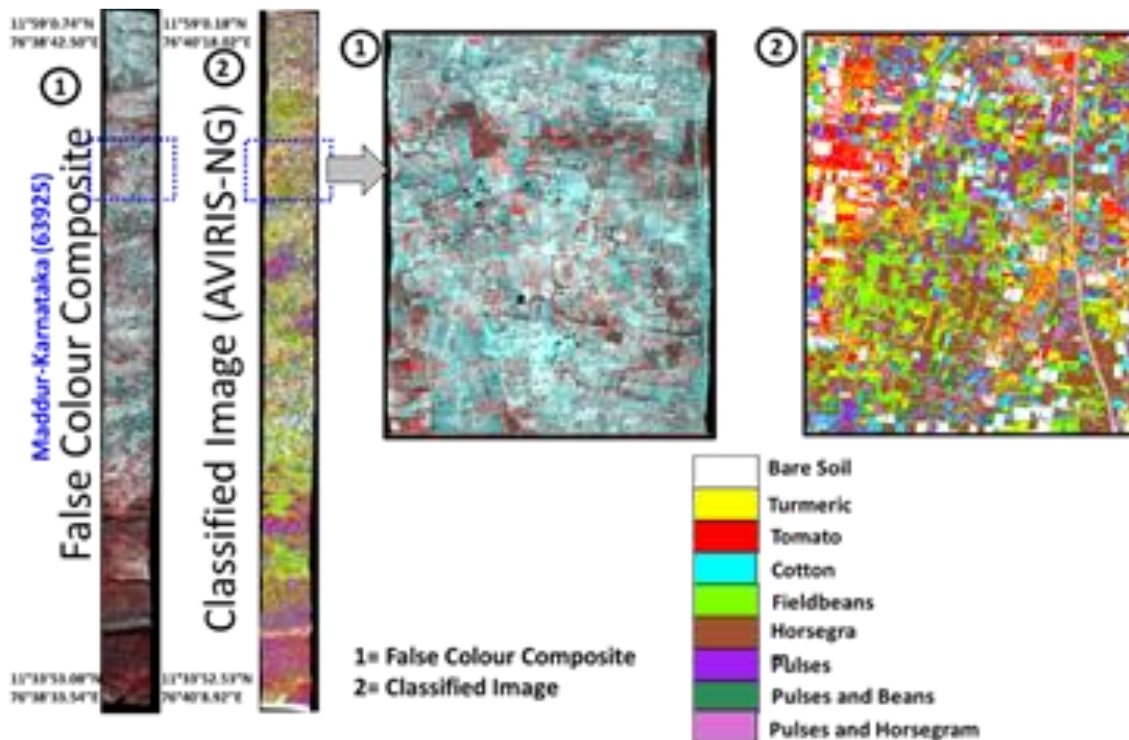


Figure 15.3. Crop classification using AVIRIS-NG data using spectral angle mapper algorithm

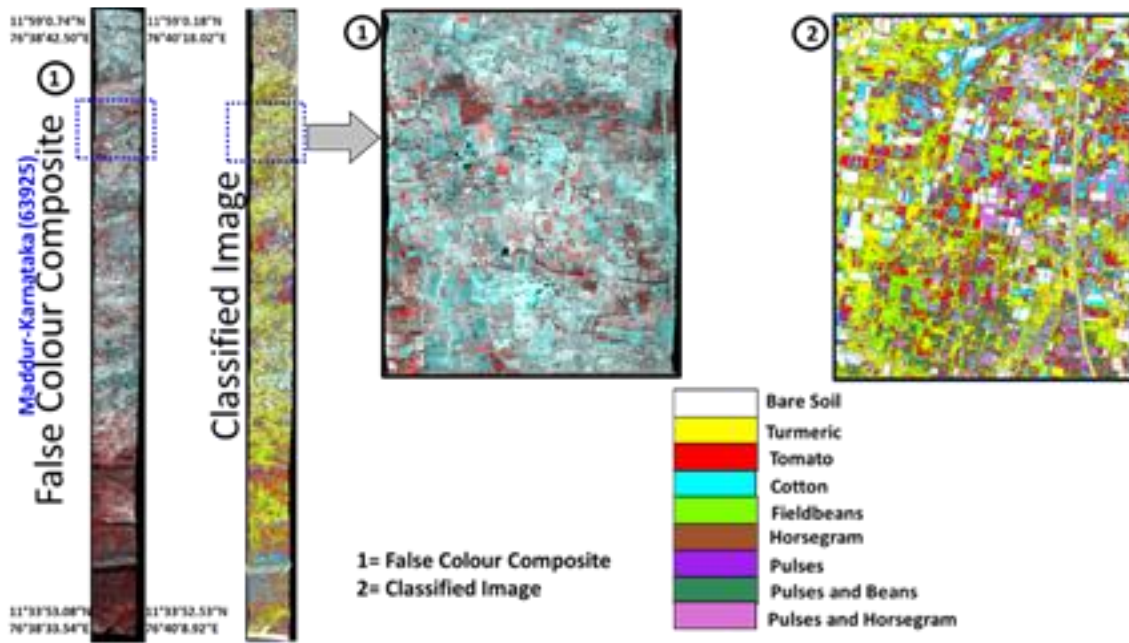


Figure 15.4. Crop classification using LISS-IV equivalent spectral data using SAM algorithm

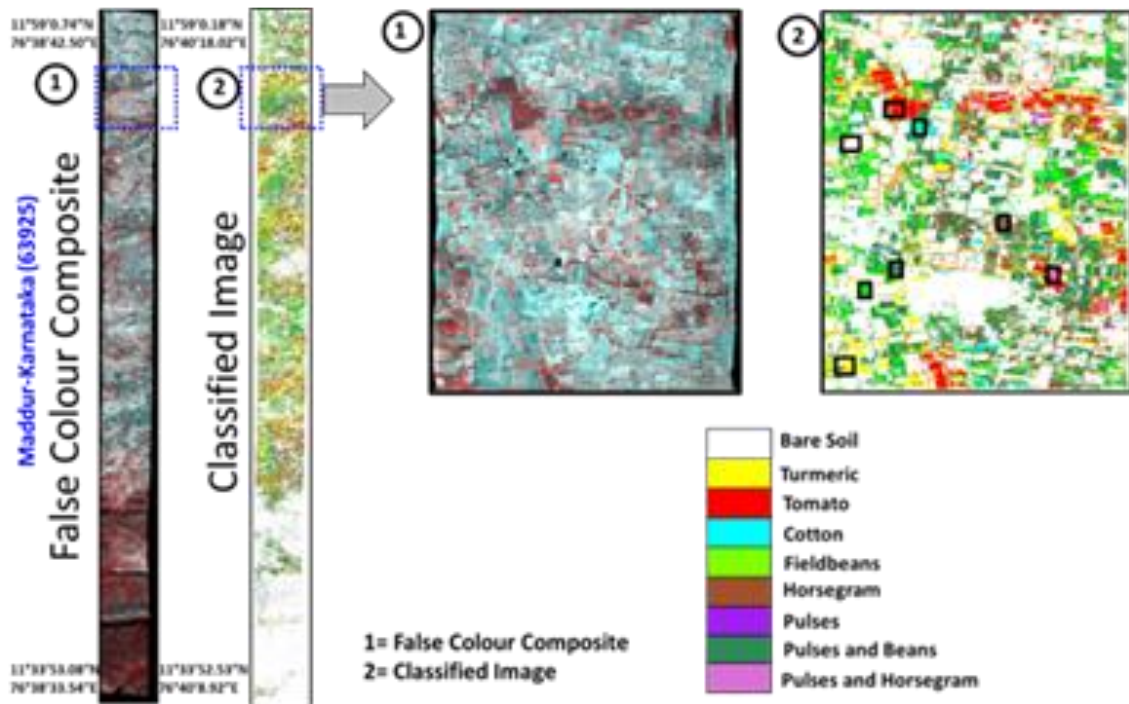


Figure 15.5. Crop classification using AVIRIS-NG data using maximum likelihood classification

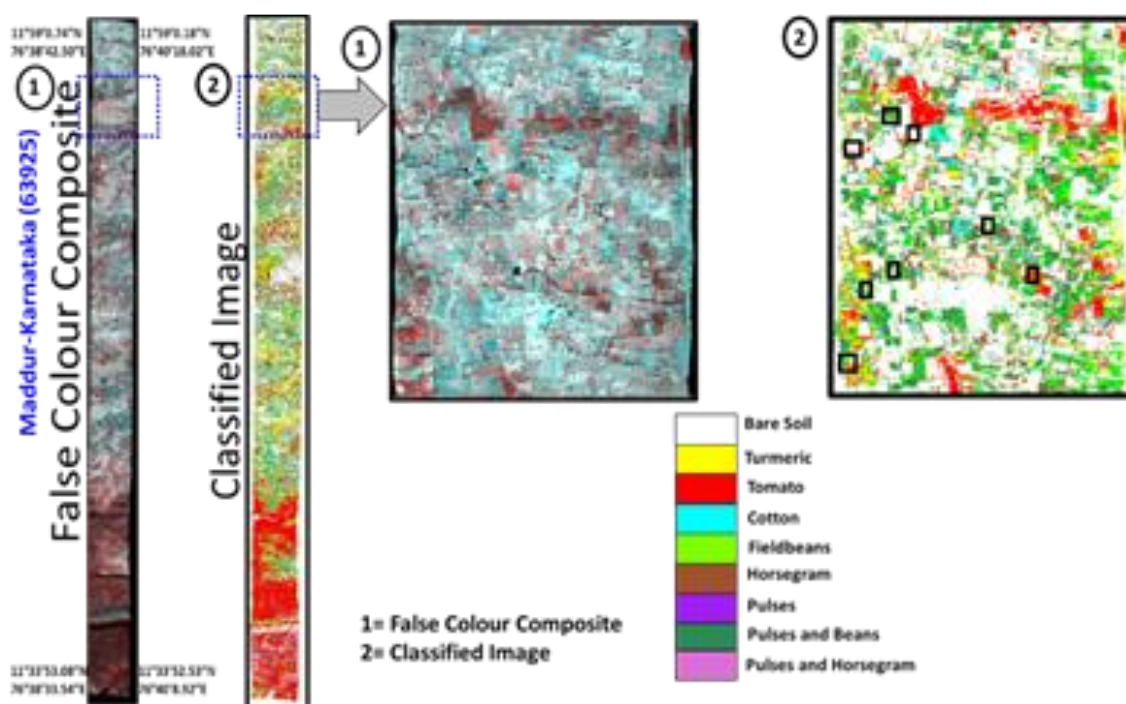


Figure 15.6. Crop classification using LISS-IV equivalent spectral data using maximum likelihood classification.

## 4.2 Linkage to societal benefits

Agriculture in India is mainly dominated by small holding farmers. Multispectral data has limitations to map crop type in heterogeneity agricultural area due to lower spectral resolution and sensor saturation. Recent advances in hyperspectral remote sensing demonstrate a great utility for crop discrimination in heterogeneous cropland. This study demonstrated that agricultural crops are better characterized, classified and mapped using AVIRIS-NG hyperspectral data in heterogeneous croplands. Hyperspectral remote sensing is well suited for crop discrimination of major and minor crops at landscape to regional level. Hence, mapping of these minor crops will boost our planning for national and international commodity market. This will also help to mapped the minor economical valuable crops such as medicinal, aromatic and cash crops. At present there is no information is available for such aforementioned crops from remote sensing data. This study also feed to design of ISRO's future hyperspectral sensors for agricultural applications.

## 5. Conclusions

- In this study, crop discrimination over AVIRIS-NG hyperspectral data and LISS-IV equivalent multispectral data is carried out successfully by application of principal component analysis and SAM and MLC classification algorithm.
- LISS-IV equivalent spectral bands showed poor classification accuracy as compare to AVIRIS-NG for same agriculture region.
- This study highlighted that hyperspectral data can improve accuracy of crop discrimination by 41 to 45% over multispectral data in heterogeneous agriculture area.
- In future, such mission gives us better understanding of high economic value minor (medicinal, aromatic, cash crops etc.) crops. Moreover, multi-year data will help us to generate spectral libraries for various crop type and soil. This will further help to understand the crop rotation at field scale.
- In future mission our target will be for discrimination of cultivar type for same crop with in a study site as well across the study sites.

## Acknowledgements

Authors would like to thank Shri A. S. Kiran Kumar, Chairman, ISRO, for his keen interest and support in the science activities of AVIRIS-NG Campaign. We would also like to thank Dr. Tapan Misra, Director, Space Applications Centre (ISRO), Ahmedabad for his kind support and encouragement to carry out this study. We would also like to extend our thanks to AVIRIS-NG Science Team for their continuous guidance and support.

## References

Ferrato L. J., Forsythe K.W., (2013) Comparing Hyperspectral and Multispectral Imagery for land Classification of the Lower Don River, Toronto, Journal of Geography and Geology, vol. 5, No.1,92-107.

Mariotto, I., Thenkabail, P.S., Huete, A., Sloncker, E.T., Platonov, A. (2013) Hyperspectral versus Multispectral crop-productivity modeling and type discrimination for the HypsIRI mission, Remote Sensing of Environment, 139, 291-305.

Ozdogan, M., Woodlock, C.E., 2006. Resolution dependent errors in remote sensing of cultivated areas. *Remote Sens. Environ.* 103, 203-217. <http://dx.doi.org/10.1016/j.rse.2006.04.004>.

Richards, J.A. and Jia, X., (1999) Segmented Principal components transformation for efficient hyperspectral remote sensing of image display and classification. *IEEE Transactions on Geoscience and Remote sensing*, 37, 538-542.

Thenkabail, P.S. (2001) Optimal hyperspectral narrowbands for discriminating agricultural crops. *Remote Sensing reviews*, 20:4, 257-291, DOI: 10.1080/02757250109532439.

Tsai, F., Lin, E.K., Yoshino, K. (2007) Spectrally segmented principal component analysis of hyperspectral imagery for mapping invasive plant species. *International Journal of Remote Sensing*, 28, 1023-1039.

## Identification and discrimination of sugarcane fresh v/s ratoon using AVIRIS-NG data

Sujay Dutta, Ashwini Muddaliar and Somnath Paramanik\*

AED/BPSG/EPISA

Space Applications Centre, ISRO, Ahmedabad, Gujarat, India

\*Coral Dept., IIT., Karagpur, India

### 1. *Scientific rationale and Objectives*

India is an agrarian economy and about two-thirds of its population are directly or indirectly involved in agriculture (National Portal Content Management Team, 2011). The agricultural sector contributes to the GDP by about 7% since 2001 (FAO, 2011). In India net area cultivated in 2011-12 is about 125.49 million hectares, or about 41 percent of the total reported area. Sugarcane occupies 4.7- 5.1 million hectares of cultivable land. India is currently the second-largest producer of sugarcane. The sugarcane crop consists of two growth stages namely sugarcane-fresh plantation (SFP) and sugarcane-ratoon (SR). The sugarcane -fresh plantation is the fresh seed that is sown in the field and has a 12 month growing season in India from February- March. Over the recent past, there has been a growing concern on the need for mapping sugarcane cropping areas in order to improve decision-making in the agricultural sector. The use of remote sensing images for identifying and mapping specific crops in the last few decades has increased rapidly. Although remote sensing has a great potential to be used with sugarcane, only a few reports have been developed in this area. There is still a lack of studies on spectral behavior using field radiometry, Hyperspectral sensors represent a further step in the continuing search for technologies to obtain information about the Earth's surface from a remote platform. Data from such systems comprise a large number of spectrally contiguous images, each acquired within narrow wave bands in the visible and infrared region of the spectrum. It is spectrally more powerful by acquiring the spectra of any target in a number of narrow spectral range. In recent years' image acquired from space platform namely hyperspectral Hyperion image acquired by the Earth-Observing (EO-1), and Airborne Visible/Infrared Imaging Spectrometer (AVIRIS), are used for improving agricultural

productivity and economy crop discrimination. The primary objective of this study is to discriminate sugarcane-fresh plantation (SFP) with sugarcane-ratoon (SR) using different classification techniques.

## 2. Study area and data used

The site selected for SFP and SR was Bharuch. Bharuch, a district in the state of Gujarat, India. It is situated on banks of Narmada river. Bharuch is geographically located at 21.7°N and 72.97°E. For the study area, data from the Next Generation Airborne Visible Infrared Imaging Spectrometer (AVIRIS-NG) was acquired on 11 February, 2016.

## 3. Methodology

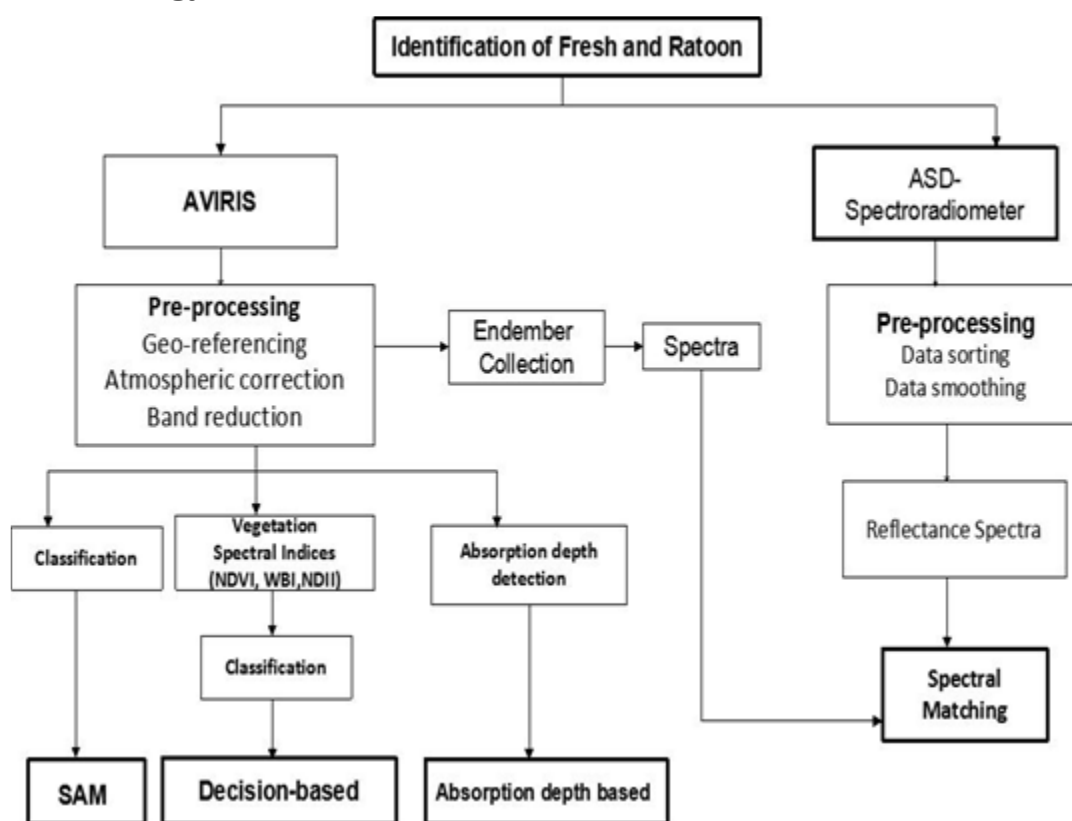


Figure 16.1. Methodology

## 4. Outcome

### 4.1 Salient findings

AVIRIS data was pre-processed and the reduced band were utilized for discriminating sugarcane fresh plantation (SFR) and Sugarcane-Ratoon (SR) Three techniques were used for

discriminating SFR and SR utilizing the AVIRIS-NG, viz. (a) Classification based on SAM; (b) Hierarchical decision rule classifier; (c) classification based on absorption depth. The SAM classification (figure 16.2 (a)) was performed without any spectral angle threshold specified to have more information on classifications between the crop classes SAM has come as a potential technique for discriminating the crop and its stages, many researchers have utilized this technique for various crop classification (Fahimnejad, et al., Apan, 2004, Shwetank et al., 2011, and Vijayan D. V., et al., 2014).

Hierarchical decision rule was utilized for classification of SFR and SR (figure 16.2(b)). Different Vegetation indices such as NDVI, WBI and NDII were. Utilizing different Spectral indices aided in understanding the combined interaction between a small numbers of wavelengths, which is adequate to describe the biochemical or biophysical interaction between light and matter. Narrowband vegetation indices have potential for crop type discrimination.



Figure 16.2. a.) SAM Classified, b.) Hierarchical Decision rule.



Figure 16.3. (a) AD (661.93-702.0nm), (b) AD (947.43-997.52nm)

Continuum Removal (CR), which is a normalization method, could emphasize the location and depth of individual absorption features by drawing a curve with the absorption value from 0 to 1 (Clark & Roush, 1984). CR is examined to show its usefulness for discriminating SFR and SR. CR was applied in two particular range of wavelength, one was applied in 661.93-702. nm (figure 16.3(a)) and other was applied in 947.43 - 997.52 nm (figure 16.3(b)). After continuum removal, absorption depth was applied to the image, which further aided in discriminating the SFR and SR. The best possible discrimination of SFR and SR can be seen in the 947.43 to 997.52 nm.

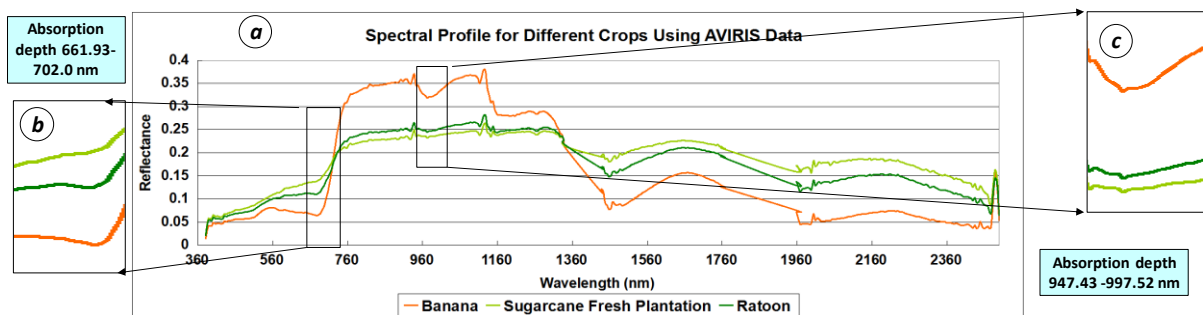


Figure 16.4. a.) AD (661.93-702.0nm), b.) AD (947.43-997.52nm)

Accuracy was carried out for SAM using Spectral matching. Ground collected ASD spectra were used as Reference (figure 16.4 (a)) and classified sugarcane (SR and SFR) areas spectra were generated with AVIRIS image, these two spectra were used for spectral matching.

Table 16.1. Percentage (%) error between retrieved Rrs and in-situ observations

<i>Classification Techniques</i>	<i>Spectral feature fitting score</i>	
	<i>Sugarcane Ratoon</i>	<i>Sugarcane Fresh plantation</i>
SAM	0.85	0.68
Hieararchial based descision rule	0.86	0.75
AD (661.93-702.0 nm) classification	0.84	0.79
AD (947.43-997.52 nm) classification	0.87	0.75

## 4.2 Linkage to societal benefits

Sugarcane production is linked to fresh and ratoon crop in India. Ratoon production declines up to half of the fresh planted crop. Knowing the areas of fresh v/s ratoon crop the production of sugar can be estimated more accurately. Therefore, in the recent past, there has been a growing concern on the need for mapping sugarcane cropping areas in order to improve decision-making in the agricultural sector. For an efficient agricultural resource management up-to-date information about the location of these crops is needed.

## 5. Conclusions

- Two or three-year data will help in better classification accuracy.
- Repeating the research is needed to establish its accuracy

## Acknowledgements

Author is grateful to Shri Tapan Mishra, Director SAC (ISRO).

## References

Fahimnejad, H., Soofbaf S.R., Alimohammadi A., Valadan Zoej, M. J., Crop Types Classification by Hyperion Data and Unmixing Algorithm, Map World Forum, GIS Development.

Apan, A., Held, A., Phinn, S, and Markley, J., 2004. Spectral discrimination and classification of sugarcane varieties using EO-1 Hyperion, Hyperspectral Imagery New Generation Sensors and Applications: Hyperspectral Sensing.

Shwetank, Jain K and Bhatia K, 2011 Development of Digital Spectral Library and Supervised Classification of Rice Crop Varieties Using Hyperspectral Image Processing Asian Journal of Geoinformatics, Vol.11, No.3.

Vijayan V, D., Ravi Shankar G., Ravi shankarT, 2014 The International Archives of the Photogrammetry, Remote Sensing and Spatial Information Sciences, Volume XL-8, 2014 ISPRS Technical Commission VIII Symposium, 09 – 12 December 2014, Hyderabad, India.

Clark, R.N., Roush, T.L., 1984. Reflectance spectroscopy: quantitative analysis techniques for remote sensing applications. *Journal of Geophysical Research*, 89(B7), pp. 6329-6340.

## Specific crop/Soil discrimination form AVIRIS Hyperspectral data

Anil Kumar, Justin George K and A. Senthil Kumar

Indian Institute of Remote Sensing, ISRO, Dehradun, India

### ***1. Scientific rationale and Objectives***

Generation of spectral library and crop/soil type discrimination.

### ***2. Study area and data used***

ICRISAT and Shadnagar (Hyderabad) Site.

### ***3. Methodology***

Crop/soil type discrimination - Our primary aim was to collect field data including crop and soil information as well as ground spectra using spectro-radiometer and soil samples from the corresponding locations, under conditions similar to flight condition. The sampling areas and sites were determined by interpretation of high resolution image (LISS IV and Cartosat) of the study area, which helped us to identify large agricultural patches and even helped us in identification of fallow as well cropped fields. The entire area was traversed with the help of satellite image and GPS. In the field, local variations were given importance, including change in soil colour, crop type and growth variations, land use land cover type etc. The study area was divided into grids for sampling purpose. The coordinates of each sampling location was recorded using GPS as well as the data was collected and uploaded using format described in Bhuvan Crop AVIRIS android app.

#### **Ground truth data collection**

Ground spectra of various targets/classes were collected using ASD Spectroradiometer. The data was collected at 1nm interval in the wavelength of 350 to 2500nm. The instrument was switched on nearly one hour before measurement, to ensure proper heating and the effect of dark current was corrected during calibration and white reference readings were also taken. The system was optimized before every spectra collection, by taking white reference

reading using reference plate/spectra to account for minute variation in illumination/local conditions.

During field campaign we have collected nearly 100 ground spectra comprising of various targets like soil, crops/vegetation, soil and vegetation, scrub land etc. Other accessory information including crop type, crop stage, crop health condition, soil type, surface wetness etc were also collected from the field.

The collected ground spectra were then grouped into various homogenous groups based on field observations. The soil spectra were grouped into three groups mainly black soil, red soil and mixed soil groups. In ICRISAT site, we could get ground spectra for nearly eight crops (cotton, red gram, bengal gram, jowar, tomato, chilli, niger and fodder grass).

Soil samples were also collected from various sampling locations, depending on the local variability and soil characteristics. The soil samples were collected by quartering process by mixing soil from different points in the area and then dividing them into required quantity (400 gm each). By this procedure, 140 soil samples were collected during the field campaign at ICRISAT and Shadnagar sites. These samples were transported to IIRS and were processed for sample preparation. The prepared samples are being analyzed to determine various physico-chemical and fertility parameters of soils from the study area.

## **4. Outcome**

### **4.1 Salient findings**

For crop/soil type discrimination, spectral Similarity Analysis between Ground Pure Spectra and Image Spectra for Different has been generated and similarity score has been generated. Classified outputs for ICRISAT area has been generated while extracting specific crop/soil types in area using segmentation based support vector machine based classification approach.

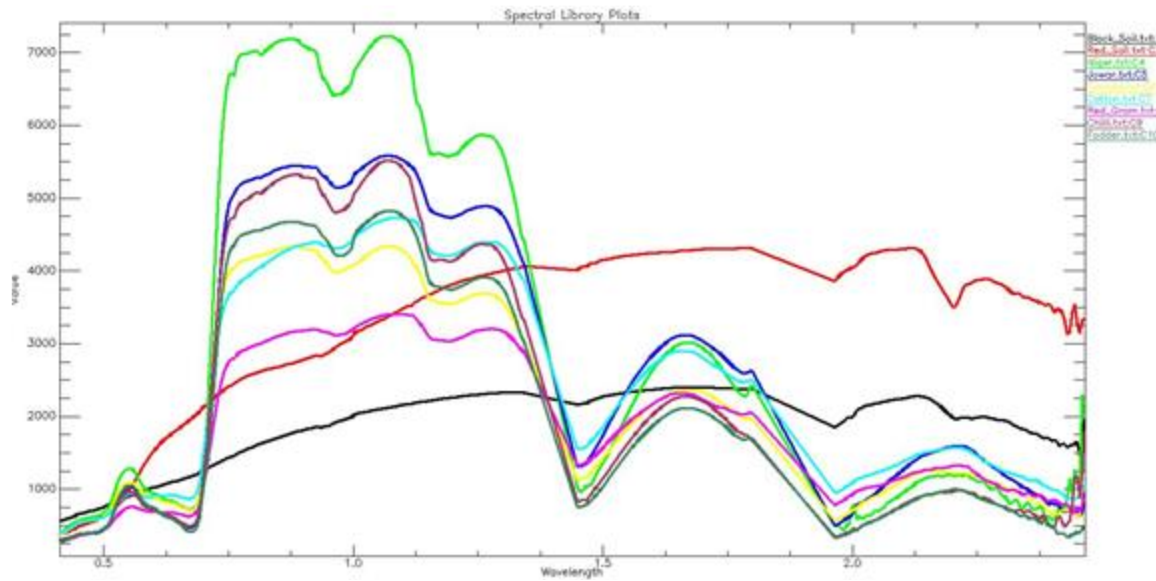


Figure 17.1. Ground Spectra for Different Crops/Soils

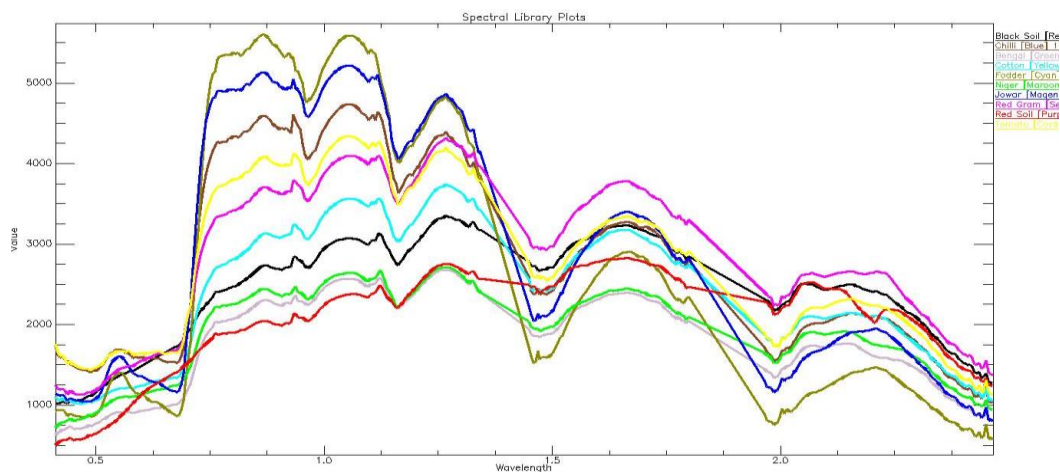
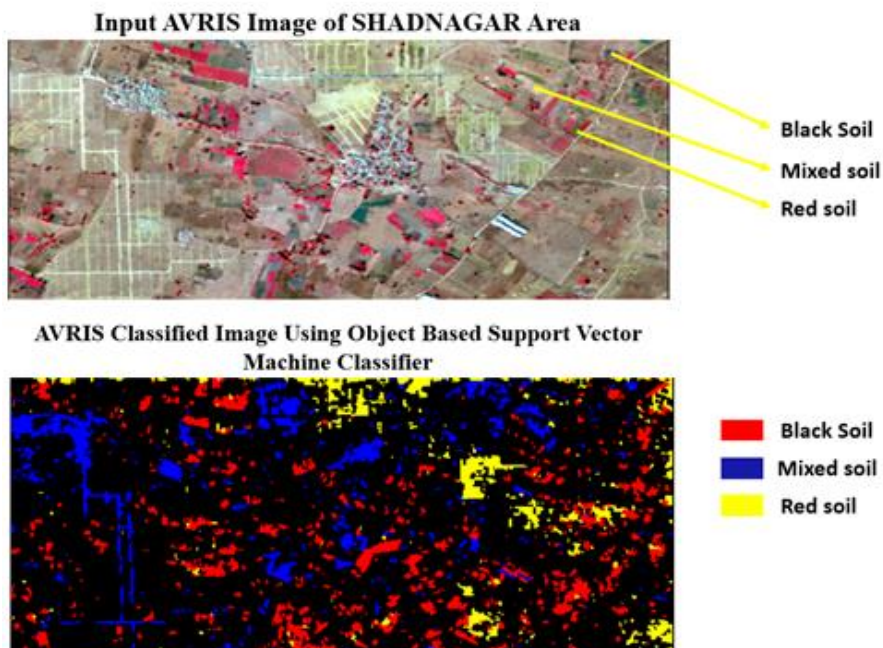
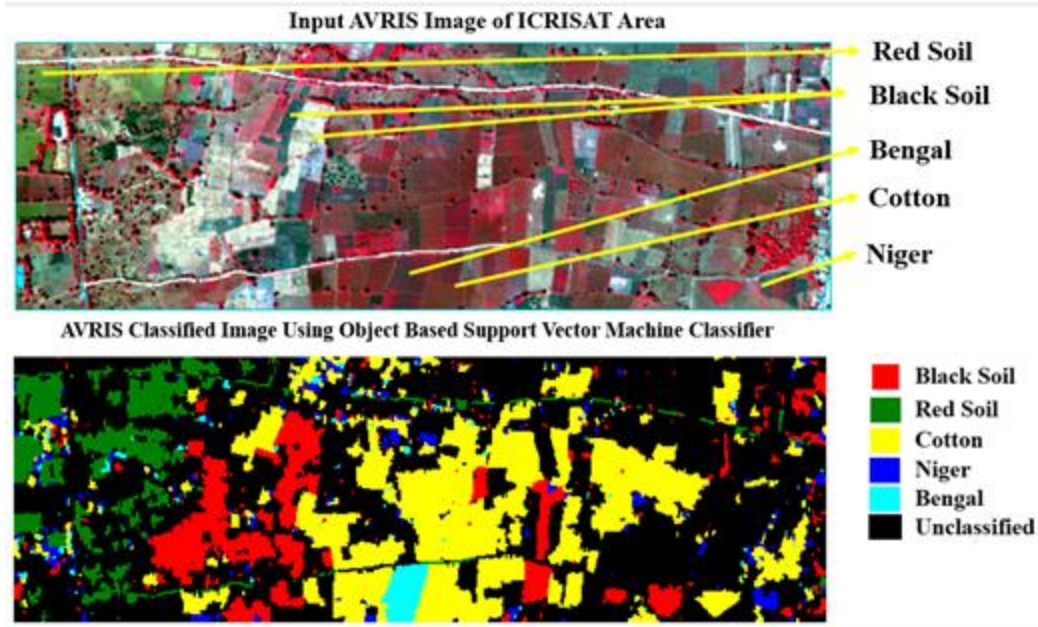


Figure 17.2. Image Spectra for Different Crops/Soils

**Similarity Scores**

Symbology	Crop/Soil	Similarity Score
	Jowar	0.897
	Chilli	0.838
	Fodder Grass	0.798
	Tomato	0.785
	Cotton	0.735
	Red Gram	0.708
	Bengal	0.698
	Niger	0.671
	Black Soil	0.590
	Red Soil	0.497



## 4.2 Target vs. Achievement

It has been tried to identify specific crop/soil type and further work has to be done on narrow based indices generation through automatic approach. For other application sites, ground truth data has been analyzed with spectral library generation and further work is in progress. It has been also tried to generate multi-spectral image bands from AVIRIS data.

### **4.3 Linkage to societal benefits**

Approach developed for specific class identification from hyperspectral data.

### **5. Conclusions**

For ICRISAT site it was possible to identify specific crop/soil types using segmentation based SVM approach and very good discrimination was found. While for Shadnagar site there was very high spectral overlap between black soil, roads and orchards. So classes' discrimination was not so good.

### **Acknowledgements**

We thank ISRO for considering IIRS to evaluate AVIRIS-NG project. Thanks to SAC and NRSC for providing AVIRIS data. We thank Director IIRS for time to time guidance for AVIRIS-NG data processing.

# Hyperspectral modeling for soil texture prediction in semi-arid tropical region of India – A case study

Justin George K, Vinay Kumar, Abhishek Danodia, Suresh Kumar and A. Senthil Kumar

Indian Institute of Remote Sensing,  
ISRO, 4 Kalidas Road, Dehradun, Uttarakhand, India

## ***1. Scientific rationale and Objectives***

In soil science, methods for mapping soil texture at various scales are needed for several applications, but typically, large numbers of samples must be collected and analyzed in order to adequately estimate the soil texture spatial variability. It is not an easy task to test each and every soil sample present on the field. The complex and expensive conventional methods and field surveys are currently driving the scientific community to develop indirect estimation methods based on proximal and remote sensors (ground based, airborne or satellite based), including reflectance spectroscopy. Remote sensed data are useful when they are combined with numerical modelling and ground based information. For studying the soil properties of large area through remote sensing we need to extract and process the small ground based information. By applying the ground based modelling over the satellite data we can predict the soil properties of whole area covered by satellite.

A number of approaches, including chemo metrics techniques or specific absorption features, have been proposed to estimate soil properties from visible and near infrared and shortwave infrared reflectance domains. These methods are low cost and can be used to characterize many soil variable e.g. soil texture, water content etc. according to their reflectance in the 400- 2500 nm wavelength range. Various laboratory methods have been developed to relate the soil spectrum to soil attributes, here we are using partial least- Squares Regression (PLSR) technique. PLS regression is particularly suited when the matrix of predictors has more variables than observations, and when there is multi-collinearity among X values. Compared to other multivariate statistical techniques, PLSR is generally preferred because it is more understandable and the algorithm is computationally faster (Curcio et al., 2013). In order to

develop a scheme for soil texture prediction using soil spectra, the study was conducted with the following objectives.

- To generate Spectral Library of the soil samples
- To generate various Reflectance transformations
- Predictive modeling of soil texture using various transformations.

## ***2. Study area and data used***

ICRISAT Site (Area id:117) and Shadnagar site (Area id: 134 & 138)

ICRISAT site is located in and around Patancheru in Sangareddy District, whereas Shadnagar site is located in Ranga Reddy District of Telangana. Both the study areas were approximately 20km x 10km (Total swath covered by airborne survey). The swath covered includes large stretches of agricultural fields, where variety of crops are cultivated throughout the year and thus was identified for crop and soil related studies using AVIRIS data. The major soil types present in both the sites are red soil, black soil and mixed soil. Shadnagar site had much more fallow area compared to ICRISAT site and was found to be much drier than ICRISAT site. Soil samples (140 nos) were collected along with their GPS locations from various sampling locations, depending on the local variability and soil characteristics.

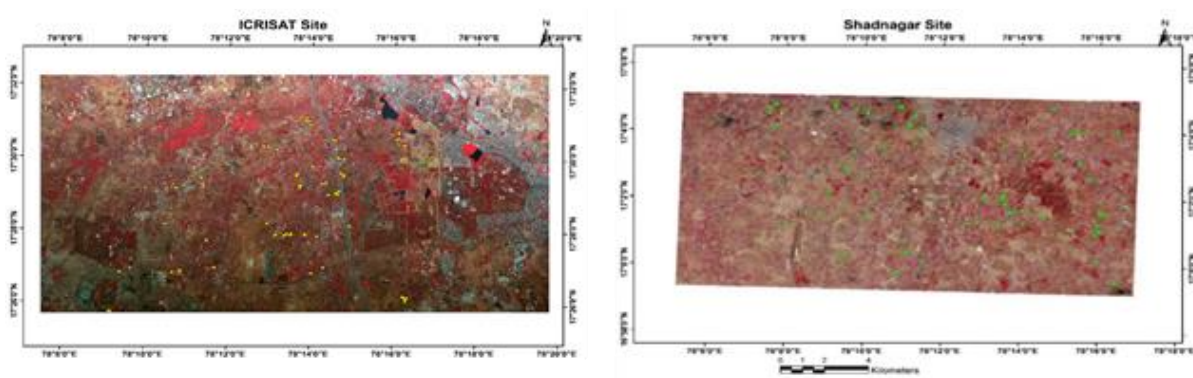


Figure 18.1. Study Area False Color Composite

## ***3. Methodology***

The overall methodology adopted in the study is depicted in the figure 18.2.

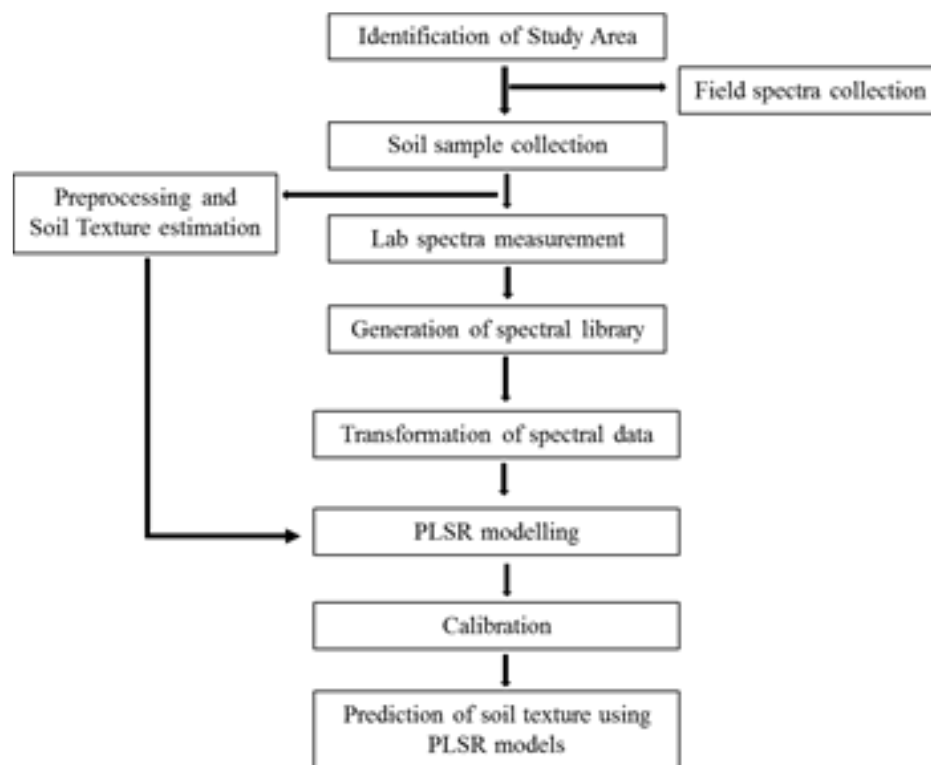


Figure 18.2. Overall methodology

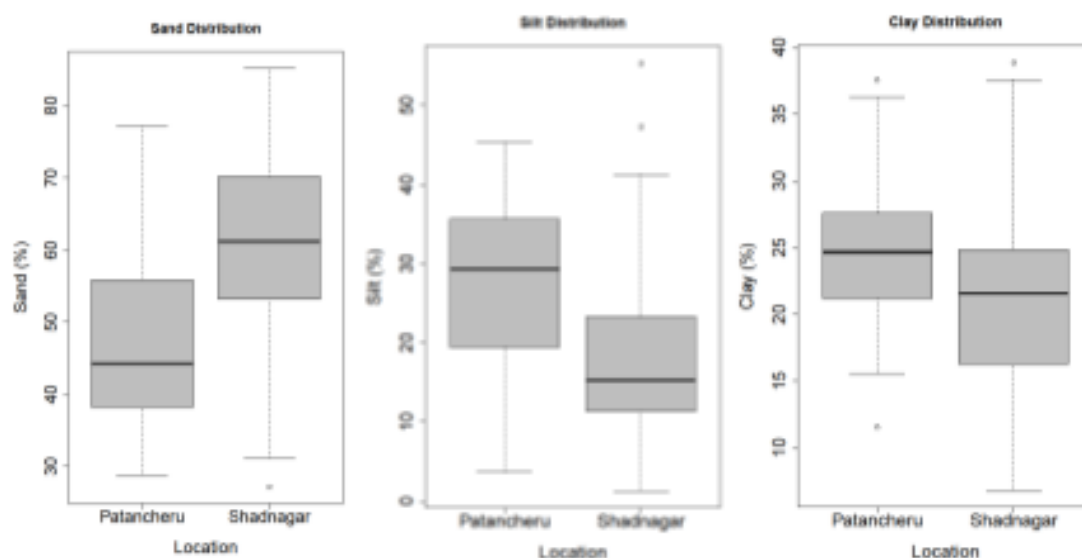


Figure 18.3. Particle size distribution of soil samples

## 4. Outcome

### 4.1 Salient findings

The textural composition of various soil samples is shown in figure 18.3. The spectral library of all the soil samples generated is shown in figure 18.4. The various significant reflectance

transformations generated using lab collected spectra are given in figure 18.5. Partial Least Square Regression technique was used for predictive modelling of soil texture using various reflectance transformations. Among the various transformations, root R showed best results for prediction of soil texture followed by reflectance and logarithmic reflectance (figure 18.5). Performance of PLSR technique for prediction of Soil texture using soil spectra was quite satisfactory. Various transformations showed promising results in modelling of sand, silt as well as clay percentages of which root R transformation showed best results for prediction of sand as well as silt using PLSR technique. The plots of textural prediction using various reflectance transformations employing PLSR modelling technique is given in Fig 6. In addition to root R transformation, other transformations such as log R and 1/R also yielded significant results for prediction of soil texture along with reflectance data (figure 18.6).

#### 4.2 Target vs. Achievement

- Generation of spectral library could be completed.
- Generation of reflectance transformations were done.
- Predictive modelling using PLSR technique was also completed.
- Identification of key wavelengths essential for soil textural prediction couldn't be done.

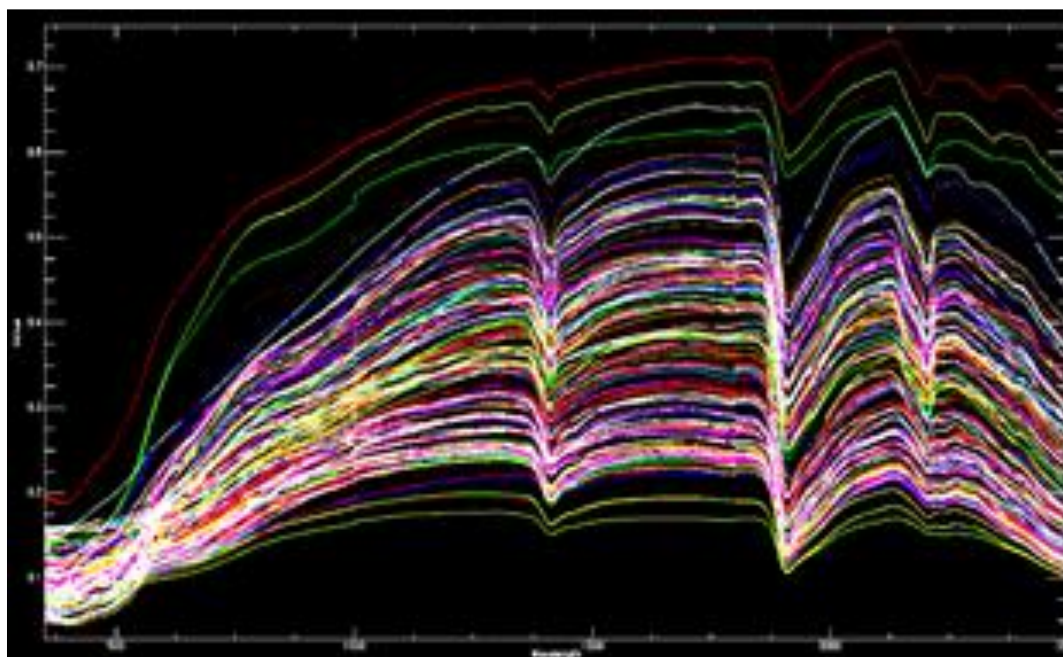


Figure 18.4. Spectral library of soil samples

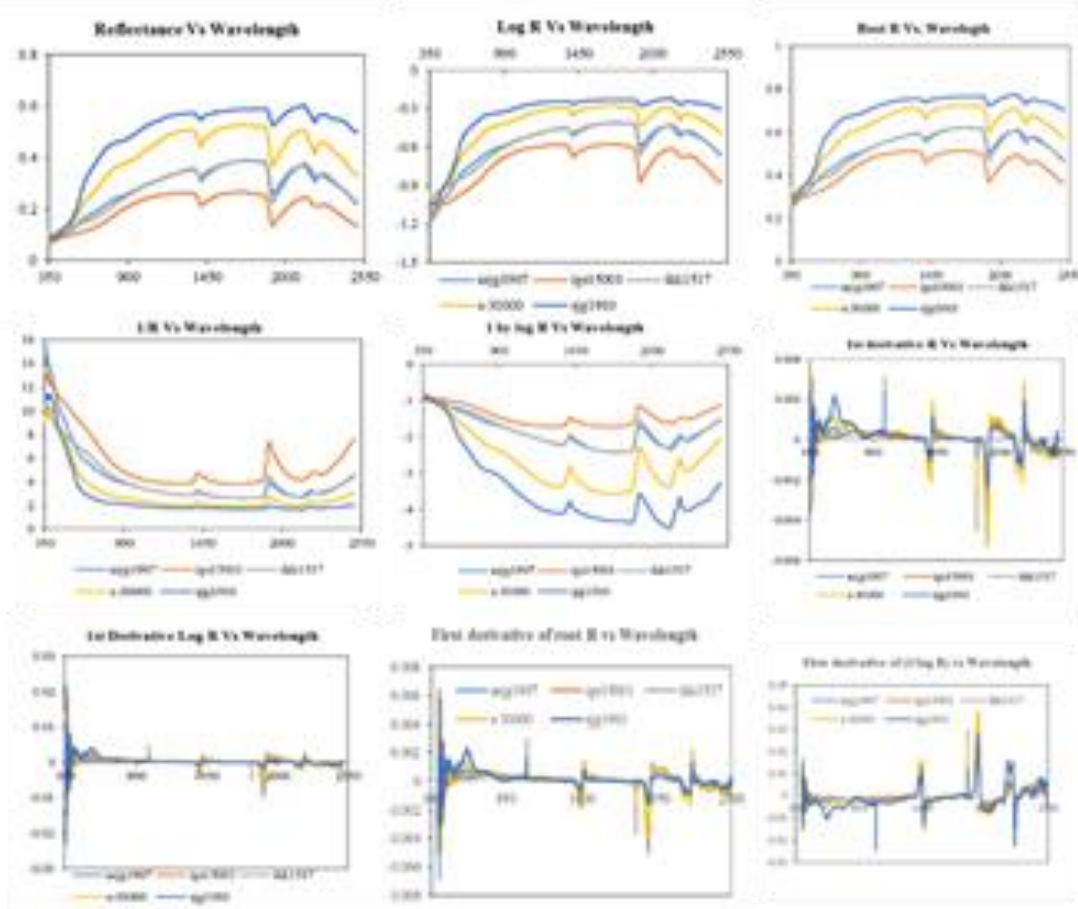


Figure 18.5. Various Spectral Reflectance transformations

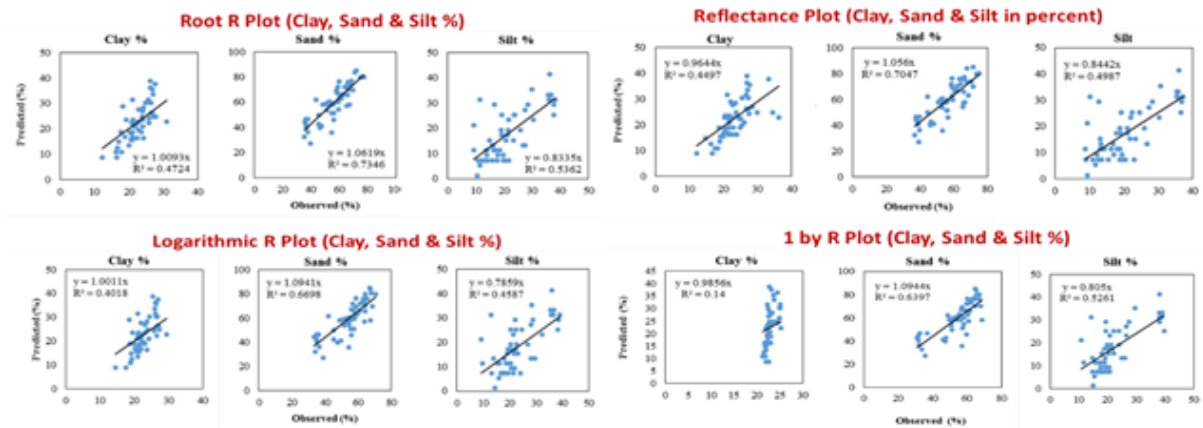


Figure 18.6. Soil textural prediction using different reflectance transformations employing PLSR technique.

### 4.3 Linkage to societal benefits

Further studies in this direction can lead to techniques for spatial mapping of various soil properties including soil texture using hyperspectral remote sensing data.

## 5. Conclusions

- The study revealed that PLSR technique performed satisfactorily well for prediction of Soil texture using soil spectra. Among the various transformations, root R transformation showed best results for prediction of sand as well as silt using PLSR technique.
- Future studies (2<sup>nd</sup> phase) should be aimed at identification of specific/particular wavelengths sensitive to various soil properties including soil textural changes, clay mineralogy etc.

## References

CAMO Inc". The Unscrambler user manual. CAMO Inc, Corvallis, OR. 1998.

Curcio, D., Ciraolo, G., Asaro, F.D., Minacapilli, M. (2013). Prediction of soil texture distributions using VNIR-SWIR reflectance spectroscopy. *Procedia Environmental Sciences* 19, 494-503.

# Crop bio-physical-chemical parameter retrieval using AVIRIS-NG data over agriculture area

Rahul Nigam and Bimal K Bhattacharya

Agriculture and Land Eco-System Division (AED), BPSG/EP  
Space Applications Centre, ISRO, Ahmedabad, Gujarat, India

## 1. *Scientific rationale and Objectives*

Weather and soil nutrient dynamics play a critical role in growth and development of agriculture crop as they responsible for exchange of energy, water and nutrients at temporal and spatial scale. Crop bio-physical and biochemical parameters such as leaf area index (LAI), chlorophyll (Cab) and leaf water content (Cw) will provide indicators to assess physiology of crop in varying conditions. Assessing crop physiology condition can indicate productivity and adaptability to environmental stress (Colombo and Parker 1999). Early detection of stress with remote sensing could help to identify stress at larger temporal and spatial scales and before damage is visible. The LAI, Cab and Cw have potential indicators of crop condition and growth. LAI and Cab have a direct role in photosynthetic processes of light harvesting and initiation of electron transport and its responsiveness to a range of stresses. Leaf bio-chemical constituents also act as potential indicators for nutritional deficiencies (Zarco-Tejada et al, 2013). These constituents can be estimated using different vegetation indices from several broad wavelength bands using multispectral bands. Attempts were made to estimate these crop constituents using multi-spectral bands with limited accuracy at spatial and temporal scale (Panda et al., 2010). The hyperspectral based indices also can't be translated to other regions. The limited use of physical principles in the construction of these indices also restricted their robustness and portability depend on targets and conditions at the time of observations (Roberts et al. 1997). The physical canopy radiative transfer model that simulate the canopy reflectance as a function of canopy bio-physical and bio-chemical parameters. Radiative transfer models establish an explicit connection between vegetation canopy reflectance and its biophysical and biochemical parameters based on physical laws with the goal of obtaining general knowledge of the physical processes involved in photon transport

within vegetation canopies in order to apply this knowledge to different situations (Jacquemoud et al., 2012). The inversion of these models can be used for retrieval of these parameters. The process of inverting a model means determining these parameters by minimizing the difference between the measured and simulated data. This motivate us to develop methodology for retrieval of crop bio-physical-chemical (B-P-C) parameters (eg.LAI, Cab) using physical modelling scheme.

## ***2. Study area and data used***

In the present study two contrasting sites i.e. Jhagdia (Gujarat) and Kota (Rajasthan) has been used selected. Jhagdia site represents heterogeneous agriculture as there were multiple crops has been reported during the time of flight. Kota site represents a homogeneous crop area and dominated with wheat crop. Airborne AVIRIS-NG campaign over Kota and Jhagdia have been conducted on 5th February 2016 and 9th February 2016 respectively. The site details are shown in figure 19.1.

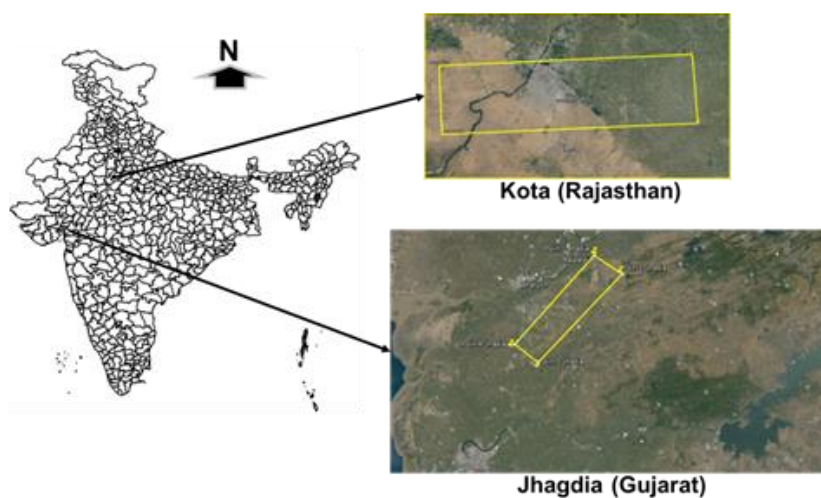


Figure 19.1. Study area

In this study Airborne Visible-Infrared Imaging Spectrometer Next Generation (AVIRIS-NG) hyperspectral data along with in situ data during the flight time has been used. AVIRIS having 425 spectral bands between 380 nm to 2500 nm. The spatial resolution is varying from 4 m to 8 m as per the altitude of the flight. The AVIRIS-NG instrument uses most advanced state-of-the-art detector array and grating for dispersion of light. Most importantly, the blazing and grooving technique employed in the grating of AVIRIS-NG could successfully maintain the

spectral as well as spatial uniformity, thus completely removing the SMILE and KEYSTONE effects that used to be the integral part of all the earlier hyperspectral instruments. In this study L-2 data is used for retrieval of bio-physical-biochemical parameters.

### 3. Methodology

One dimensional (1-D) canopy radiative transfer simulation model, PROSAIL, which is the combined form of PROSPECT and SAIL, is used in this study for retrieval of canopy parameters. The PROSPECT simulates reflectances at leaf level and SAIL (Scattering by Arbitrary Inclined Leaves) addresses the directionality. The model simulates reflectance as using leaf bio-physical-chemical constituents such as leaf structure parameter ( $N$ ), chlorophyll ( $a + b$ ) content ( $Cab$ ), leaf equivalent water thickness ( $Cw$ ), leaf dry matter content ( $Cm$ ), leaf area index ( $LAI$ ), leaf inclination angle ( $LIA$ ), hotspot parameter ( $SL$ ), horizontal visibility ( $vis$ ), sun zenith angle ( $\theta_s$ ), view zenith angle ( $\theta_v$ ), relative azimuth angle ( $\phi_{sv}$ ) and soil albedo ( $\rho_s$ ). The model is calibrated with in-situ data for different model absorption coefficients for chlorophyll, water and biomass. The CRT model is customized for 224 AVIRIS-NG spectral bands. The model will simulate 224 bands in forward simulation as per the given inputs. The various input parameters of models were divided into number of intervals within their theoretical lower and upper limits to cover whole dynamics of crops as per the in-situ observations and reported literature. All the combination of different inputs according to their limits and intervals resulted various scenarios for respective soil type. For chlorophyll retrieval and leaf area index different bands as per the decorrelation based technique were used for their retrieval. For chlorophyll four (451, 551, 656, 686 nm) and LAI six (451, 551, 686, 797, 857, 882 nm) were used. The overall flow of methodology has been shown in Figure 19.2.

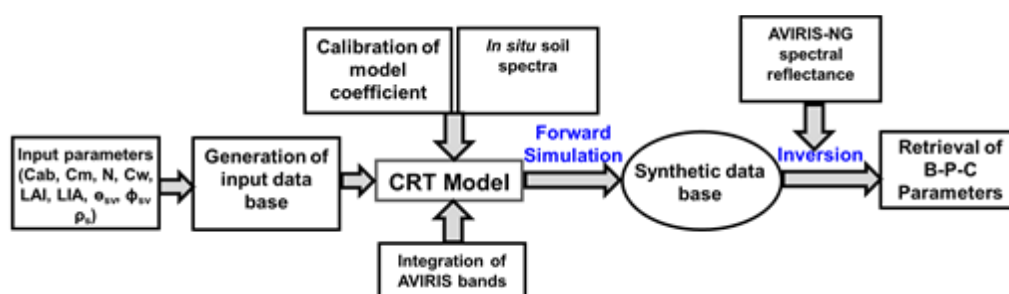


Figure 19.2. Flow of methodology for retrieval of B-P-C canopy parameters using RT model.

The calibrated CRT model is run over different LAI values as shown in figure 19.3. A cost function ( $S$ ) was used that represented the sum of square differences between AVIRIS pixel band reflectance and model simulated band reflectance. Minimum of the cost function was obtained using least square approach which gives unique value of LAI and chlorophyll for a given set of observed reflectance using unique LUT respectively. This approach is similar to the variational method in which difference of error is minimized but differ in the sense of observation error covariance matrices. This may be the scope of future research under that variational approach (Barker et al., 2004) and can be used to retrieve the LAI from observed reflectance. In variational method, cost function, which is a function of total variance, is minimized.

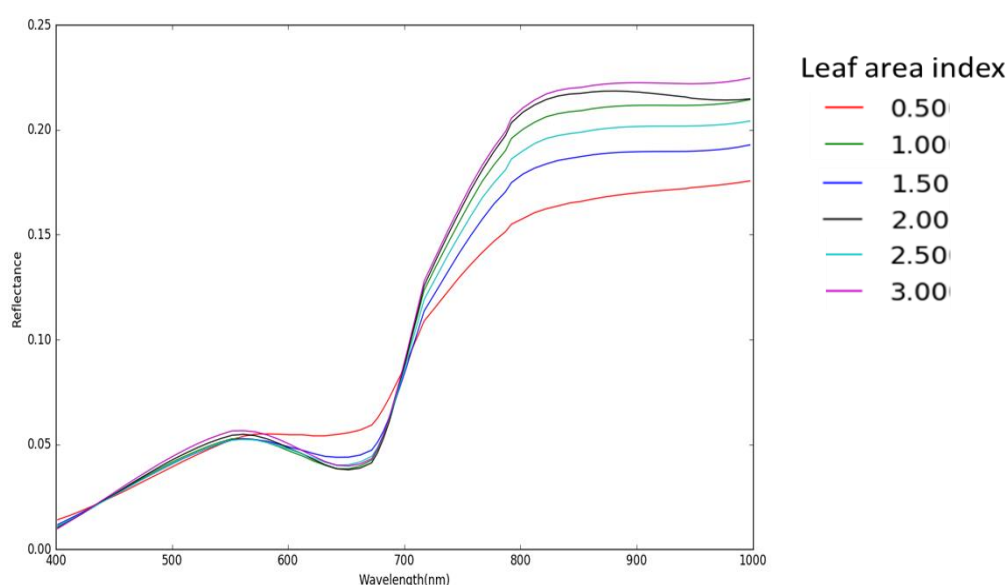


Figure 19.3. Forward simulation of calibrated CRT model over various LAI ranges

## 4. Outcome

### 4.1 Salient findings

Through decorrelation method of AVIRIS-NG data six (451, 551, 686, 797, 857, 882 nm) and four (451, 551, 656, 686 nm) spectral narrow bands for LAI and chlorophyll are identified for retrieval using canopy radiative transfer (CRT) model. The generated LUT from CRT model is used for retrieval of LAI and chlorophyll for respective selected bands. LAI is retrieved over homogenous agriculture area of Kota (Rajasthan) covering crop such as wheat, mustard, beans, garlic, fenugreek, coriander, peas and onion. The 70 percent of agriculture area is

dominated by wheat crop and rest by covered by other crops. The LAI of each crops showed the different ranges from 1-7 as shown in figure 19.4. The validation from in situ data showed the error of 15.7% from mean data as shown in figure 19.5.

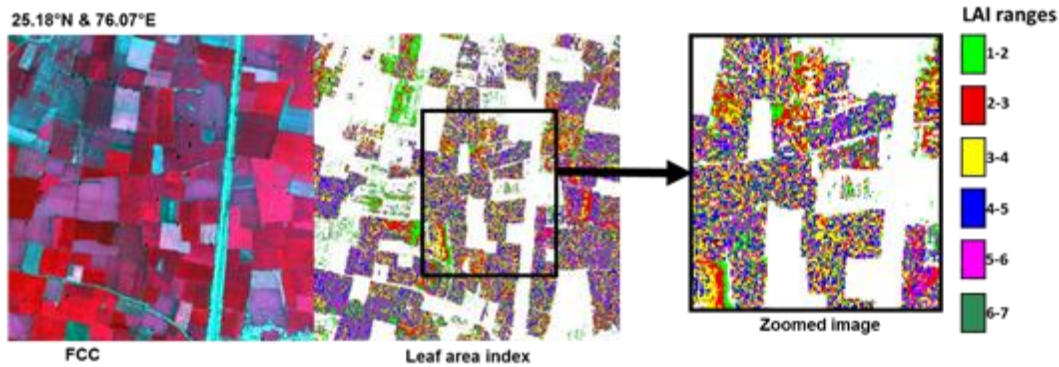


Figure 19.4. Retrieval of agricultural leaf area index using radiative transfer method over AVIRIS-NG data (Site: Kota; Flight date 5 February 2016)

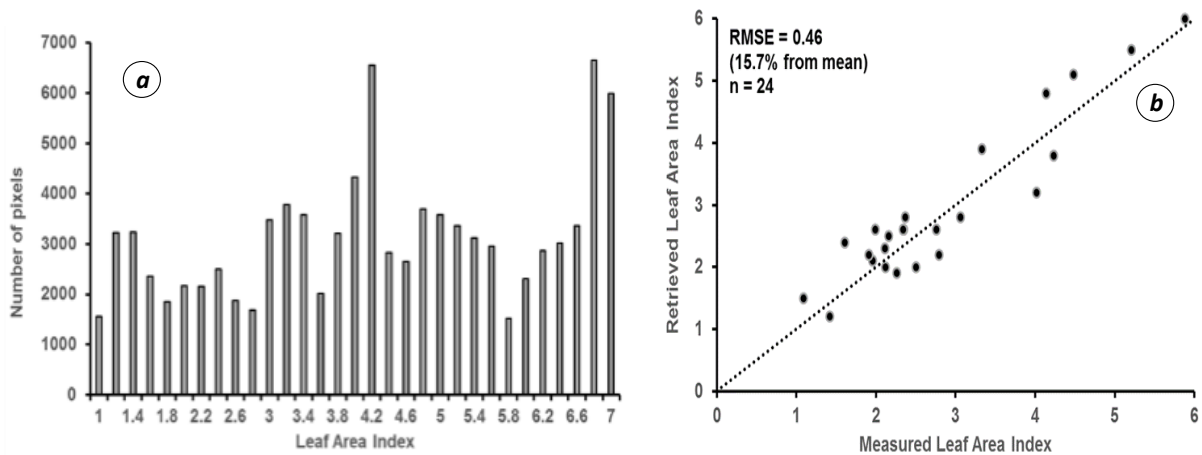


Figure 19.5. (a) Histogram of LAI and (b) validation of retrieved LAI from CRT model measured data

Cab is retrieved over heterogeneous agriculture area of Jhagdia (Gujarat) covering crop such as wheat, sugarcane, banana, onion and pigeon pea. The 50 percent of agriculture area is dominated by wheat and sugarcane crop and rest by covered by other crops. Chlorophyll content within a crop showed its health status. The crops having less Chlorophyll of each crops showed the different ranges from 5-45  $\mu\text{g cm}^{-2}$  as shown in figure 19.6. The validation from in situ data showed the error of 21.5% from mean data as shown in figure 19.7 for various crop.

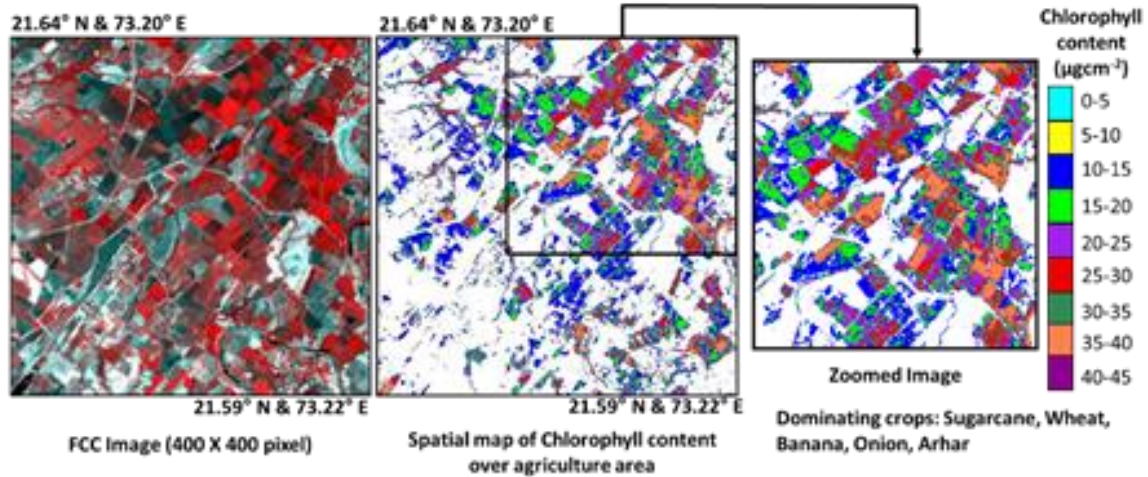


Figure 19.6. Leaf Chlorophyll content from AVIRIS NG using forward and inversion of Canopy Radiative Transfer Model (Site: Jhagdia, (Gujarat) AVIRIS Flight date 9th Feb 2016)

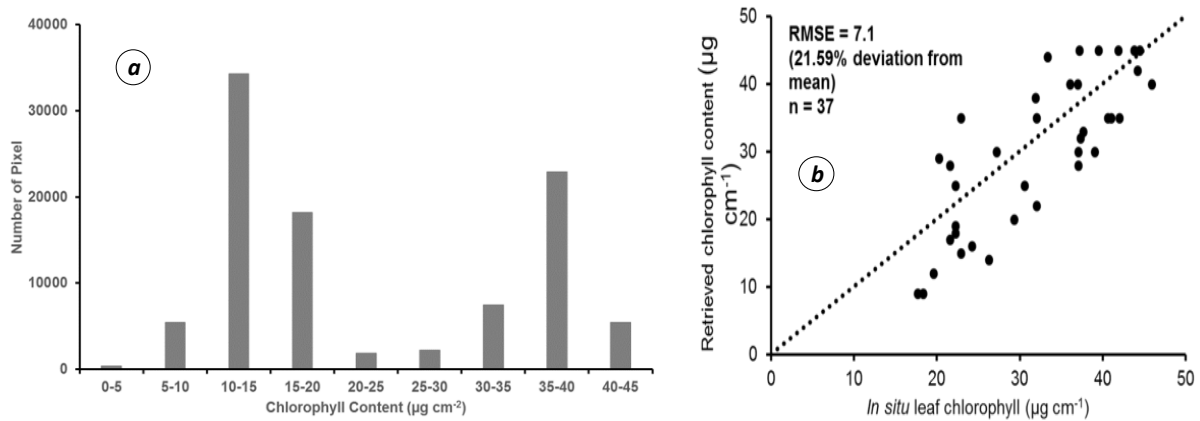


Figure 19.7. (a) Histogram of Chlorophyll and (b) validation of retrieved Chlorophyll from CRT model with in situ data

### 4.2 Target vs. Achievement

Target	Achievement	% remaining
Retrieval of bio-physical and chemical canopy parameters over five study sites (Kota, Jhagdia, Maddur, Raichur, Sunderbans) for agriculture applications.	Retrieval and validation of LAI and chlorophyll has been done over three site.	40%

### 4.3 Linkage to societal benefits

Early detection of crop stresses and monitoring of health is paramount importance in agriculture for national food security. The early detection of stress helps for advance application of farm management practices to avoid enormous farm losses. Crop bio-physical-biochemical parameter are the indicators of crop health. The deviation in core crop

parameters such LAI, chlorophyll and leaf water content from normal leads to stress. The persistent low values of crop parameters indicate poor crop health and finally it will reflect on yield. Hence to avoid yield losses the advance estimate of these parameters will help farmers for decision making at farm scale. Moreover, presently the aim of the government agencies is to reduce the cost of crop production by avoiding over use of water, fertilizer and pesticide. Further these retrieved crop parameters from hyperspectral data at high spatial resolution will help us to know the status of crop health lead to open a way for precision farming.

## **5. Conclusions**

- In the present study crop LAI and chlorophyll has been targeted for retrieval.
- The retrieval algorithm has been developed and will further validated over different set of crop season and also helps to identify the narrow spectral bands for retrieval of crop LAI and chlorophyll. These narrow band able to improve the accuracy of the retrieved parameters as compared to multispectral data.
- In future mission other canopy bio-physical-chemical parameters such as carotenoids, xanthophylls and fluorescence to be targeted for generation of crop photosynthesis efficiency map.
- Future mission will further help us to understand the crop chemistry to segregate biotic and abiotic stresses.

## **Acknowledgements**

The authors would like to thank Shri. A.S. Kiran Kumar, Chairman, ISRO for his encouragement and motivation for AVIRIS campaign. The authors would also like to thank Shri Tapan Misra Director, SAC for constant guidance. The authors also thank Dr Rajkumar Deputy Director, EPSA, SAC and Dr Prakash Chauhan Group Director BPSG, EPSA for their critical comments and wonderful suggestions that substantially improved the clarity of this study.

## **References**

Barker, D.M., Huang, W., Guo, Y.R., Bourgeois, A.J., Xiao, Q.N. (2004). A three dimensional variational data assimilation system for MM5: implementation and initial results. *Mon. Weather Rev.* 132, 897–914.

Colombo, S.J., and W.C. Parker. 1999. Does Canadian forestry need physiology research? For. Chronicle 75:667–673.

Jacquemoud, S., Verhoef, W., Baret, F., Bacour, C., Zarco-Tejada, P.J., Asner, G.P., Francois, C., Ustin, S.L., 2009. PROSPECT + SAIL models: a review of use for vegetation characterization. Remote Sens. Environ. 113, S56–S66

Panda, S.S, Hogeboom, G. and Paz, J.O. (2010). Remote Sensing and Geospatial Technological Applications for Site-specific Management of Fruit and Nut Crops: A Review. Remote Sensing 2010, 2, 1973-1997.

Roberts, D.A., Green, R. and Adamd, J.B. (1997). Temporal and Spatial Patterns in Vegetation and Atmospheric Properties from AVIRIS. Remote Sensing of Environment, 62,233-240.

Zarco-Tejada P.J, Morales, A. Testi, L. and Villalobos, F.J. (2013). Spatio-temporal patterns of chlorophyll fluorescence and physiological and structural indices acquired from hyperspectral imagery as compared with carbon fluxes measured with eddy covariance. Remote Sensing of Environment. 133, 105-115.

## Exploring AVIRIS-NG Data for Crop and Soil Studies

Rojalin Tripathy, K N Chaudhari, Mehul Pandya and Bimal K Bhattacharya

Agriculture and Land Eco-System Division (AED), BPSG/EP  
Space Applications Centre, ISRO, Ahmedabad, India

### **1. Scientific rationale and Objectives**

Quantification of crop biochemical and biophysical attributes such as the plant Nitrogen content, plant water content, chlorophyll and leaf area index can provide indicators of crop stress status and indirectly the plant productivity status. Hyperspectral remote sensing techniques have the advantage of providing unique absorption feature of each element in contrast to the multispectral remote sensing where because of the broad band the signature is the resultant of average signature in a number of narrow band that leads to misinterpretation of the property (crop and soil) under study, especially the chemical constituents. Hyperspectral (narrow band) indices have been shown to be crucial for providing additional information with significant improvements over broad bands, in characterizing, mapping and quantifying biophysical and biochemical parameters of agricultural crops. Recent advances in hyperspectral remote sensing demonstrate great utility for a variety of crop monitoring applications (Sahoo et al. 2015). There are many studies conducted on a wide array of crops and their biophysical and biochemical variables such as yield, chlorophyll content, nitrogen content, carotenoid pigment, plant biotic stress, plant moisture and other biophysical variables. These studies give a measure of the current, proven experimental capabilities and operational applications, and stimulates investigations of new and ambitious applications (Sahoo et al. 2015).

Looking at the advantages of hyperspectral remote sensing using AVIRIS-NG and the wide applicability of narrow band vegetation index, the present study was carried out with an overall goal of exploring the applicability of various hyperspectral vegetation index from AVIRIS-NG data for crop and soil research with the following broad objectives.

- Discrimination of crop type, crop stage and crop cultivar;

- Estimation of plant biochemical and biophysical parameters from AVIRIS-NG;
- Assessing biotic (Disease, insect infestation) and abiotic stress (Nitrogen, water) in different crop;
- Estimate soil properties (N and organic carbon and moisture) using AVIRIS-NG.

## ***2. Study area and data used***

The study area constituted an approximate area of 8x40 km in Anand district of Gujarat state. The area covers the research farms of Anand Agricultural University and the adjoining agricultural area. Major crops in this area during the campaign were wheat at different stage, mustard, chickpea, Oat, Amaranth, potato, tomato, brinjal, chilli, different cultivars of tobacco at different stages, fodder maize at different stage, pearl millet, cabbage, fodder sorghum, amaranthus and fennel. We could find the mustard crop affected by aphid (80 % infestation) and chickpea infested with blight disease. Soil type in the study area varied in nutrient content and texture Most soils are sandy loam. Climate of the study area is semi-arid with an average annual rainfall of about 750 mm. Rabi season daily average temp varied from 20 to 25°C.

## ***3. Methodology***

The AVIRIS-NG image was classified into areas with different crop types using SAM classifier with endmembers from known locations. Empirical regression models were generated using VIs from ground spectra and was inverted in AVIRIS-NG scene for generating the map of the respective property. The overall methodology is depicted in figure 20.1.

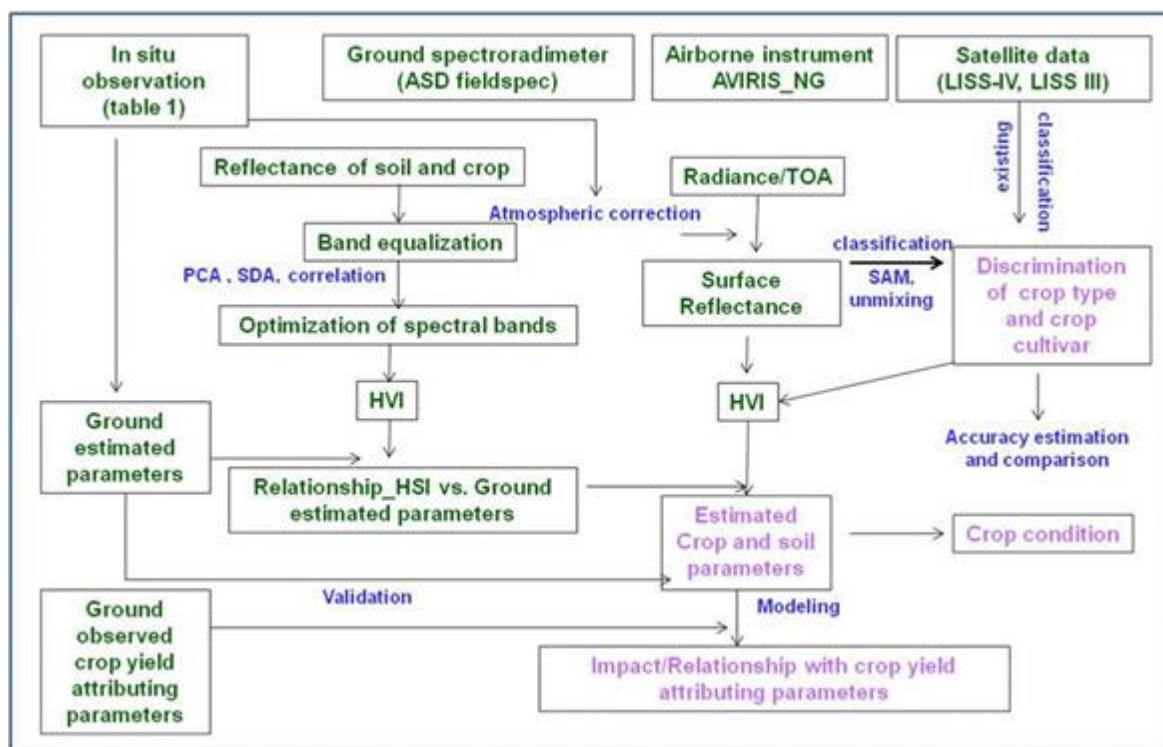


Figure 20.1. Flow chart for estimating biochemical and biophysical properties of crop and soil from AVIRIS-NG

## 4. Outcome

### 4.1 Salient findings

**Crop type discrimination:** SAM classified image is depicted in Figure 20.2 (a). The end-member spectras are used for classification. The analyzed scene of the AVIRIS-NG showed clear discrimination of 8 different crop types.

**Growth stage and varietal identification in different crops:** We found wheat and tobacco at three different stages and the spectral signature in each stage was found to be different in NIR (780-870 nm) and red edge region (670-720 nm) both in ground spectra and AVIRIS-NG spectra. Due to lack of sufficient data point further analysis could not be done. Similarly, for varietal difference in wheat and tobacco we could find significant difference in spectral signature at red edge, NIR and SWIR (1500-1800) band but the results could not be conclusive as number of data point is less.

**Biotic stress in different crops:** Biotic stress was observed in brinjal, chickpea and mustard crops. Shifting of red edge to longer wavelength was observed in all healthy plant as compared to diseased plant.

**Crop biochemical properties and biophysical properties using AVIRIS-NG:** Three major biochemical parameters (Plant N, Chlorophyll, water) and one biophysical parameter (LAI) was considered for this study. The biochemical properties from the collected samples during ground campaign were estimated in AAU, Anand using standardized procedure. The models developed for estimating these parameters in AVIRIS-NG scene are depicted in Figure 20.2.

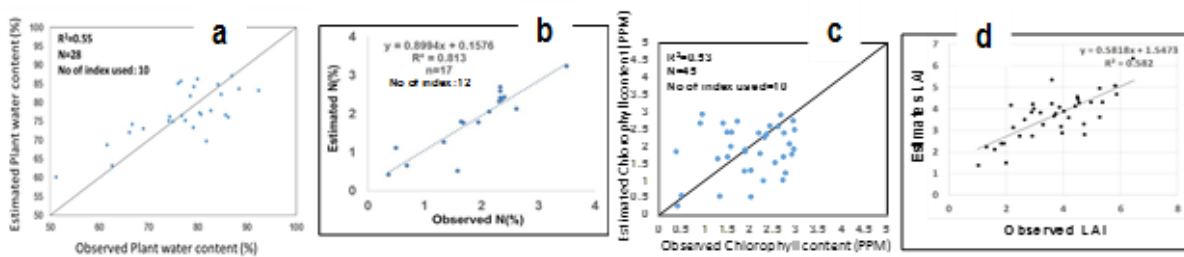


Figure 20.2. Models developed for estimating (a)Plant N content, (b) plant water content, (c) plant chlorophyll and (d) Leaf area index.

The resulted map of the two plant properties using these model along with the validation of the result with independent set of observation are depicted in figure 20.3 (Plant N content) and figure 20.4(LAI).

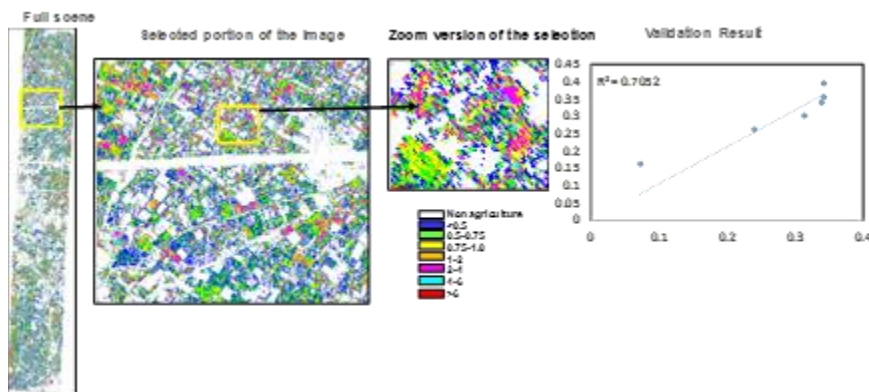


Figure 20.3. Plant N content map over AVIRIS-NG scene.

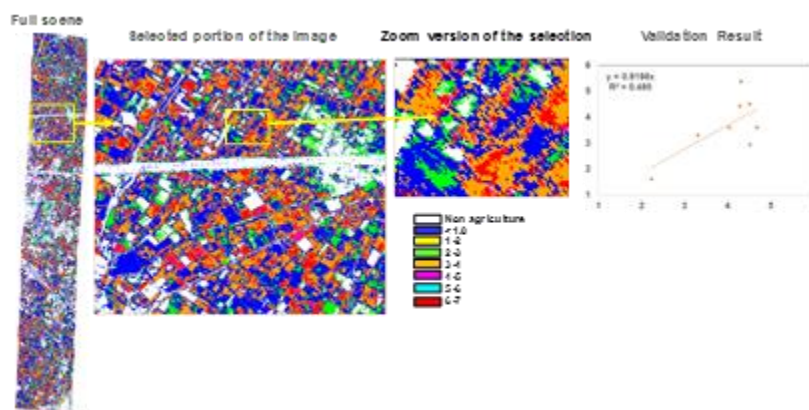


Figure 20.4. LAI map over AVIRIS-NG scene along with validation result with ground.

## 4.2 Target vs. Achievement

S. No	Targets	Achievement
1	Discrimination of crop type, crop stage and crop variety	20 % (Discrimination of crop type was carried out for one scene)
2	Estimating Plant N, water, chlorophyll content and LAI	25 % (Estimated over one scene)
3	Finding out the optimum no of bands for estimating plant biochemical content	--
4	Estimating Soil chemical properties	10 % (Lab estimation of soil organic C and available N, analysis of soil spectra) Modeling is remaining

## 4.3 Linkage to societal benefits

- Plant N content at finer resolution could be used as an input for precision agriculture
- Farmers can be advised proper time of fertilizer application based on the instantaneous plant N content.

## 5. Conclusions

- The results from the present study concluded that AVIRIS-NG could help to classify crops at finer spatial resolution (5m) and hence could be used for classifying mixed agriculture area with fragmented field size.
- Narrowband indexes could be used for assessing crop nitrogen and water status.
- The VIs at red edge region could be used for crop N stress assessment.

## Acknowledgements

Authors are grateful to Shri. Tapan Misra Director, SAC for his encouragement and keen interest for this study. Authors are thankful to Dr. Raj Kumar, DD EPSA and Dr. Prakash

Chauhan GD, BPSG, BPSG for their valuable suggestions for the advancement of the study. Our sincere thanks are due to Ms. Rucha Dave and team from AAU, Anand for their valuable participation in the ground campaign. We acknowledge NASA for providing the level1 data from AVIRIS-NG.

## **References**

Sahoo R. N., Ray, S. S. and Manjunath, K. R. 2015. Hyperspectral remote sensing of agriculture, Current Science, 108: 848-859.

# Hyper Spectral Sensing of Crops under Varying Conditions of Soil Wetness

Chandrasekar K, Srikanth P, Abhishek Chakraborty and Karunkumar Choudary

Agricultural Sciences Applications Group,  
National Remote Sensing Centre, Hyderabad, India

## ***1. Scientific rationale and Objectives***

Crop water stress is the most predominant reason for the crop damage and yield loss. It is an important indicator to the condition of the crops physiological status (Carter, 1991; Peñuelas et al., 1994; Stimson et al., 2005). It also helps in assessment of drought and to take informed irrigation decisions (Peñuelas et al., 1993). Monitoring the various facets of moisture in the soil and crop will help in better management of crop. The crop or vegetation water status information can be derived from water absorption bands with centres at approximately 970, 1200, 1450, 1950 and 2250 nm (Sims & Gamon, 2003). There are several water sensitive indices that can be derived using various combinations of NIR and SWIR narrow band wavelengths available with the AVIRIS-NG data. Several studies in the past have developed spectral indices that use these water bands for detection of plant water stress, relative water content, leaf water potential and water content as percent of dry matter (Sims & Gamon, 2003). However, each index is designed to highlight certain parameter.

The water stress/surplus could happen during any phase of the crop. When the water stress happens during the peak vegetative stage of the crop, it could not be discerned as the green canopy above indicates a healthy crop by vegetation indices. Further during the early phase of the crop when the fields have very poor canopy cover, the vegetation index shows up very low values despite the field is saturated with water. In this study it is envisaged to derive the water sensitive indices from the AVIRIS-NG data to evaluate its sensitivity for the determination of liquid water content in the soil and crop under various conditions of soil wetness.

The major objectives of the study are:

- Determination of the suitable narrow band water index which is sensitive to soil and crop liquid water content.
- To determination of water index which is suitable for the early and late phase of the crop season.
- To discern the start of the season under irrigated agro-ecosystem using water indices.

## 2. Study area and data used

The study area is Nagarjuna Sagar command area. The AVIRIS L2 data supplied by the JPL is used in this study.

## 3. Methodology

The AVIRIS-NG L2 data provided by Space Application Centre, Ahmedabad were used in this study. The AVIRIS-NG L2 data was geometrically corrected and all the individual strips were mosaiced. The ground truth information was transferred to the AVIRIS-NG data. The spectral signature for each of the ground truth sites was derived and plotted. The candidate vegetation and water indices were derived for the entire site. The water indices are:

- Normalized Difference Water index (NDWI)
- Normalized Difference Infrared Index (NDII)
- Land Surface Water Index (LSWI)
- Water Index (WI)

$$NDVI = \frac{\rho_{862} - \rho_{661}}{\rho_{862} + \rho_{661}} \quad \text{Rouse et al.}$$

$$NDWI = \frac{\rho_{862} - \rho_{1242}}{\rho_{862} + \rho_{1242}} \quad \text{Gao B.}$$

$$NDII = \frac{\rho_{862} - \rho_{1664}}{\rho_{862} + \rho_{1664}} \quad \text{Hardisky et al.}$$

$$LSWI = \frac{\rho_{862} - \rho_{2130}}{\rho_{862} + \rho_{2130}} \quad \text{Chen et al.}$$

$$WI = \frac{\rho_{900}}{\rho_{970}} \quad \text{Peñuelas et al.}$$

The indices values for the ground truth sites and for known features were derived and plotted. Regression analysis was carried out between vegetation index and water indices for two

cases. 1. Dry soil to dense crop cover and 2. Wet soil to dense crop cover. Scatter plot of NDVI vs all the water indices was plotted and analysed. The dry edge and wet edge from the NDVI vs water index scatter plot was determined to derive the Standardized Water Content Index (SWCI) of the investigated water indices. The overview of the methodology followed is given in figure 21.1.

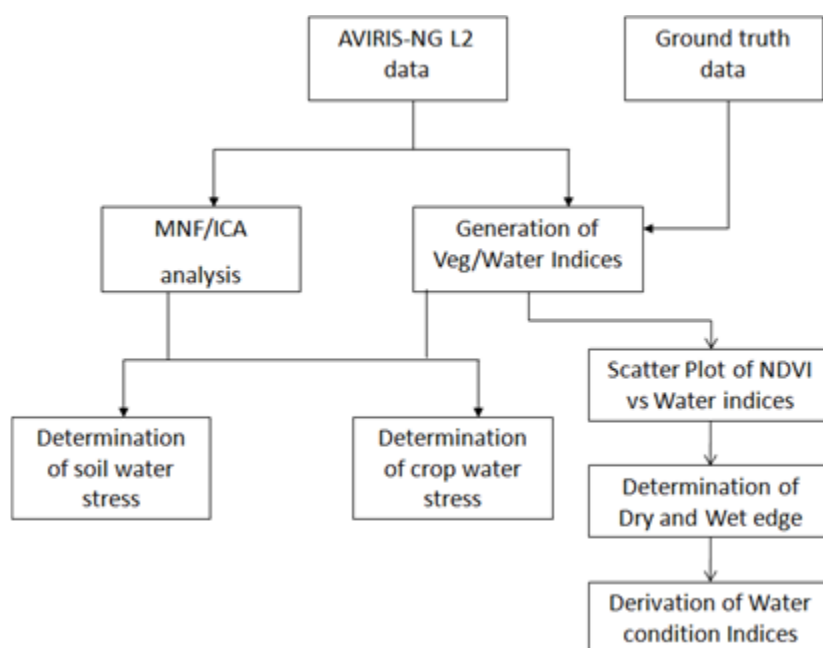


Figure 21.1. Overview of the methodology

## 4. Outcome

### 4.1 Salient findings

The spectral signature of various crops and other features observed during the ground truth was plotted with wavelength on x-axis and reflectance on the y-axis. It can be observed from the figure 21.2 that irrigated fields were having the least reflectance among all the features in the red-NIR region. The healthy crops were having highest reflectance in the NIR region while the bare dry soils were having the highest reflectance in the SWIR region.

Using the reflectance values of the water sensitive wavelength from the AVIRIS-NG data, the NDVI, NDWI, NDII, LSWI and WI were derived for the Nagarjuna Sagar study area (figure 21.3). It can be observed that all the water indices were able to identify the irrigated fields. However, the NDWI and WI were not sensitive to the crop liquid water content as they did not pick the dense crop canopy. On the contrary the LSWI and NDII displayed high values for both wet soil

as well as for the healthy crops. Figure 21.4 shows the scatter plot of the NDVI with all the water indices to determine the dry and wet edge. Using the current NDVI, dry and wet edge, the Standardized Water Content Index (SWCI) of the respective water index was derived.

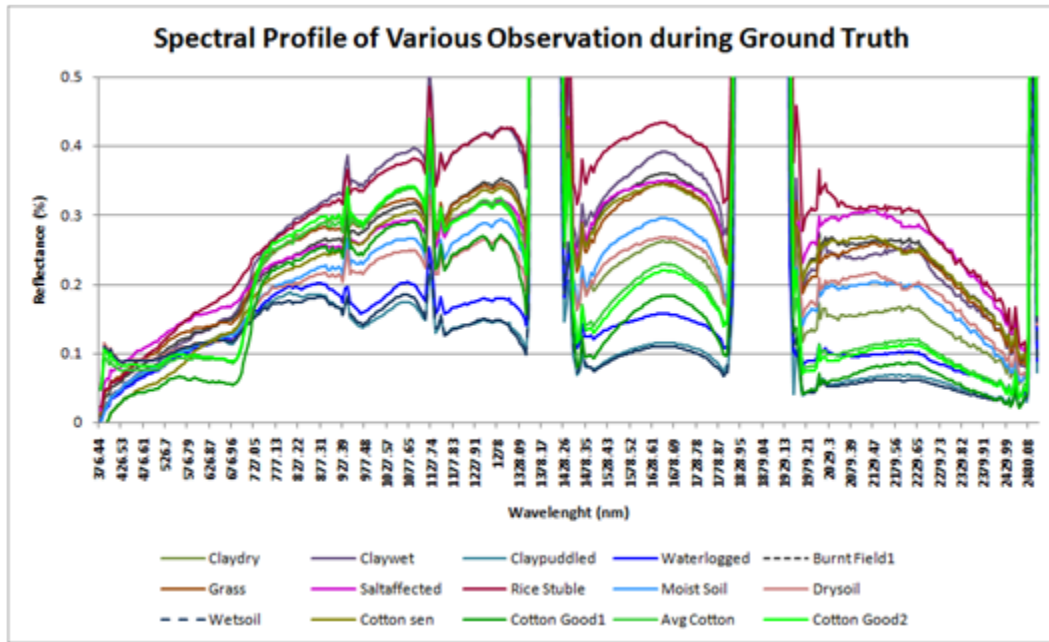


Figure 21.2. Spectral profile of various features observed during ground truth

By using the dry and wet edge the Standardized Water Content Index (SWCI) for all the water indices was derived. Figure 21.5 show the SWCI for various ground truth sites. It can be observed that whenever there is excess water in the field due to irrigation or standing water the SWCI of the water indices showed higher values and vice versa. Among the SWCIs the SWCI of LSWI showed better dynamic range compared to others while the SWCI of WI show the least dynamic range.

$$SWCI(NDWI) = \frac{(NDWI_i - NDWI_{dryedge})}{(NDWI_{wetedge} - NDWI_{dryedge})}$$

$$SWCI(LSWI) = \frac{(LSWI_i - LSWI_{dryedge})}{(LSWI_{wetedge} - LSWI_{dryedge})}$$

$$SWCI(NDII) = \frac{(LSWI_i - LSWI_{dryedge})}{(LSWI_{wetedge} - LSWI_{dryedge})}$$

$$SWCI(WI) = \frac{(WI_i - WI_{dryedge})}{(WI_{wetedge} - WI_{dryedge})}$$

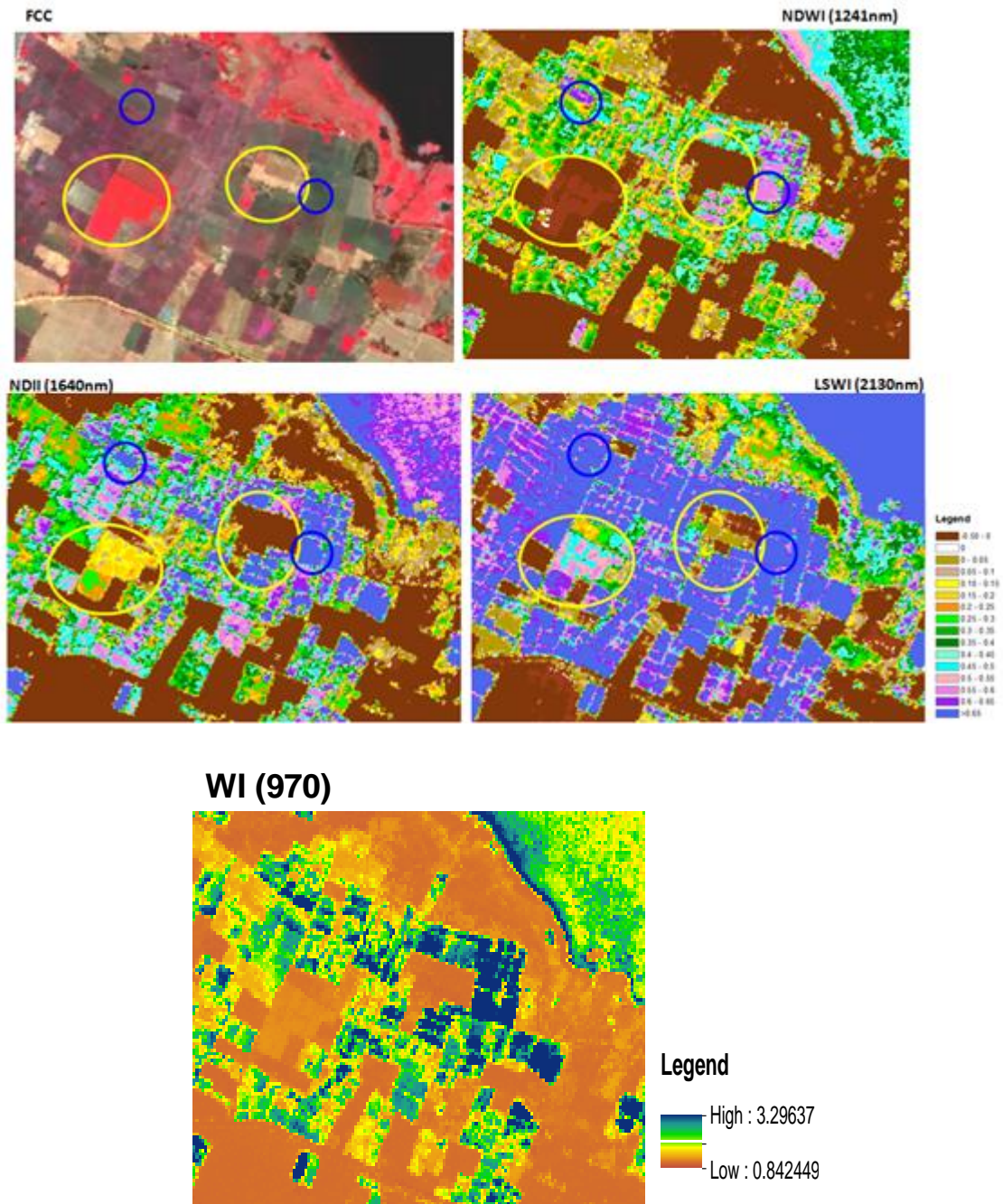


Figure 21.3. FCC image and Water Indices of the Nagarjuna Sagar command area

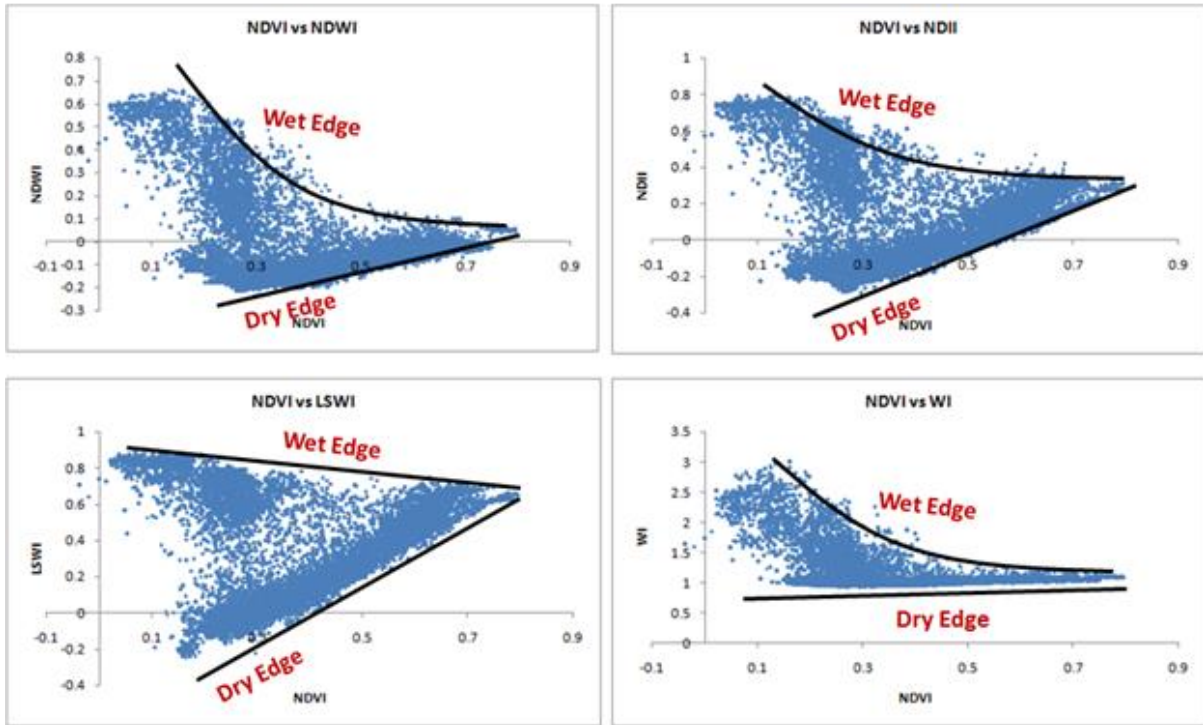


Figure 21.4. Scatter plots of NDVI vs NDWI, NDII, LSWI and WI

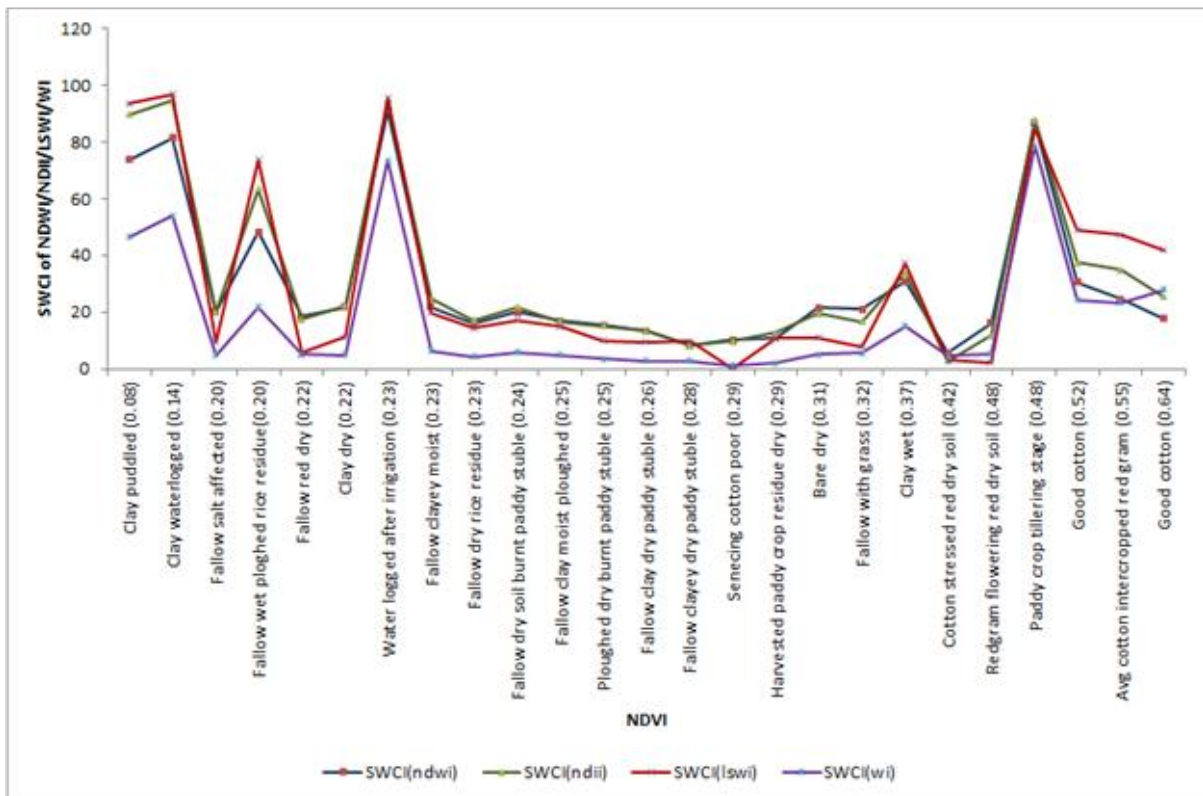


Figure 21.5. Plot of the Standardize Water Condition Index of NDWI, NDII, LSWI and WI

## 4.2 Target vs. Achievement

<b>Activity</b>	<b>% Remaining</b>
Data Preparation	10%
Validation	20%
Report Preparation	50%

## 4.3 Linkage to societal benefits

The results showed that the NDWI which used the 1240 nm and WI which uses the 970 nm are good in determination of flooded and saturated. However, these indices get saturated at higher NDVI. Hence NDWI and WI are more suitable to identify the irrigated fields during early part of the crop season. These indices can be well used to determine the start of the season under irrigated agricultural ecosystem and during the early monsoon season to determine the first soaking rain which makes soil conducive for sowing. On the other hand, the LSWI and NDII were sensitive to crop moisture content throughout the entire NDVI dynamic range and hence it can be used to monitor the crop liquid water stress during all stages of the crop.

## 5. Conclusions

- The NDWI is suited for determination of the flooded and saturated fields during the early part of the season.
- The LSWI is sensitive to the crop moisture content for the entire dynamic range of NDVI and hence can be used to monitor crop water stress throughout the crop season.

## Acknowledgements

The authors wish to thank Director, Associate Director and Deputy Director (RSA), NRSC for their constant encouragement and guidance in this study. Thanks are also due to colleagues in NRSC, SAC and the students of JNTU who provided support during the ground truth campaign.

## References

Carter, G. A. 1991. Primary and secondary effects of water content on the spectral reflectance of leaves. *American Journal of Botany*, 78(7), 916– 924.

Chen, D., Huang, J., Jackson, T.J., 2005. Vegetation water content estimation for corn and soybeans using spectral indices derived from MODIS near- and short-waveinfrared bands. *Remote Sens. Environ.* 98 (October (2–3)), 225–236.

Gao, B., 1996. NDWI—A normalized difference water index for remote sensing of vegetation liquid water from space. *Remote Sens. Environ.* 58, 257–266.

Hardisky, M.A., Klemas, V., Smart, R.M., 1983. The influence of soil salinity, growthform, and leaf moisture on the spectral radiance of *Spartina alterniflora* canopies. *Photogramm. Eng. Remote Sens.* 49, 77–83.

Peñuelas, J., Filella, I., Biel, C., Serrano, L., Save, R., 1993. The reflectance at the 950–970 nm region as an indicator of plant water status. *Int. J. Remote Sens.* 14, 1887–1905.

Rouse, J.W., 1974. Monitoring the vernal advancement and retrogradation (greenwave effect) of natural vegetation. Final rep. NASA/GSFC, Greenbelt, MD.

Sims, D. A., & Gamon, J. A. (2003). Estimation of vegetation water content and photosynthetic tissue area from spectral reflectance: A comparison of indices based on liquid water and chlorophyll absorption features. *Remote Sensing of Environment*, 84, 526– 537.

# Wheat yellow rust identification through AVIRIS-NG data

Sujay Dutta, Somnath Paramanik\* and Bimal K Bhattacharya

AED/BPSG/EP  
Space Applications Centre, ISRO, Ahmedabad, Gujarat, India  
\*Coral Dept., IIT., Kharagpur, W, B., India

## 1. *Scientific rationale and Objectives*

Stripe rust appears periodically on wheat crop and includes heavy losses in yield. For reducing crop disease infection and yield loss, earlier detection of pest or disease damage in crops needed. The common method for detection of pest or disease damage in crops is by visual inspection of the foliage in the field. But manually it is a labour intensive and costly. Remote sensing provides an alternative cost effective method to obtain detailed spatial information for entire crop field at frequent intervals during the cropping season. But in the case of pest and disease identification hyperspectral data or hyperspectral remote sensing techniques is very useful due to its high spectral and spatial resolution. For this type of identification there are some hyperspectral vegetation indices like DSWI, LRDSI etc. Even the absorption properties of the vegetation spectra from hyperspectral data is very useful for detection of disease whereas it is not able to do from multispectral data due to extrapolation of data.

Objective: Identification of wheat rust disease of wheat crop using hyperspectral remote sensing techniques and the developed image based algorithms.

## 2. *Study area and data used*

- Rupnagar or Ropar district in Punjab. It is located at 30.97° N, 76.53° E.
- Spectroradiometer ASD data was collected for 9 disease infested sites. AVIRIS (L2 processed) data was taken for the study area for date of pass February 17, 2016.

### 3. Methodology

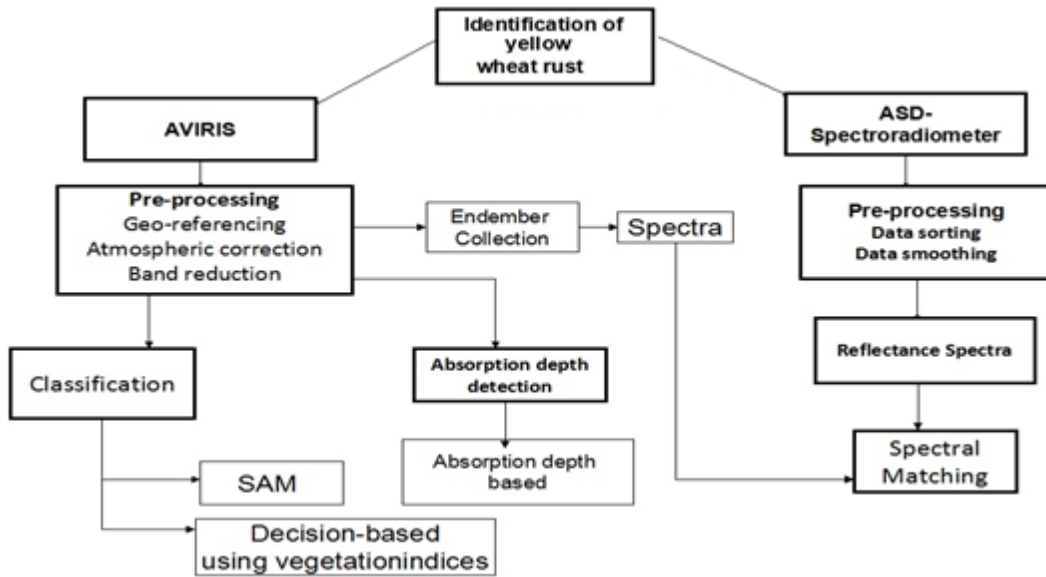


Figure 22.1. Flowchart for complete work.

#### a) Plotting of ASD data after sorting and absorption feature analysis

In Reflectance spectroscopy techniques for plant identification, characteristics of the plant reflectance spectrum is utilized. This plot (figure 22.2) shows the different spectral signature of healthy and disease wheat. The healthy and diseased spectra was discriminated based upon the magnitude of reflectance.

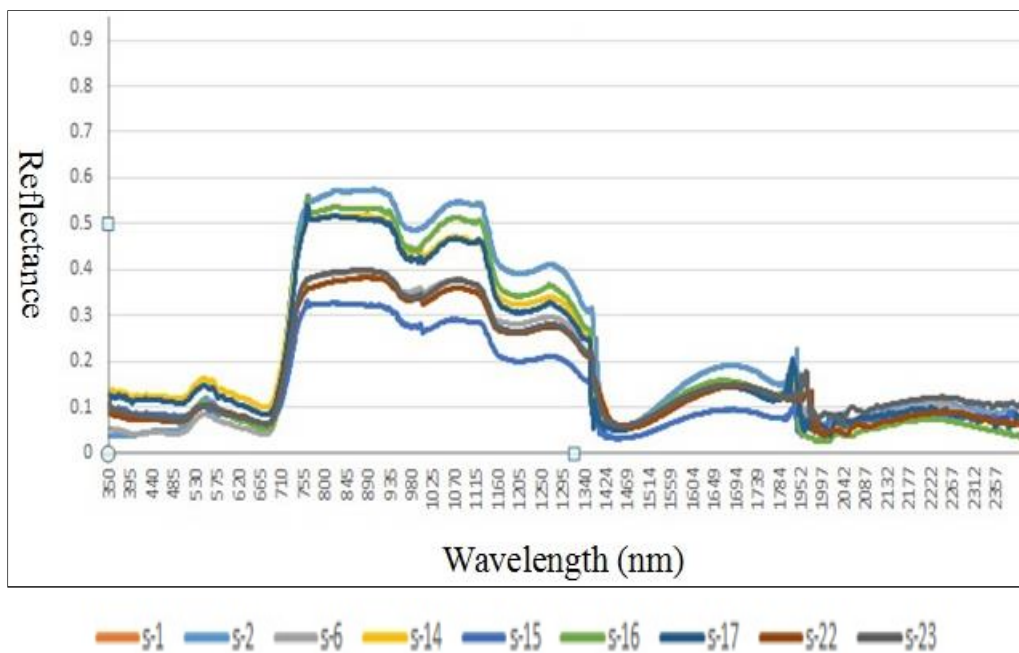


Figure 22.2. Band range selection for wheat disease identification.

Table 22.1. Absorption features analysis of ASD data of the site Roper, Punjab.

Site	Wavelength range	Band depth	Area	FWHM
15	760-790	0.019	45.4091	8.0643
	1660-1820	0.062	13.9101	10.1057
	2014-2160	0.245	10.4899	27.3323
	2257-2322	0.0456	5.0643	18.6015
	2322-2389	0.0425	5.1665	23.0661
16	760-812	0.0563	27.5761	21.8549
	1660-1820	0.2965	23.1748	73.8521
	2225-2360	0.0613	8.0359	84.2578
17	760-900	0.1377	48.9194	40.3721
	1660-1820	0.0409	21.4935	37.1559
	2014-2160	0.1744	11.5105	27.9738
	2322-2389	0.1982	4.5521	16.2915
22	1660-1820	0.0208	21.0099	23.8596
	1968-2016	0.0293	2.2269	3.228
	2016-2190	0.1347	12.2569	30.0429
	2220-2350	0.0425	10.0393	69.0462
23	1660-1820	0.0838	31.0932	63.4281
	1968-2016	0.009	3.7886	3.6876
	2016-2190	0.1357	18.3712	32.7319
	2220-2350	0.0865	14.3019	25.9012

From the Table 22.1, analysis of the ASD data of the Roper site -17 is recorded as the highest wheat rust disease in wheat crop as according to the ASD spectra with the disease scoring of 80S. For the site of 22, it had the minimum wheat rust disease, score was 20S. The Fraunhofer lines were removed from the reflectance image and non-vegetation areas were masked out using two indices (NDVI, DSWI).

#### b). Classification techniques

Masked out image was used for further classification. Different classification techniques were applied for wheat rust identification 1) SAM classification 2) Index based classification and 3) Absorption band depth based classification after continuum removal.

## 4. Outcome

### 4.1 Salient findings

**SAM classification:** MNF transformation, pixel purity index, end member selection was carried out. Spectral Angle Mapper (SAM) (Figure 22.3) algorithm was applied in this work. The spectral signatures for crops were collected using field GPS plot.

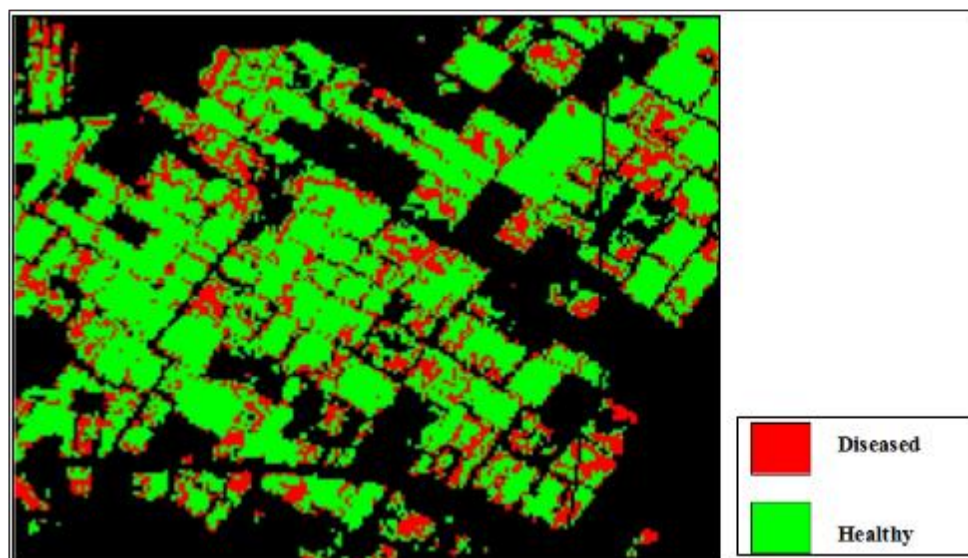


Figure 22.3. SAM classified image.

### Index based classification

Two spectral disease indices (LRDSI-1 and 2) were developed by Ashourloo D. (2014) based on the reflectance at the 605, 695 and 455 nm wavelengths. In both the indices, the  $R^2$  between the estimated and the observed was high as 0.94. Huang et al. (2007) found that the level of yellow rust disease in wheat can be related to a photochemical reflectance index ( $R^2 = 0.97$ ). The healthy and diseased wheat field in present study site were identified using two indices Leaf Rust Disease Severity Index (LRDSI) (Ashourloo D., et al., 2014) and photochemical reflectance index (Huang et al., 2007). For this classification technique using this rust index, LRDSI the threshold value was fixed in the range of 7.5-7.9 and 8-8.4 for healthy and diseased wheat field, respectively based on ground point observation. But according to the current work it was the combination of 655 nm and 455 nm, which gave precise and more accurate results (figure 22.4).

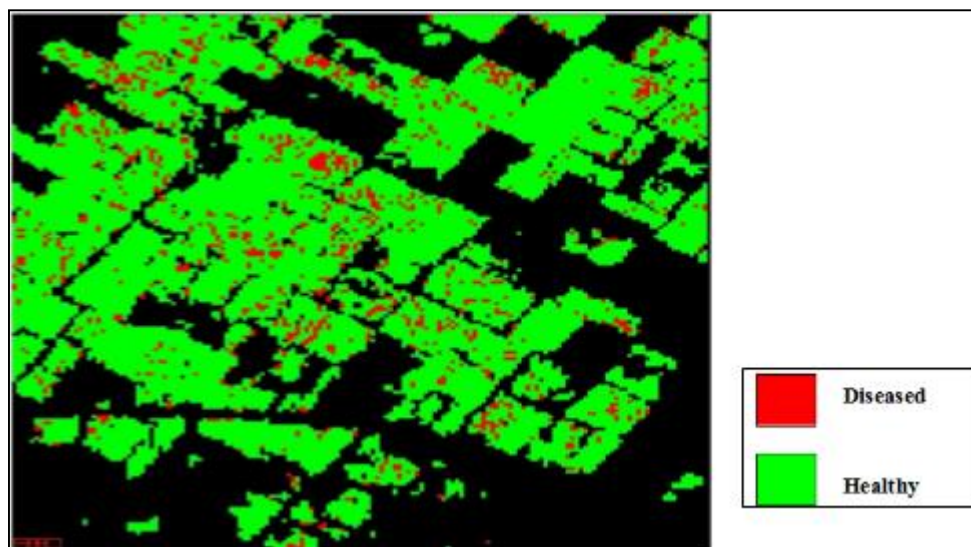


Figure 22.4. Index based classified image

### **Absorption band depth based classification after continuum removal**

In the present study, the ASD spectra and spectra from AVIRIS image of healthy and diseased field were compared (figure 22.5). The absorption depth feature extraction was done for two regions in Visible and SWIR region. The range, 662-702 nm and 2155-2175nm were selected according to the spectral absorption behavior and response of 1st order derivative. The value of absorption depth in the range of 662-702nm were 0.25-0.356, 0.201-0.238 and for the range of 2155-2175nm, it was 0.07-0.146, 0.03-0.068 respectively, for healthy and diseased wheat. Then two ranges were combined and it was the final output of absorption band depth based classification (figure 22.6), where the green indicates the healthy wheat field and the red spot indicates the yellow wheat rust infestation in the field. In the green region (500–660 nm), the relatively higher reflectance of healthy leaves compared to the medium and severely damaged leaves of wheat is expected since the green region is characterized by relatively higher reflectance due to chlorophyll content (Kumar et al., 2003).

Similar work done by Mirik et al. (2007), reported that canopies of wheat infested by Russian wheat aphids showed that the reflectance in the near infrared region was low and reflectance in the visible range was high in the spectrum when compared with non-infested canopies. Yang et al. (2005) studied stress in wheat canopies caused by green bug infestation using multispectral radiometry. Their results demonstrated that reflectance from a band centered

at 694 nm, and vegetation indices derived from bands centered at 800 and 694 nm were the most sensitive to identifying the damage due to green bug infestation.

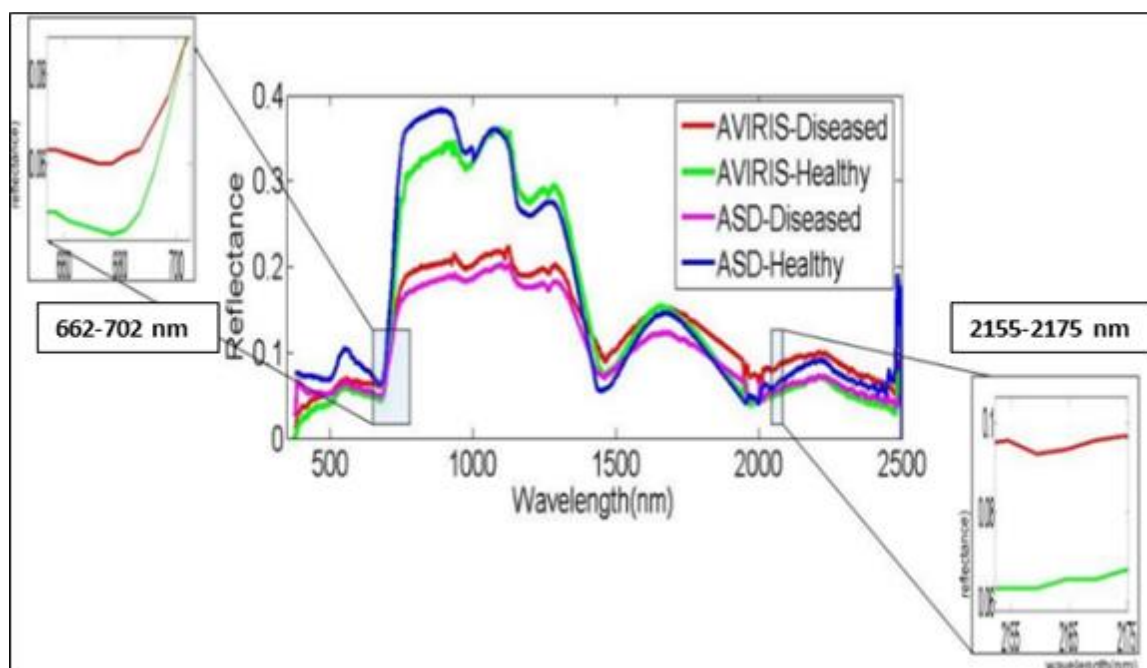


Figure 22.5. Band range selection for wheat disease identification

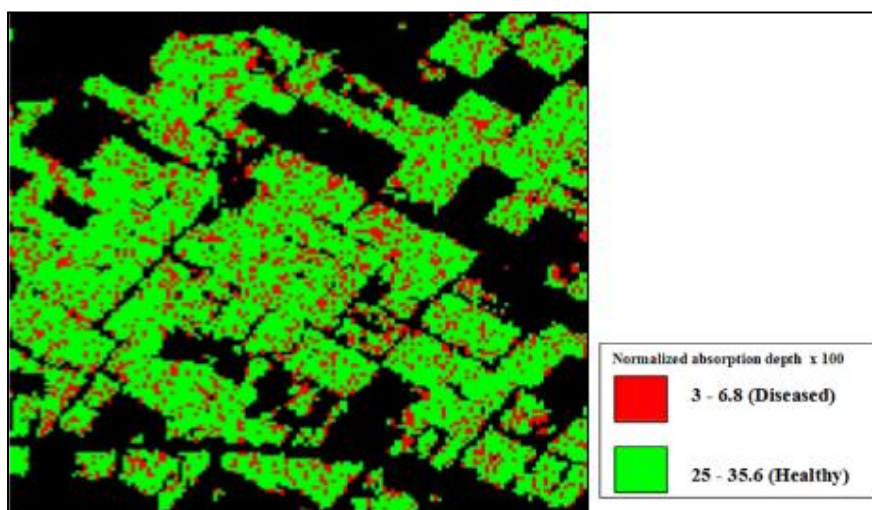


Figure 22.6. Absorption depth based classified image

Output of the work validated with the help of ground observation points and Spectral Feature Fitting (SFF). Taking the spectra from the ASD spectroradiometer and image spectra then with the ENVI tool, Spectral feature fitting (SFF) generated the matching score. On the basis of this spectral matching score it was validated. For healthy wheat spectral feature fitting (SFF) score was 0.914 and for wheat rust it has 0.936 SFF w.r.t. field (ASD) spectroradiometer data.

## 4.2 Target vs. Achievement

Since the target site for wheat rust was not available therefore number of sample points falling under the AVIRIS data was too meagre. The identified site is slotted to be flown in Phase – II. The repeated experiment in phase –It will establish the authenticity of the procedure in versatile field conditions in reality.

## 4.3 Linkage to societal benefits

Identification of rust disease is a very time consuming, laborious for farmers and more expensive for large study area that's why this type of research work is needed. It will help the farmers for early detection of rust disease due to synoptic view of the crop through remote sensing and also help the Ministry of Agriculture for making a quick statistic about productivity, yield, and its losses.

## 5. Conclusions

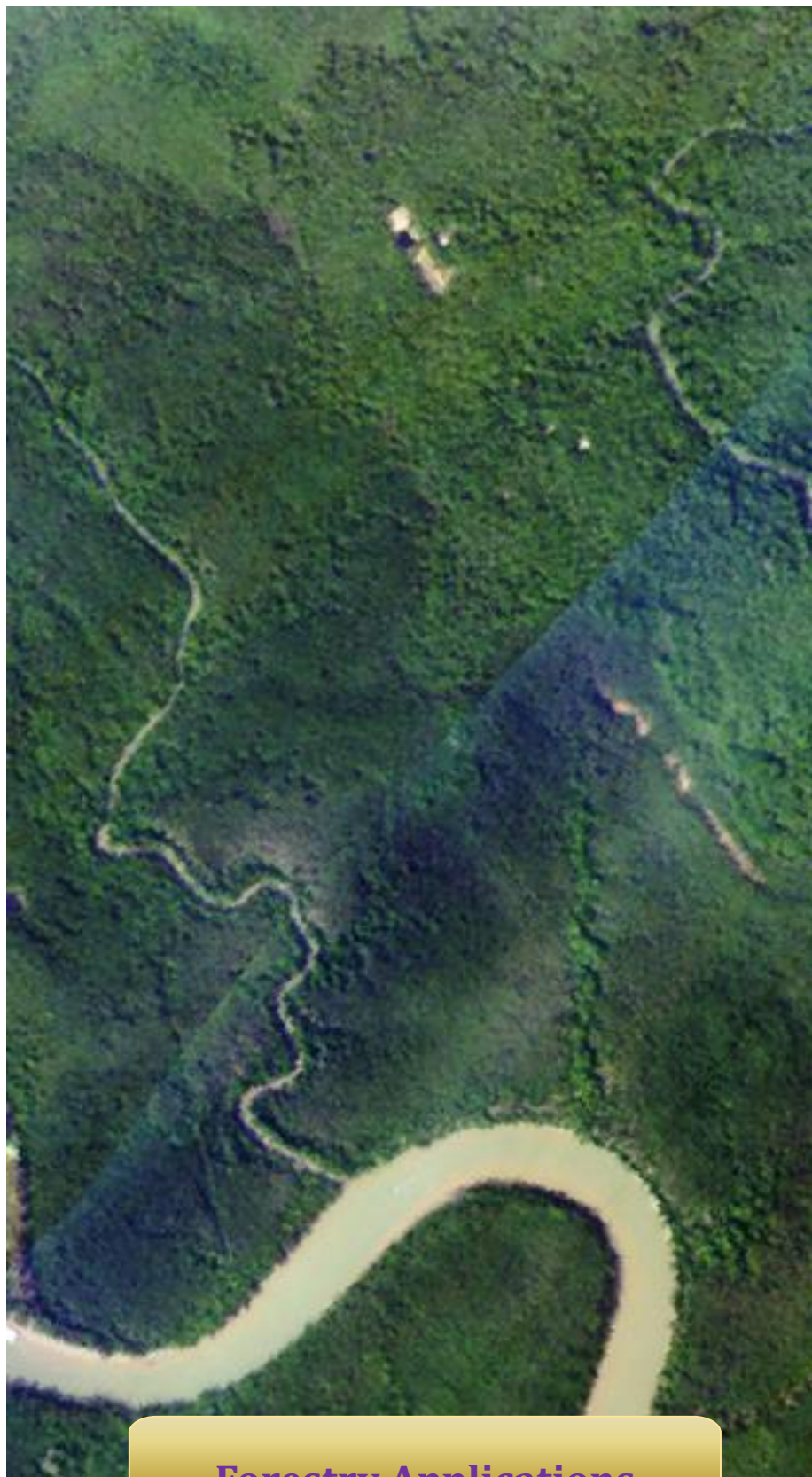
- Discrimination of healthy and diseased wheat fields was found to be better with the help of spectral absorption depth analysis. In absorption depth analysis classification 662-702 nm and 2155-2175 nm wavelength were chosen similar to LRDSI values (the 605, 695, 800 and 455 nm) observed by Ashourloo D (2014), which aided in improving the classification and showed a better promising capabilities for discriminating of healthy v/s diseased wheat.
- Results of the classifications algorithm indicate that SAM based classification and Indices based classification (LRDSI and PRI) were capable to discriminate between healthy v/s rust diseased wheat fields. Repeat experiment is needed to establish procedure as a fool proof methodology.

## Acknowledgements

Authors are grateful to Shri Tapan Misra, Director, SAC (ISRO), Ahmedabad for the funds, support and encouragement to carry out this study and JPL (NASA) team for providing the AVIRIS data for R&D project for this study. Authors are grateful to ground Engineers who worked in tandem with JPL team for acquiring the data in India.

## References

- Ashourloo D., Mobasheri M.R., Huete A. (2014). Developing two spectral disease indices for detection of wheat leaf rust (*Puccinia triticina*). *Remote Sensing* 6, 4723–4740.
- Huang, W., Luo, J., Zhang, J., Zhao, J., Zhao, C., Wang, J., et al. (2012). Crop Disease and Pest Monitoring by Remote Sensing. *Remote Sensing- Applications* 31–76.
- Kumar, S., Ghosh, J., & Crawford, M. M. (2001). Best-bases feature extraction algorithms for classification of hyperspectral data. *IEEE Transactions on Geoscience and Remote Sensing*, 39(7), 1368–1379. doi:10.1109/36.934070.
- Mirik M., Michels G.J., Kassymzhanova-Mirik S., Elliott N.C. (2007). Reflectance characteristics of Russian wheat aphid (Hemiptera: Aphididae) stress and abundance in winter wheat. *Computers and Electronics in Agriculture* 57, 123–134.
- Yang Z., Rao M.N., Elliott N.C., Kindler D., Popham T.W. (2005). Using ground based multispectral radiometry to detect stress in wheat caused by greenbug (Homoptera: Aphididae) infestation. *Computers and Electronics in Agriculture* 47, 121–135.



**Forestry Applications**

### Summary

Assessment of forest biodiversity, its health assessment and fuel load are essential for devising better forest management policies and climate mitigation and wild life sustainability. The forestry applications have newer areas of applications using AVIRIS-NG data. In one of the studies the  $\alpha$ -diversity (Shannon Diversity Index) has been computed and spatially mapped in Mudumalai region of Tamil Nadu. Spectral-Angle Mapper (SAM)- based species classification has also been carried out. There are two studies carried out for Mangroves ecosystem, according to one study carried out for Sundarbans around 70% of mangrove species were correctly classified with respect to ground-truth verification results. It has also been demonstrated that fine resolution AVIRIS-NG hyperspectral data is capable of discriminating various mangrove species. Another study on Mangrove ecosystem in Bhitarkanika has also shown on species-level classification using bands centred around 714, 719, 724 and 729 nm and biochemical analysis leading to forest health assessment using the sensitive band regions centred around 440, 680 and 800nm. The moist deciduous forest ecosystem of Shoolpaneshwar has also been studied for its forest fuel load which is indicator of potential areas for forest fire hazard.

# Mapping Forest Diversity using Airborne Hyperspectral Data

J. Singhal, C.S. Reddy, Rakesh, G. Rajashekar, C.S. Jha

Forestry and Ecology Group, National Remote Sensing Centre, Hyderabad

## ***1. Scientific rationale and Objectives***

Accurate knowledge of the distribution of species can form a critical component for managing ecosystems and preserving biological diversity. Hyperspectral remote sensing data with a greater number of bands and narrower bandwidths can be effectively used for vegetation studies. In this study we try to characterize the  $\alpha$ -diversity of a forest by estimating Shannon index  $H'$  for the selected region. Dominant species in the study area were also mapped using AVIRIS data.

## ***2. Study area and data used***

21.7 km<sup>2</sup> area in Mudumalai Wildlife Sanctuary were selected for species mapping using AVIRIS hyperspectral data. Study area is covered under tropical dry and moist deciduous forest. Field inventory data collected at 21 sample plots (0.1 ha) were used to identify dominance species in the study area. Plots were selected considering the vegetations types over the regions, GBH (girth at breast height), height, species name etc were recorded at each plot. Geographic coordinates of each quadrat were collected using GPS.

Species information collected during field survey were used to identify dominance species/community at the particular location. AVIRIS images for the given area is used to collect the image spectra for the corresponding species/community class using the geographic location of the plot in image. A subset of 14.5 km<sup>2</sup> were used for mapping  $\alpha$ -diversity.

## ***3. Methodology***

The following methodology was applied to L2 corrected AVIRIS datasets of the Mudumalai region:

- Out of 425 bands, the high noise bands were removed from the dataset manually and 381 bands were used for further analysis.
- Principal component analysis (PCA) was applied to the spectral data followed by a principal component (PC) selection to decrease spectral dimensionality.
- A subset of pixels was randomly selected from the entire mapped landscape, and the spectral space containing this subset is partitioned into spectral species using k-means clustering, and the location of the centroid of each spectral space was saved.
- The hyperspectral data was gridded in 100mX100m kernels. Within each mapping unit, each image pixel is assigned to a given spectral species, with a maximum of 40 spectral species per kernel (or “digital plot”), based on the minimal Euclidean distance between the pixel and the previously defined centroids.
- A spectral species distribution is obtained for each mapping unit. The Shannon index ( $\alpha$ -diversity) was computed from this distribution.
- Field inventory data were used to obtain the dominant species in study area. Image spectra were collected for the dominant species using the geographic location of the field plots recorded during field survey.
- Spectral Angle Mapper classification technique was used for species mapping using image spectra.

## ***4. Outcome***

### **4.1 Salient findings**

A map which is proportionally representative of the  $\alpha$ -diversity of the region was obtained through this technique (figure 23.1), which may be used for analysis of relation between diversity and spatial and topographical features.

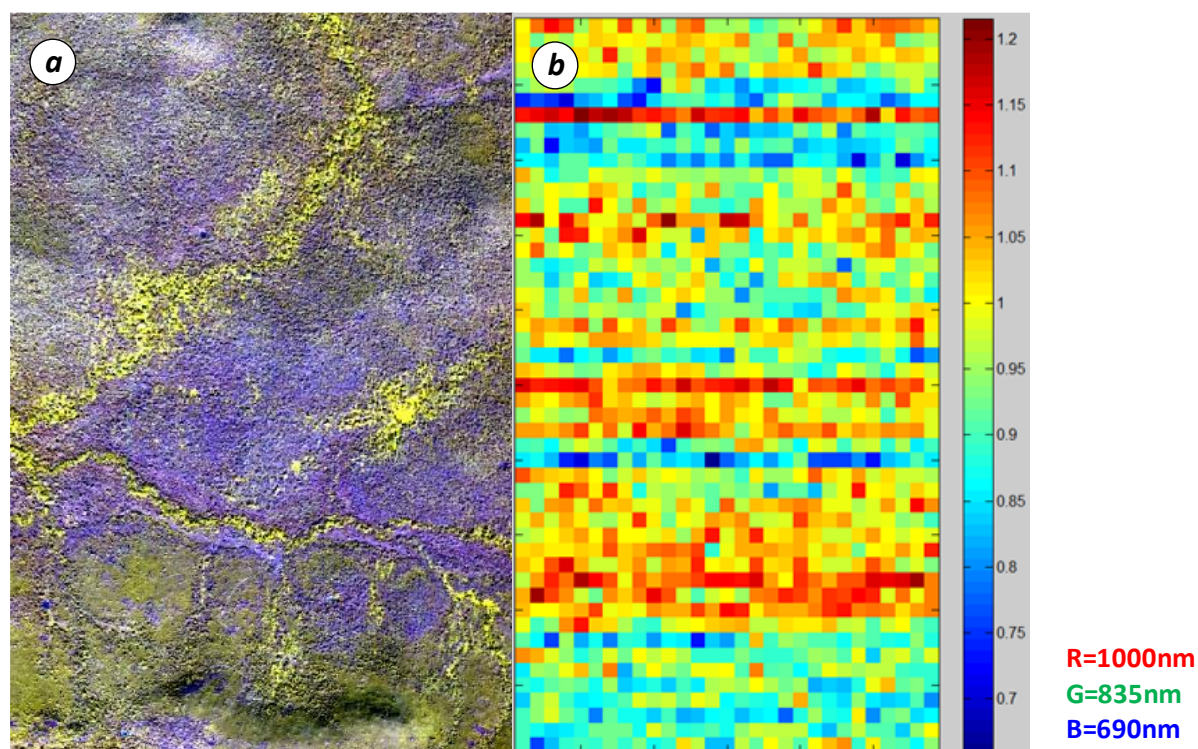


Figure 23.1. (a) Hyperspectral Data; (b) Shannon Diversity Index

Field inventory data were used to identify the dominance species and community type in the study area. Geographic location recorded during field survey were used to collect the image spectra for each class. Dominant species in the study area are *Anogeisuslatifolia*, *Terminalia alata*, *Grewiatilifolia*, *Mangiferaindica*, *Shorearoxburghi*, and *Tectonagrandis*.

SAM classified species map is shown in figure 23.2. Area covered under dominance of different species are given in Table 23.1. SAM classification shows that nearly 40% area is dominated by *Anogesuslatifolia* and 27.5 % by *Tectonagrandis*.

#### 4.2 Target vs. Achievement

S. No.	Targets	Completion
1.	$\alpha$ -diversity mapping	Done
2.	Species mapping	Dominant species has been mapped in Mudumalai using image spectra
3.	Species Map Validation	To be done
4.	Calibration and Validation of $\alpha$ -diversity map	To be done
5.	Systematic field sampling with field spec	To be done

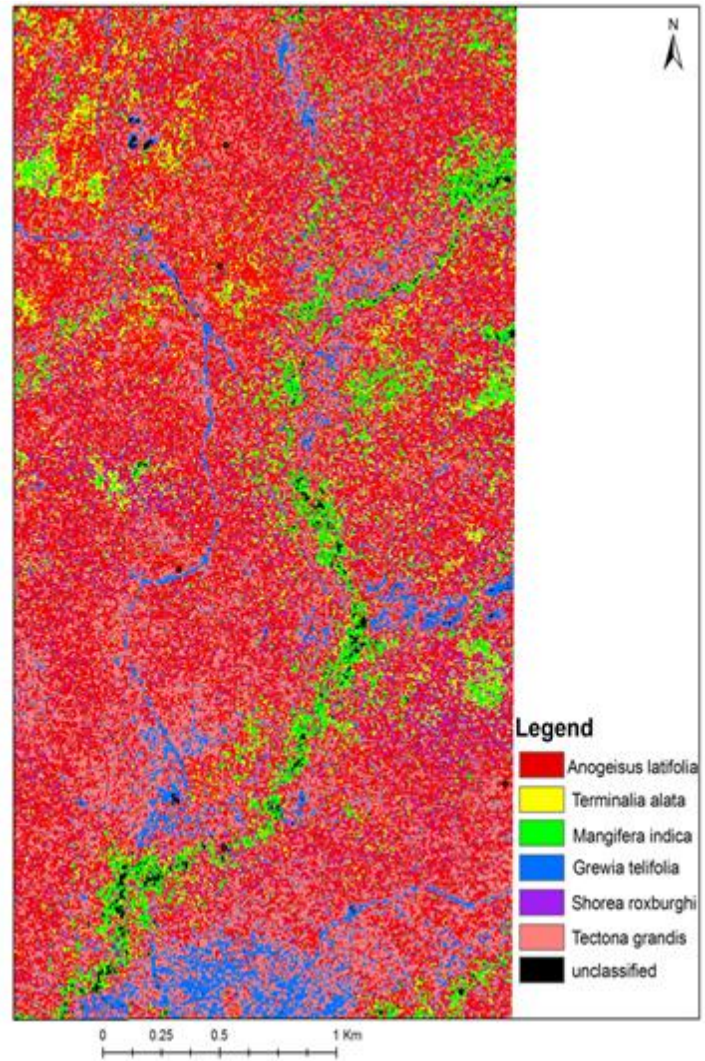


Figure 23.2. SAM based species classified map for study area

Table 23.1. Area under different Species dominance

<b><i>Class</i></b>	<b><i>Area (km<sup>2</sup>)</i></b>	<b><i>Percentage</i></b>
Anogesuslatifolia	8.6	39.8
Terminalia alata	2.2	10.1
Grewiatilifolia	1.2	5.6
Mangiferaindica	1.6	7.4
Shorearoxburghi	1.9	8.8
Tectonagrandis	6.0	27.5
Unclassified	0.2	0.8

### **4.3 Linkage to societal benefits**

This study used AVIRIS data in forest species and  $\alpha$ -diversity mapping at community level. Accurate knowledge of the distribution of species will help the scientific community in better understanding and managing ecosystems and preserving biological diversity.

## **5. Conclusions**

This study conclude that AVIRIS data can be used in Species mapping and  $\alpha$ -diversity mapping at community level. Field inventory required to validate the results.

## **Acknowledgements**

We are thankful to Director, NRSC and Deputy Director, RSA, NRSC for suggestions and encouragements. We are also thankful to AVIRIS team for providing the AVIRIS data.

# Mangrove Species Discrimination using Hyperspectral data

Nilima Rani Chaube and Arundhati Misra

MTDD/AMHTDG/EP  
Space Applications Centre, ISRO, Ahmedabad, Gujarat, India

## ***1. Scientific rationale and Objectives***

The coastline in the estuarine Bengal is the India's largest mangrove known as Sunderbans, which is currently a UNESCO site for its potential and importance in preserving eco systems under threat by human settlements & activities. This ecosystem with the mangroves, is the habitat of the large variety of wild animals i.e. royal Bengal tiger and crocodiles, various reptiles, venomous snakes, insects, marine creatures and migratory birds. The primary productivity of mangroves is higher than many terrestrial ecosystems, therefore they act as carbon sink of blue carbon (oceanic carbon). Mangroves differ from other aquatic and terrestrial plants of same family due to their morphological and physiological features such as aerial roots, vivipary, salt tolerance, capacity to survive in anaerobic conditions. Due to floristic diversity of mangroves, 55-90 mangrove species are being reported worldwide. Unambiguously accepted true mangrove species are Rhizophora, Ceriops, Kandelia, Bruguiera, Avicennia and Aegiceras etc. while Acanthusilicifolius, Nypafruticans are treated as mangrove associates.

## ***2. Study area and data used***

Study area, Site No. 154 is shown with flight lines along with SAC processed L2 data for total and classified mangrove portion shown in figure 24.1. Ground Truth data is used to develop hyperspectral signature of various mangrove species.

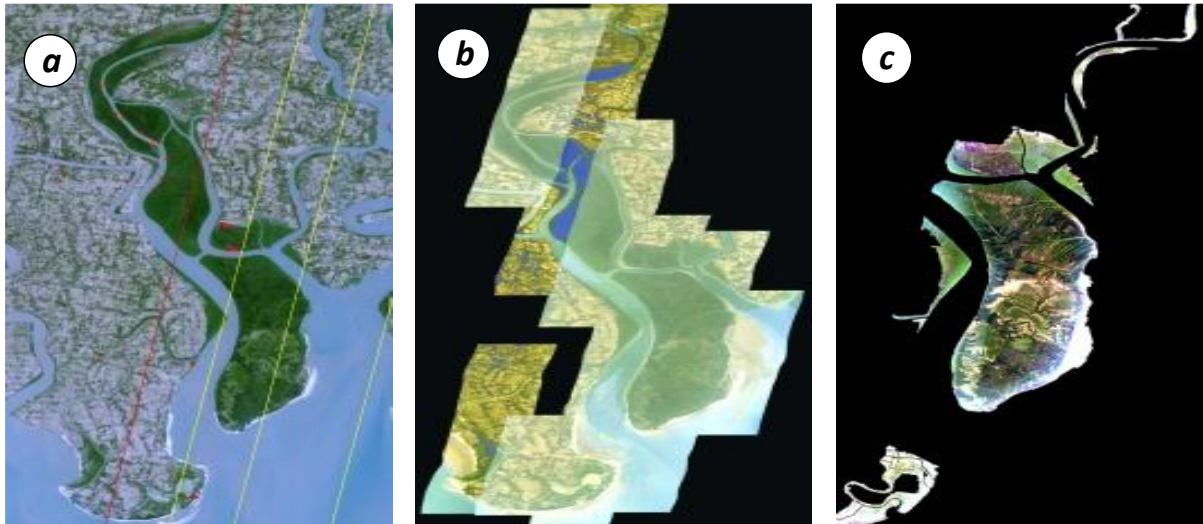


Figure 24.1. (a) Study area; (b) Total Mangrove Coverage in AVIRIS-NG; (c) Classified Mangrove portion

### 3. Methodology

Methodology flow is shown in figure 24.2. Wavelength sensitivity analysis is carried out on GT data and according to that 339 bands out of 425 bands are selected for processing. Hyperspectral signature for various mangroves is given in figure 24.3.

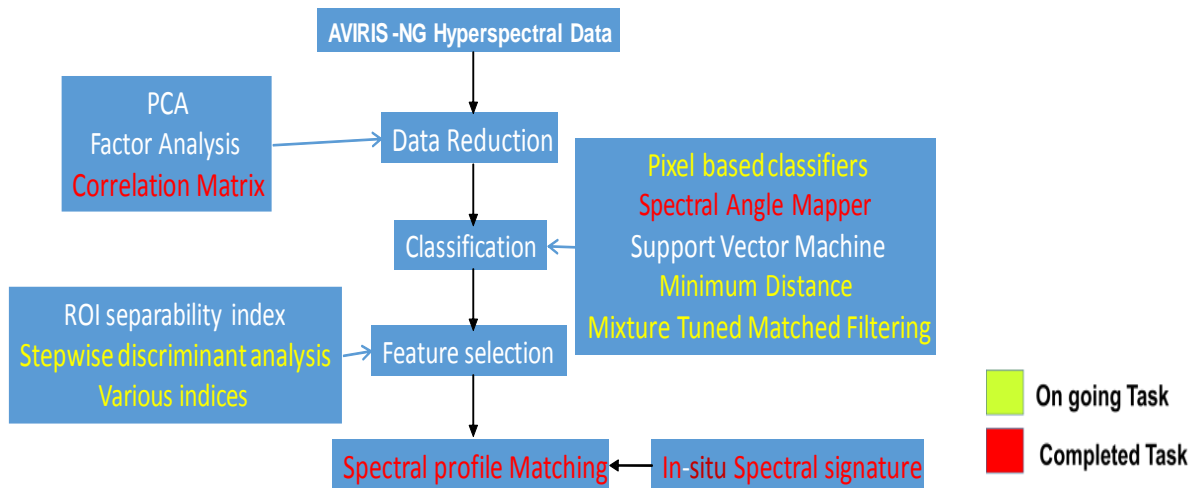


Figure 24.2. Methodology

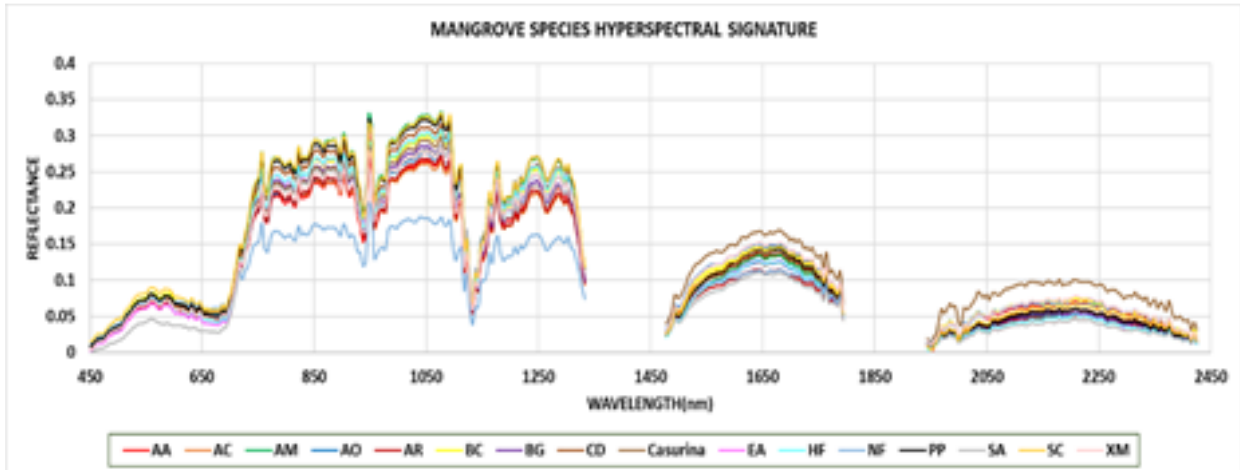


Figure 24.3. Hyperspectral signature of various mangrove species

### 4. Outcome

#### 4.1 Salient findings

15 mangrove species out of 19 species are discriminated using AVIRIS-NG data over Bhagwatpur and Lothian Islands as shown in figure 24.4. This data also has capability to distinguish fresh and marine water as depicted in figure 24.5 over Henry Island. Results are validated with GT at Bhagwatpur, Lothian and Henry islands [1][2]. Various indices for forest health are under study along with the lab results of leaf bio-chemical analysis for various mangrove species. Printice, sushni islands have radiometry problem and will be taken up in subsequent processing.

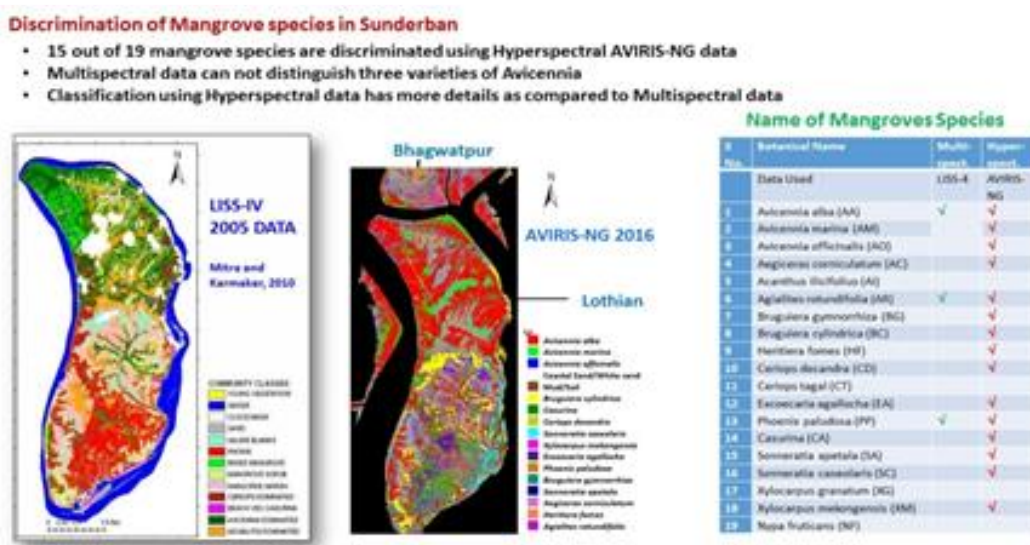


Figure 24.4. Comparison of classified Multispectral and Hyperspectral data

**Discrimination of fresh & marine water using AVIRIS-NG**

- Hyperspectral data can distinguish fresh and marine water
- Pond water and the water in river channel have different composition
- Some of the mangrove and mangrove associates are also classified using AVIRIS-NG data

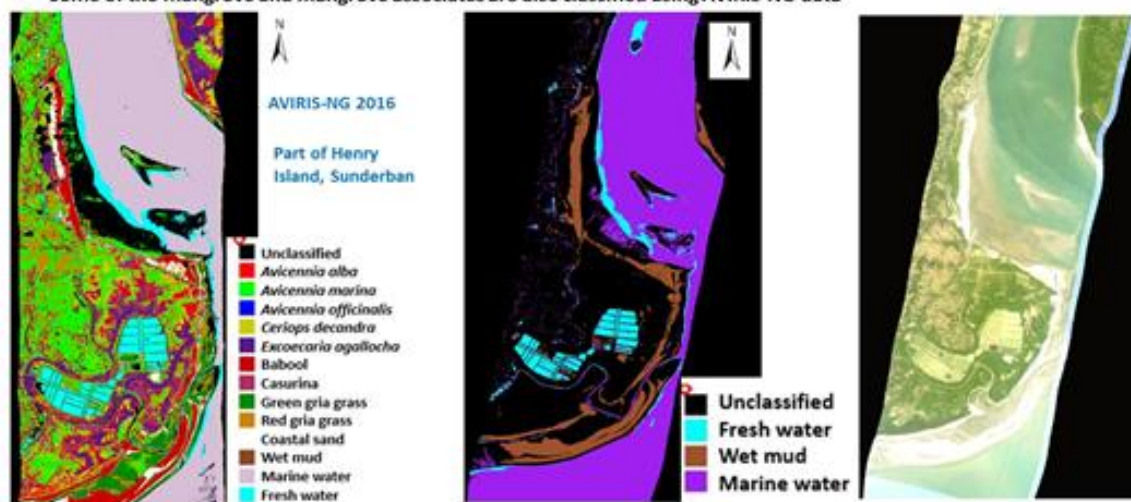


Figure 24.5. Capability to discriminate fresh and marine water

## 4.2 Target vs. Achievement

70 % mangrove species have been classified and verified with GT [3] for more than 50% of mangrove coverage in study site.

Classification of Prentice, Sushni and Fresergunj	Not done
Various indices analysis	Is in progress
Development of other classification techniques	Is in progress

## 4.3 Linkage to societal benefits

Mangroves play a major role in supporting biodiversity, providing economic and ecological security to the coastal communities, mitigating the effects of climate change and global warming. Various other functions performed by mangrove ecosystems are water filtration, nutrient cycling, fisheries support, carbon sequestration, medicinal and food sources, habitat for a wide range of species, land building process, tourism support and aesthetics. India is at 11th position considering the global mangrove cover. Forest of India has reported the mangrove cover of the country as 4628 sq km (FSI, 2013). About 55 mangrove species belonging to 22 genera and 18 families are found in India. West Bengal and Orissa have the richest mangrove forests of the country.

To encounter the seasonal variability of various mangrove species multiple AVIRIS-NG airborne data is required. The study will help in mangrove forest management in choosing plantation sites for conservation of this ecosystem.

## **5. Conclusions**

- Fine resolution AVIRIS-NG hyperspectral data is capable of discriminating various mangrove species. Somewhere mangrove canopy is not filling the 5 m<sup>2</sup> area of 1 resolution cell of AVIRIS-NG data.
- AVIRIS-NG fine resolution airborne is required to study seasonal variation & floristic diversity of various mangroves in future.
- From this study we will establish the requirement to develop new techniques/methods using Hyperspectral remote sensing data to estimate mangrove cover. This will be finally fed into our future spaceborne hyperspectral missions.

## **Acknowledgements**

Authors are grateful to Shri Tapan Misra, Director, SAC and Dr. Rajkumar, DD, EPSA for their support in carrying out this activity.

## **References**

- Chaube, N. R. and Maity, S. (2016). In-situ ground truth measurements for the project titled: Mangrove Species Discrimination using Hyperspectral data”, SAC/EPSA/GHCAG/MHTD/TR/02/2016, March-2016
- Chaube, N. R. and Misra, A. (2017). Mangrove species discrimination using AVIRIS-NG”, SAC/EPSA/GHCAG/MHTD/TR-01/Mar2017
- Mitra, D. and Karmaker, S. (2010). Mangrove classification in Sundarban using high resolution multi-spectral remote sensing data and GIS”, Asian Journal of Environment and Disaster Management, Vol. 2, No. 2 (2010) 197–207, doi:10.3850/S179392402010000268.

# Mangrove ecosystem analysis – A perspective of hyperspectral remote sensing

Nikhil Lele and TVR Murthy

Muktipada Panda, Sushanta Das and R.N. Samal

AED/BPSG/EPISA, Space Applications Centre, ISRO, Ahmedabad, Gujarat, India  
Chilika Development Authority, Odisha, India

## ***1. Scientific rationale and Objectives***

Hyperspectral imagery is acquired using imaging spectrometry, the simultaneous acquisition of images in many narrow (band width less than 10 nm), contiguous spectral bands. As band widths are narrow, local variations in absorption features can be detected that might otherwise be masked within the broader bands of multispectral scanner systems. Hyperspectral scanners mostly cover the 400-2500 nm spectral region, enabling the availability of much broader continuous spectrum than that available with multispectral scanners. This increases the possibilities of determining the characteristic spectral features for analysis, classification and monitoring cover types and processes (Goetz, 1995).

Several attempts have been made using multispectral observations for species-level classification (Rohde & Olson, 1972, Skidmore, 1989). Yet, it is difficult to identify boundaries between vegetation communities. In a coastal wetland environment like mangroves, classification becomes complex due to spectra from water, soil, wet soil, herbaceous vegetation, emergent vegetation, etc. However, hyperspectral narrow spectral channels offer potential to detect and map spatial heterogeneity in vegetation (Hestiret al, 2008; Vaiphasaet al, 2007; Schmidt and Skidmore, 2003).

### **Objectives:**

- Analysis of the in situ spectral signatures for discriminating and mapping mangrove vegetation.
- Species level classification of mangrove ecosystem.
- Estimating biophysical and biochemical properties of mangrove vegetation.

## 2. Study area and data used

Bhitarkanika National Park, in the lower reaches of the Dhamra-Patsala-Maipura River, is an important mangrove ecosystem along the east coast of India. The National Park comes under Rajnagar division in Kendrapada district of Odisha and is located between 20.51°N -20.85°N and 86.75°E – 87.2°E. The estuaries, at the mouth of the river Brahmani, Baitarani, Dhamra, and a large number of ramifying creeks, channels, and distributaries have given rise to luxuriant growth of mangroves. Following are the various field data, ancillary data and remotely sensed data were used during the study:

- Field data- Field data collection was carried out in two teams visiting different places and taking observations using variety of field instruments. Sunphotometer, ozonometer, digital plant canopy imager (Leaf Area Index measurement), portable photosynthesis system (photosynthesis rates), collection of leaf for measurement of lab-based pigments, phytosociological survey of vegetation, etc.
- Remote sensing data- IRS Resourcesat 2- LISS 4 data.

## 3. Methodology

Hyperspectral data typically comes in huge number of bands. Data processing was carried out by geo-correction and converting data to reflectance image. Study area is covered by 6 runs of the flight.

In situ spectroradiometer data was analyzed for similarity and dissimilarity among dominant mangrove species, that was subsequently used in classification of air-borne data. D-matrix given by Price (1994) was used for knowing similarity among species.

$$D = \left[ \frac{1}{\lambda_b - \lambda_a} \int_{\lambda_a}^{\lambda_b} [S_1(\lambda) - S_2(\lambda)]^2 \right]^{1/2}$$

Spectral Angle Mapper (SAM) method was used for classification of mangrove ecosystem and using end-member spectra from the reflectance data. Vegetation analysis was varied out by analyzing the red-edge position of various species. Using the combination of Enhanced Vegetation index and Structure Insensitive Pigment Index (SIPI) a spatial map of forest health

was derived. Forest health across same species was analyzed for its spectral characteristics. In addition, V-NIR hyperspectral imager was used to capture images of vegetation in 96 spectral bands. Field data collection included collecting data for atmospheric parameters, required for image correction, spectroradiometer data of each species, collection of leaf samples for pigments and lab analysis for the same. Detail flowchart of methodology is shown in figure 25.1.

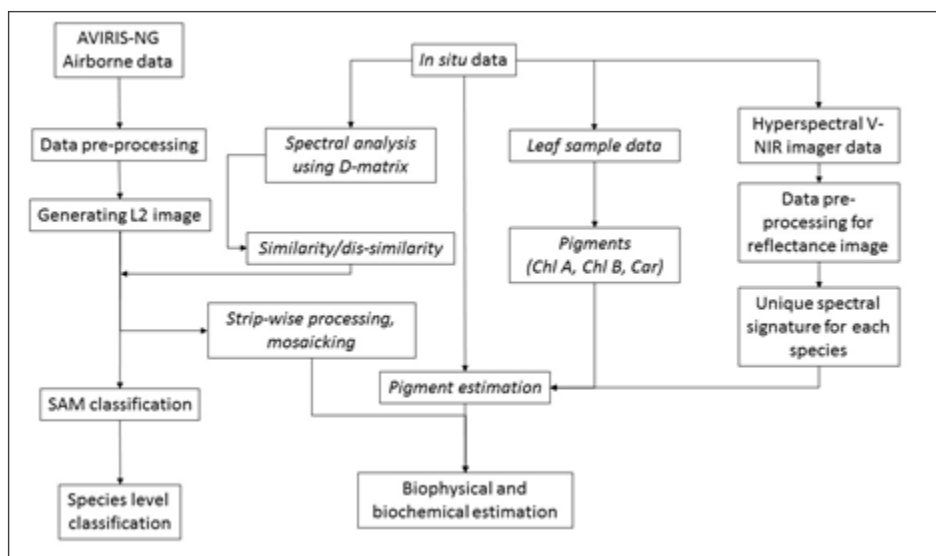


Figure 25.1. Flowchart showing detail methodology

## 4. Outcome

### 4.1 Analysis of *in situ* spectra

Analysis of *in situ* spectra provided a clue for knowing a priori which species are separable from each other, before classification. Higher the value in D –matrix, better is the separability from other one. Table 25.1 shows D Matrix values indicating separability of one species from the other.

### 4.2 Forest discrimination using Spectral Angle Mapper(SAM)

On the basis of ground truth information, end-member spectra were collected and AVIRIS-NG data was classified using SAM algorithm. Dominant species such *Avicennia alba*, *A. officinalis*, *A. marina*, *Excoecaria agallocha*, *Heritiera fomes* were mapped. Certain parts of Bhitarkanika are grasslands which were clearly discriminated using hyperspectral data. Two runs out of complete flight are processed and 3 are under processing.

Table 25.1. Spectral separability analysis using D-matrix. Species with higher difference in the values are better separable in spectral domain

<i>D Matrix</i>		AM	AO	EA	HF	RM	SM	CD	BP	HF-EA	KC	XG
	AM											
	AO	0.058										
	EA	0.033	0.045									
	HF	0.045	0.082	0.039								
	RM	0.110	0.054	0.098	0.136							
	SM	0.117	0.062	0.103	0.139	0.019						
	CD	0.093	0.149	0.121	0.106	0.196	0.203					
	BP	0.051	0.027	0.049	0.082	0.064	0.069	0.135				
	HF-EA	0.068	0.060	0.041	0.057	0.100	0.098	0.151	0.065			
	KC	0.025	0.035	0.028	0.059	0.086	0.094	0.115	0.033	0.062		
	XG	0.033	0.038	0.013	0.047	0.091	0.096	0.124	0.043	0.045	0.023	
	Minimum	0.025	0.027	0.013	0.047	0.019	0.069	0.115	0.033	0.045	0.023	
	Maximum	0.117	0.149	0.121	0.139	0.196	0.203	0.151	0.065	0.062	0.023	

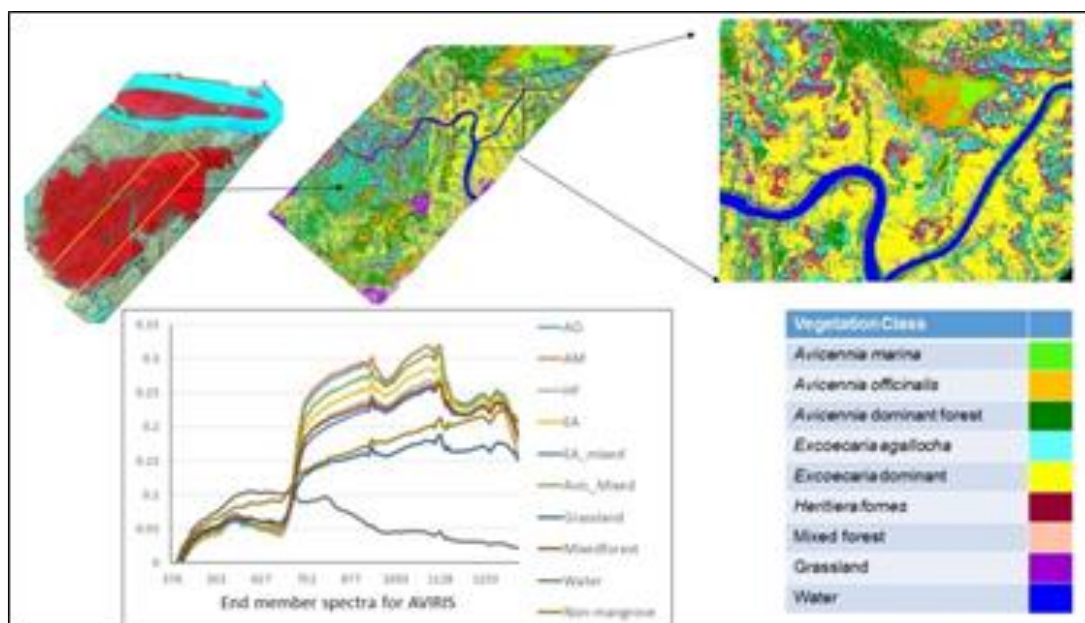


Figure 25.2. Mangrove forest discrimination based on SAM depicting dominant mangrove species

### 4.3 Better separability using hyperspectral data

Along with Hyperspectral data, IRS Resourcesat 2 LISS 4 multispectral data of 5.8-meter resolution were acquired and was subjected to supervised classification.

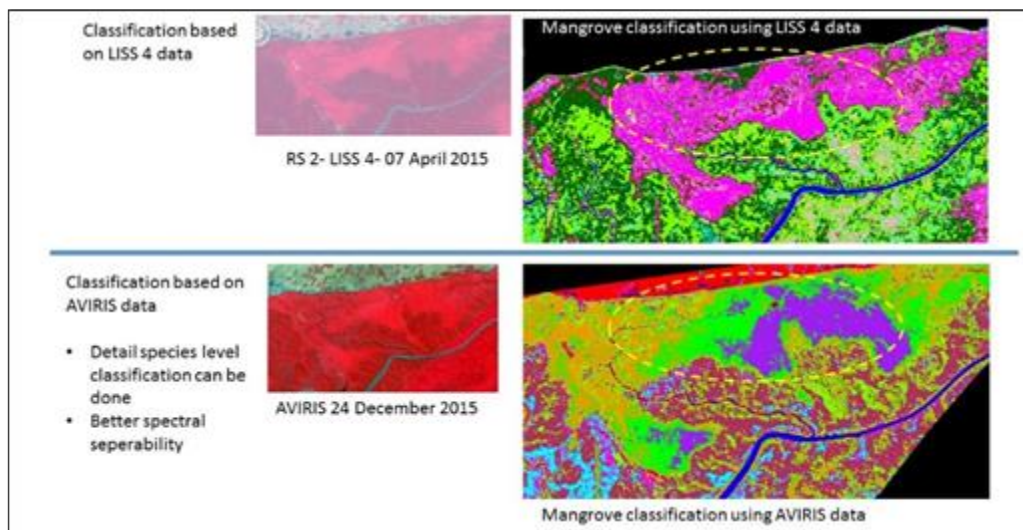


Figure 25.3. Comparison of classification using Resourcesat 2 LISS 4 multispectral data and AVIRIS hyperspectral data. Better class separability due to higher spectral & spatial resolution was achieved.

It was found that Hyperspectral data allowed identifying more number of classes because of its better spectral resolution as shown in figure 25.3. The spatial resolution of hyperspectral data was nearly 5 m, which is almost similar to spatial resolution of LISS 4.

#### 4.4 Mangrove forest health assessment

Forest health assessment was analysed for various species based on EVI (Enhance Vegetation Index) and SIPI (Structure Insensitive Pigment Index) that makes use of 440 nm, 680nm & 800 nm. Health assessment was done in 2 ways:

- Difference in vegetation reflectance- in red and NIR wavelengths. Qualitative health condition of the same species under similar densities had shown pronounced differences (higher the reflectance, better the health).

- Red-edge position:

In stress affected / less healthy plants, chlorophyll absorption is affected, which is seen in the vegetation spectra, particularly in red-edge position. Lower values of red-edge were found in stressed (less healthy) vegetation as shown below.

*Excoecariaagallocha*: 714 & 729 nm; Mixed forest :714 & 719 nm;

*Avicenniamixed forest*: 719 & 724 nm (as less healthy & healthy, respectively)

Also, areas close to creeks and jetty as well as along the walkways were found to have less healthy vegetation as seen in figure 25.4.

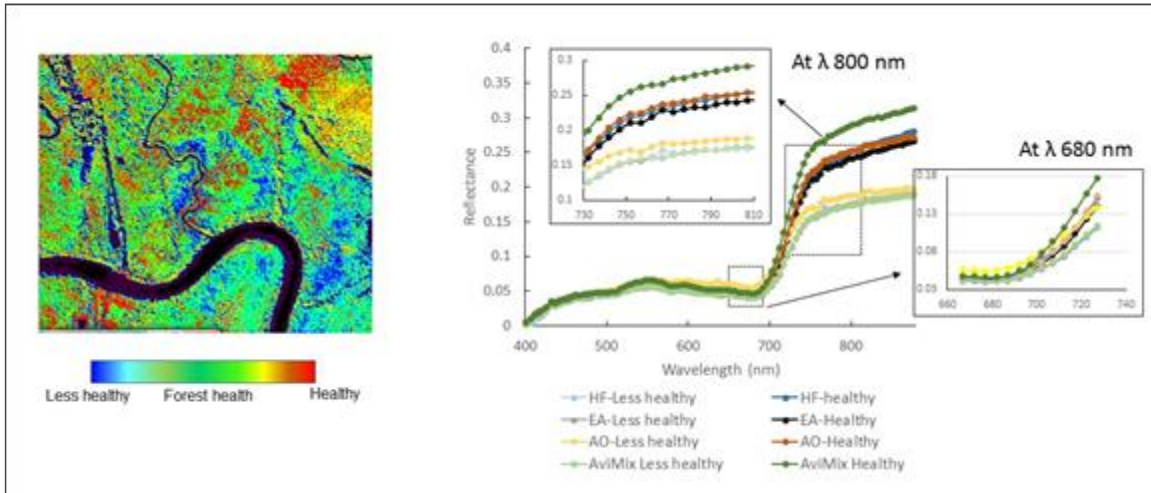


Figure 25.4. Mangrove forest health assessment.

### 4.5 Utility of Hyperspectral canopy imager

Hyperspectral V-NIR Imager that captures target image in 96 bands (350 nm to 1025) was used in this campaign. Forest canopy was chosen as target for taking the such photograph. figure 25.5 shows spectra derived from hyperspectral.

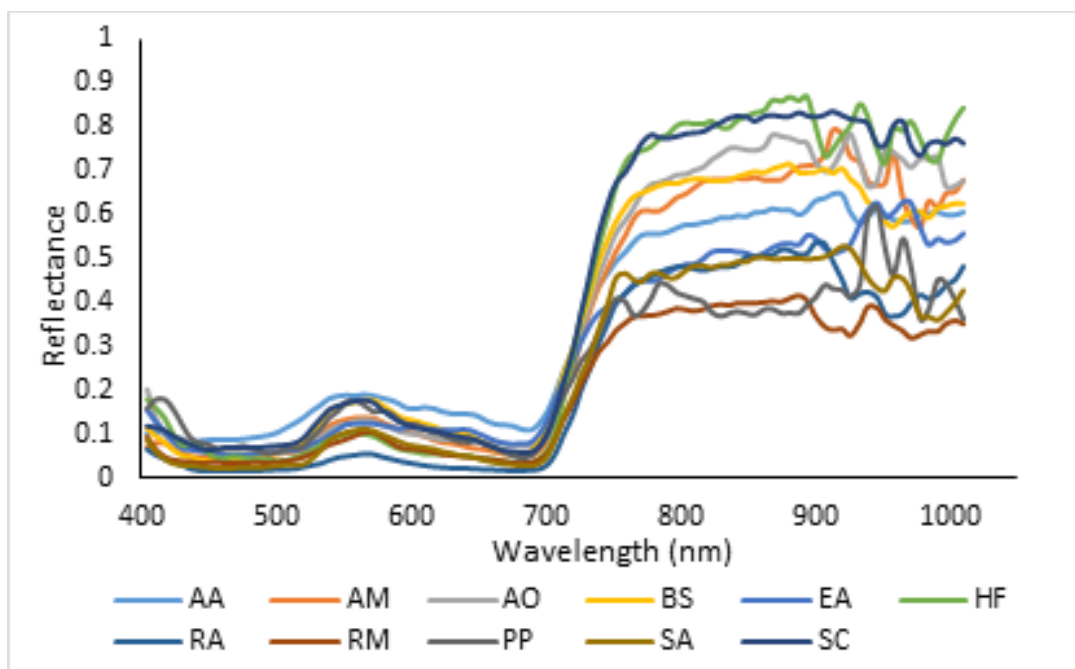


Figure 25.5. Spectra from hyperspectral imager for dominant mangrove species

### 4.6 Target vs. Achievement

Sr No.	Achievement (Objective / activities)	% completed
1	Analysis of the in situ spectral signatures for discriminating and mapping mangrove vegetation.	Complete

2	Species level classification of mangrove ecosystem	80% over; Accuracy assessment remaining.
3	Estimating biophysical and biochemical properties of mangrove vegetation	50 % over
4	Additional activities - Forest health assessment	80% over
5	Analysis from Hyperspectral V-NIR Imager	70 % over

#### 4.7 Linkage to societal benefits

- Species level mapping of forest enables forest administrators to prepare managements plans. In place like national park, status of biodiversity and such maps help in societal education and awareness for visitors.
- Biochemical constituents such as presence of phenolics, aromatic materials have high economic importance. Some of the forest species exhibit these unique materials that may have economic potential.

### 5. Conclusions

- Hyperspectral data allowed better class separability owing to its higher spectral resolution.
- Overall health condition on the vegetation (that may be combined defect of degradation / drought / disease) can be detected by means of hyperspectral data.
- It allows for estimation of pigments and plant biochemical constituents that are otherwise not detectable using merely multi-spectral observations.

Following activities can be accomplished in 2<sup>nd</sup> phase of AVIRIS campaign:

- Biochemical analysis of certain parameters like nitrogen, lignin and cellulose requires special precaution for fixing and preservation of samples in field, followed by laboratory analysis. These estimations can be attempted in next phase.
- Seasonal variation in mangrove phenology as well as changes in pigments during these phases can be studied. Particularly, in *Excoecaria* species deciduous nature is more prominent as compared to other species, and is found commonly at Bhitarkanika.

### Acknowledgements

We are obliged to DrTapan Mishra, Director, Space Applications Centre (SAC), providing all the necessary facilities to carry out this work. We are grateful to Dr Raj Kumar, Deputy

Director, (EPSA) and Dr. Prakash Chauhan, Group Director (BPSG) for necessary support and suggestions during the campaign. We are thankful to Dr Bimal K Bhattacharya- Head (AED) and Project Director (AVIRIS-NG) for his continuous involvement throughout the campaign and time to time guidance. We express our gratitude to PCCF (Principal Chief Conservator of Forests), Odisha forest department for giving necessary permissions and thank Forest department of Odisha for required support during field work.

## References

Goetz, A.F.H. 1995. Imaging spectrometry for remote sensing: vision to reality in 15 years. In M.R. Descour, J.M. Mooney, D.L. Perry, and L. Illing (Eds.), *Imaging Spectrometry*, Vol. 2480, (pp. 2-13). Bellingham, WA: The International Society for Optical Engineering (SPIE).

Hestir, E.L., Khanna, S., Andrew, M.E., Santos, M.J., Greenberg, J.A. Rajapakshe, S.S. and Ustin, S.L. 2008. Identification of invasive vegetation using hyperspectral remote sensing in the California Delta ecosystem. *Remote Sensing of Environment*, 112, pp. 4034-4047.

Price, J. C. 1994. How unique are spectral signatures? *Remote Sensing of Environment*, 49, 181–186.

Schmidt, K.S. and Skidmore, A.K. 2003. Spectral discrimination of vegetation types in a coastal wetland. *Remote Sensing of Environment*, 85, pp. 92-108.

Vaiphasa, C.K., Skidmore, A.K., de Boer, W.F. and Vaiphasa, T. 2007. A hyperspectral band selector for plant species discrimination. *ISPRS Journal of Photogrammetry and Remote Sensing*, 62, pp. 225-235.

# Mapping vegetation parameters for fuel load estimation in Shoolpaneshwar forests using AVIRIS-NG

C. P. Singh and Jakesh Mohapatra

AED/BPSG/EP  
Space Applications Centre, ISRO, Ahmedabad, Gujarat, India

## ***1. Scientific rationale and Objectives***

Fire fuel analysis is primarily based on indices which can show the bulk amount of green vegetation or greenness, the water content of the vegetation and dry or senescent carbon which can highlight non-photosynthetic vegetation (NPV). If fire fuels are located beneath a closed canopy, they may not be detected by this technique. However, in Shoolpaneshwar area the AVIRIS-NG data acquisition coincided with the prime senescence period for the deciduous trees of the area. Therefore, the deciduous trees having large amount of leaf litter on the surface were prone to encounter possible fire outbreak due to high presence of fire fuel. The areas having green canopy with good canopy closure is expected to reduce the detection of fire prone dry shrubs beneath the green canopy because dry or senescent indices are only sensitive to the top layer of the vegetation, causing the dry vegetation beneath it to be obscured by the upper layer of green vegetation. However, Shoolpaneshwar area mostly having deciduous forest and density of forest being moderate fire fuel detection has been attempted.

## ***2. Study area and data used***

Shoolpaneshwar forest area is a wildlife sanctuary which has vast, undulating terrain with good forest cover at the congregation of Vindhyan-Satpura hill ranges. The forest area rated as one of the best and thickest in Gujarat state, is situated between 21°30'51" – 21°52'55"N and 73°38'55" – 73°44'52"E covering approximately 397 km<sup>2</sup> area (as per flight plan, figure 26.1). The sanctuary has two distinct forest types viz. Southern Tropical Moist Deciduous Forest, sub type slightly moist teak forests 3B/C1C and Southern Tropical Dry Deciduous Forests, sub type dry teak forests 5A/C1B (Champion & Seth, 1968). The area is generally hilly and rugged with precipitous slopes at most of the places. The soils in this area vary in color,

texture, depth and stoniness depending upon the rock and topography. There are three main seasons - Monsoon, which extends from June to October, winter from November to February and summer from March to June (defined by the senescence in the sanctuary). The area receives an annual rainfall of 100 to 125 cm. The summers are hot while the winters are pleasant.

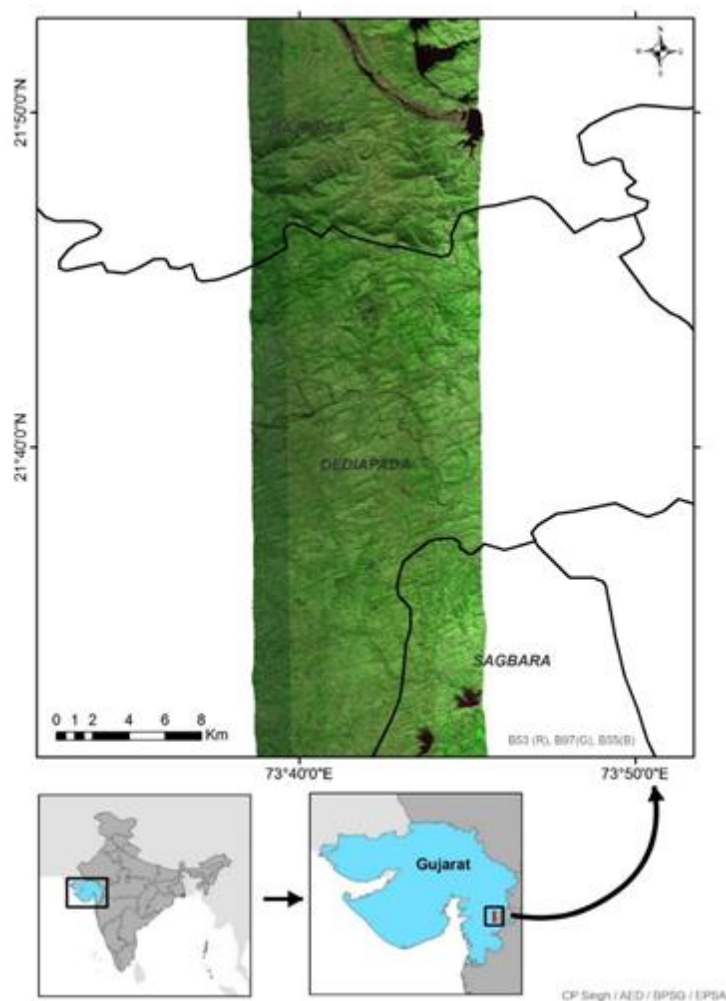


Figure 26.1. Study area map showing AVIRIS data over part of Shoolpaneshwar forest.

The two forest types found in the area are not distinctly reflected on topography. The moist teak forests are found in Fulsar, Piplod, and Sagai ranges of the sanctuary. The composition of teak is usually 25% of the total stand. The dry teak forests also occur in the same locality within a short distance but mostly on poor soils, hill ridges and areas subjected to biotic interference. Under storey consisting of *Dendrocalamus strictus* (bamboo), is a characteristic feature of this area. There are about 575 species of flowering plants in this area. Ground cover

consists of evergreen to semi evergreen species and occurrence of woody climbers is common feature. This area can be categorized into different strata. The top strata are occupied by the trees, which consist of *Tectonagrandis*(teak), *Terminalia cranulata*(sadam), *DalbergiaSissoo*(sisam), *Anogeissuslatifolia*, *Lanneacoromandelica*, *Garugapinnata*, *Mitragynaparvifolia*, *Lagerstroemia parviflora*, *Diospyrosmelanoxylon* (timru), *Soymidofebrifaga*, *Terminalliabellerica*, *Madhucaindica* (mahuda), *Emblicaoofficialis* (amla), *Acacia catechu* (khair), *Sapindustrifolatus* (aritha), *Ougeiniaoojeinensis* (tanachh), *Jatropha curcus* (karanj) and rest are other species.

### 3. Methodology

The AVIRIS-NG calibrated reflectance product was used for estimation of following important narrowband indices:

- Modified Red Edge Normalized Difference Vegetation Index (MRENDVI), This index is a modification of the Red Edge NDVI that corrects for leaf specular reflection. It capitalizes on the sensitivity of the vegetation red edge to small changes in canopy foliage content, gap fraction, and senescence to detect vegetation stress conditions (Sims & Gamon, 2002). The value of this index ranges from -1 to 1. The common range for green vegetation is 0.2 to 0.7.

$$MRENDVI = \frac{\rho_{750} - \rho_{705}}{\rho_{750} + \rho_{705} - 2 * \rho_{445}}$$

- Moisture Stress Index (MSI), This a reflectance measurement that is sensitive to increasing leaf water content. As the water content of leaves in vegetation canopies increases, the strength of the absorption around 1599 nm increases. Absorption at 819 nm is nearly unaffected by changing water content, so it is used as the reference. This index is useful for fire hazard condition analysis (Jackson et al., 2004). The MSI is inverted relative to the other water VIs; higher values indicate greater water stress and less water content. MSI is defined by the following equation:

$$MSI = \frac{\rho_{1599}}{\rho_{819}}$$

The value of this index ranges from 0 to more than 3. The common range for green vegetation is 0.4 to 2.

- Plant Senescence Reflectance Index (PSRI)

This is designed to maximize the sensitivity of the index to the ratio of bulk carotenoids (for example, alpha-carotene and beta-carotene) to chlorophyll. An increase in PSRI indicates increased canopy stress (carotenoid pigment), the onset of canopy senescence, and plant physiological stress detection (Merzlyak et al, 1999). PSRI is defined by the following equation:

$$PSRI = \frac{P_{680} - P_{500}}{P_{750}}$$

The value of this index ranges from -1 to 1. The common range for green vegetation is -0.1 to 0.2.

By comparing the results of different VIs in a particular category, and correlating these to field conditions measured on site, we could assess that above indices will do the best job of modelling the variability of fuel load in the given area. These indices are used in mapping relative amounts of vegetation components, which were then integrated through overlay analysis in terms of assessing fire fuel load. To calculate fire fuel, we first computed the narrowband greenness indices and selected MRENDVI. Further, indices indicating level of canopy water content were tested and MSI was found suitable. Lastly the indices indicating dry vegetative material were evaluated and PSRI was found most suitable. Equal weightages were given to one representative from each category and values were stretched from 1 to 9 (ten classes) with 9 being most heavily loaded with fuel.

## **4. Outcome**

### **4.1 Salient findings**

The output of individual indices is given in figure 26.2 and overlay analysis based forest fuel load map is given in figure 26.3.

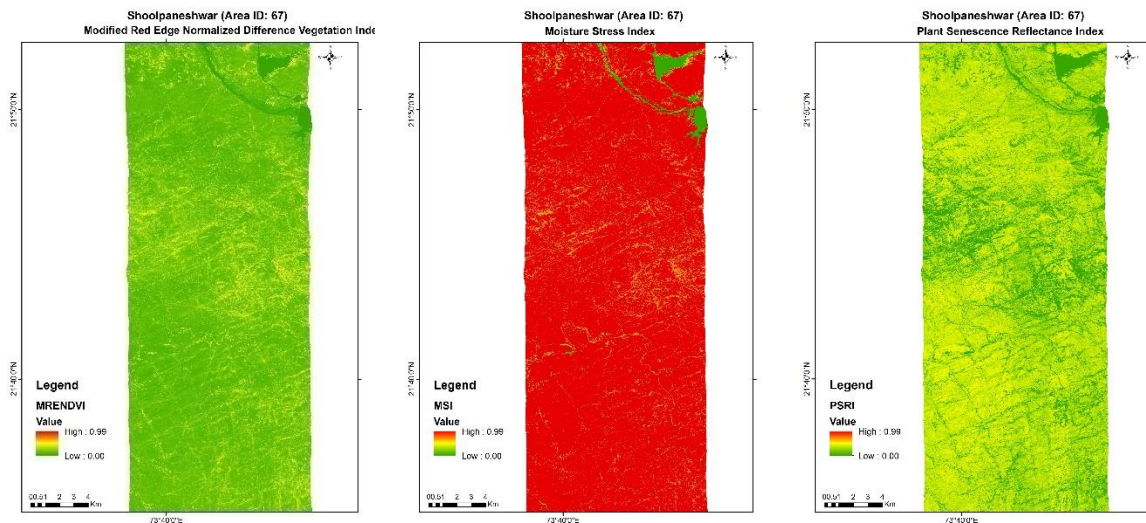


Figure 26.2. Vegetation indices (MRENDVI, MSI, PSRI) for fuel load estimation

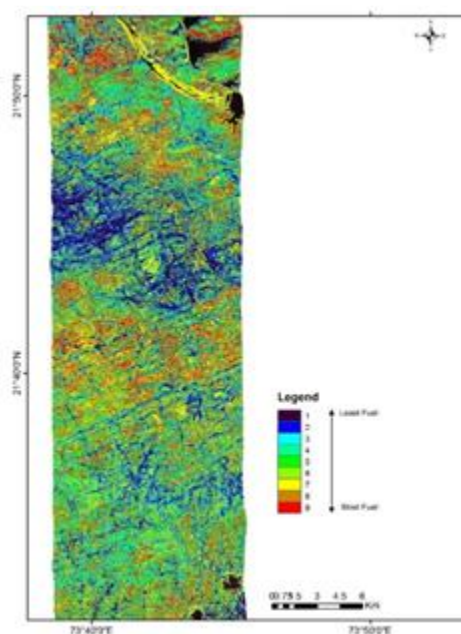


Figure 26.3. Forest fuel load map of Shoolpaneshwar forest using AVIRIS based vegetation indices

The fuel load data could not be directly validated in absence of field experiments designed for computing the litter biomass and moisture content, however, vicarious validation was attempted with the actual fire counts in different categories of fuel load ranging from 1 – 9. It was interesting to note that only 38% of fire events were falling in the category range of 5 – 9 (Table 26.1 & Figure 26.4). However, the dryness conditions would have changed over period of time and newer scenarios would have developed at the later dates.

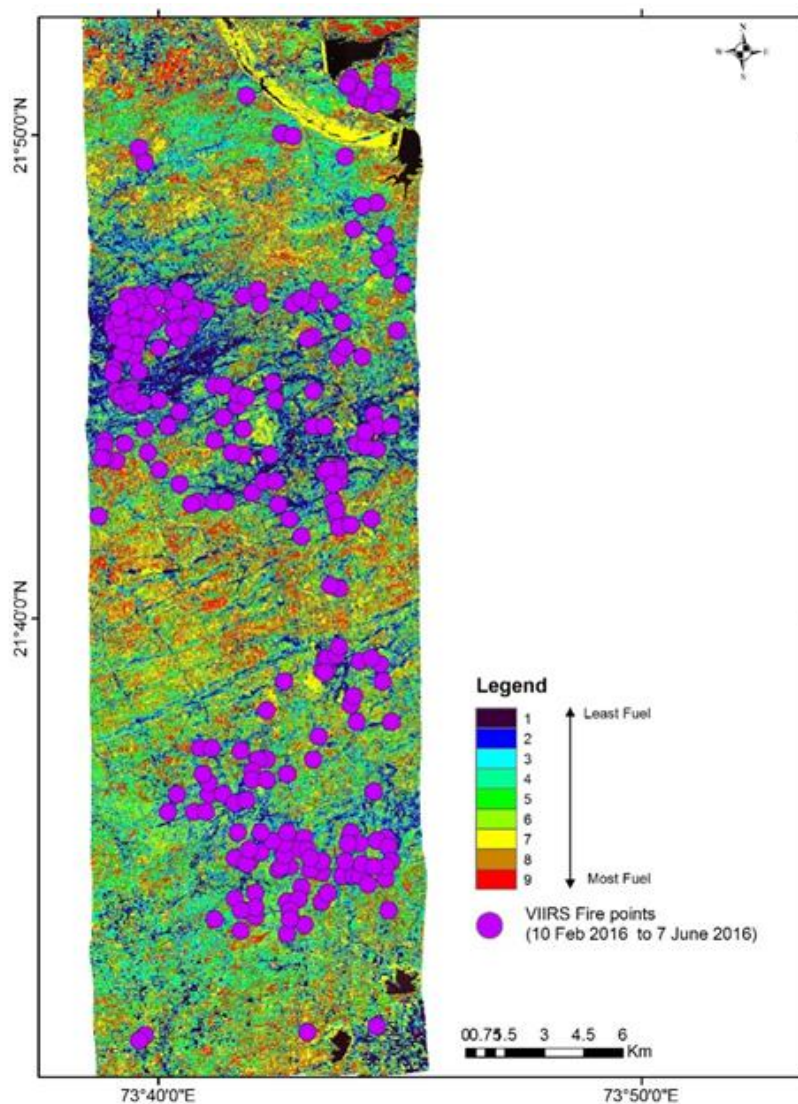


Figure 26.4. Vicarious validation of fuel load using active fire points detected after acquisition of AVIRIS-NG data

Table 26.1. Records of VIIRS detected fire during 10 Feb 2016 to 7 June 2016) on underlying fuel condition as detected by AVIRIS-NG on 08 Feb 2016

<i>SN</i>	<i>Fuel Load Rank</i>	<i>Fire frequency %</i>
1	1	20
2	2	22
3	3	16
4	4	4
5	5	8
6	6	14
7	7	6
8	8	5
9	9	6

## 4.2 Target vs. Achievement

<i>Sr No.</i>	<i>Achievement (Objective / activities)</i>	<i>% completed</i>
1	Species level classification	20%
2	Estimating biophysical and biochemical properties	50 %
3	Forest fuel load assessment	80%
4	Ecological diversity indices	10 %

## 4.3 Linkage to societal benefits

This kind of operational products can be very useful for forest managers in order to protect the forest resources.

## 5. Conclusions

- AVIRIS-NG data with higher spectral and spatial resolution provided us with unique opportunity to carry out the biochemical level spectroscopy of the forest landscape in Shoolpaneshwar.
- Overall stress and dryness condition of the deciduous forest could be detected by means of AVIRIS-NG data.
- It allowed us to accurately estimate the plant level greenness or senescence conditions and availability of material as fuel which was not possible through available multi-spectral observations.

Following activities can be accomplished in 2nd phase of AVIRIS campaign

- The second phase of observation can greatly enhance the information content and learning of the subject. We are now equipped with duff moisture meter which will be able to give us direct measurement of fuel moisture content.

## Acknowledgements

We are highly indebted to Tapan Mishra, Director, Space Applications Centre, for providing all the necessary facilities to carry out this work. We are grateful to Dr RajKumar, Deputy Director, (EPSA) and Dr. Prakash Chauhan, Group Director, BPSG for their support and suggestions during various reviews. We are thankful to Dr Bimal K Bhattacharya- Head (AED) and PD, AVIRIS-NG for his guidance and untiring efforts towards completion of our goals. We also express our gratitude to team of MS University, Baroda and Gujarat Forest Department for field support.

## References

Champion, H.G. and Seth, S.K. (1968). A Revised Survey of the Forest types of India. Manager of Publications, Government of India, Delhi, India, xxviii+404pp.

Sims, D. and J. Gamon, 2002. Relationships Between Leaf Pigment Content and Spectral Reflectance Across a Wide Range of Species, Leaf Structures and Developmental Stages. *Remote Sensing of Environment*, 81: 337-354.

Jackson, T.L., D. Chen, M. Cosh, F. Li, M. Anderson, C. Walthall, P. Doriaswamy, and E.R. Hunt, 2004. Vegetation Water Content Mapping Using Landsat Data Derived Normalized Difference Water Index for Corn and Soybeans. *Remote Sensing of Environment* 92:475-482.

Merzlyak, J.R., A.A. Gitelson, O.B. Chivkunova, and V.Y. Rakitin, 1999. Non-destructive Optical Detection of Pigment Changes During Leaf Senescence and Fruit Ripening. *Physiologia Plantarum* 106:135-141.



## Geological Applications

### Summary

Mineral exploration potential for existing mining areas and to find out new mining areas and zones for hydro-thermal alterations is the key societal benefit area where there is large scope of applicability of imaging spectroscopy. The primary objectives of the studies on geology are to recognize various mineralogical and lithological units within the target areas and map them with the support of their representative hyperspectral signature analysis; and on the other end to categorize the future exploration target sites based on various geo-physico-chemical parameters. Initial analysis of AVIRIS-NG data over Jahazpur and surrounding mineralized belts of Rajasthan divulged exciting results in terms of host rock characterization. The spectral analysis of these areas suggest that the principle mineralogies are Mg-Carbonates, Talc bearing lithologies and other associated clay minerals, i.e. Montmorillonite and Kaolinite. Spectral analysis over Ambaji and the surrounding areas revealed that the western part of the study area is mainly dominated by the Calcite while the northern and eastern parts consist of clay minerals containing Al-OH bonds. In addition, in the representative reflectance spectra, a shift in absorption wavelength is notified which may be due to the subtle compositional variation of carbonates, between Calcite and Dolomite. Most of the minerals show the deepest absorption feature at the wavelength range of 2.0 – 2.5  $\mu\text{m}$  in their characteristic spectra. The mapping of this absorption feature on the area can be useful for further exploratory analysis. The AVIRIS-NG data of the study areas of Sittampundi Layered Complex, Erode, Tamilnadu, Bhukia Bhimsore area, Banswara, Rajasthan and Wajrakarur, Andhra Pradesh have been analysed to comprehend the exploration value of AVIRIS-NG derived spectral anomaly. These datasets are demarcating the abundance of patchy exposures of Chromite and Dolomite in Sittampundi areas. The AVIRIS-NG data are also useful for recognizing the Kimberlite and Dolomite in Wajrakarur and Bhukia areas, respectively. Additionally, the Serpentine mineralization was confirmed on the South-eastern part of Dungarpur, Rajasthan during the ground study, which is a martian analog. This gives the information about the hydrothermal alteration process in the martian past.

# **A mineralogical appraisal of Jahazpur and adjoining areas of Rajasthan as revealed by AVIRIS-NG imaging spectrometer**

Satadru Bhattacharya, Aditya K. Dagar and Sumit Pathak

Planetary Sciences Division, BPSG/EPSC  
Space Applications Centre, ISRO, Ahmedabad, Gujarat, India

## ***1. Scientific rationale and Objectives***

Of late, imaging spectroscopy has become an invaluable tool for detection and mapping of minerals/ mineral assemblages and for identification of signatures/indicators for mineral exploration. Recent advancements in the field of hyperspectral remote sensors, both airborne and space-borne, along with the very advanced and fast computing systems have made it possible to detect and quantify various earth resource materials (Goetz 2009; Goetz et al. 1985; Clark et al. 1990). Therefore, there is a paradigm shift in the field of remote sensing from remotely identifying an object to remote quantification. One of the earliest applications of hyperspectral remote sensing identified was geological mapping and its commercial role in mineral exploration (Goetz 2009).

Remote imaging spectrometers provide information on the physico-chemical characteristics of rocks and soils and surface geochemistry of an area in a spatial context thereby helping in delineating exploration targets for metals and industrial minerals (Kruse 1988). Visible/near-infrared (VNIR) spectroscopy in the spectral range of 0.4 – 2.5  $\mu\text{m}$  provide detailed information about many important earth surface minerals (Clark et al. 1990). Studies on laboratory spectroscopy (Hunt and Salisbury 1970; Clark et al. 1990) and data using remote imaging spectrometers (Kruse 1988, Kruse et al. 1990, Staenz and Williams 1997, Kruse et al. 2003, Neville et al. 2003; Bhattacharya et al. 2012) have well established its efficiency in mineral identification, quantification, mapping and exploration (Goetz 2009).

In view of the above, a two-day airborne campaign was carried out over the mineralized belt of Jahazpur, Rajasthan, India involving Airborne Visible-Infrared Imaging Spectrometer – Next

Generation (AVIRIS-NG) instrument during February 04-05, 2016 to carry out remote geochemical mapping of the study area and delineation of potential future exploration targets within the studied region. This was the first ever airborne campaign of AVIRIS-NG over Indian territories courtesy a joint venture between ISRO and JPL-NASA.

### **Objectives**

- The primary objective of the present study is to map diverse mineralogical and/or lithological entities present within the study area based on spectral signature studies, which is otherwise not possible using a broad-band remote sensor.
- To identify the future exploration targets within the study area based on physico-chemical parameters such as mineralogy, structure, lineament distribution, degrees of weathering and leaching, presence of hydrothermal alteration zones & gossans etc.

## ***2. Study area and data used***

The study area is situated in the south eastern part of the Aravalli craton and primarily represents a low-grade metasedimentary sequence (greenschist facies) (Gupta et al. 1981) sharing a thrust contact with the rocks of the Mangalwar complex in the northwest and separated from the Vindhyan sediments by the Great Boundary Fault (GBF) of Rajasthan in the southeast. The area comprises mostly of the lithoassemblages belonging to the Jahazpur Group and Hindoli Group (table 27.1 and figure 27.1). The Jahazpur rocks form two linear belts, namely, the eastern Jahazpur belt and the western Jahazpur belt. The former is enclosed within a sequence of turbidite-volcanic association of the Hindoli Group, while the latter unconformably overlies the Hindoli sequence. Jahazpur Group of rocks comprise polymictic conglomerate, gritty quartzite, orthoquartzite, arkose mica schist, chert, breccia, dolomitic marble, carbonaceous phyllite and BIF that overlies the Hindoli Group unconformably and shares a tectonized contact, occurring between southeast of Nandrai in Bhilwara district to Naenwa in Tonk district. The western margin of the western Jahazpur belt shares a thrust contact with the migmatites and gneiss of Mangalwar Complex that have been juxtaposed on the Jahazpur belt. In the eastern Jahazpur belt, the base of the Jahazpur sequence overlying the Jahazpur Granite (c.a. 2.5 Ga equivalent to Berach Granite) is marked by a pebbly quartzite and arkose bed and an overlapping Jahazpur dolomite (GSI Miscellaneous Publication No. 30, Part 12, 2011).

The Lower Proterozoic supracrustal rocks of the Jahazpur Group of Bhilawara Supergroup are found to have potential for base metal mineralization. The intracratonic failed rifts of eastern and western Jahazpur belts represent a classic example of SEDEX type base metal mineralization. The host rocks for base metal mineralization at Jahazpur include dolomite, dolomitic marble, carbonaceous phyllite, Banded Iron Formation (BIF) and dolomite with BIF. Old workings can be seen in the study area in association with ferruginous cherty-breccia and BIF belonging to Jahazpur group. Bedrock sampling in the area had revealed concentrations of Pb up to 1.4% and Zn up to 0.37% (GSI Miscellaneous Publication No. 30, Part 12, 2011). Galena is also found to be present in the mine dumps. Chalcopyrite stringers are seen in the mine dumps of a dolomitic marble quarry near Bedunda village (figure 27.2).

JPL-L2 reflectance product of AVIRIS-NG (AVIRIS, 2007) has been used for the present study. A total of six scenes were acquired during February 04-05, 2016 covering Jahazpur and adjoining regions of Rajasthan. AVIRIS-NG instrument measures the reflected solar radiation in the spectral range of ~376-2500 nm at a spectral resolution of 5 nm over 425 contiguous spectral channels. The aircraft was flown at an altitude of approximately 8 km providing a ground resolution cell of roughly 8 m. In addition to that, ASD FieldSpec4 Hi-Res spectrometer has also been utilized in the spectral range of 350-2500 nm to obtain the in situ as well as lab-based reflectance spectra of rocks and soil samples collected from the field.

Table 27.1. The stratigraphic succession as given by G.S.I.

Era/ Peiod	Gelological Cycle	Group	Lithology
Quarternery	-	-	Alluvium, blown sand
UpperProterozie	VindhyanSupergroup	Bhander Group	Shale, snadstone and limestone
PROTHROZOIC	Delhi Super Group	Kumbhalgarh Group	Calc-Schist, gneisses, marble, garnet-boititeschust, migmatites
		Gogunda Group	Quartzite, biotite schist, Calcschist, hornblende schist
ARCHEAN	Aravalli Super Group	Dovda Group	Quartzite, dolomite marble, dolomite, amphibolites, cals-silicates rocks, biotite schist, quartz-biotite gneiss and migmatites
	Igneous activity/Intrusives		Dolerite dykes and sills
	BhilwaraSupergroup	Ranthambor Group	quartzite, shales and slates

Era/ Peiod	Geological Cycle	Group	Lithology
		<b>Igneous activity/ Intrusives</b>	<b>Berach granite and gneisses Jahajpur granite</b>
		Pur-Banera Group	Calc-schist, gneisses, banded magnetite-quartzite, dolomitic marble, quartzite, garnet-mica schist and amphibolites
		<b>Jahajpur Group</b>	<b>Dolomite, Phyllite, Quartzite</b>
		<b>Hindoli Group</b>	<b>Shales, slates, phyllites, metagrawacke, limestone, dolomite, quartzite, mica shist, meta basics, volcanics.</b>
		<b>Mangalwar Complex</b>	<b>Migmatites, gneisses, mica schist, garnetiferous mica schist, para-amphibolites silicified mica schist.</b>
		Sandmata Complex	Para-gneisses, migmatites, pyroxene-granulites, amphibolites, biotite-ultranatic rocks.
		Igneous activity/ Intrusive	Acidic and mafic bodies

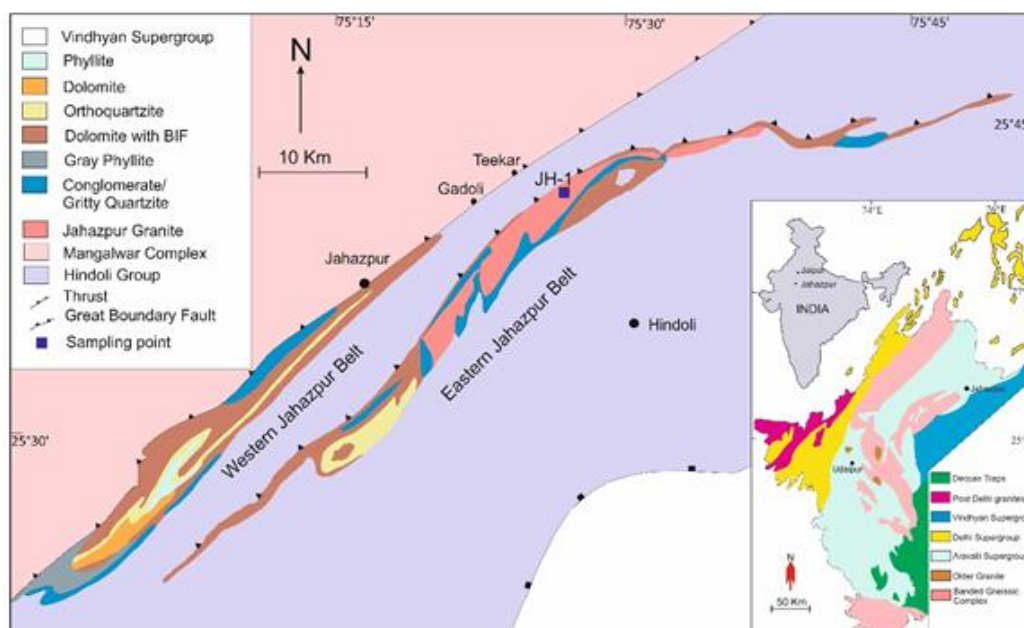


Figure 27.1. Lithological map of Hindoli-Jahazpur Group modified after Pandit et al., 2003 by Dey et al., 2016



Figure 27.2. Stringers of chalcopyrite (CuFeS<sub>2</sub>) within dolomitic marble

### **3. Methodology**

The primary goal of the present study is to characterize the host rock for base metal mineralization in the Jahazpur belt using AVIRIS-NG apparent reflectance product (L2) as provided by NASA-JPL. A total of six AVIRIS-NG scenes have been acquired and stitched to prepare a seamless mosaic of the study area using ENVI s/w. The host rock for the base metal as well as soapstone occurrences in the studied region predominantly comprises of dolomite, dolomitic quartzite and dolomite with BIF. The AVIRIS-NG data was first divided into two sets based on the spectral range. The first spectral subset covers the VNIR range from ~376-1770 nm and the second spectral set ranges from ~1954-2500 nm. NDVI image was generated for masking vegetation and water bodies present within the scene. Advanced hyperspectral techniques, namely, Integrated Band Depth (IBD) for 2200-, 1000- BD, 2300-nm are employed on the spectral subsets of AVIRIS-NG mosaic in order to identify the mineral endmembers and their spatial distributions within the study area. Finally, Spectral Feature Fitting (SFF), a least square regression based technique between the unknown spectra and standard reference spectra, implemented in “Spectral Analyst” and “Mapping Methods” tools of ENVI have been applied to identify the minerals present in the scene. A score of 0–1 was generated for SFF, where a value of 1 indicated a perfect match showing the exact mineral type. End member spectra were matched with those of the minerals as available in the United States Geological Survey Spectral Library (Bhattacharya et al., 2012).

## 4. Outcome

### 4.1 Salient findings

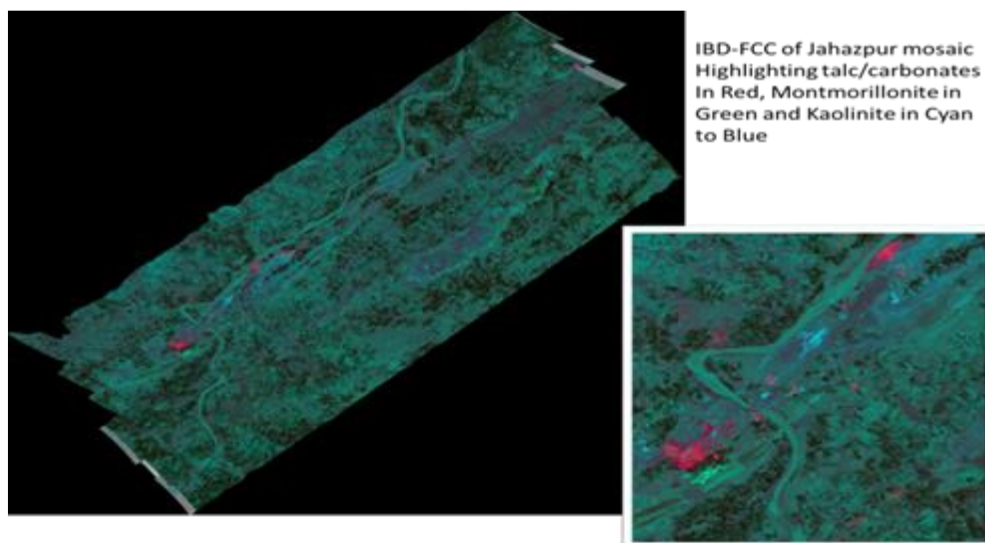


Figure 27.3. Integrated Band Depth (IBD) based FCC of Jahazpur and adjoining regions highlighting Mg-carbonate and talc-bearing exposures in red, Montmorillonite-bearing localities in Green and kaolinite-bearing locales in cyan

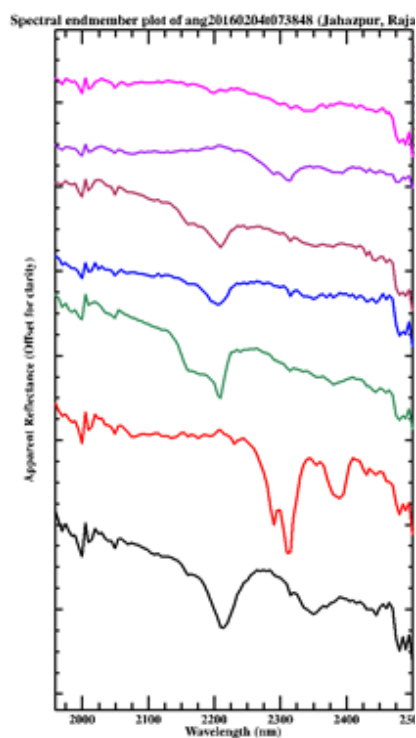
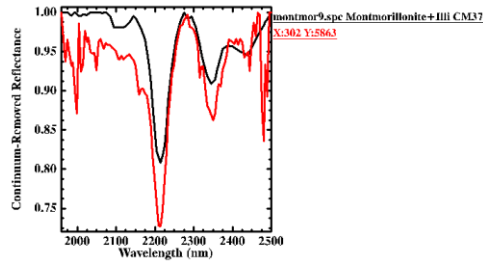


Figure 27.4. Spectral endmembers derived from the IBD-based FCC mosaic of Jahazpur and the spectra were compared with the mineral spectra of USGS Library generating a score between 0-1 through least square regression method implemented as Spectral Feature Fitting (SFF) in ENVI



Unknown: X:302 Y:5863

Library Spectrum	Score	SFF
montmor9.spc Montmor	[0.960]	{0.960}
illite5.spc Illite I	[0.957]	{0.957}
muscovib.spc Muscovi	[0.957]	{0.957}
muscovi1.spc Muscovi	[0.956]	{0.956}
illite3.spc Illite I	[0.956]	{0.956}
cinnabar.spc Cinnaba	[0.956]	{0.956}
perthite.spc Perthit	[0.956]	{0.956}
illite2.spc Illite I	[0.956]	{0.956}
cookeit2.spc Cookeit	[0.955]	{0.955}
lepidol3.spc Lepidol	[0.955]	{0.955}
montmora.spc Montmor	[0.955]	{0.955}
muscovia.spc Muscovi	[0.955]	{0.955}
mizzoni1.spc Mizzoni	[0.955]	{0.955}
muscovi5.spc Muscovi	[0.955]	{0.955}
muscovi7.spc Muscovi	[0.955]	{0.955}
muscovi9.spc Muscovi	[0.955]	{0.955}
lepidol5.spc Lepidol	[0.954]	{0.954}
quartz4.spc Quartz G	[0.954]	{0.954}
muscovi8.spc Muscovi	[0.954]	{0.954}
spodumen.spc Spodume	[0.954]	{0.954}
cordieri.spc Cordier	[0.954]	{0.954}
montmor5.spc Montmor	[0.954]	{0.954}
muscovic.spc Muscovi	[0.954]	{0.954}
desertv2.spc Desert_	[0.954]	{0.954}
muscovi6.spc Muscovi	[0.954]	{0.954}
muscovid.spc Muscovi	[0.954]	{0.954}

Figure 27.5. Spectral plot of mineral endmembers obtained after known vs. unknown analysis with reference to the USGS mineral spectral library

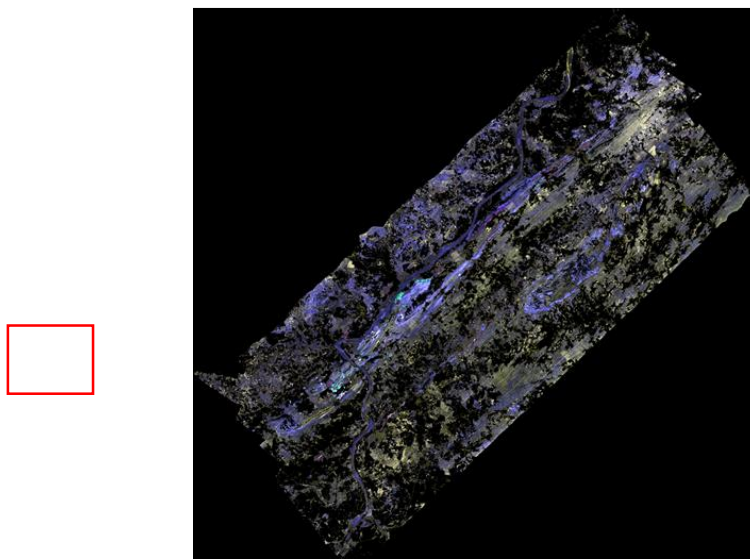


Figure 27.6. SFF-based FCC of the Jahazpur mosaic highlighting Mg-carbonate-bearing lithologies in maroon, talc in aquamarine to light green and kaolinite/montmorillonite-bearing regions in purple to blue to white

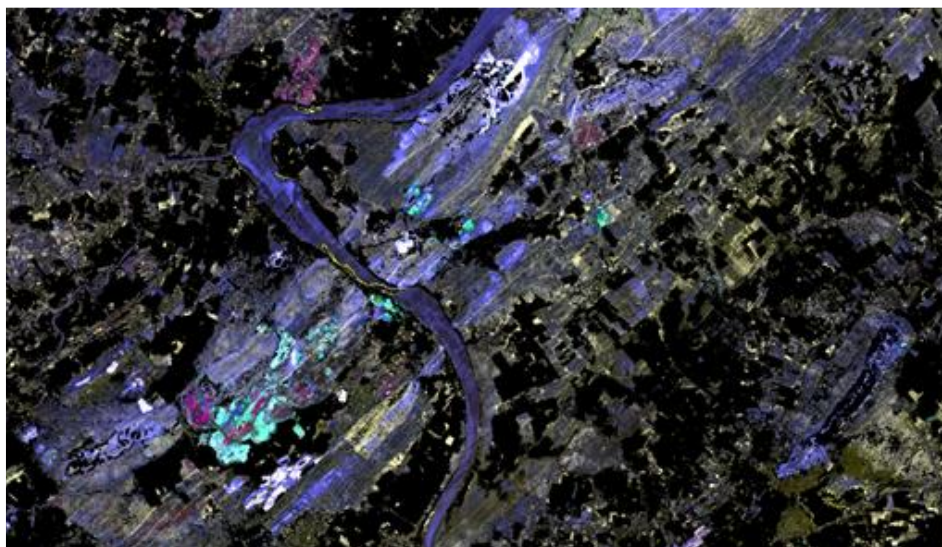


Figure 27.7. Zoomed-in portion marked by red rectangular box in Figure 27.6

Preliminary analysis of AVIRIS-NG data over Jahazpur and surrounding mineralized belts of Rajasthan reveals exciting results in terms of host rock characterization. In the present study, IBD-parameters have been developed to completely characterize absorption features arising due to electronic transition of  $Fe^{3+}$  in the crystal lattice of Fe-oxides and oxyhydroxides and those arising due to combination tones of metal-OH stretching and bending and also due to combination and overtones of  $CO_3$  fundamentals.

#### **4.2 Target vs. Achievement**

25% of the work has been carried out. In the next phase, spectral band parameters will be estimated from the in situ and lab-based spectral data of the rocks and soil samples collected from the study area. Also, geochemical analyses will be taken up for selected samples and finally a spectral-compositional analysis will be carried out. An attempt will be made to study the degree of alteration that the rocks under study have suffered and also to study the efficiency of airborne hyperspectral data in bringing out the variations in the grades and compositions of carbonates and talc and other associated clay minerals.

#### **4.3 Linkage to societal benefits**

This study is extremely important in identifying potential future exploration targets based on the presence of mineral indicators, stratigraphic locations, favourable structures and other parameters. The present study area is already known for its base metal deposits and very good quality soapstones.

## 5. Conclusions

- High SNR values of AVIRIS-NG data is crucial in discriminating different mineral phases present in the study area.
- IBD-based mineral indices have been developed to detect and map the presence of key indicator minerals
- Mineral endmembers have been identified and matched with standard reference spectra of the minerals using Spectral Feature Fitting technique
- Finally, SFF-based classified map has been generated to depict the spatial distribution of rocks and indicator mineral assemblages that host base metal mineralization in the study area.
- Second phase of AVIRIS-NG Campaign over the existing sites as also over few new sites would be extremely encouraging in further establishing the potential of hyperspectral remote sensing in the field of mineralogical/compositional mapping and mineral exploration.

## Acknowledgements

We would like to thank Shri Tapan Misra, Director, SAC for providing this unique opportunity to participate in the AVIRIS-NG Science Campaign. Thanks are due to Dr. Rajkumar, DD, EPSA and Dr. Prakash Chauhan, GD, BPSG for their keen interest in this study. The constant encouragement received from Dr. A. S. Arya, Head, PSD is thankfully acknowledged. Last but not the least we thank Dr. Bimal K. Bhattacharya, Team Leader, AVIRIS-NG Science Campaign and Head, AED for his overall guidance and invaluable suggestions.

## References

AVIRIS, 2007. AVIRIS Workshop Bibliographies. <http://aviris.jpl.nasa.gov/html/aviris.biblios.html> (accessed April 20, 2009).

Bhattacharya, S., Majumdar, T. J., Rajawat, A. S., Panigrahi, M. K., Das, P. R. (2012), Utilization of Hyperion data over Dongargarh, India, for mapping altered/weathered and clay minerals along with field spectral measurements. *International Journal of Remote Sensing*, 33(17), 5438-5450, Taylor & Francis.

Clark, R. N., G. A. Swayze, R. Wise, E. Livo, T. Hoefen, R. Kokaly, and S. J. Sutley (2007), USGS digital spectral library splib06a: U.S. Geological Survey, Digital Data Series 231, <http://speclab.cr.usgs.gov/spectral.lib06>.

Clark, R. N., T. V. V. King, M. Klejwa, and G. A. Swayze (1990), High spectral resolution reflectance spectroscopy of minerals, *JGR*, 95 (12), 653-12,680.

Dey, B., Das, K., Dasgupta, N., Bose, S. and Ghatak, H. (2016). Zircon U-Pb SHRIMP dating of the Jahazpur granite and its implications on the stratigraphic status of the Hindoli-Jahazpur group, Seminar Abstract Volume: Developments in Geosciences in the Past Decade - Emerging Trends for the Future & Impact on Society & Annual General Meeting of the Geological Society of India, 2016.

Geology and mineral resources of Rajasthan (2011). Geological Survey of India Miscellaneous Publication No. 30, Part 12, 3rd Revised Edition.

Goetz, A.F.H., 2009. Three decades of hyperspectral remote sensing of the Earth: A personal view. *Remote Sens. Environ.*, doi: 10.1016/j.res.2007.12.014.

Gupta, S.N. Arora, Y.K., Mathur, R.K., Iqballuddin, Prasad, B., Sahai, T.N. and Sharma, S.B., 1981. Lithostratigraphic map of Aravalli region, southeastern Rajasthan and northern Gujarat, Geol. Surv. Ind. Publication, Hyderabad.

Hunt, G.R. And Salisbury, J.W., 1970, Visible and near infrared spectra of minerals and rocks: I. Silicate minerals. *Modern Geology*, 1, pp. 283–300.

Kruse, F.A., 1988, Use of airborne imaging spectrometer data to map minerals associated with hydrothermally altered rocks in the Northern Grapevine Mountains, Nevada and California. *Remote Sensing of Environment*, 24, pp. 31–51.

Kruse, F.A., Boardman, J.W. and Huntington, J.F., 2003, Comparison of airborne hyperspectral data and EO-1 Hyperion for mineral mapping. *IEEE Transactions on Geoscience and Remote Sensing*, 41, pp. 1388–1400.

Kruse, F.A., Kierein-Young, K.S. And Boardman, J.W., 1990, Mineral mapping at Cuprite, Nevada with 63 channel imaging spectrometer. *Photogrammetric Engineering and Remote Sensing*, 56, pp. 83–90.

Kruse, F.A., Lefkoff, A.B., Boardman, J.B., Heidebrecht, K.B., Shapiro, A.T., Barloon, P.J. and Goetz, A.F.H., 1993, The Spectral Image Processing System (SIPS) – interactive visualization and analysis of imaging spectrometer data. *Remote Sensing of Environment*, 44, pp. 145–163.

Neville, R.A., Levesque, J., Staenz, K., Nadeau, C., Hauff, P. And Borstad, G.A., 2003, Spectral unmixing of hyperspectral imagery for mineral exploration: comparison of results from SFSI and AVIRIS. *Canadian Journal of Remote Sensing*, 29, pp. 99–110.

Pandit, M.K., Sial, A.N., Malhotra, G., Shekhawat, L.S. and Ferreira, V.P. (2003). C-, O-isotope and whole-rock geochemistry of Proterozoic Jahazpur carbonates, NW Indian Craton. *Gondwana Research*, 6(3), 513-522.

Staenz, K. And Williams, D.J., 1997, Retrieval of surface reflectance from hyperspectral data using a look-up table approach. *Canadian Journal of Remote Sensing*, 23, pp. 354–368.

Staenz, K., 2009. Terrestrial imaging spectroscopy – some future perspectives. *Personal Communication*.

# Analysis of AVIRIS data for mineralogical mapping in parts of Ambaji, Gujarat

Hrishikesh Kumar

Space Applications Centre, ISRO, Ahmedabad, Gujarat, India

## 1. Introduction

Hyperspectral remote sensing or imaging spectrometry is a technique in which images are acquired in very narrow, contiguous spectral band (Goetz et al., 1985). Imaging spectroscopy is capable of providing high resolution spectra of material present within a resolution cell and aid in its identification. It is powerful, rapid, inexpensive and non-destructive technique commonly used in identification of minerals and in some instances determination of their abundance (Goetz et al., 1985; Lang et al. 1987; Kruse, 1988; Kruse et al., 1993; Crowley, 1993; Mustard and Pieters, 1987).

Identification of minerals based on study of their reflectance spectra is enabled by presence of diagnostic absorption feature arising from electronic transition, vibrational modes, charge transfer processes and other processes (Hunt, 1977). Imaging spectrometers such as AVIRIS and HyMAP have been flown on aircraft and have mapped chemical composition of surficial materials upto 50  $\mu\text{m}$  ((Buckingham and Sommer, 1983) and monitored dynamic changes in ice, vegetation and other surface processes on earth (e.g., Bedini, 2009, Crowley, 1993, Vane et al., 1993; Cocks et al., 1998; Green et al., 1998; Painter et al., 2003; Asner et al., 2004, 2007). Hyperspectral datasets are particularly useful for mapping key iron mineralogy such as haematite, goethite and jarosite as well as clay minerals (Clark et al., 1990). Due to presence of contiguous spectral channels and improved spectral resolution in hyperspectral data, we can map subtle differences in surficial mineralogy (Ruitenbeek et al, 2005, References). Imaging spectrometry datasets have also been used to map hydrocarbon induced alteration (Petrov et al., 2008, Khan and Jacobson, 2008).

Multispectral and hyperspectral remote sensing has been utilized for mapping hydrothermally altered rocks (e.g., Crosta et al., 2003, Kruse et al, 1988, Kruse et al., 2006,

refernces). Mapping of altered rocks is important as they host various minerals deposits and can provide precious information for mineral exploration programmes. Physical and chemical changes induced by alteration produces mineral assememlages which are diagnostic of alteration zones. Many minerals present within the alteration zones have absorption feature near 2.20 micro caused by comination of tones of -OH fundamental stretch and AL-OH fundamental bending (Hunt and Ashley, 1979).

Present report describes evaluation of high resolution AVIRIS data acquired over parts of Ambaji region, Gujarat for mineral mapping. First we describe main rock type, their visible and near infrared spectra acquired in wavelength region 0.4-2.5 micro Second we describe AVIRIS data and methodology used in this study. Finally, we present the results of our analysis.

## ***2. Study area and data used***

In the present study AVIRIS-NG data acquired over parts of Ambaji region (figure 28.1), Gujarat is analyzed to map the surficial mineralogy.

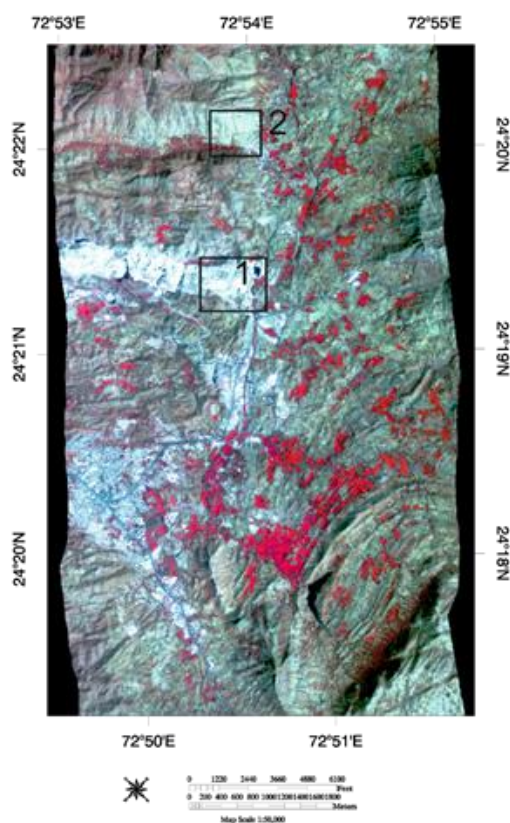


Figure 28.1. AVIRIS colour infrared image of the study area. At location 1, marble quarries exist. Pink granite is exposed at location 2.

In the present study, we have used hyperspectral data acquired by AVIRIS-NG in February, 2016 over parts of Ambaji, Gujarat. The data is collected in 425 bands covering wavelength region 0.37 to 2.5  $\mu\text{m}$  with spectral resolution of 5 nanometre. AVIRIS sensor was flown onboard ISRO aircraft at an altitude of 6 km. The image was acquired on 2<sup>nd</sup> February 2016 at a very high spatial resolution of  $\sim 8$  m.

Absorption by atmospheric constituents (e.g. water vapour, carbon dioxide and ozone) and spectral mixing complicate the process of direct determination of surficial composition. Atmospheric correction of hyperspectral data is required before analysis and interpretation of absorption features associated with minerals. In the present study, we have used atmospherically corrected level 2 data, provided by Jet Propulsion Laboratory (JPL).

### ***3. Methodology***

#### **3.1 Continuum removal**

Data acquired is affected by presence of continuum which affects analysis and interpretation of absorption features and needs to be removed from the spectra. Continuum was defined for each spectrum by finding local maxima and then fitting straight line between these points. Afterwards, continuum was divided by original spectrum to normalize the absorption bands to a common reference (Clark and Roush, 1984). The continuum removed reflectance was used in further studies related to identification of absorption wavelength and depth of absorption feature.

#### **3.2 Masking of vegetation and water**

In order to map minerals/altered minerals in study region we first mask the vegetation cover as it may adversely impact the mineral mapping. In order to mask the vegetation, Normalized Difference Vegetation Index (NDVI) was used. Using hit and trial method, threshold value of -0.55 was used to mask the vegetation in our study site. Further, water bodies were also masked by using Normalized Difference Water index (NDWI). Figure 28.2 shows masked vegetated and water pixels. No computations are performed in masked areas which also saves computing time in analysis of high volume hyperspectral data.

### 3.3 Mapping of Carbonates

Carbonates are one of the most dominant mineral present in our study area. The reflectance spectra of carbonates show several diagnostic absorption feature in SWIR region at 2.12-2.16, 2.30-2.35 and 2.50-2.55  $\mu\text{m}$  (Hunts and Salisbury, 1971). The absorption bands occurring in region 2.50 to 2.55 and 2.30-2.35 are strongest, while those occurring in 2.12-2.16  $\mu\text{m}$  are weakest. One other important absorption feature of carbonates is located at 1.9  $\mu\text{m}$  but is not very useful for satellite based studies as these absorption features are often masked by atmospheric water vapour or sometimes by fluid inclusions in minerals. Further, as AVIRIS-NG collects spectra over 0.4 to 2.5  $\mu\text{m}$ , the strong absorption feature occurring in 2.50-2.55  $\mu\text{m}$  cannot be utilized in this study. These absorption features of carbonates occurring at longer wavelength region (SWIR region) is attributed to vibrational processes. The observed absorption features are due to planar shape of  $\text{CO}_3^{2-}$ . Combination of four fundamental vibrational modes (symmetric stretch, the out of plane bend, the asymmetric stretch and the in plane bend) and overtone bands of  $\text{CO}_3$  results in above mentioned absorption features in carbonates. Changes in composition of carbonates cause shift in band positions (Gaffey, 1986). Carbonate absorption feature occurring near 2.30-2.35  $\mu\text{m}$  helps in discrimination between calcite and dolomite. Dolomite shows absorption near shorter wavelength (2.32  $\mu\text{m}$ ) as compared to calcite (2.35  $\mu\text{m}$ ).

We have exploited this property to study the variations of carbonate mineralogy in our study site. Continuum removed spectra was analysed at every pixel to determine the wavelength corresponding to minimum reflectance in region 2.30-2.35  $\mu\text{m}$ . Band depth is also calculated as it is an important parameter and varies due to mineral abundance and grain size.

### 4.4 Integrated band depth analysis

Integrated Band Depth (IBD) is a mineral indicator parameter developed by Mustard et al., (2011). It captures the fundamental mineralogical variations of the surface as it exploits the nature of crystal field absorptions at diagnostic absorption feature. We have used IBD at 2.30 and 2.20  $\mu\text{m}$  as indicator of carbonates and clays. Following equations were used to compute IBD for carbonate and clay

**For carbonates:**

$$\sum_{n=0}^{44} 1 - \frac{R(2189+5n)}{R_c(2189+5n)} \quad \dots (1)$$

**For clays**

$$\sum_{n=0}^{21} 1 - \frac{R(2134+5n)}{R_c(2134+5n)} \quad \dots (2)$$

Here, R refers to reflectance at a given wavelength;  $R_c$  is continuum reflectance and is represented as straight line across the absorption band. Width of the absorption feature is determined by initial and final wavelength. In case of calcite it is determined by wavelength 2189 and 2409  $\mu\text{m}$ . Numbers 5 represents spectral resolution of the sensor and specifies the wavelength interval in nanometers, and n is the number of channels over which integration is performed.

### 3.5 Mapping deepest absorption feature in SWIR region (2.0-2.5 $\mu\text{m}$ )

Several minerals such as phyllosilicate, carbonates and sulphates have diagnostic absorption feature in SWIR region and are called infrared active. Therefore, mapping of wavelength position of deepest absorption feature and its depth is very important for exploratory analysis of surficial composition and broad identification of mineral groups. Following methodology was adopted for mapping of deepest absorption feature:

Continuum was first removed from the spectra to highlight diagnostic absorption features. Continuum was removed for each pixel by calculation of convex hull and its subsequent division as described in Clark and Roush, 1984. To calculate the wavelength position of deepest absorption feature, methodology described in Rodgers et al., 2012 was used. In this method, wavelength position corresponding to deepest absorption feature is determined. Considering wavelength corresponding to lowest reflectance as centre, two other consecutive wavelengths are chosen and a quadratic polynomial is fitted through these three points. This can be represented by the following equation:

$$w(x) = ax^2 + bx + c$$

where  $x$  represents wavelength and  $w(x)$  is interpolated reflectance and  $a, b, c$  are coefficients of the equation. The minimum value of this equation is represented by:

$$w_{min} = \frac{-b}{2a}$$

where  $w_{min}$  is interpolated wavelength position corresponding to minimum reflectance,  $a$  and  $b$  are coefficients of the quadratic equation. Further depth of the absorption feature was computed using following equation:

$$D = 1 - R(w_{min})$$

where  $R(w_{min})$  is the reflectance corresponding to deepest absorption feature. At every pixel of image wavelength and corresponding band depth was calculated.

#### 4. Results

Figure 28.2 shows mask of vegetation and water. For geological applications, presence of vegetation and water on surface obscures the expression of surficial mineralogy and needs to be masked. These masks were used in mapping of minerals in the area.

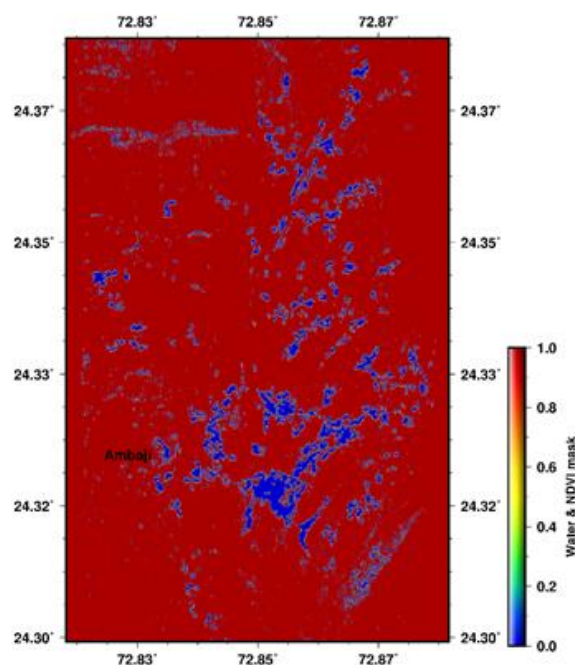


Figure 28.2. Mask of pixels (Blue colour) containing vegetation and water is prepared using NDVI and NDSI. Masking is done to avoid erroneous interpretation of absorption features in terms of surficial mineralogy.

Shown in figure 28.3 (A) is wavelength at which deepest absorption feature occurs in SWIR region (2.0 to 2.5  $\mu\text{m}$ ). Band depth of corresponding deepest absorption features are shown in figure 28.3 (B). It is noted that for most of the region deepest absorptions occur in wavelength region 2.26 to 2.34 (shown in yellow colour, figure 28.3 (A)) with moderate to low band depth ( $<0.22$ ) indicating a calc-silicate terrain in general. At locations, marked in rectangle 2 in figure 28.3(A), the deepest absorption feature occurs at 2.30 to 2.35 indicating presence of relatively pure carbonates. Band depth values are also high ( $>0.25$ ) indicating their abundance and relatively fresh exposures of carbonates at these locations. North of location 2, small patch (shown as rectangle 1, figure 28.3 (A)) depicting absorption near 2.20  $\mu\text{m}$  is indicative of presence of clay minerals. South of the open cast mine, at Ambaji, several clusters showing absorption near 2.0  $\mu\text{m}$  occur. These may be due to presence of residual carbon dioxide absorption features which is not completely removed during atmospheric correction of AVIRIS data.

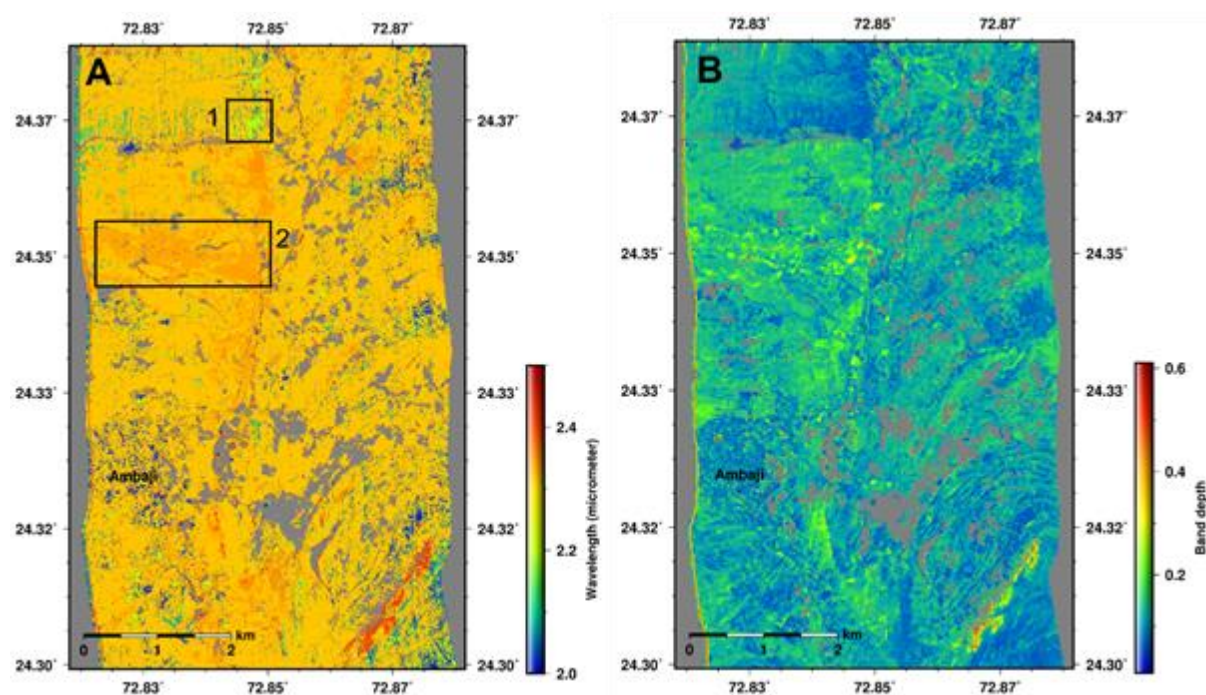


Figure 28.3. Map depicting spatial variations of deepest absorption feature in SWIR (2.0-2.5  $\mu\text{m}$ ).

Region bounded by rectangle 1 has absorption feature in 2.32 -2.35  $\mu\text{m}$ , indicating presence of carbonates. Small zone shown in rectangle 2 has absorption feature near 2.20  $\mu\text{m}$  due to presence of clay minerals (A). Band depth corresponding to deepest absorption feature is shown in figure B.

#### 4.1 Spectral data analysis

Based on above analysis of deepest absorption features, detailed analysis of image spectra at locations showing 2.20 and 2.32  $\mu\text{m}$  absorption band was carried out. During the field campaign, rock samples corresponding to various lithologies exposed in the region were collected for detailed laboratory based study. Exposures of marble and pink granite as seen in field is shown in figure 28.4. Spectra of various rock samples were collected using Spectroradiometer present at SAC-ISRO. Figure 28.5 shows comparison of image spectra with field spectra for carbonate. Field spectra of marble collected from marble mine (shown as rectangle 1 in figure 28.1) shows absorption feature at 1, 1.4, 1.9, 2.31 and 2.39  $\mu\text{m}$ . Absorption feature occurring at 1  $\mu\text{m}$  is possibly due to presence of iron while those occurring at 1.4 and 1.9 are attributed to presence of hydroxyl ions in crystal structure. A very strong absorption feature is observed at 2.32  $\mu\text{m}$  is attributed to vibrational process. Due to presence of diagnostic absorption band at 2.32, mineral is identified as dolomite which shows absorption band at shorter wavelength region as compared to calcite. Figure 28.6 shows reflectance spectra of pink granite exposed at location marked as 2 in figure 28.1. Field based spectra shows absorption feature near 1.0, 1.4, 1.9, 2.20 and 2.38  $\mu\text{m}$ . Absorption feature at 1  $\mu\text{m}$  is due to presence of iron.



Figure 28.4. Field photographs of marble quarry exposed at location 1 (Figure 28.1) and pink granite at location 2 (Figure 28.1).

Here also absorption features, indicative of hydroxyls are seen near 1.4 and 1.9  $\mu\text{m}$ . A major absorption feature at 2.20  $\mu\text{m}$  along with several minor absorption features at 2.17, 2.31 and 2.38  $\mu\text{m}$  is noticed. Based on diagnostic absorption features, in particular shape and position of absorption feature near 2.20, mineral is identified as Kaolinite. It is noted that diagnostic

absorption features of both the minerals (carbonate and Kaolinite) present in SWIR region are nicely captured by AVIRIS-NG (figure 28.5(B) and figure 28.6 (B)).

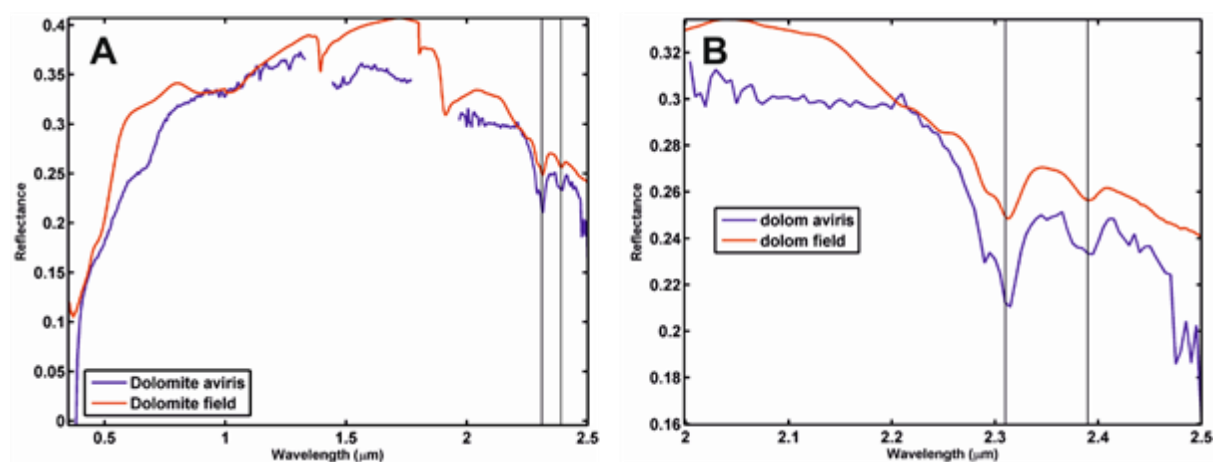


Figure 28.5. Inter-comparison of dolomite (a mineral present in marble) spectra of AVIRIS-NG and field (A). Enlarged view of spectral matching in SWIR region is shown in figure B. Diagnostic absorption features at 2.32 and 2.38  $\mu\text{m}$  in SWIR match nicely. However, in VNIR region, presence of strong atmospheric water absorption band near 1.4 and 1.9  $\mu\text{m}$  obscures the absorption features in image spectra.

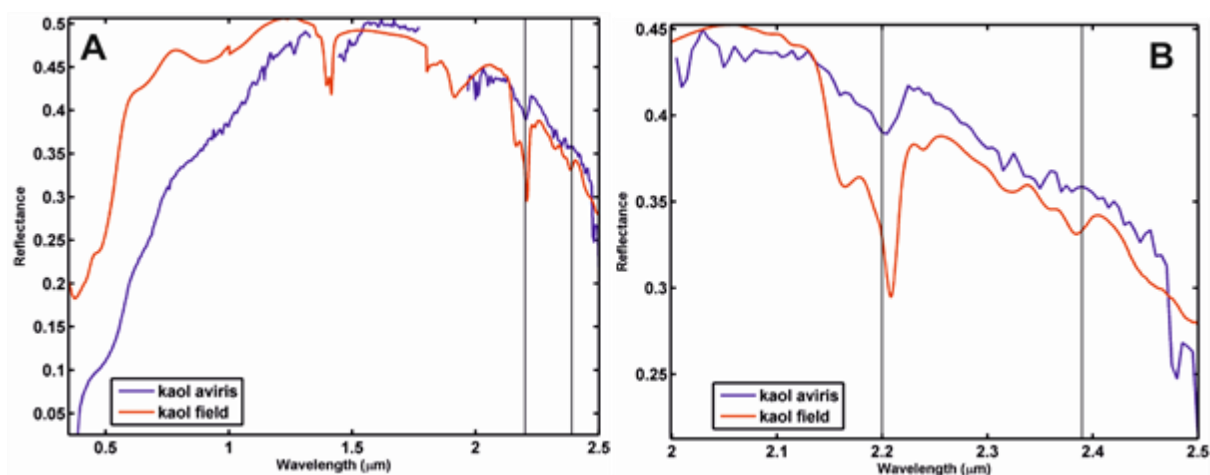


Figure 28.6. Inter-comparison of field reflectance spectra of kaolinite (mineral present in pink granite) with image spectra (A). Enlarged view of spectral matching in SWIR region is shown in figure B. Kaolinite has dominant absorption feature near 1.0, 1.4, 1.9, 2.17, 2.21, 2.32 and 2.38  $\mu\text{m}$ . Shape of absorption feature at 2.21  $\mu\text{m}$  is diagnostic of Kaolinite.

However, kaolinite which has absorption feature near 1.4 and 1.9  $\mu\text{m}$  (hydroxyls absorption feature) are not picked by AVIRIS-NG due to presence of strong atmospheric water absorption bands at these wavelength regions. Comparison of image spectra and United States Geological Services (USGS) provided library spectra is shown in figure 28.7 and figure 28.8. Diagnostic

absorption features for carbonates (figure 28.7) and Kaolinite (figure 28.8) of library and image spectra are in good agreement.

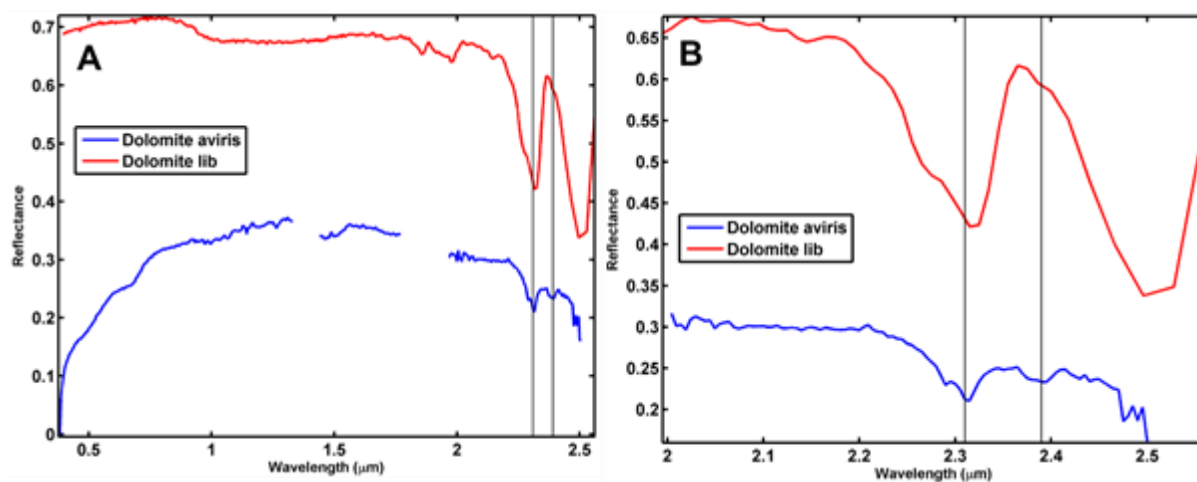


Figure 28.7. Inter-comparison of image spectra with library spectra of mineral dolomite in 0.4-2.5  $\mu\text{m}$  and 2.0 – 2.5  $\mu\text{m}$  range. Absorption features of image and library spectra are in good agreement.

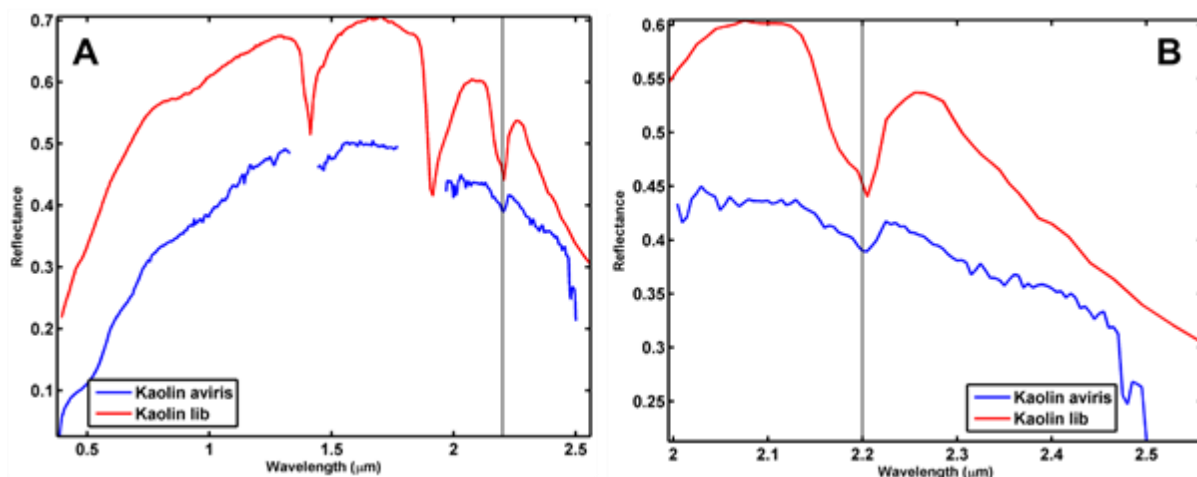


Figure 28.8. Inter-comparison of image spectra with library spectra of mineral Kaolinite in 0.4-2.5  $\mu\text{m}$  and 2.0 – 2.5  $\mu\text{m}$  range. Absorption features of image and library spectra are in good agreement.

## 4.2 Mapping variations in carbonate mineralogy

In order to understand the variations of 2.30-2.35  $\mu\text{m}$  absorption feature due to differences in carbonate chemistry, we have mapped the deepest absorption feature occurring between 2.30 and 2.40  $\mu\text{m}$  in open cast marble mine located north of Ambaji town. Figure 28.9 shows spatial distribution of absorption features occurring between 2.30 and 2.40  $\mu\text{m}$  and their band depth is shown in figure 28.7 (B).

It is clearly seen that, mine area (marked as 1) in the figure 28.9 (A) has dominant absorption occurring near 2.32  $\mu\text{m}$  while at small patch (marked as 2), dominant absorption wavelength is located near 2.34  $\mu\text{m}$ . The observed difference in wavelength of absorption may be due to subtle variations in carbonate composition. Absorption feature at 2.32  $\mu\text{m}$  is due to presence of dolomite ( $\text{CaMg}(\text{CO}_3)_2$ ) while those occurring at higher wavelengths i.e. at 2.34  $\mu\text{m}$  may be attributed to presence of calcite ( $\text{Ca}(\text{CO}_3)_2$ ) as presence of Magnesium (Mg) in crystal structure of carbonates causes absorption feature to shift towards shorter wavelengths.

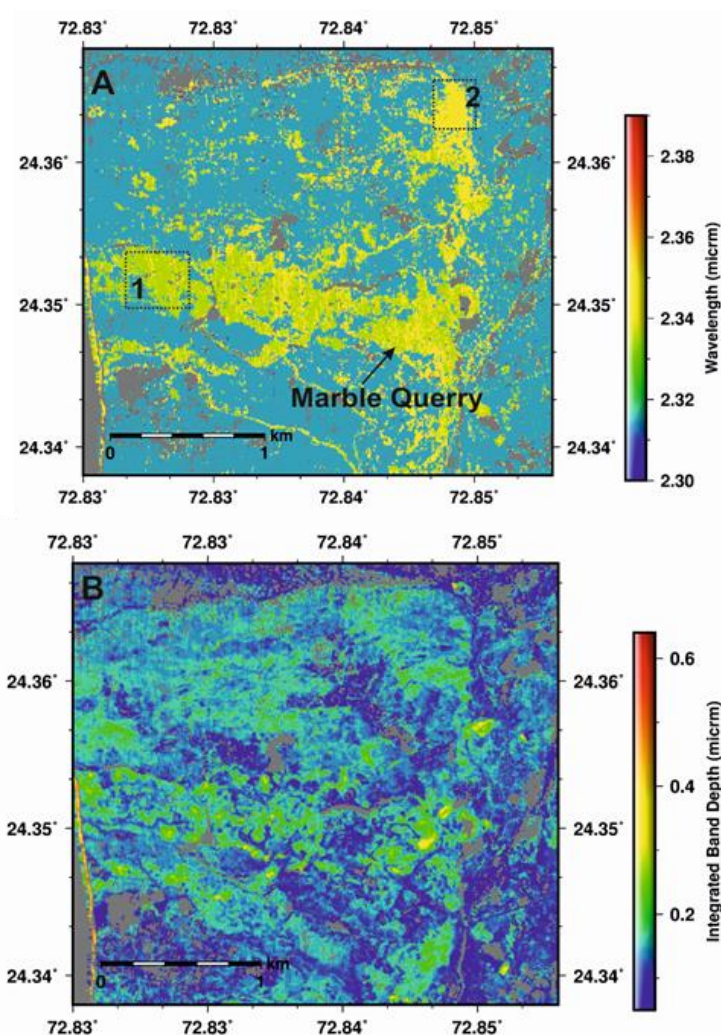


Figure 28.9. Mapping of subtle differences in carbonate mineralogy is depicted (A). Region bounded by rectangle 1, has dominant absorption near 2.32 indicating presence of dolomite. Location 2 shows dominant absorption near 2.34 due occurrence of calcite. Very high spectral resolution of AVIRIS-NG (5nm) has enabled differentiation of carbonates based on subtle shifting of absorption features in 2.30-2.35  $\mu\text{m}$ . Shown in figure B is corresponding band depth of absorption feature.

### 4.3 Use of IBDs for carbonate and clay mapping

Integrated Band Depths (IBD) calculated over certain chosen wavelength ranges keeping in view of diagnostic absorption feature of the mineral are important parameter for mapping and understanding of surficial mineralogy of the area of interest. In this study, we used IBD at 2.20 and 2.30  $\mu\text{m}$  as indicators of clay and carbonate mineralogy respectively. Figure 28.10 shows IBD for 2.30  $\mu\text{m}$  wavelength indicating absorption due to carbonate minerals. It is clearly noted that the regions having abundant and fresh carbonates have very high band depth ( $> 4$ ) while regions with relatively weak carbonate features and calc-silicate rocks have low band depth. During field visit, at one of the locations (marked as rectangle 1, figure 28.1), quarry of marble was observed. Several small mine locations in and around Ambaji are also detected from IBD image. This technique is capable of mapping occurrences of fresh carbonate deposits within region of interest.

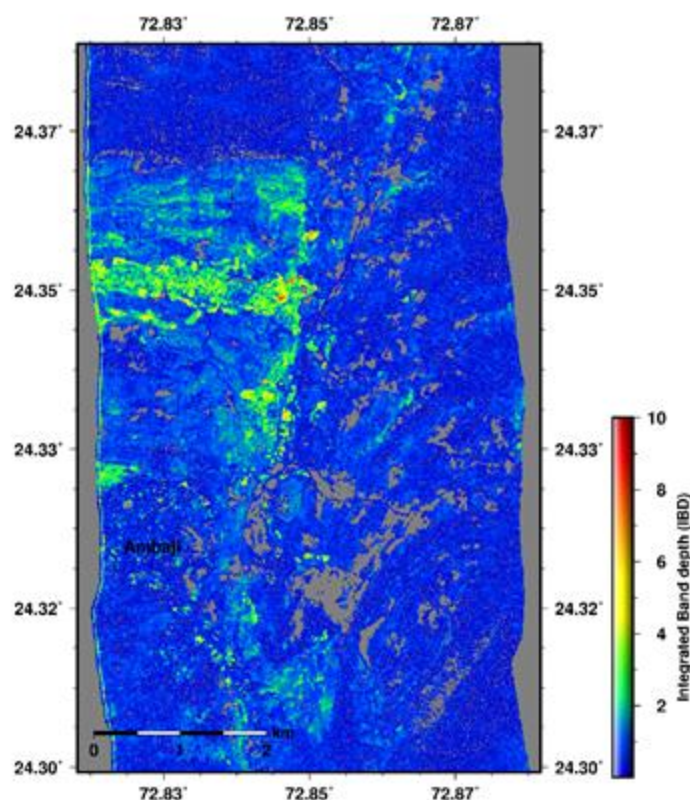


Figure 28.10. Integrated band depth at 2.30  $\mu\text{m}$  showing spatial distribution of carbonate minerals. Regions appearing in greenish to reddish tone have high IBDs ( $>2$ ) and depict presence of carbonate.

Figure 28.11 shows distribution of IBD for 2.20  $\mu\text{m}$ . It is noted that areas with high IBD values (0.55-1) are representative of clay minerals having relatively strong absorption feature near 2.20  $\mu\text{m}$ . Analysis of reflectance spectra over the regions of high IBD confirms this. In region shown in rectangle 2 in figure 28.1 is location where pink granites are exposed as observed during field visit. Analysis of field spectra of pink granites also shows an absorption feature near 2.20  $\mu\text{m}$  probably due to conversion of feldspar, a mineral present in granite to clays (Kaolinite) due to chemical weathering.

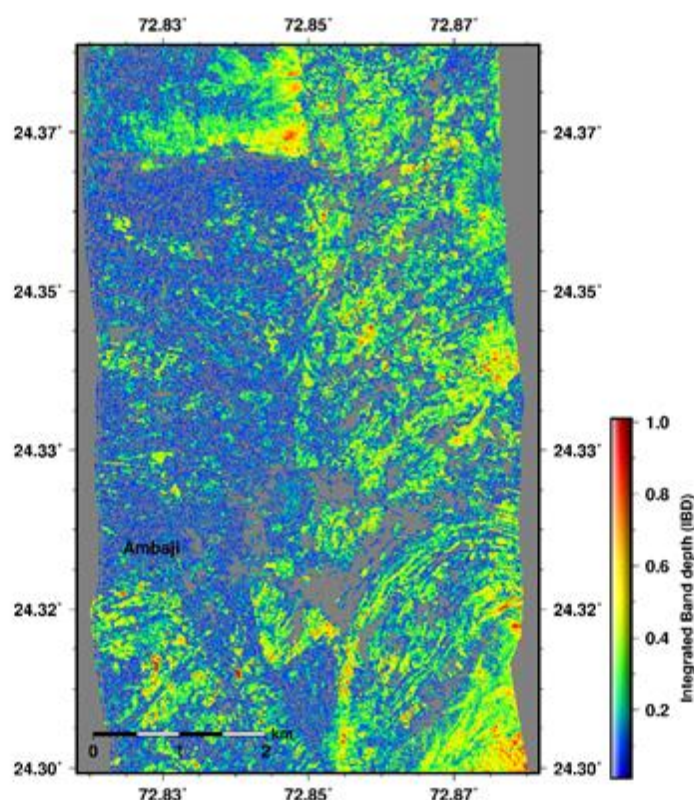


Figure 28.11. Integrated band depth at 2.20  $\mu\text{m}$  showing spatial distribution of clay minerals. Higher value of IBD is semi-quantitative measure of abundance. It is evident that eastern and northern part of the study area have high IBD ( $> 0.35$ ) due to occurrence of clay mineral (identified as Kaolinite).

Based on analysis of IBDs at 2.30 and 2.20  $\mu\text{m}$ , thresholds were applied to detect areas with relatively high band depths. Stronger the band depth, more is abundance of the mineral (assuming grain size to be constant). Figure 28.12 and figure 28.13 represent the regions where possibility of finding marble and Kaolinite are high respectively. Identification of marble/carbonate rich zones (figure 28.12) outside the known marble quarry can be used to

locate new marble mines. In addition to marble quarries, several patches of pure carbonates are delineated which may be targeted for marble exploration. Mapping of spatial distribution of clay minerals (figure 28.13) which are indicators of hydrothermal alteration is of immense significance in mineral exploration projects. It helps in narrowing the regions for intense field based mapping and sampling to locate mineral deposits.

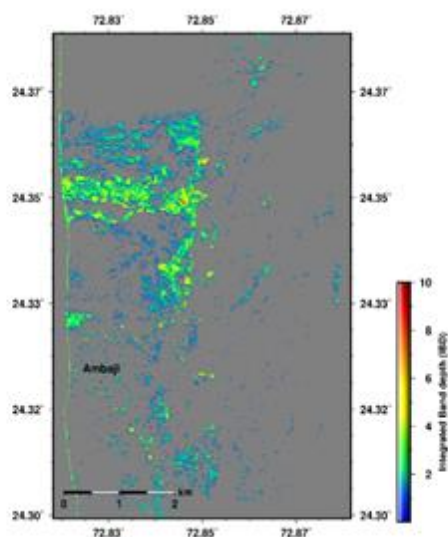


Figure 28.12. Map showing regions having occurrence of relatively pure carbonate minerals obtained by applying threshold ( $> 0.2$ ) on  $2.30 \mu\text{m}$  IBD image.

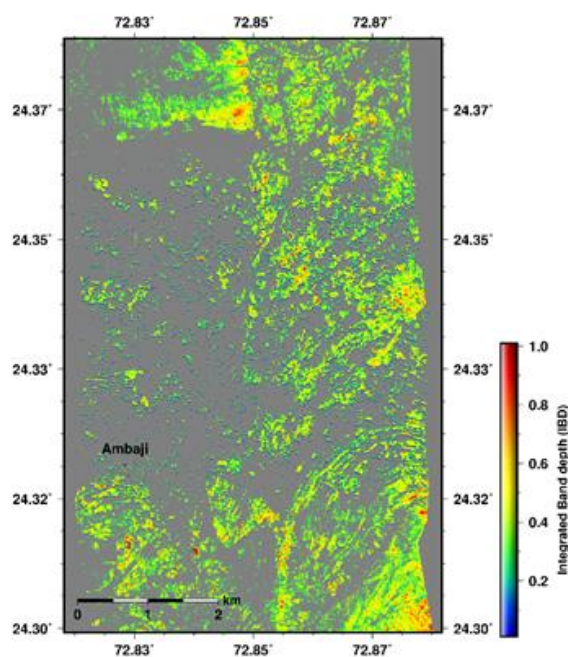


Figure 28.13. Map depicting regions having dominant presence of clay minerals obtained by applying threshold ( $> 0.35$ ) on  $2.20 \mu\text{m}$  IBD image.

## 5 Conclusions

Following are the conclusions which emerge from the study:

- Mapping of deepest absorption feature in wavelength range 2.0-2.5  $\mu\text{m}$  where most of the minerals have their diagnostic absorption feature is useful for exploratory analysis of the data. It gives an overview of surface mineral diversity/mineral group likely to be present in the study area. Zones of interest can be identified and taken up for detailed spectroscopic analysis.
- Inter-comparison of image, library and laboratory based spectra reveals that diagnostic absorption features present in SWIR region are in good agreement. However, presence of strong atmospheric water absorption at 1.4 and 1.9  $\mu\text{m}$  corrupts the image thereby, hindering inter-comparison.
- Integrated Band Depth (IBDs), developed by exploiting diagnostic absorption features of minerals is a very reliable indicator of spatial distribution of mineral. Interpretation of IBD image along with band depth image helps in understanding the spatial distribution as well as their abundance if grain size is assumed to be constant over the region.
- Shift in absorption wavelength due to subtle mineralogical variations of carbonates is useful for discrimination between calcite and dolomite.
- Based on the analysis of above mentioned datasets, it is clear that western part of the study region is dominated by calcite. In northern most part as well as most of the eastern part we have presence of clay mineral containing AL-OH bonds.

## Acknowledgements

Author would like to place deep sense of gratitude to TapanMisra, Director, SAC for his keen interest and encouragement during study. Thanks are due to Dr. A.S. Rajawat, Head, Geosciences Division, Dr. Rajkumar, DD EPSA and Dr. Bimal Bhattacharya, Science Leader, AVIRIS-NG for their help and encouragement during the study. Author thanks Satadru Bhattacharya for his help and guidance provided in field data acquisition and fruitful discussions. Help provided by Aditya Dagar and Sumit Pathak during field work is thankfully

acknowledged. All scientists and engineers involved in operation of AVIRIS-NG mission are acknowledged.

## References

Asner, G. P., Knapp, D. E., Kennedy-Bowdoin, T., Jones, M. O., Martin, R. E., Boardman, J., & Field, C. B. (2007). Carnegie airborne observatory: in-flight fusion of hyperspectral imaging and waveform light detection and ranging for three-dimensional studies of ecosystems. *Journal of Applied Remote Sensing*, 1(1), 013536-013536.

Asner, G. P., Nepstad, D., Cardinot, G., & Ray, D. (2004). Drought stress and carbon uptake in an Amazon forest measured with spaceborne imaging spectroscopy. *Proceedings of the National Academy of Sciences of the United States of America*, 101(16), 6039-6044.

Bedini, E. (2009). Mapping lithology of the Sarfartoq carbonatite complex, southern West Greenland, using HyMap imaging spectrometer data. *Remote Sensing of Environment*, 113(6), 1208-1219.

Buckingham, W. F., and Sommer, S. E. (1983). Mineralogical characterization of rock surfaces formed by hydrothermal alteration and Weathering-Application to remote sensing: *Economic Geology*, v. 78, no. 4, p. 664-674

Clark, R. N., & Roush, T. L. (1984). Reflectance spectroscopy: Quantitative analysis techniques for remote sensing applications. *Journal of Geophysical Research: Solid Earth*, 89(B7), 6329-6340.

Clark, R. N., King, T. V., Klejwa, M., Swayze, G. A., & Vergo, N. (1990). High spectral resolution reflectance spectroscopy of minerals. *Journal of Geophysical Research: Solid Earth*, 95(B8), 12653-12680.

Cocks, T., Jenssen, R., Stewart, A., Wilson, I., and Shields, T., 1998, The HyMap TM airborne hyperspectral sensor: The system, calibration and performance, in *Proceedings of the 1st EARSeL workshop on Imaging Spectroscopy*, Zurich, p. 37–42.

Crosta, A. P., De Souza Filho, C. R., Azevedo, F., & Brodie, C. (2003). Targeting key alteration minerals in epithermal deposits in Patagonia, Argentina, using ASTER imagery and principal component analysis. *International journal of Remote sensing*, 24(21), 4233-4240.

Crowley, J. K. (1993). Mapping playa evaporite minerals with AVIRIS data: A first report from Death Valley, California. *Remote Sensing of Environment*, 44(2), 337-356.

Goetz, A. F. H., Vane, G., Solomon, J. E., and Rock, B. N. (1985). Imaging spectrometry for earth remote sensing: *Science*, 228, 1147-1153

Green, R.O., Eastwood, M.L., Sarture, C.M., Chrien, T.G., Aronsson, M., Chippendale, B.J., Faust, J.A., Pavri, B.E., Chovit, C.J., Solis, M., Olah, M.R., and Williams, O. (1998). Imaging Spectroscopy and the Airborne Visible/Infrared Imaging Spectrometer (AVIRIS). *Remote Sensing of Environment*, 65(3), 227–248

Hunt, G. R., & Ashley, R. P. (1979). Spectra of altered rocks in the visible and near infrared. *Economic Geology*, 74(7), 1613-1629.

Khan, S. D., & Jacobson, S. (2008). Remote sensing and geochemistry for detecting hydrocarbon microseepages. *Geological Society of America Bulletin*, 120(1-2), 96-105.

Kruse, F. A. (1988). Use of Airborne Imaging Spectrometer data to map minerals associated with hydrothermally altered rocks in the northern Grapevine Mountains, Nevada and California: *Remote Sensing of Environment*, v. 24, no. 1, pp. 31-51.

Kruse, F. A. (1988). Use of airborne imaging spectrometer data to map minerals associated with hydrothermally altered rocks in the northern Grapevine Mountains, Nevada, and California. *Remote Sensing of Environment*, 24(1), 31-51.

Kruse, F. A., Perry, S. L., & Caballero, A. (2006). District-level mineral survey using airborne hyperspectral data, Los Menucos, Argentina.

Lang, H. R., Adams, S. L., Conel, J. E., McGuffie, B. A., Paylor, E. D., and Walker, R. E. (1987). Multispectral remote sensing as stratigraphic tool, Wind River Basin and Big Horn Basin areas, Wyoming: *American Association of Petroleum Geologists Bulletin*, 71, 4, 389-402.

Mustard, J. F., Pieters, C. M., Isaacson, P. J., Head, J. W., Besse, S., Clark, R. N., ... & Runyon, C. J. (2011). Compositional diversity and geologic insights of the Aristarchus crater from Moon Mineralogy Mapper data. *Journal of Geophysical Research: Planets*, 116(E6).

Painter, T.H., Dozier, J., Roberts, D.A., Davis, R.E., and Green, R.O. (2003). Retrieval of subpixel snow-covered area and grain size from imaging spectrometer data: *Remote Sensing of Environment*, 85, 64–77, doi: 10.1016/S0034-4257(02)00187-6.

Petrovic, A., Khan, S. D., & Chafetz, H. S. (2008). Remote detection and geochemical studies for finding hydrocarbon-induced alterations in Lisbon Valley, Utah. *Marine and Petroleum Geology*, 25(8), 696-705.

Rodger, A., Laukamp, C., Haest, M., & Cudahy, T. (2012). A simple quadratic method of absorption feature wavelength estimation in continuum removed spectra. *Remote Sensing of Environment*, 118, 273-283.

Vane, G., Green, R. O., Chrien, T. G., Enmark, H. T., Hansen, E. G., & Porter, W. M. (1993). The airborne visible/infrared imaging spectrometer (AVIRIS). *Remote Sensing of Environment*, 44(2-3), 127-143.

## AVIRIS-NG data for mineral exploration studies

Arindam Guha, Komal Pasricha, Subhendu Modal\* and K. Vinod Kumar

Geosciences Group, National Remote sensing Centre, Balanagar, Hyderabad

\*Department of Geophysics, Indian Institute of Technology (ISM), Dhanbad

### **1. Scientific rationale and Objectives**

In recent times, spectral profiles of rocks and minerals collected within the spectral domain of 0.4-2.5 micrometer have been used as key in delineating economic mineral/metal bearing rocks such as bauxite, limestone, chromitite, iron-oxide rich banded iron formation, kimberlite and other important host rocks for mineralization (Bedini et al., 2011, Guha et al., 2013 Rajendran et al., 2012). Specially, carbonate rocks and chromitite were mapped using broad band ASTER data of ASTER in selected areas in the country (Guha, et al.) Further attempt has been made to delineate surface alteration features associated with hydrothermal and supergene enrichment (Bedini, 2010; Chen et al., 2007). In this regard, space borne and airborne hyperspectral data are being used worldwide. In India, there are ample scopes to utilize high spectral resolution data with finer spatial resolution to delineate exploration targets. Under tropical climate of the country, however, many of such rocks, specially rocks of mafic and ultramafic composition either have scanty or have intensely weathered exposures., Many of the rocks known for its economic and petrogenetic importance have been covered with regolith and related land covers. Therefore, it is a challenge to delineate such rocks with limited spatial extent but immense exploration utility. In present study, Advanced space borne infrared spectrometer (AVIRIS) data were processed and analyzed for few study areas known for the occurrence for economic rocks like kimberlite, chromite and dolomite. Within this setup, important rock types having distinct mineralogical and spectral characters were present as patches.

- Comparative evolution of ASTER and AVIRIS data for delineating spectrally conspicuous but spatially restricted targets like chromitite& kimberlite.
- Mapping of dolomite and any intrafacies variation within dolomite.

## 2. Study area and data used

Table 29.1 provides details of the study area has been given.

Table 29.1. Details of the study

<b>Name of the area</b>	<b>State</b>	<b>Geological significance</b>	<b>Data used</b>
Sittampundi Layered Complex	Erode, Tamilnadu	Known for chromitite and host rocks of Platinum Group of elements	AVIRIS data, VNIR-SWIR bands of ASTER data, spectral profiles of rocks, ground geophysical data on magnetic anomaly
Bhukia, Bhimsore area	Banswara, Rajasthan	Mapping of carbonate and mapping of phosphate within carbonate.	AVIRIS data, VNIR-SWIR bands of ASTER data, spectral data of rocks, X ray diffraction data and Petrography
Wajrakarur	Guntakal, A.P	This area is characteristic of Kimberlite, (diamond bearing rocks). They have petrogenetic significance (pristine mantle composition). Serpentine rich analogue for planetary research	AVIRIS data, VNIR-SWIR bands of ASTER data, spectral data of rocks, X ray diffraction data and Petrography

## 3. Methodology

AVIRIS level 1B data were calibrated using physics based atmospheric correction module using FLAASH (Fast line of sight atmospherically analysis corrected spectral hypercube) software which was developed based on implemented MODTRAN 4 atmospheric correction model (FLAASH, 2009). Spectral integrity of image spectra was confirmed using the AVIRIS resampled laboratory spectra (FLAASH, 2009). Spectral details of targets and associated rocks were collected a-priori in laboratory. Mineralogical data and the relative abundance of minerals was ascertained using quantitative petrography. Different spectral mapping methods were utilized to delineate the target (i.e. chromitite, dolomite and kimberlite). Results were validated based on field data on chromite exposure and also using ground magnetic data. Methodology is discussed in the figure 29.1.

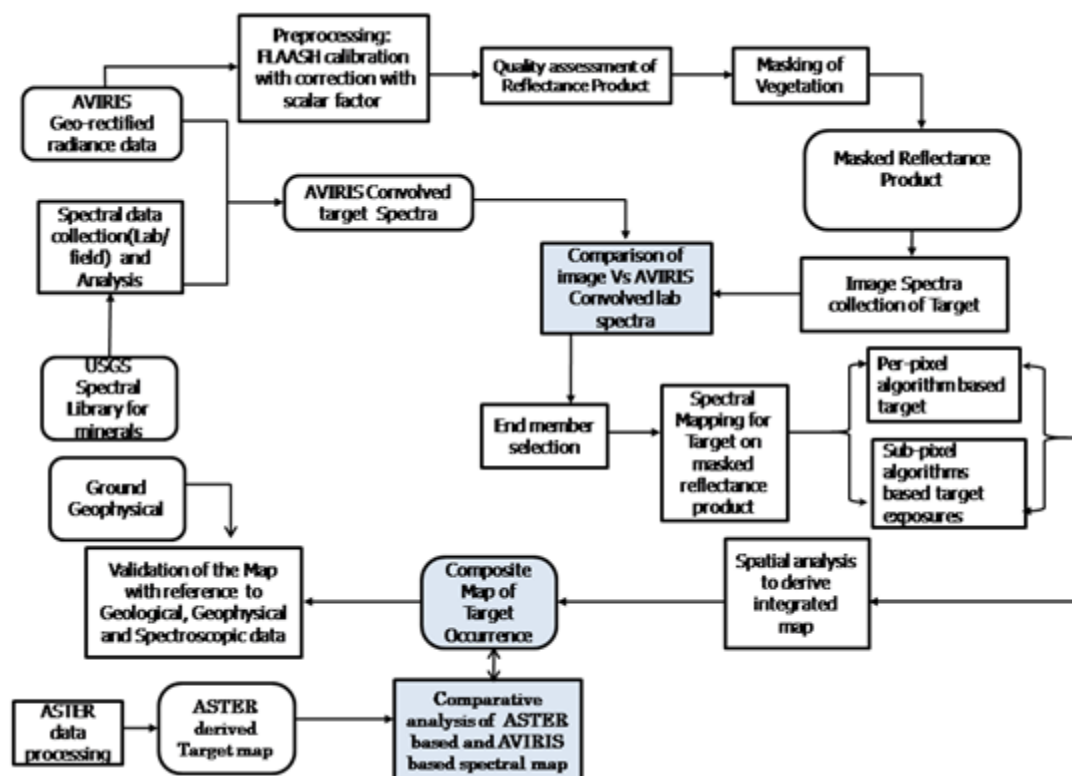


Figure 29.1. Flow chart of methodology.

## 4. Outcome

### 4.1 Salient findings

In this report, results of AVIRIS data processing for chromitite have been discussed. In the Sittampundi layered complex, chromitite occur as band and lenses within the anorthosite at the western fringe of layered complex (figure 29.2 (a)) (Ramadurai et al.,1975). In addition to chromitite, mafic rocks like orthopyroxenite and metagabbro (mafic cumulates of layered intrusion) occur at the eastern part of the study area(figure 29.2(a)). Most of these rocks are known for high magnetic anomaly than the plagioclase rich rock anorthosite. Anorthosite is the main country rock in the layered complex Therefore, ground magnetic data have been collected for the area with approximate 500-800-meter interval to delineate chromite or mafic cumulate within anorthosite. The data were processed to derive ground magnetic anomaly (figure 29.2(b)). Chromitite is also known for high magnetic anomaly. Two distinct areas have been analyzed in detail with respect to magnetic anomaly (figure 29.2(c)). One study area is known for chromitite occurrence and other area is known for meta gabbro occurrence. Precision magnetometer was used for collecting magnetic data.

In the study area, chromitite is associated with anorthosite, metagabbro and granodiorite gneiss (figure 29.3 a-d). Microphotograph of the rocks were made and analyzed to identify dominant minerals in major rocks (figure 29.3 f-h). These data are used to understand the mineralogical significance of absorption feature imprinted in the spectral profiles of the major rock units of layered complex (figure 29.3). AVIRIS Level 1B data were processed to derive minimum noise fraction (MNF) composite. This image was proved suitable for delineating gabbro, gneiss and anorthosite from each other (figure 29.4). But sub-pixel mapping was implemented to delineate chromitite; which are known for patchy and small sized exposure. Adaptive coherence estimator (ACE) mapping method was implemented to delineate chromitite in AVIRIS and ASTER data. Chromite exposure patches were delineated in AVIRIS data in accordance with field data and magnetic anomaly (Figure 29.5 a and c). Same spectral mapping method was also applied to calibrated ASTER data to delineate chromitite. However, ASTER derived chromitite map was characterized with false positives and fresh exposures were missed (figure 29.5 b).

Few of the pixels in ASTER based chromitite map were related with chromitite dump and associated red soil. In the broad band and coarse spatial resolution bearing ASTER data, iron rich soil and chromite have strong correlation in their spectral signature. Therefore, larger pavements of iron rich soil with chromite dump were delineated as anomaly while real, small sized chromitite exposures which were getting subdued in ASTER derived chromite map.

We have also processed AVIRIS data for parts of Bhukia and Bhimsore area. Initial results have been obtained. Spectral mapping applied on AVIRIS data could delineate dolomite band with less false positives than that of the spectral map derived using same mapping algorithm (match filtering method) (Figure 29.6 a and b). Results were validated using available geological map (updated with field input).

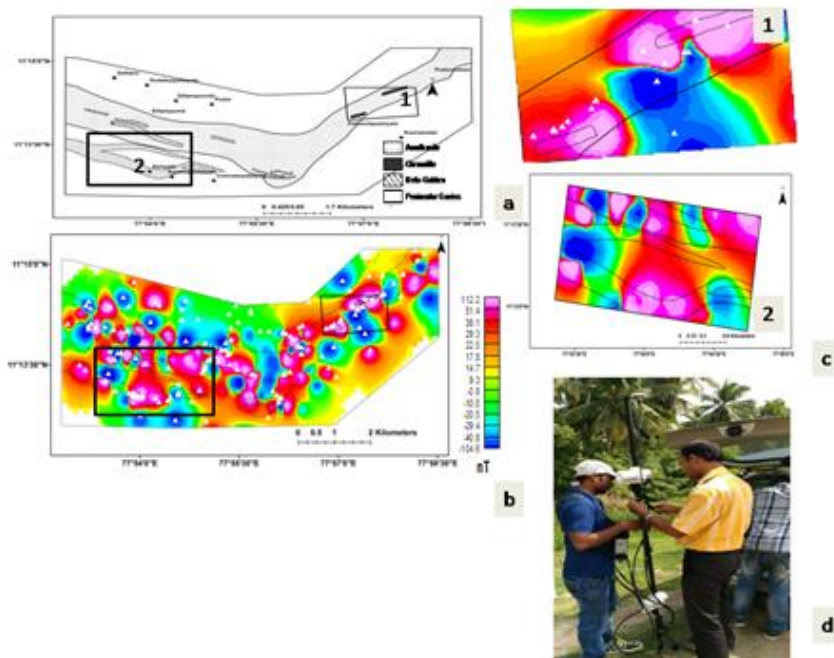


Figure 29.2. Geological map of Sittampundi Layered complex. b. 2D map ground magnetic anomaly. C. Enhanced portion of magnetic anomaly map for two sub areas one for chromitite and other for meta-gabbro.

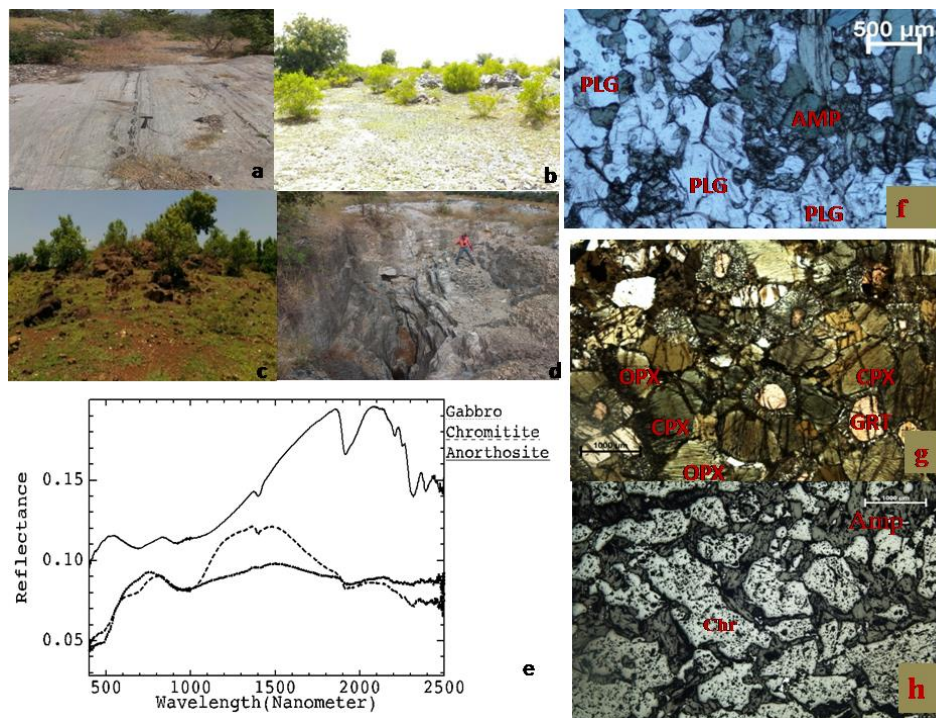


Figure 29.3. Field exposures of granodiorite gneiss(a), anorthosite(b) meta gabbro(c) and chromitite(d). e. Spectral profiles of major rocks of the study area. Microphotograph of anorthosite(f), meta-gabbro (g) and chromitite(h). PLG= Plagioclase. OPX=Orthopyroxene, CPX=Clinopyroxene, AMP= Amphibole and CHR=Cromitite.

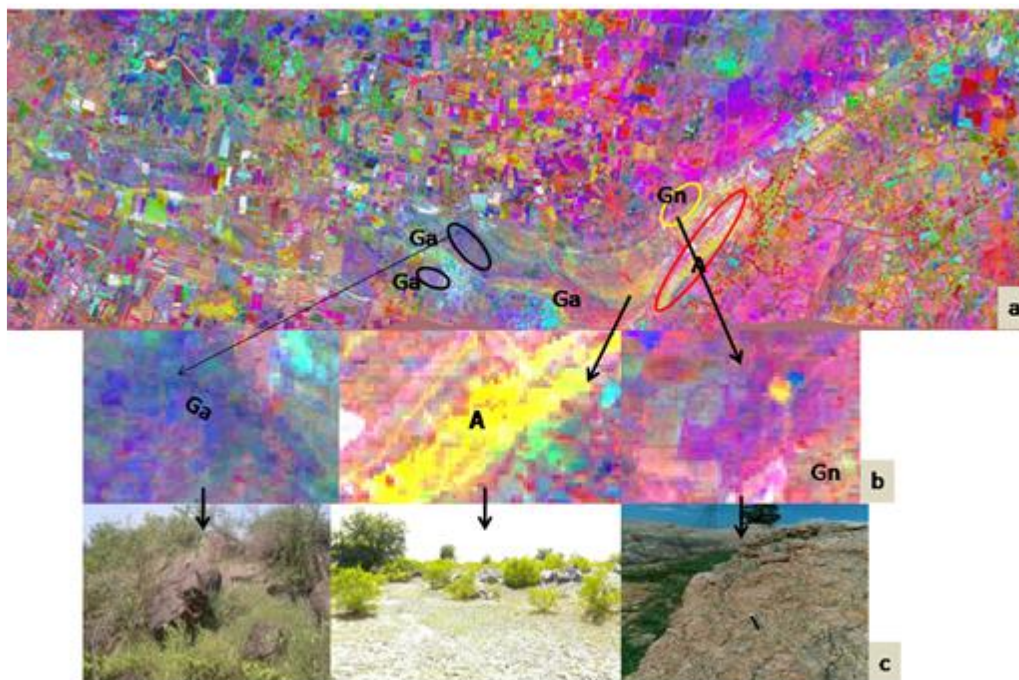


Figure 29.4. MNF composite of AVIRIS Level 1B data delineating major rocks of the area. Enhanced part of the image composite (b) of different rocks were shown with corresponding field photograph of different rocks.

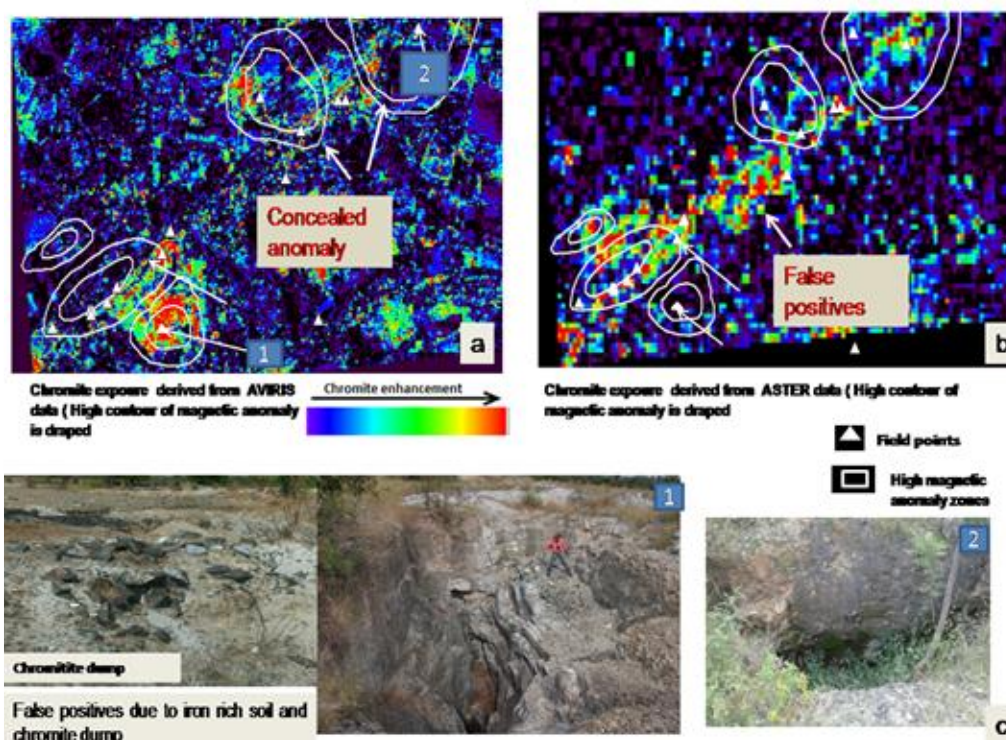


Figure 29.5. MNF composite of AVIRIS Level 1B data delineating major rocks of the area. Enhanced part of the image composite (b) of different rocks were shown with corresponding field photograph of different rocks.

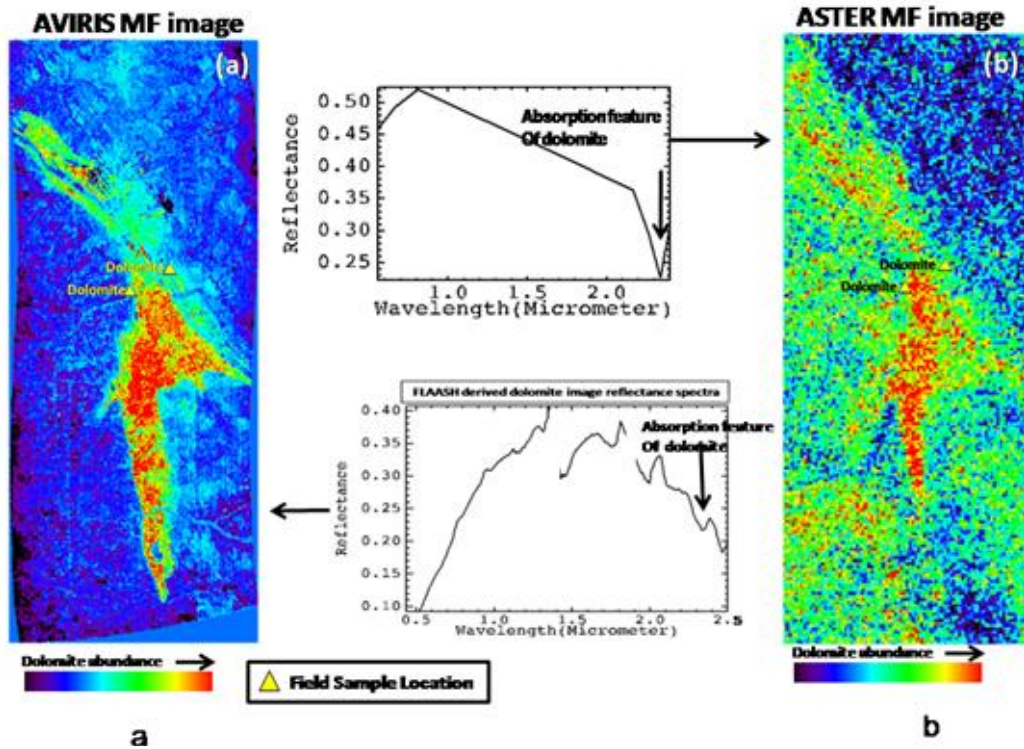


Figure 29.6. AVIRIS based dolomite map prepared using image spectra of dolomite (from mine area).  
 b. ASTER based dolomite map derived from broad band ASTER image spectra of dolomite.

### 4.6 Target vs. Achievement

Details of the progress are summarized below:

<b>Name of the Study area and target rock</b>	<b>Proposed Activity</b>	<b>Status or progress so far</b>	<b>Percentage of work completed till date</b>
Sittampundi Layered Complex (Erode, Tamilnadu) Target rock: Chromite	Pre-processing, Processing of ASTER and AVIRIS data to delineate major components of layered complex, validation, Comparison between ASTER & AVIRIS data output, field validation and validation with respect to geophysical data	Completed activity: Collection of all field data and ancillary data, Petrography of rocks, Laboratory spectral data collection and analysis for rock types, geological data base preparation ASTER data pre-processing and Processing. Preprocessing and processing of AVIRIS (level 1B) data, spectral mapping for delineating meta-gabbro, anorthosite and validation with field data and geophysical data. Planned activity: Final validation in field and report/paper documentation	80%

Bhukia, Bhimsore area (Banswara, Rajasthan) Target rock: dolomite	Pre-processing, Processing of ASTER and AVIRIS data, mapping, validation, Comparison between ASTER & AVIRIS data output.	Completed activity: Collection of field data, spectral data collection and analysis for rock types, geological data base preparation. AVIRIS-ASTER data pre-processing, Processing of AVIRIS and ASTER data, Comparative analysis of AVIRIS and ASTER data for mapping dolomite Planned activity: Investigate any intrafacies variation is observed in the dolomite, validation and report preparation	40%
--	--	---	-----

#### 4.7 Linkage to societal benefits

It will provide input to mineral exploration for the country.

### 5. Conclusions

Results of the AVIRIS data are analyzed in light of geophysical anomaly and field data on occurrence of rock exposures to understand the exploration value of AVIRIS derived spectral anomaly. For chromite, good correspondence was observed between spectral anomaly, geophysical anomaly and the presence of scattered targets. Initial study on chromite and dolomite has brought out the fact that AVIRIS data is better in delineating patchy exposures of chromitite and dolomite with less positive in comparison to ASTER data. Similar approach will be followed for kimberlite and dolomite. In dolomite, attempt will be made to understand the potential of AVIRIS data in estimating grade variation.

### References

- Bedini, E., 2011 Mineral mapping in the Kap Simpson complex, central East Greenland, using HyMap and ASTER remote sensing data. *Advances in Space Research*. 47, 60-73.
- Brandmeier, M., 2010. Remote sensing of Carhuarazo volcanic complex using ASTER imagery in Southern Peru to detect alteration zones and volcanic structures – a combined approach of image processing in ENVI and ArcGIS/ArcScene. *Geocarto International*. 25, 629-648.
- Chen, X., Warner, T., Campagna, D.J., 2007. Integrating visible, near-infrared and short-wave infrared hyperspectral and multispectral thermal imagery for geological mapping at Cuprite, Nevada. *Remote Sensing of Environment*. 110, 344-356.

FLAASH Module, 2009. Atmospheric Correction Module: QUAC and FLAASH User's Guide; Version 4.7; ITT Visual Information Solutions: Boulder, CO, USA, p. 44.

Guha, A., Rao, A., Ravi, S., Vinod Kumar, K., Dhananjaya Rao, E.N., 2012. Analysis of the potentials of kimberlite rock spectra as Spectral end member – a case study using kimberlite rock Spectra from the Narayanpet kimberlite Field (NKF), Andhra Pradesh. *Current science* 103, 1096-1104.

Guha Arindam, Vinod Kumar K, Jeyaseelan A.T., Dhananjaya Rao E.N., Parveen, Reshma.2014. An image processing approach for converging ASTER derived spectral maps for limestone mapping-a case example for Kolhan limestones, Jharkhand, India- *Current Science*, Vol. 106, No.1, 40-49.

GuhaArindam, Ghosh B., Vinod Kumar, K, Chowdhary, S.2015. Implementation of reflection spectroscopy based new aster indices and principal components to delineate chromitite and associated ultramafic-mafic complex in parts of Dharwar craton, India, *Advances in Space Research(Elsevier)*, 56 (2015) 1453–1468.

Rajendran, S., Al-Khribash, S., Pracejus, B., Nasir, S., Humaid Al-Abri, A., Kusky, T.M., Ghulam, A., 2012. ASTER detection of chromite bearing mineralized zones in Semail Ophiolite Massifs of the northern Oman Mountains: Exploration strategy. *Ore Geology Reviews* 44 121–135.

Ramadurai, S., Sankaran, M., Selvan, T., Windley, B., 1975. Stratigraphy and structure of sittampundi complex, Tamil-Nadu, India. *Journal of the Geological Society of India* 16, 409-430.

Khan, S.D., Mahmood, K., 2008. The application of remote sensing techniques to the study of ophiolites. *Earth Science Reviews*. 89, 135–143.

Kraut, S. Scharf, L. L. and Butler, R. W, 2005.The adaptive coherence estimator: a uniformly most-powerful-invariant adaptive detection statistic. *IEEE Transactions on Signal Processing*, 53,427-438.

# Identification of Terrestrial analogues of Noachian period of Mars using AVIRIS-NG data

Nirmala Jain, Tapas Martha, Priyom Roy and K. Vinod Kumar

Geosciences Group, National Remote Sensing Centre,  
ISRO, Balanagar, Hyderabad, India

## ***1. Scientific rationale and Objectives***

Currently, the only way to explore Mars is via data sent back from unmanned orbiting spacecraft and rovers, and through the study of Martian meteorites. However, it is widely recognized that interpretations of Mars must begin by using the Earth as a reference. This introduces the concept of terrestrial analogues, which are places on Earth that approximate the geological and environmental conditions on Mars and other planetary bodies, either at the present-day or sometime in the past. Water plays an important role in the formation of hydrated minerals. Hydrated minerals have been detected from orbital investigations in previous studies for Mars. Most commonly detected are phyllosilicates, carbonates and hydrous sulfates. Present work is to study the processes of formation of aqueous minerals from Nili Fossae, Mars region using hyperspectral datasets from the imaging spectrometer, Compact Reconnaissance Imaging Spectrometer for Mars (CRISM) onboard Mars Reconnaissance Orbiter (MRO). Nili Fossae is located in Northern Hemisphere of Mars. It has previously been mapped by aqueous minerals such as phyllosilicates, carbonates of Noachian period. To understand the processes of formation of these minerals Udaipur, Zabar Dungarpur and Ambaji region of Rajasthan are selected as a Martian analogue sites in the present study. Study of phyllosilicates and carbonates from the surface of Mars and from terrestrial analogue sites will help to understand the past environmental history of Red Planet.

## ***2. Study area and data used***

The analysis of hyperspectral datasets is carried out to understand the processes of formation of hydrothermally altered minerals using AVIRIS-NG and ASD Field Spec spectro-radiometer

for Dungarpur and Udaipur (Rajasthan) and Ambaji (Gujarat). Hyperspectral datasets by MRO-CRISM is used for the study of above minerals from Nili Fossae, Mars.

### 3. Methodology

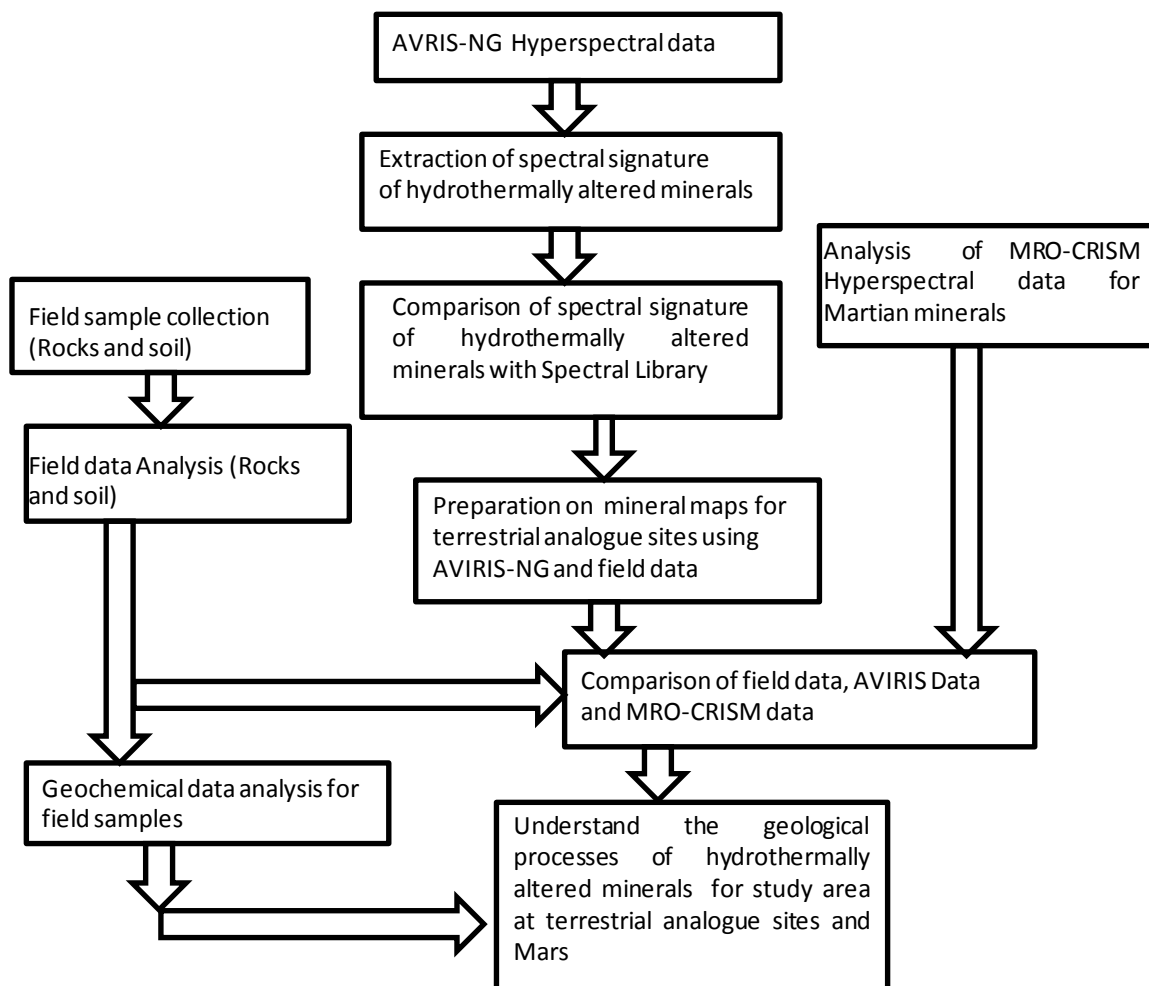


Figure 30.1. Flow chart shows the detail methodology of the study

## 4. Outcome

### 4.1 Salient findings

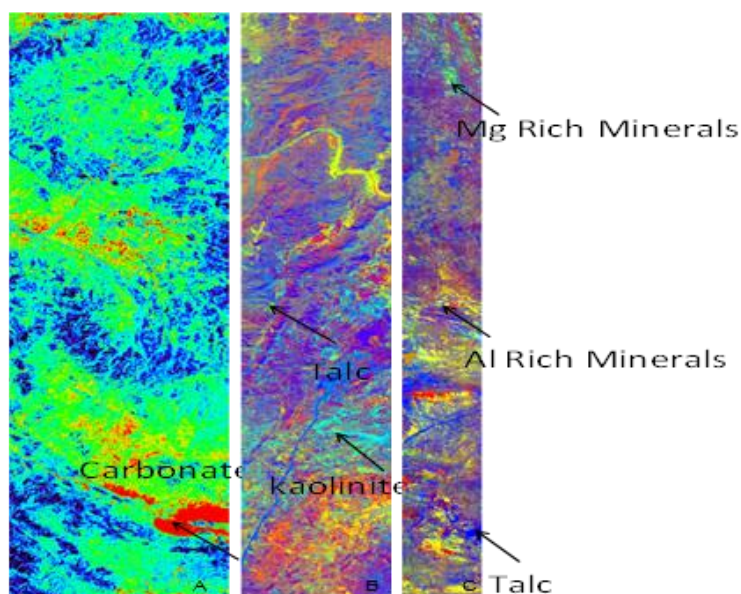


Figure 30.2. Hydrothermally altered minerals around Ambaji and Dungarpur region. A) Carbonate deposits (red) found near Ambaji B) deposits of kaolinite (cyan) and talc (yellowish green) found near Dungarpur C) deposits of Mg rich minerals (yellowish green), Al rich minerals (Cyan) and talc (dark blue) found near Dungarpur area.

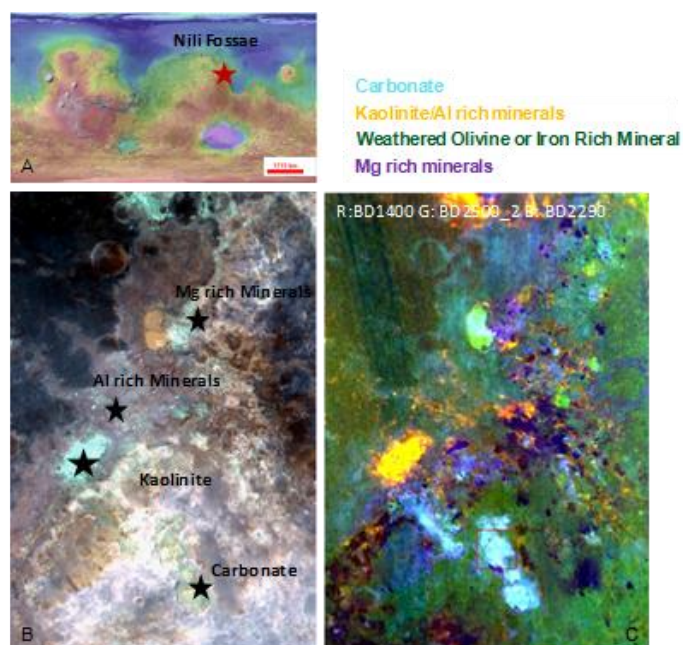


Figure 30.3. Hydrothermally altered minerals at Nili Fossae region of Mars. A) Location of Nili region on Mars Orbiter Laser Altimeter (MOLA) data, B) CRISM image shows the location of different hydrothermally altered minerals, C) MRO-CRISM band parameters such as BD1400, BD2500\_2 and BD 2290 were used to highlight the regional extent of the hydrothermally altered minerals.

## 4.2 Target vs. Achievement

<i>Target</i>	<i>Achievement</i>	<i>Remaining Work (%)</i>
Identification of aqueous minerals (phyllosilicates and carbonates) using AVIRIS-NG data.	Target is completed for the study area such as Ambaji (Gujarat) and area around Dungarpur (Rajasthan)	0%
Combine study of spectroscopic analysis of field samples, AVIRIS-NG data sets and MRO-CRISM data sets for hydrothermally altered mineral from Mars and terrestrial analogue	Field work is completed. In-situ data of rock and soil samples for hydrothermally altered minerals were collected from Ambaji and area around Dungarpur. Analysis of field samples and Mars data are under process.	(80%)
To understand the processes of formation of hydrothermally altered minerals from terrestrial analogue in order to understand the past aqueous environment of Mars.	Literature on processes of formation of hydrothermally altered minerals from Nili Fossae region, Mars and from terrestrial analogue is under progress.	(70%)

## 4.3 Linkage to societal benefits

The work will help to understand the Martian mineralogy, particularly the occurrence of and cause of the presence of a group of minerals of past Martian period. It will also identify the terrestrial analogues of Mars which will aid future planetary exploration.

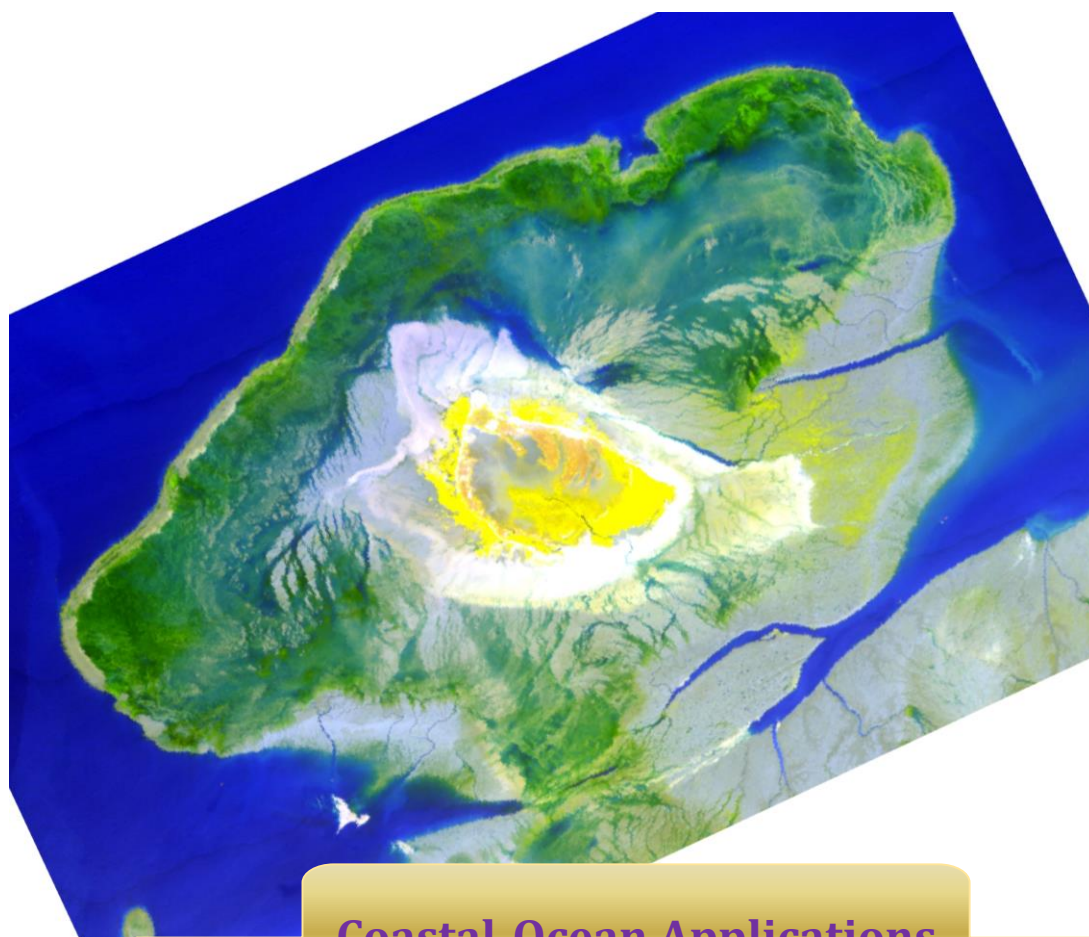
## 5. Conclusions

The south east part of Dungarpur (Rajasthan) contains deposits of serpentine minerals which is collected during field survey. This mineral gives the information of hydrothermal alteration processes occurred in past history of Mars. During the first campaign of AVIRIS-NG, this area is not cover. It will be helpful, if the second campaign of AVIRIS-NG will cover this region.

## References

Geological Survey of India, Misc. Publication, Government of India, Controller of Publication, No. 30 Part 12 • 3rd Revised Edition, ISSN 0579-4709, PGSI.327, 7000-2010 (DSK-II).

Geological Survey of India, Contributed by Shri Benudhar Behera.



## Coastal-Ocean Applications

### Summary

Characterization of suspended sediments along the coastal region is crucial in deciphering the coastal processes contributing to the distribution of terrigenous flux in the marine environment. Marine macro-algae are primary producers in coral reef ecosystems and are equally important to human life as a source of food, fodder, fertilizers, medicines and raw materials for cosmetic industries. Mapping of the extent of invader species shall help to check its further growth, coastal sewage and its spread along the coast, coastal classification maps help in fixing the coastal management plans. Species of *Sargassum* are used for alginate and liquid seaweed fertilizer production in India. Accordingly, species level map of marine macro-algae in a coral reef environment can help in building a geospatial inventory of macro-algal resources. Studies have been carried out in Gulf of Kachchh in Gujarat, south Karnataka coast in Mangalore region and Chilika lagoon in Odisha to characterize and understand the spectral signatures of various nearshore water quality parameters, to derive coastal bathymetry, benthic habitat and understand spectral signature of coastal land cover and landform, discrimination and mapping of three dominant brown macro-algae species of Sargassaceae family in Pirotan reef of Gulf of Kachchh. Largely, linear spectral unmixing and spectral angle mapper (SAM) were used for coastal studies. The characteristic triple peaks at 575, 600 and 650 nm appeared in case of all the three macroalgae species, with the third peak recording a negative shift of the order of 4 nm, i.e. at 646 nm. The spectral convexity in the 840 to 940 nm region is indicative of ripple effects of marginal water column on the macroalgae species. The future attempts will be to assess sediment size, composition, co-habitation of Sargassaceae species and identification and abundance mapping of red algae or Rhodophyta group.

# Application of hyperspectral data in Coastal Zone Studies

Ratheesh R, Preeti Rajput, Arunkumar SVV, A.S. Rajawat, Rakesh Baral,  
Ateeth Shetty, R.N. Samal and K.S. Jayappa

GSD/GHCAG/EP  
Space Applications Centre, ISRO, Ahmedabad, Gujarat, India

## ***1. Scientific rationale and Objectives***

Characterisation of suspended sediments along the coastal region is the crucial parameter in deciphering the coastal processes contributing to the distribution of terrigenous flux in the marine environment. The sediment size and compositional parameters of the suspended sediment possess unique signature of the source and thereby determining the sediment concentration, composition and size parameters is critical in understanding the sink to source pathway of the terrigenous influx.

The sediment dynamics within the Gulf of Kachchh has been a region of constant scientific interest owing to the high sediment concentration in a macro tidal environment. Mangalore city, along the southern coast of India is host to major port, fishing harbour and chemical industries. The discrimination and monitoring of sewages, chemical effluents and oil spill is vital aspect in maintaining the fragile coastal ecosystem. These activities impugning on the sea is regulated through CRZ notification of 2011 and hyperspectral data possess the potential to identify these coastal pollutants. Deriving coastal bathymetry data for shallow water region is another potential application of hyperspectral data which shall lead to access of updated bathymetry for nearshore modelling. Eutrophication of coastal water is another serious aspect where the hyperspectral data can be used viably by estimating the nutrients of the water column. Chilika Lagoon, along the east coast of India, is a closed system where eutrophication is a serious issue affecting the fishing community and the fragile ecosystem. Hyperspectral data has an upper hand in assessing water quality parameters and shall be used in discriminating the benthic habitat within the clear waters of Chilika lagoon.

## Detailed objectives

- Spectrally discriminate coastal sediments in terms of composition and size parameters using hyperspectral and in situ data.
- Map the regional distribution of sediments based on composition, size and concentration and infer the sediment source sink pathway.
- Understand the spectral signatures of various nearshore water quality parameters such as pollutants/sewage/oil slicks etc. within CRZ classes.
- Deriving coastal bathymetry and validation using in situ measurements
- Assess the water quality parameters for eutrophication studies within Chilika Lagoon viz TSM, Phytoplankton pigments (Chl-a, Chl-b, Chl-c), nutrients (nitrate, phosphate, ammonia), CDOM, diffuse attenuation coefficient.
- Classify the benthic habitat using hyperspectral data
- Understanding spectral signatures of various coastal land cover and landform classes and ecologically sensitive area.

## 2. Study area and data used

- Gulf of Kachchh in Gujarat (68.930-70.400 E 22.410-22.680 N)
- South Karnataka coast around Mangalore region (74.620-74.940E 12.790-13.270N)
- Chilika lagoon and environs, Odisha (84.940-85.770E 19.300-19.980N)

## 3. Methodology

To cater different objectives, different hyperspectral techniques are applied. The conceptual flow diagram of methodology is given in Figure 31.1.

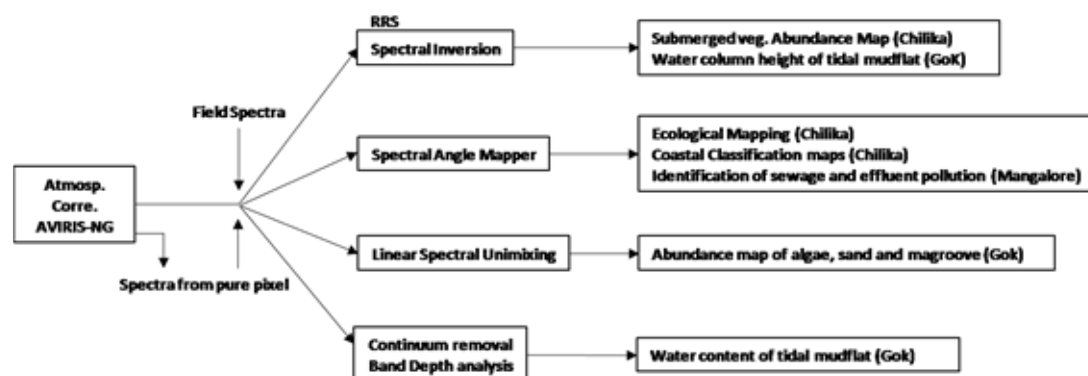


Figure 31.1. Conceptual Methodology.

## **Spectral inversion techniques**

Bio-optical models, which makes use of optimization techniques to assess water quality and bottom properties through inversion of the remotely sensed data (Giardino et al. 2012) are used to estimate water column depth of tidal mudflats along Gulf of Kachchh and to map the abundance of submerged benthic vegetation in Chilika region. The bio-optical model is based on the principle that the above water remote sensing reflectance is expressed as a function of radiance reflectance which is approximated as the sum of contributions from the water column and the bottom. The contribution from water column is estimated based on IOPs (total absorption coefficient and total backscattering coefficient), which are modeled as a function of concentration of water constituents and the bottom albedo is expressed as sum of relative distribution of different substrate albedo.

## **Linear Spectral unmixing**

Linear spectral unmixing technique is used to determine relative abundance of algae, sand and mangroves within the tidal mudflats of Gulf of Kachchh to establish a methodology towards estimating stability index of mudflats. In linear spectral unmixing method, the reflectance at each pixel level is assumed to be a combination of reflectance of each material or endmember. ASD spectra collected during the field campaign are used as the endmember spectra to determine the abundance map.

## **Spectral Angle Mapper**

Spectral angle mapper (SAM) technique is used to generate coastal classification map along the Chilika region and to map the pollutions of the Mangalore coast. Ecological mapping of Chilika is also carried out through SAM technique. In SAM, the similarity between two spectra is determined by calculating the angle between the spectra and treating them as a vector in a space with dimensionality equal to the number of bands.

## **4. Outcome**

### **4.1 Salient findings**

Bio-optical models were used to inverse the RRS spectra of atmospherically corrected AVIRIS-NG image to estimate abundance map of submerged aquatic vegetation of Chilika Lagoon. Figure 31.2 shows the abundance map of submerged aquatic vegetation in the Chilika

region. Spectral inversion technique has also been applied to estimate water column height over the tidal mudflat in Gulf of Kachchh. Figure 31.3 shows the water column height estimated from spectral inversion. Model is optimized using insitu observed reflectance of bottom features. Spectral Angle Mapper technique has been used to generate coastal classification map at Chilika mouth (figure 35.4).

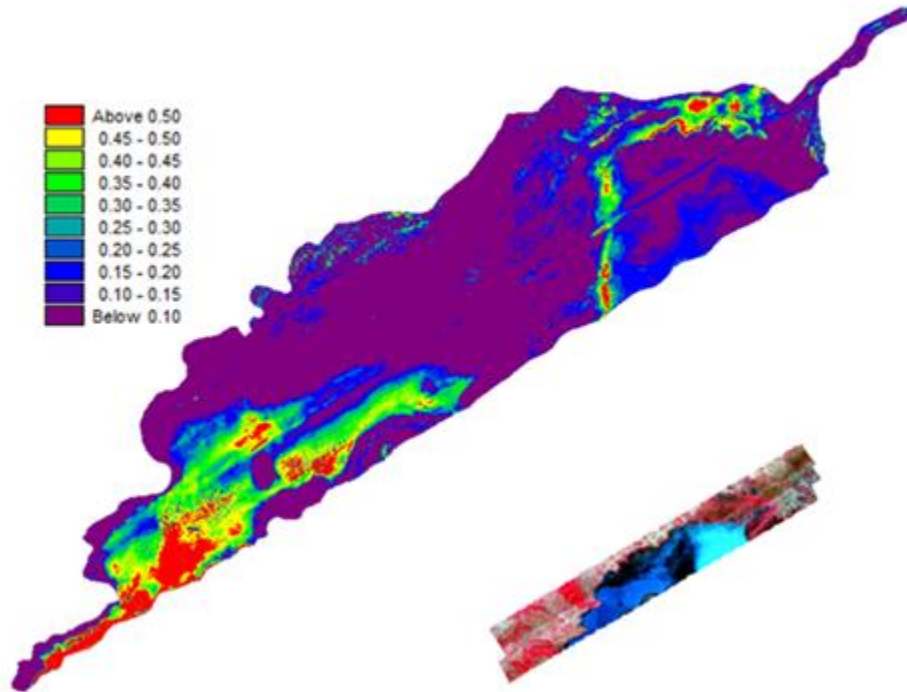


Figure 31.2. Abundance map of submerged aquatic vegetation in Chilika Lagoon

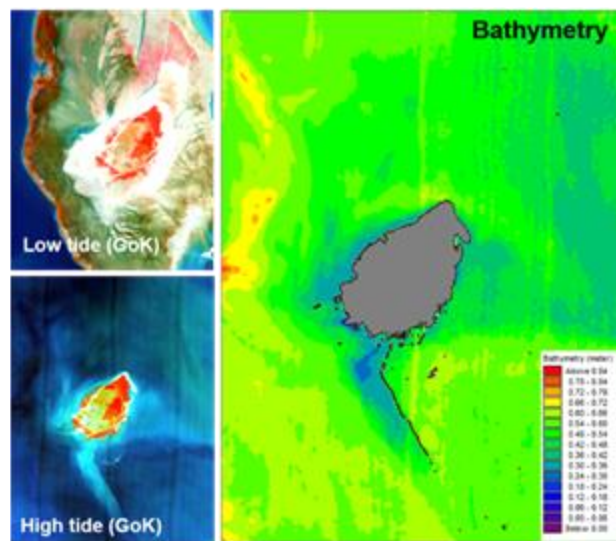


Figure 31.3. Water Column height estimation using spectral inversion technique

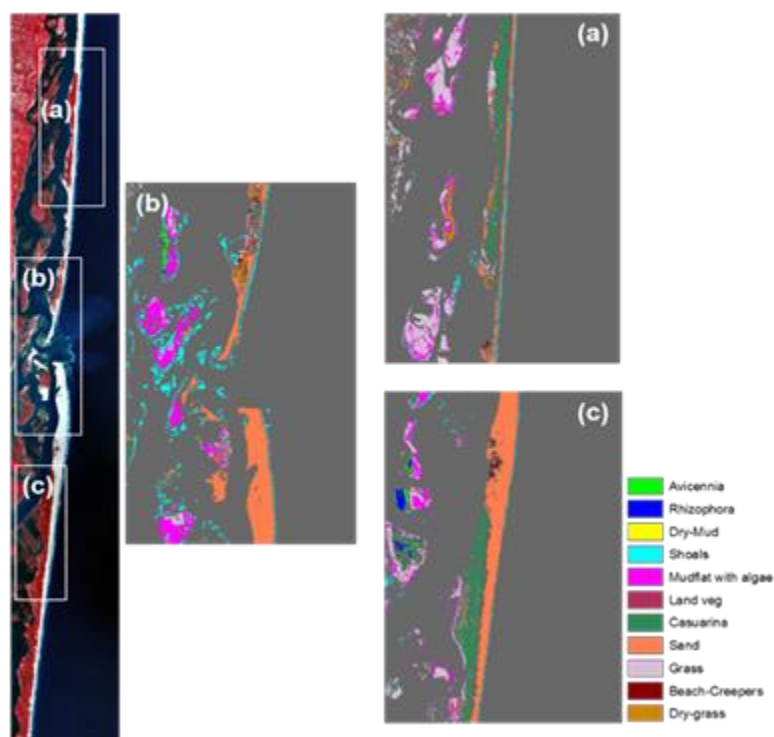


Figure 31.4. Coastal classification map

Using AVIRIS-NG, species-wise classification of mangrove (*Avicennia* and *Rhizophora*) were made and from land vegetation, *Casuarina*, beach creepers and dry grass were able to be discriminated. Ecological monitoring within Chilika Lagoon is carried out by mapping the area covered with *Phragmites karka* an invader species, whose alarming growth along the northern region is deteriorating the ecological condition. The spread of biomass accumulation is also mapped within the Chilika Lagoon which indicates the severity of eutrophication. Coast of Chilika is also affected with floating aquatic vegetation that prohibits the flow of water which adversely affect the ecological condition. Field observed spectra of floating grass, biomass accumulation and *Phragmites karka* are used to map their spread within Chilika Lagoon. Coastal waters affected by sewage pollutions at Mangalore coast is mapped using SAM method. Field observed spectra are used to map the sewage contaminations at Gurupur, and Netravati river (figure 35.5).

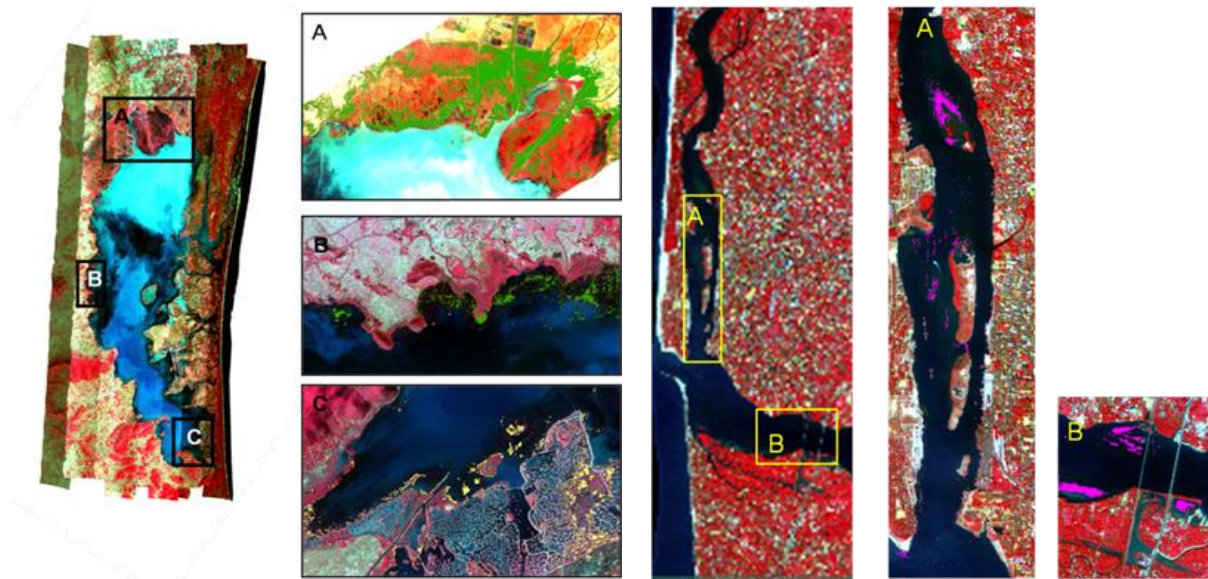


Figure 31.5. Mapping of different ecological parameters within Chilika Lagoon and sewage pollutions near Mangalore coast.

A method has been developed to determine the stability index of mudflat at Gulf of Kachchh with different weightage given to parameters (Smith et al. 2003) determined using AVIRIS-NG datasets. Abundance map of algae, sand, mangrove and mud is prepared using LS unmixing of the data, where in situ and pure pixel spectral values are chosen as the endmembers. Water content is estimated from band depth analysis of the continuum removed spectra of AVIRIS-NG. The specific absorption band at  $0.97 \mu\text{m}$  is used to estimate the water content (Verpoorter et al 2014). Different parameters estimated using AVIRIS-NG towards the development of mudflat stability index is shown in figure 31.6.

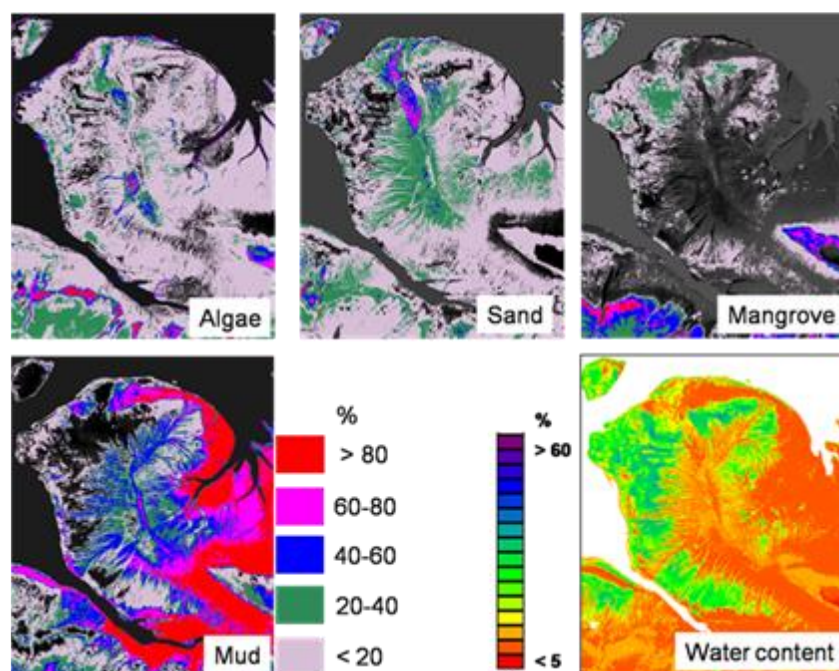


Figure 31.6. Abundance map of different coastal features and moisture content at Gulf of Kachchh.

## 4.2 Target vs. Achievement

Sl no	Targets	Achievement
1	Spectral discrimination of coastal sediments	Have carried out studies, but have not succeeded in discriminating based on composition and size.
2	Understand spectral signatures of various nearshore water quality parameters	75 %
3	Derive Coastal bathymetry	80 %
4	Benthic habitat	80 %
5	Understand spectral signature of coastal land cover and landform	75 %

## 4.3 Linkage to societal benefits

The following maps shall benefit the coastal community in delivering management plans

- Mapping of the extent of invader species within Chilika shall help to check its further growth
- Coastal sewage and its spread along Mangalore coast.
- Coastal classification maps.

## 5. Conclusions

- Various techniques like, spectral inversion using bio-optical model, spectral angle mapper, linear spectral unmixing and continuum removal and band depth analysis are applied to the AVIRIS-NG images of Chilika Lagoon, Mangalore coast and Gulf of Kachchh to deliver the different objectives under coastal applications of AVIRIS-NG.
- Abundance map of submerged benthic vegetation.
- Water column height of tidal submerged tidal mudflats.
- Coastal classification map with species-wise identification of mangrove and identification of different coastal vegetations.
- Ecological mapping of Chilika Lagoon, where major ecological issues like extent of growth of invader species, area of biomass accumulation and coastal region affected with floating grass are carried out.
- Abundance map of different parameters within the tidal mudflat.
- In the second phase, rigorous campaign with selection of specific source of coastal pollution, observation of underwater optical backscattering for bio-optical models, species wise identification of submerged vegetations, beach sediment size and compositional characteristics.

## Acknowledgements

We express our sincere gratitude to Shri TapanMisra, Director and Dr Raj Kumar for providing overall guidance and support. We are grateful to DrManimurali and his team for participating in the field campaign at Gulf of Kachchh.

## References

Smith G, A. Thomson, I. Möller, J. Kromkamp (2003), Potential of hyperspectral imaging to assess the stability of mudflatsurfaces by mapping sediment characteristics, Remote Sensing for Environmental Monitoring, GIS Applications, and Geology II, Proceedings of SPIE Vol. 4886, 330-341.

Verpoorter, C., V. Carrère, and J.-P. Combe (2014), Visible, near-infrared spectrometry for simultaneous assessment of geophysical sediment properties (water and grain size) using the

Spectral Derivative–Modified Gaussian Model, *Journal of Geophysical Research, Earth Surface*, 119,2098–2122.

Giardino, C, G Candiani, M Bresciani, Z Lee, Gagliano S and M Pepe (2012), BOMBER: A tool for estimating water quality and bottom properties from remote sensing images, *Computers & Geosciences* 45, 313-318.

# Study of Coral Reef Environment based on Airborne Hyperspectral Imaging with AVIRIS-NG Sensor

Nandini Ray Chaudhury, Mohit Arora, Ashwin Gujrati,  
Rakesh Patel\*, Devanshi Joshi\* and Harshad Patel\*

Space Applications Centre, ISRO, Ahmedabad, Gujarat, India

\*GEER Foundation, Gandhinagar, Gujarat, India

## 1. *Scientific rationale and Objectives*

Coral reefs represent a classic case of an optically complex shallow water target. As an underwater remote sensing target, coral reefs appear as mosaics of diverse substrates or bottom types when viewed from the space. Spectral nature of the remotely sensed data has been recognized as the basic link between coral reef substrates and remotely sensed images (Hochberg and Atkinson 2003). Imaging spectrometry remains a promising field for coral reef remote sensing especially for substrate detection, characterization and mapping.

In case of Indian coral reefs, high-resolution multispectral sensors have been successful only to map macroalgae (Bahuguna et al. 2013) but could never classify the different pigment groups.

The objectives of the current study are:

- Detection and mapping of emergent/submerged macrophytes/macroalgae in coral reef environment.
- Habitat discrimination into benthic and litho-substrate zones.

## 2. *Study area and data used*

The study area comprises of Pirotan reef (22°34'41"- 22°37'06" N latitude; 69°55'54"- 69°58'57" E longitude), which is identified as a core part of Jamnagar Marine National Park situated in the Jamnagar-Okha coastal segment of the Saurashtra peninsula, in the interior of southern part of Gulf of Kachchh. Pirotan is a fringing type of reef with an island in its core and lies to the north of Jindra bet. Pirotan Island is located 22 km off the coast, consisting of mangrove, coral reef, seagrasses, algae, invertebrates and low tide beaches. The island has

an area of 3 sq km. Pirotan Island is one of the most popular MNP site where visitors/tourists are normally permitted.

Data used: AVIRIS-NG data (JPL L2 product) dated 14.02.2017 (from sortie 3) along with in situ hyperspectral data collected with HR1024 spectrometer have been used for this study.

### 3. Methodology

This study used the established mapping algorithm: Spectral Angle Mapper (SAM) to map the brown macroalgae species. In situ spectral reflectance of brown macroalgae species were measured on Pirotan reef, synchronous to AVIRIS-NG flight on 14.02.2017. The resulting spectral library was used as a reference spectral library for extracting the end-member spectra from the target pixels of geo-registered AVIRIS-NG (JPL L2 reflectance) data. A multi-radian approach was initially employed to visualize the species level classified maps on smaller spatial subsets. The final classified map of brown macroalgae for the whole of Pirotan reef was generated with 0.1 radian as the minimum threshold angle.

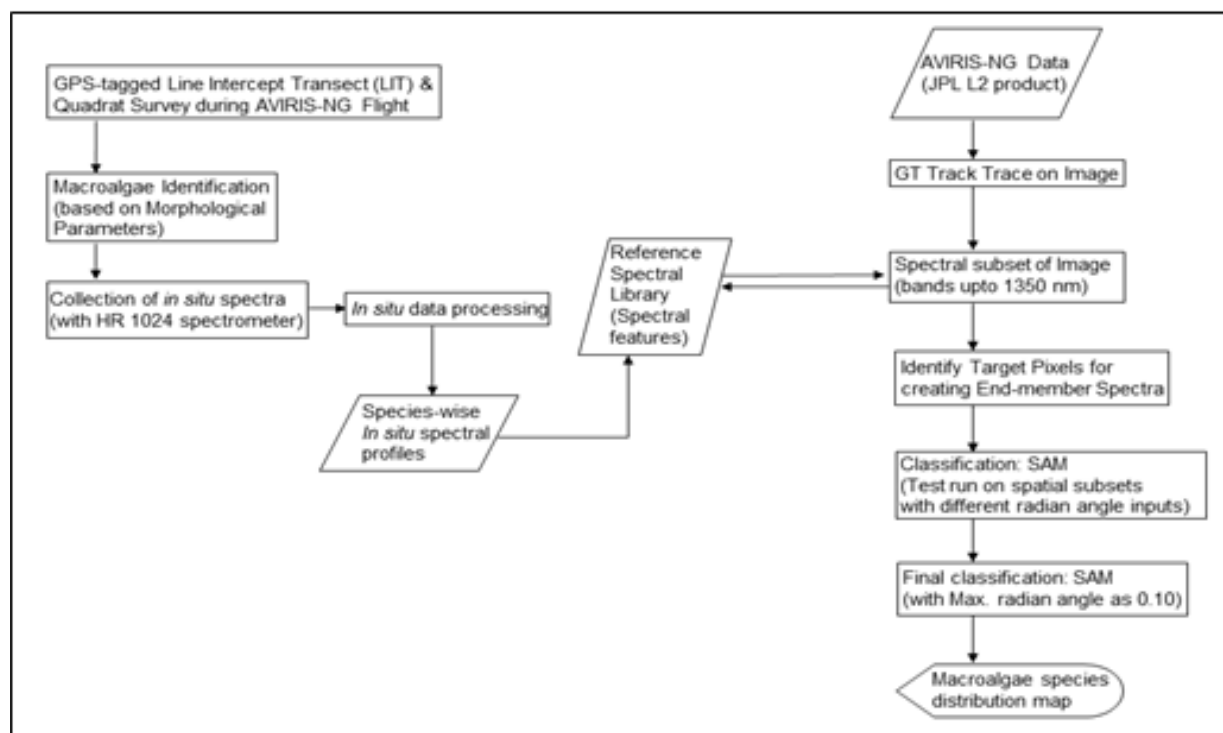


Figure 32.1. Flow chart showing the methodology

## 4. Outcome

### 4.1 Salient findings

Spatial distribution of brown macroalgae belonging to Sargassaceae Family was mapped for Pirotan reef from the AVIRIS-NG data. Three species have been identified: *Sargassum tenerrimum*, *Sargassum prismaticum* and *Cystoseira indica*. These brown macroalgae contain auxiliary carotenoid pigment: fucoxanthin which absorbs a broader section of light in the blue and green wavelength regions than the primary pigment of chlorophyll alone (Fong and Paul 2011). The characteristic triple peaks at 575, 600 and 650 nm appear in case of all the three species, with the third peak recording a negative shift of the order of 4 nm, i.e. at 646 nm. The spectral convexity in the 840 to 940 nm region is indicative of ripple effects of marginal water column on the macroalgae species. The mapped distribution shows microhabitat preferences of the macroalgae species: *S. tenerrimum* and *S. prismaticum* inhabiting the outer reef flat while *C. indica* is found as an ubiquitous species inhabiting both outer and inner reef flats of the Pirotan reef. This is due to the species preference of the bottom substrate. *S. tenerrimum* and *S. prismaticum* inhabit zones with hard rocky bottom while *C. indica* prefers a soft substrate like coralline sand (Jha et al. 2009).

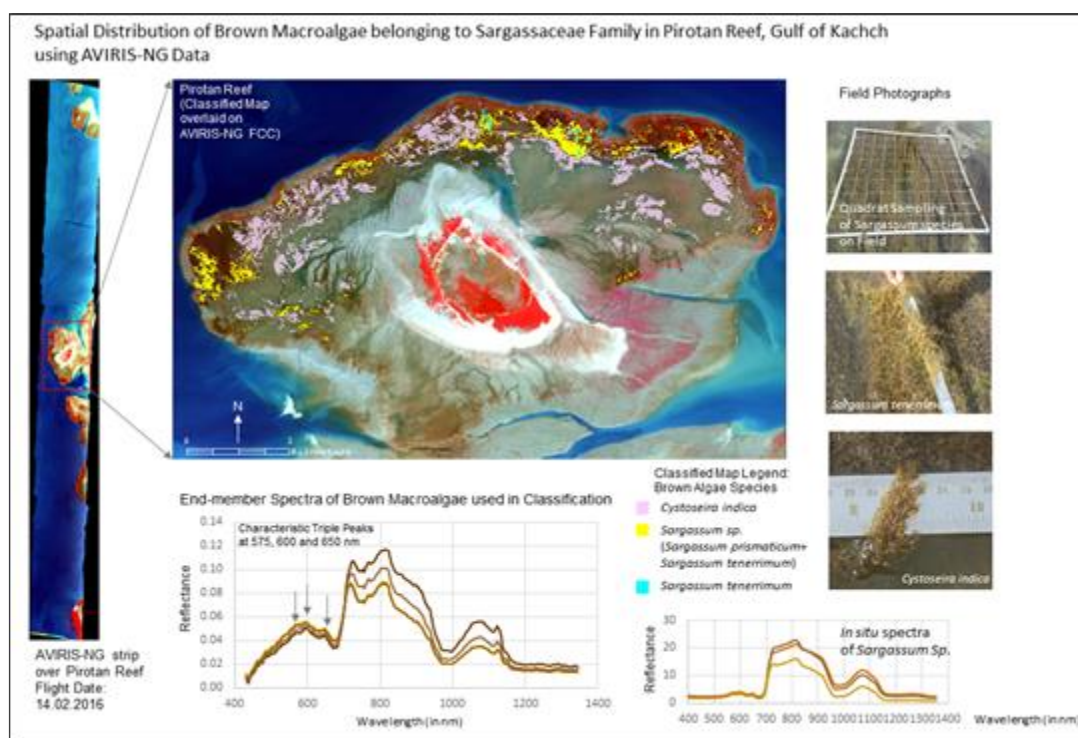


Figure 32.2. Species level distribution map of Sargassaceae Family in Pirotan reef

## 4.2 Target vs. Achievement

	<i>Targets</i>	<i>Achievement</i>
Objective 1	100%	50%
Objective 2	100%	Will be attempted after completion of Objective 1.

## 4.3 Linkage to societal benefits

Marine macroalgae are primary producers in coral reef ecosystems and are equally important to human life as a source of food, fodder, fertilizers, medicines and raw materials for cosmetic industries. Species of Sargassum are used for alginate and liquid seaweed fertilizer production in India. Accordingly, species level map of marine macroalgae in a coral reef environment can help in building a geospatial inventory of macro-algal resources.

## 5. Conclusions

- Characteristic triple peak feature present for all three Sargassaceae species.
- Negative shift, of the order of 4nm observed for the third peak (i.e. at 646 nm).
- Co-habitation of Sargassumtenerrimum and Sargassumprismaticum species yet could not be separated through simple SAM classification of AVIRIS-NG data.
- Cystoseiraindica is found as a ubiquitous species as compared to S. tenerrimum and S. prismaticum species which show their microhabitat preference towards outer reef flat.
- Repeat campaign on the same site and same time can help in validation of the species level macroalgae maps with additional work on Red Algae or Rhodophyta group which was not sufficiently covered in the first phase of the AVIRIS-NG campaign.

## Acknowledgements

The project team acknowledges the encouragement and support of Director, Space Applications Centre, ISRO in conducting the study. The team acknowledges the support of Director, GEER Foundation, Gandhinagar, in facilitating the field campaign. The support, guidance and encouragement received from Deputy Director, EPSA, SAC, Group Director, BPSG and AVIRIS-NG Science Team Leader and Head, AED are acknowledged with thanks.

## References

Bahuguna, A., Ray Chaudhury, N., Bhattji, N., Ajai and Navalgund, R.R. 2013. Spatial inventory and ecological status of coral reefs of the Central Indian Ocean using Resourcesat-1. *Indian Journal of Geo-marine Sciences*. 42(6), pp. 684-696.

Fong, P. and Paul, V.J. 2011. Coral reef algae. In: *Coral reefs: An ecosystem in transition* (Ed. Dubinsky, Z. and Stambler, N.), Springer, pp. 241-272.

Hochberg, E.J. and Atkinson, M.J. 2003. Capabilities of remote sensors to classify coral, algae and sand as pure and mixed spectra. *Remote Sensing of Environment*. 85, pp. 174-189.

Jha, B., Reddy, C.R.K., Thakur, M. C., Rao, M.U. 2009. *Seaweeds of India*. Springer, 215p.

# Simultaneous Validation Programme Undertaken for Hyper-Spectral Data to be Acquired from AVIRIS Flights

P. V. Nagamani<sup>1</sup>, A. Hakeem<sup>1</sup>, V. M. Chawdary<sup>2</sup>, Ch. V. Jayaram<sup>2</sup>, Neetu Chakov<sup>2</sup>, Umamaharswara Rao<sup>1</sup>, Anirban Akhand<sup>3</sup>, Abhra Chanda<sup>3</sup>

<sup>1</sup>National Remote Sensing Centre (NRSC), ISRO, Hyderabad

<sup>2</sup>Regional Remote Sensing Centre-East, NRSC, ISRO, Kolkata

<sup>3</sup>School of Oceanographic Studies, Jadavpur University (SOS, JU), West Bengal

## 1. Scientific rationale and Objectives

- In-situ bio optical and biogeochemical measurements of Hugli Estuary along with AVIRIS validation.

## 2. Study area and data used

- Lower Reaches of Hugli Estuary
- Site ID: 152 & 132 (OSG/ECSA)
- Site ID: 153 (water resources group + OSG)

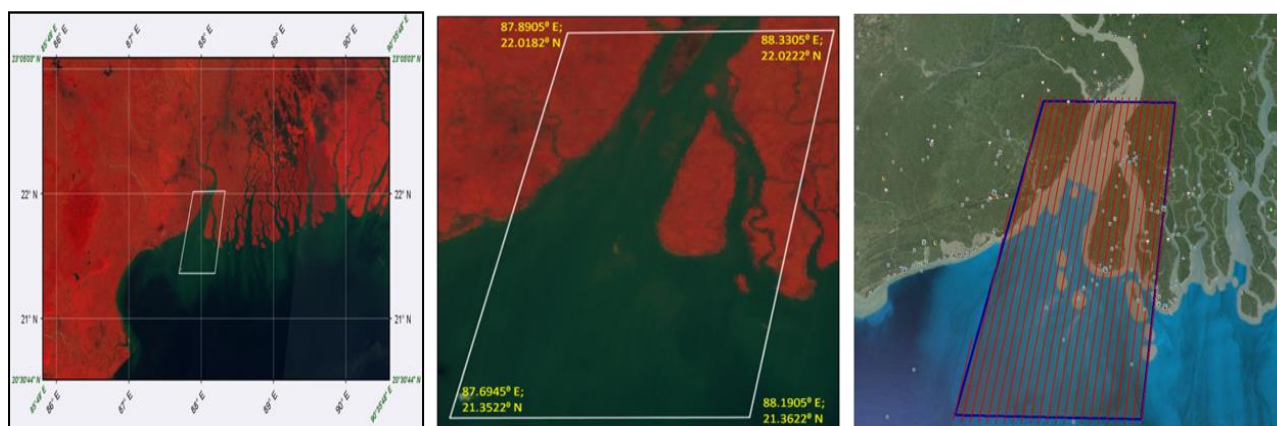


Figure 33.1. The scan lines of proposed AVIRIS-NG flight lines in the upper reaches of Hooghly and Saga Island

### 3. Methodology

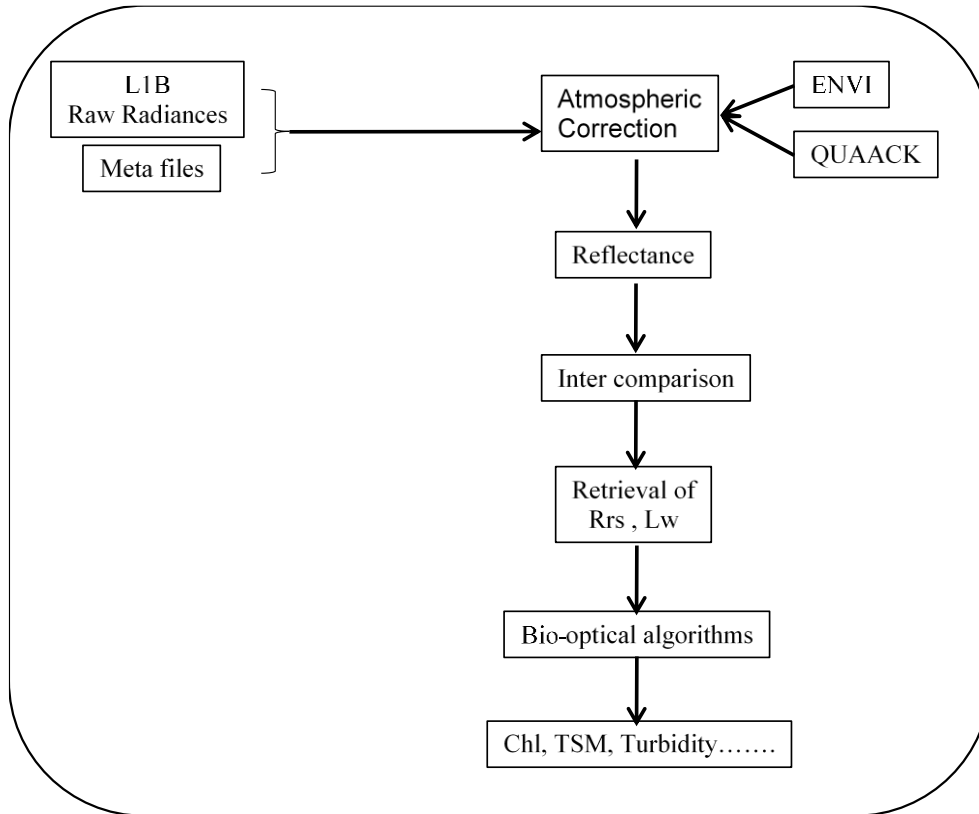


Figure 33.2. Flow chart showing the methodology adopted to retrieve the Geophysical products from AVIRIS-NG

### 4. Outcome

#### 4.1 Salient findings

##### Remote Sensing Reflectance Spectra

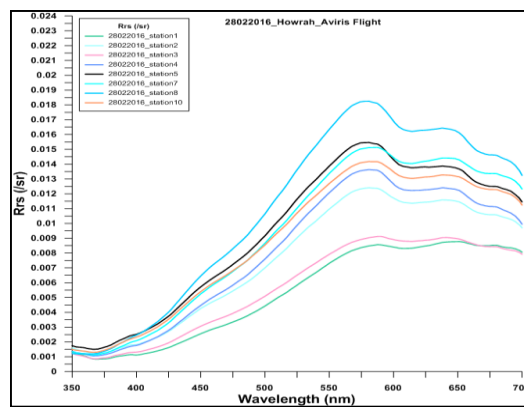


Figure 33.3. Remote sensing reflectance spectra collected on 28th February 2016, at Howrah

## Evaluation of atmospheric correction algorithms

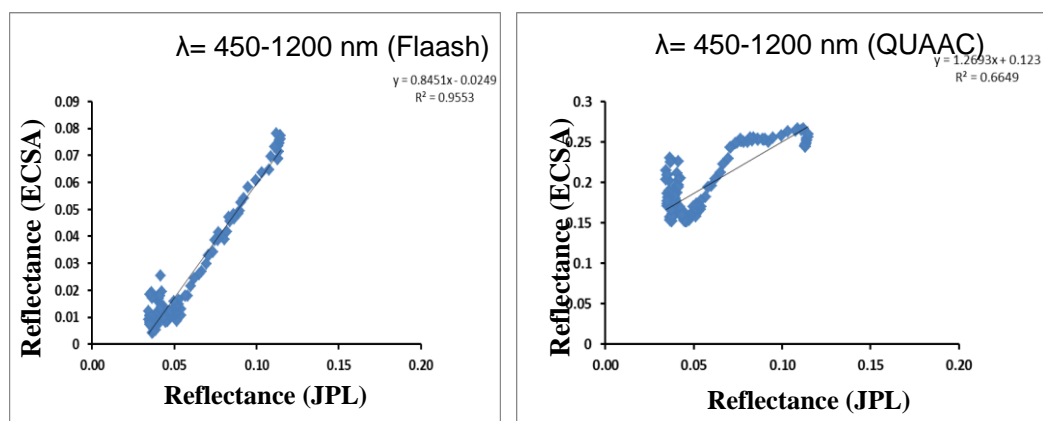


Figure 33.4. Comparison of ENVI (a) Flaash and (b) QUAACK atmospheric correction algorithms to derive the reflectances from AVIRIS-NG

## Validation of reflectance and chlorophyll

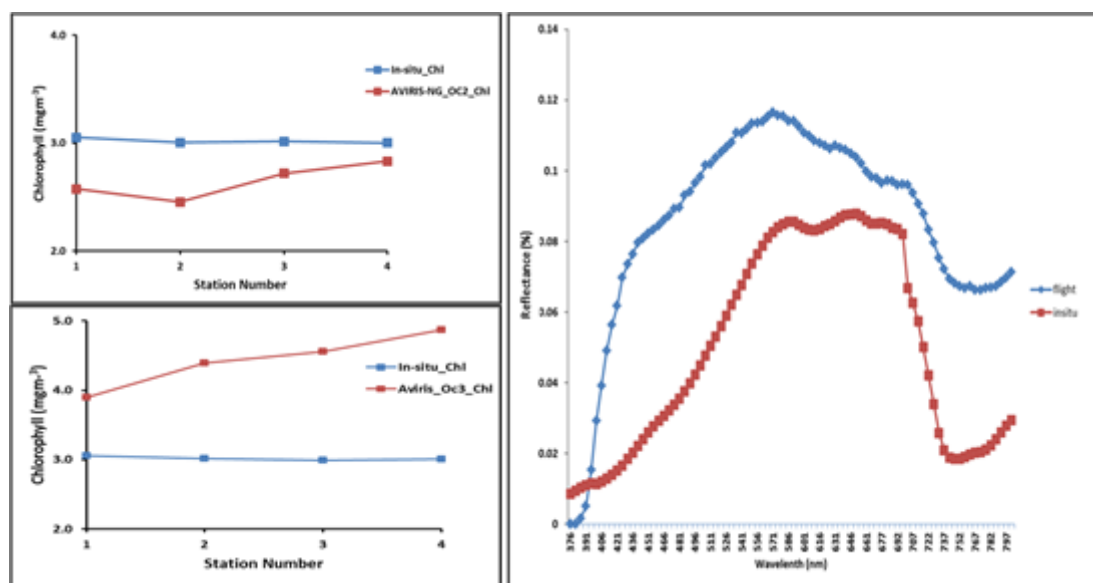


Figure 33.5. Validation of in-situ and AVIRIS-NG reflectances and chlorophyll

## Retrieval of chlorophyll

- Phytoplankton Functional Types like (i) Micro (ii) Pico and (iii) Nano planktons were identified (IOCCG 15, 2014; Hirata et al., 2011)
- Particulate Organic Carbon (POC) derived (Stramki et al., 2008)
- Total suspended Sediment (TSM) estimated using existing algorithms like (i) TASSAN (1994) (ii) TOPLISS (1990) and (iii) in-house.

- TOPLISS algorithm works in better quantification of TSM

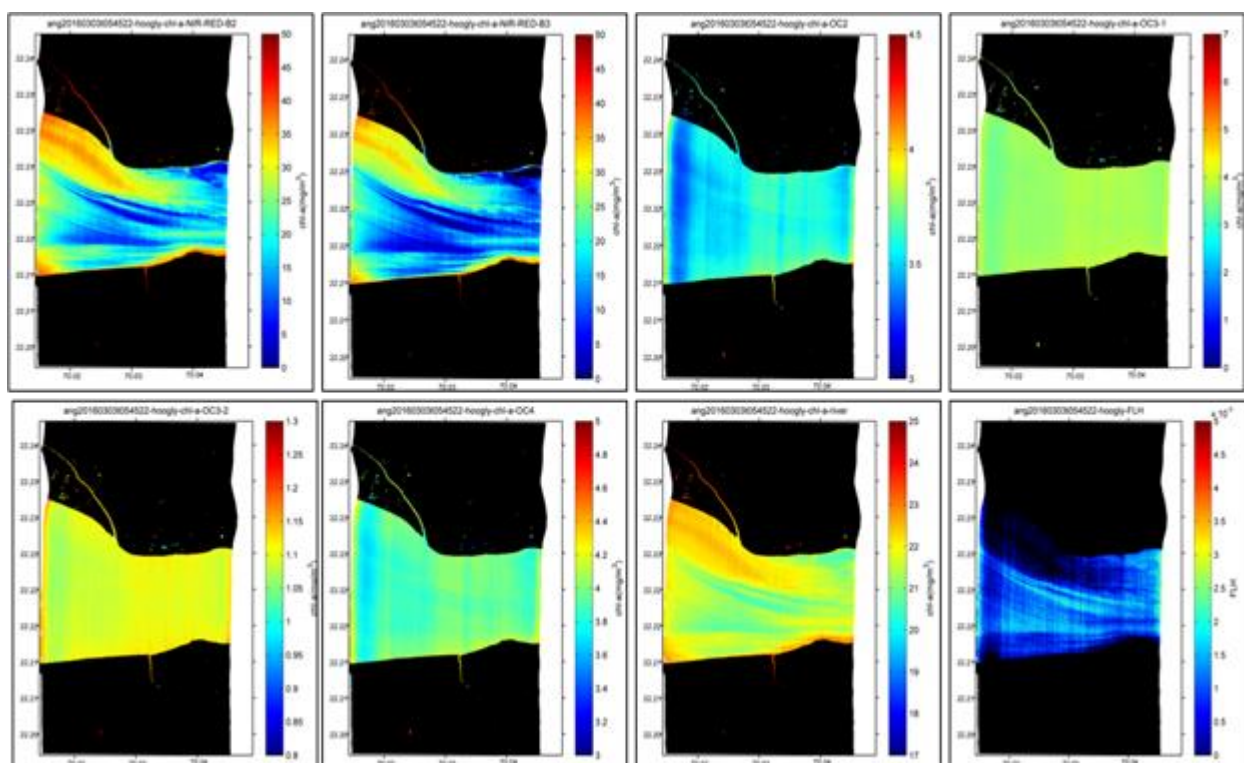


Figure 33.6. Retrieval of chlorophyll concentration and TSM in the Hooghly estuary using various chlorophyll algorithms and the bottom right figure shows the FLH fluorescence

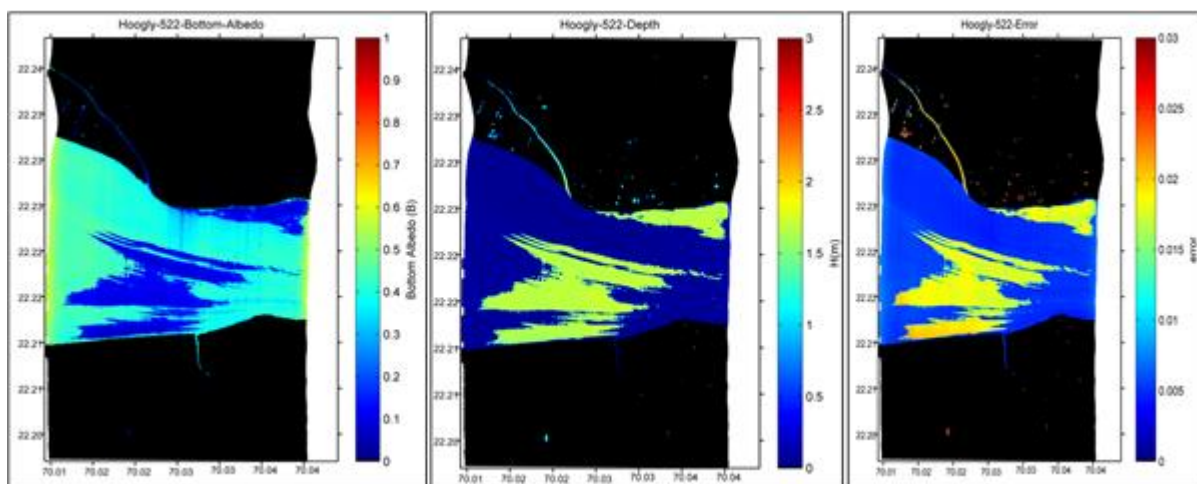


Figure 33.7. Representation of (a) bottom albedo (b) Depth and (c) error estimation while deriving these two parameters

25.02.2015 (Bagbazaar to Batanagar)							
Sample no.	1	2	3	4	5	6	7
time	10.00 AM	10.25 AM	10.58 AM	11.23A M	12.00 PM	12.41PM	1.05PM
Latitude	22°35' 29.5"	22°34' 22.85"	22°33' 17.95 "	22°32' 55.6"	22°33' 17.3"	22°33' 45.51"	22°33' 22.86"
Longitude	88°20' 53.5"	88°20' 30.5"	88°19' 34.28 "	88°18' 58.4"	88°16' 50.72"	88°14' 54.68 "	88°14' 14.218 "
water temp °c	24.7	24.6	24.8	24.8	24.9	24.8	25
salinity (µS/cm)	367	364	364	364	370	370	375
pH	7.533	7.557	7.501	7.76	7.84	7.8	7.69
UWPAR (µ mol m-2 s-1)	15.28	33.74	34.9	44.88	20.35	27.42	5.26
LUX	56400	61100	43000	76700	58000	30900	21400
DO (mg/l)	6.72	6.72	7.06	7.06	6.72	6.48	6.48
Turbidity (NTU)	49.4	60.7	113	57	44.6	43.6	160
Depth (m)	7.8	11.2	10.2	17.3	14	12.3	8.2
Chl-a (mg m-3)	9.45	9.98	8.65	11.2	10.22	10.11	9.75
HCO3-	120	124	127	124	127	127	134
Total alkalinity (µ mol/kg)	2031	2088	2143	2088	2143	2143	2257
fCO2 in (µ atm)	4664	4529	5306	2840	2426	2658	3620
pCO2 in (µ atm)	4664	4529	5306	2840	2426	2658	3620

26.02.2016 (Bagbazaar to Batanagar)									
Sample no.	1	2	3	4	5	6	7	8	9
TIME	9.10 AM	9.45 AM	10.08 AM	10.44 AM	11.05 AM	11.40 AM	11.59 AM	12.45 AM	1.21 AM
Latitude	22°36' 15.9"	22°35' 32.52 "	22°34' 6.04 "	22°33 ' 0.9"	22°33' 9.87"	22°33' 27.29 "	22°33' 46.7 "	22°31' 34.22"	22°30' 55.05 "
Longitude	88°21' 50.166 "	88°20' 16.17"	88°20' 16.17 "	88°19' 14.01 "	88°17' 58.8 "	88°16' 18.24"	88°14' 29.9"	88°14' 21.03 "	88°12' 47.5 "
water temp °c	24.7	24.8	24.8	24.9	24.9	24.9	25	25.1	25.3
salinity (µS/cm)	371	370	366	367	379	361	369	369	379
pH	7.97	7.9	7.89	7.82	7.69	7.76	7.73	7.71	7.65
UWPAR (µ mol m-2 s-1)	32.16	12.03	15.57	11.34	22.56	26.98	28.43	4.35	5.23
LUX	54400	60700	57100	22000	54000	59000	66500	13300	17920
DO (mg/l)	6.48	6.75	6.92	6.75	6.92	6.75	6.41	6.75	6.92
Turbidity (NTU)	112	37.2	52.4	48.1	59.8	101	36.4	76.2	96.2
Depth (m)	3.5	7.3	8.4	10	3.9	13.5	16.8	7.5	10.7

Chl-a (mg m-3)	10.9	10.48	7.07	10.82	10.43	10.55	9.86	11.27	10.08
HCO <sub>3</sub> -	120	134	120	129	131	134	120	124	134
Total alkalinity (μ mol/kg)	2031	2257	2031	2169	2214	2257	2031	2088	2257
fCO <sub>2</sub> in (μ atm)	1696	2219	2045	2572	3546	3074	2970	3202	3987
pCO <sub>2</sub> in (μ atm)	1696	2219	2045	2572	3546	3074	2970	3202	3987

28 .2 .16 (Bagbazaar to Batanagar)										
Sample no.	1	2	3	4	5	6	7	8	9	10
TIME	9.05 AM	9.25 AM	9.40 AM	9.55 AM	10.14 AM	10.40 AM	11.39 AM	12.00 PM	12.17 PM	12.28 PM
Latitude	22°36' 19.22 "	22°3 5' 44.5 "	22°34' 39"	22°3 4' 0.1"	22°32 ' 51.88 "	22°33' 41"	22° 31' 9.74"	22° 31' 0.28 "	22° 31' 0.1 "	22°31' 11"
Longitude	88°21' 41.6 "	88°2 1' 3.2"	88°20' 34.08 "	88°2 0' 2.5 "	88°18' 16.4 "	88°15' 42.96 "	88° 12' 52.3 "	88° 13' 17.7"	88° 13' 40.9 "	88° 13' 43.9 "
water temp °c	25	25	25	25.1	25.1	25.2	25.2	25.2	25.3	25.3
salinity (μS/cm)	362	362	364	365	368	383	374	372	373	372
pH	7.86	7.8	7.73	7.77	7.72	7.34	7.33	7.45	7.44	7.42
UWPAR (μ mol m-2 s-1)	16.63	16.97	11.45	42.8	20.78	27.55	81.46	69.01	66.08	66.72
LUX	61800	62300	42400	75500	40500	85600	94700	90000	89500	87300
DO (mg/l)	6.59	6.78	7.06	6.78	6.78	6.78	6.59	6.78	7.06	6.78
Turbidity (NTU)	67.7	61.6	46.5	32.6	49.7	30.3	58.5	53.8	61.2	56.1
Depth (m)	4.5	8.8	8.2	4.9	14.1	8.2	11.5	8.7	4.7	5.9
Chl-a (mg m-3)	11.21	10.38	8.25	10.57	9.85	9.59	8.95	8.59	8.69	7.96
HCO <sub>3</sub> -	130	130	126	120	120	124	128	130	134	134
Total alkalinity (μ mol/kg)	2200	2200	2131	2031	2031	2086	2160	2200	2257	2257
fCO <sub>2</sub> in (μ atm)	2380	2735	3116	2711	3044	7535	7982	6163	6479	6785
pCO <sub>2</sub> in (μ atm)	2380	2735	3116	2711	3044	7535	7982	6163	6479	6785

29.02.16 (Diamond Harbour)					
Sample no.	1	2	3	4	5
TIME	13.14 PM	13.35 PM	14.00 PM	14.23 PM	15.12 PM
Latitude	22 °10.998'	22 °10' 35.7"	22° 09 ' 53.50"	22° 09' 36.4"	22° 08' 45.60"
Longitude	88° 11.386'	88 °11' 14.6 "	88° 11' 19.50 "	88 °11' 57.9 "	88 °12' 14.30 "
water temp °c	27.1	26.9	26.1	27.6	27.1
salinity (mS /cm)	5.51	6.16	8.02	8.14	9.43
pH	7.925	7.968	7.936	7.982	7.921
UWPAR (μ mol m-2 s-1)	7.81	72.62		42.91	32.49
LUX	90700	90700	85100	82800	63900
DO (mg/l)	6.21	6.47	6.21	6.21	6.47
Turbidity (NTU)	435	32.3	502	52.4	47.1
Depth (m)					
Chl-a (mg m-3)	4.53	4.12	4.26	3.98	3.85
HCO3-	216.22	195.3	198.63	199.02	189.65
Total alkalinity (μ mol/kg)	3647	3294	3351	3357	3199
fCO2 in (μ atm)	2674	2084	2244	1946	2072
pCO2 in (μ atm)	2674	2084	2244	1946	2072

01.03.16 (Diamond Harbour)									
Sample no.	1	2	3	4	5	6	7	8	9
TIME	9.09 AM	9.24 AM	10.13 AM	11.03 AM	11.45 AM	12.27 PM	12.55 PM	13.31 PM	14.22 PM
Latitude	22 °10'46 "	22 °09' 34.6 "	11 °10.9 93'	22 °07' 47"	22° 3' 45.0"	22° 02' 53.5"	22 °02'05 3"	22°01' 45.8"	22° 00.75 2
Longitude	88° 11' 21.6"	88 °12' 4.8"	88° 11.39 6'	88° 12' 385"	88 °12' 37.1"	88 °11' 50.5"	88 °11.56 0"	88° 11' 10.3"	88 °10.8 82'
water temp °c	26.5	26	25.8	26.3	27.4	27.9	28.3	26.9	26.3
salinity (mS /cm)	4.03	4.54	4.55	3.98	5.79	9.06	9.41	8.76	11
pH	7.964	7.935	7.985	7.991	8.021	8.011	7.992	8.023	8.029
UWPAR (μ mol m-2 s-1)	34.34	31.25	37.98	6.56	56.33	38.53	22.05	34.96	2.42
LUX	67300	64000	73200	87800	91200	95300	57500	55100	24200
DO (mg/l)	6.32	6.54	6.54	6.11	6.49	6.31	6.19	6.18	6.08

Turbidity (NTU)	59.7	257	256	122	54.6	36.9	34.8	33.5	236
Depth (m)	5.12	4.94	4.75	5.1	4.26	4.11	3.89	4.21	3.92
HCO <sub>3</sub> <sup>-</sup>	192.37	201.17	197.84	197.65	194.13	190.22	189.83	190.61	192.21
Total alkalinity (μmol/kg)	3245.06	3393.51	3337.33	3334.13	3274.75	3208.79	3202.21	3215.37	3242.36
fCO <sub>2</sub> in (μatm)	2244	2454	2138	2162	1878	1737	1808	1685	1583
pCO <sub>2</sub> in (μatm)	2244	2454	2138	2162	1878	1737	1808	1685	1583

## 4.2 Target vs. Achievement

The proposed target was to validate the in-situ and flight reflectance and the chlorophyll in the proposed sites/ locations and this has been achieved 100%.

## 4.3 Linkage to societal benefits

The accurate estimation of Geophysical parameters in the turbid coastal waters will help in improving the coastal fisheries and local / regional climatic change studies.

The Hyperspectral data collected in these waters will help us in understanding the spectral variability of green to low to high turbid regions is Howrah and Hooghly estuary. These spectra will serve as a base and reference spectra for the future field work and upcoming ocean colour sensors.

## 5. Conclusions

- The first phase of AVIRIS helped us in planning the collection of Hyperspectral data in-situ simultaneous to the flight.
- This first phase gave us lot of understanding the in-sights in to the data processing schemes and atmospheric correction procedures that needs to be adopted for processing the Hyperspectral data and selecting the most suitable among the existing ones in the ENVI package itself.

However,

- Need to have another filed campaign of AVIRIS-NG in near future for better understanding of the coastal oceans and the estuarine water systems at the head of the Bay of Bengal and some of the riverine systems as well.
- In the second phase, more detailed and site specific flight runs closely spaced between adjacent flight runs during clear atmospheric conditions is needed for better quality of data and to obtain good results for working towards the upcoming new Hyperspectral sensors of ISRO like GISAT and PACE missions.

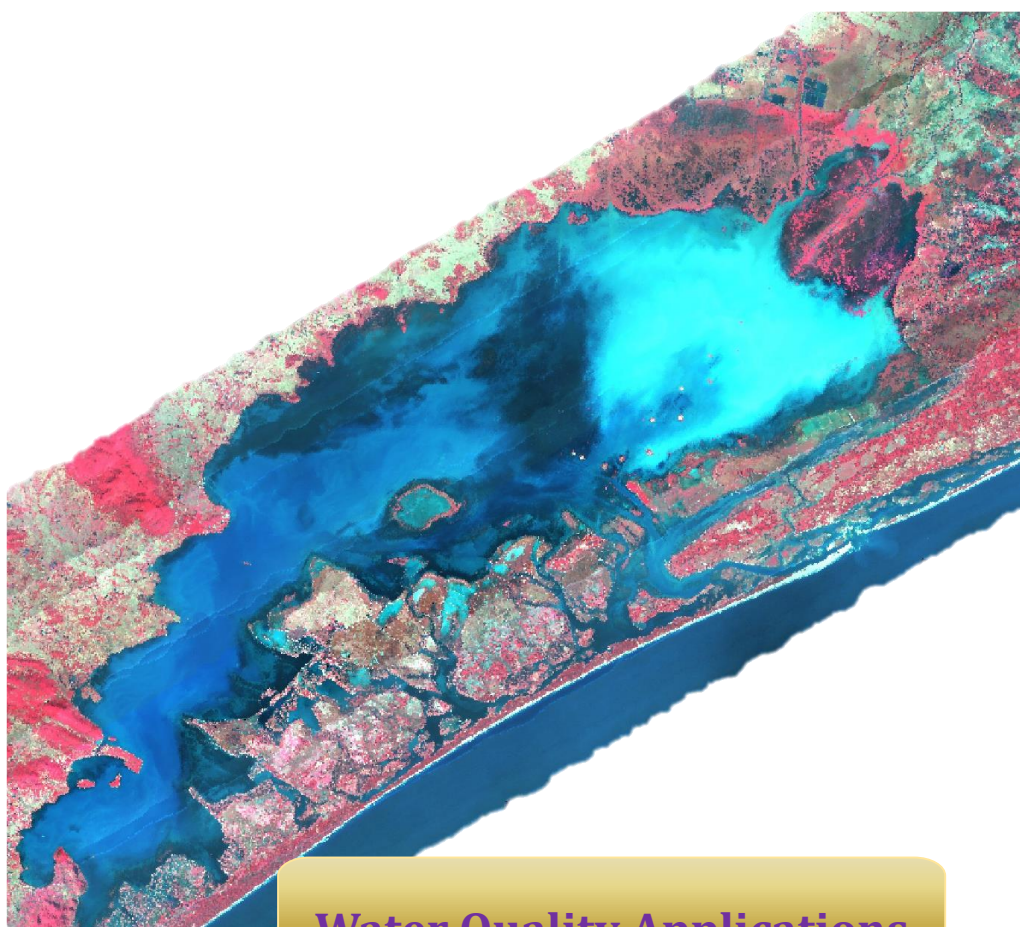
### **Acknowledgements**

The team sincerely thanks Director, NRSC and AVIRIS team for supporting the work and providing the opportunity to work with this mission. We also thank all the participants and their respective collaborative agencies (IMMT, Bhubaneswar and Andhra University, Visakhapatnam) for providing the necessary facilities to carry out the field work without any problem.

### **References**

IOCCG 5, Phytoplankton Functional Types from Space, Edited by Shubha Sathyendranath, 2014.

Natália De Moraes Rudorff & Milton Kampel (2012) Orbital remote sensing of phytoplankton functional types: a new review, *International Journal of Remote Sensing*, 33:6, 1967-1990, DOI: 10.1080/01431161.2011.601343.



## Water Quality Applications

### Summary

Water pollution is a major environmental issue in India. The largest source of water pollution in India is untreated sewage. Other sources of pollution include agricultural runoff and unregulated small scale industry. Most rivers, lakes and surface water in India are polluted. Hyper spectral remote sensing is a valuable tool for monitoring the water quality parameters from rivers and water bodies providing the synoptic view of spatial distribution of the chemical and physical properties. The variation in water quality parameters like Suspended Solids, Chlorophyll-a and Coloured Dissolved Organic Matter, affects the spectral characteristics of water in visible and near infrared electromagnetic spectrum (400-800 nm). Studies have been carried out in Ganga River and Chilika lagoon in Odisha to characterize and understand the spectral signatures of various water quality parameters and bottom depth. Largely, empirical, semi-analytical, linear spectral unmixing and spectral angle mapper (SAM) were used for water quality studies. A simulated database has been generated using bio-optical algorithms that generate remote sensing reflectance (400-800 nm) for all possible combinations of water quality parameters and bottom depth. Based on the above mentioned methodologies, turbidity maps were generated for both the study areas. The study will be used to generate water quality maps over inland water bodies, especially over the Ganga river basin. The hot-spots of point source pollution due to sewerage discharges from drainage can also be identified using hyperspectral meter level spatial resolution imagery. This will provide very useful information to pollution control agencies for finding out potential location of water quality contamination.

## Assessment of Water Quality in River Ganga using AVIRIS NG Hyperspectral Data

K. Abdul Hakeem, Annie Maria Issac and Karthik Reddy

Water Informatics & Quality Division, Water Resources Group,  
Remote Sensing Applications Area, National Remote Sensing Centre, Hyderabad, India

### 1. *Scientific rationale and Objectives*

Water pollution is a major environmental issue in India. The largest source of water pollution in India is untreated sewage. Other sources of pollution include agricultural runoff and unregulated small scale industry. Most rivers, lakes and surface water in India are polluted. Hyper spectral remote sensing is a valuable tool for monitoring the water quality parameters from rivers and water bodies providing the synoptic view of spatial distribution of the chemical and physical properties. The variation in water quality parameters like Suspended Solids, Chlorophyll-a and Coloured Dissolved Organic Matter, affects the spectral characteristics of water in visible and near infrared electromagnetic spectrum. The concept of concurrent observations: collection of water samples during the imaging time by airborne hyper spectral imaging sensor; and the correlation between the spectral signatures and water quality parameters will provide scope for effective use of air borne hyper spectral imaging for the estimation of water quality parameters. Various studies as shown in the table shown below have been carried for assessing water quality parameters using hyper spectral data.

Study Area	Parameters	Bands or Band Ratios or Band Differences Used (nm)	Reference
Mississippi River, USA	Turbidity	705	Olsman et al, 2013
	TSS	705	
	NVSS	705 & 705/670	
	VSS	705/670	
	Chlorophyll a	705/670, 705/620, 705/592	
Ohio River, USA	Turbidity	675-700, 710-740	Shafique et al, 2003
	Chlorophyll a	705/675	
	Total Phosphorous	(554/740)-(620-740) & log (554/675)	
Neuse River, USA	Suspended Solids	30 bands between 400-700 nm	Karsaka et al, 2004
	Chlorophyll a		
	Dissolved Organic Carbon		

The objectives of this study are:

- Analysis of spectral signatures from airborne hyper spectral sensor with reference to various water quality parameters for the selected river reaches of Ganga along with field measured spectra.
- Development of relationships between water quality parameters and hyper spectral data over selected reaches of Ganga River.

## ***2. Study area and data used***

More than 500 million people live along the Ganges River. An estimated 2,000,000 persons ritually bathe daily in the river, which is considered holy by Hindus. Ganges river pollution is a major health risk. In view of this, it was proposed to carry out the study as part of ISRO-NASA collaboration by acquiring AVIRIS-NG data over few reaches of main stem of Ganga River. Initially, few sites were identified between Kannauj and Varanasi, the most polluted sector of the river. Due to security restrictions they were not considered and alternatively another four sites were identified downstream of Varanasi. The four sites are near Buxar & Bhagalpur in state of Bihar, and Howrah & Hooghly in state of West Bengal (Figure 34.1).



Figure 34.1. Index Map of Study Area.

Orthorectified and atmospherically corrected reflectance data (unitless quantities from 0 to 1, scaled by a factor of 10000) of AVIRIS-NG L2 product is used in the study. Each site was covered in three strips as shown in following table.

Site Name	Strip No	Flight Date	Flight Time (GMT)	Flight Time (IST)
Buxar	1	23-Feb-2016	06:09:14	11:39:14
Buxar	2	23-Feb-2016	06:17:37	11:47:37
Buxar	3	23-Feb-2016	06:26:39	11:56:39
Howrah	1	27-Feb-2016	06:31:44	12:01:44
Howrah	2	03-Mar-2016	05:10:27	10:40:27
Howrah	3	03-Mar-2016	05:19:46	10:49:46

### **3. Methodology**

Globally two approaches are followed for retrieving water quality parameters using hyperspectral data. Either semi-empirical method (Olsman et al, 2013) or analytical method (Karsaka et al, 2004) is followed. In the first approach, simple linear regressions are used to determine the relationships between single and combinations of bands and water quality parameters. In the other approach, the reflectance/radiative transfer model used to quantify and simulate the individual contributions of the water constituents to the reflectance measured by the remote sensors. In the present study, the turbidity of water sample collected is compared with spectral profile of water. Using Spectral Angle Mapper (SAM) algorithm, the hyperspectral image is classified to generate spatial turbidity map.

### **4. Outcome**

#### **4.1 Salient findings**

Analysis of spectral profiles from AVIRIS-NG data shows higher reflectance in the region of 540-620 nm and the magnitude of reflectance is higher in case of Howrah compared to Buxar site. This indicated higher level of suspended sediment concentration in Howrah. Based on the spectral profile, turbidity maps are generated for both the study areas. It shows the spatial variability in Turbidity across the Ganga River. Further analysis needs to be carried out to compare the AVIRIS-NG spectral profile with reference spectral library of water. In addition to this, effect of chlorophyll-a concentration on spectral response pattern of water needs to be analysed.

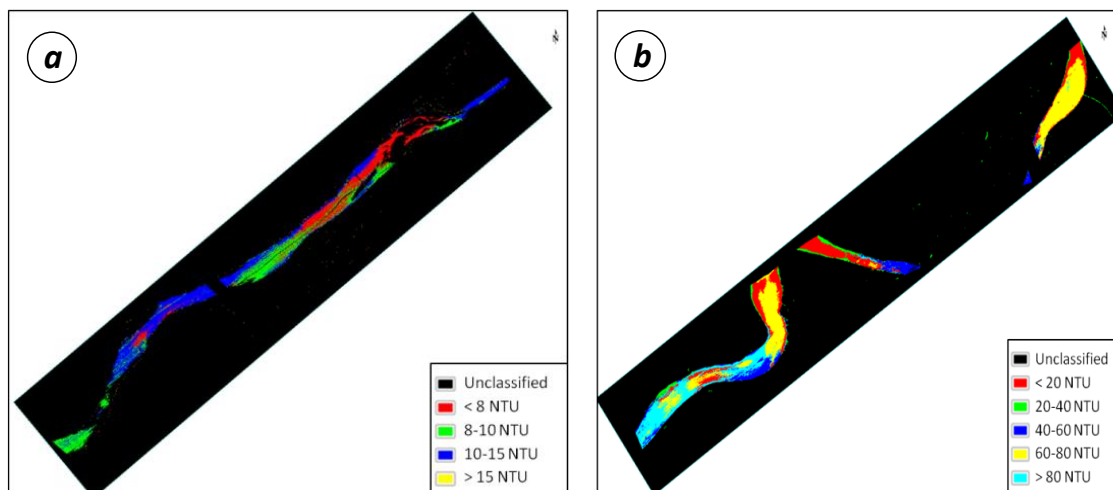


Figure 34.2. a.) Turbidity map of Ganga River near Buxar, b.) Turbidity map of Hooghly River near Howrah.

### 4.3 Linkage to societal benefits

Based on the results from the study, water quality maps need to be generated using satellite data for the Ganga River. This will provide synoptic view of the water quality status over space and time. This is expected to provide guidance to the implementing agencies for pollution abatement in River Ganga.

### References

- Jensen, J.R. (2007). *Remote Sensing of the Environment*, 2<sup>nd</sup> Edition, Pearson Prentice Hall.
- Karsaka et al, (2004). AVIRIS measurement of Chlorophyll a, suspended minerals, dissolved organic carbon and turbidity in Neuse River, Carolina, PE&RS, January 2004, pp 125-133.
- Mahtab A. Lodhi, Donald C. Rundquist, Luoheng Han, Mark S. Kuzila, (1997). The Potential for Remote Sensing of Loess Soils Suspended In Surface Waters, JAWRA, 33(1) 1997, pp 111–117.
- Olmanson et al, (2013). Airborne hyper spectral remote sensing to assess spatial distribution of water quality characteristics in large rivers: The Mississippi River and its tributaries in Minnesota, *Remote Sensing of Environment* 130 (2013), pp 254-265.
- Shafique et al (2003). Hyper spectral remote sensing of water quality parameters for large rivers in the Ohio River Basin. First Interagency Conference on Research in the Watersheds. Benson, Arizona, October 27–30, 2003. Washington, DC: USDA Agric. Res. Serv.

## Water Quality Studies in Chilika Lake

Vaibhav Garg, Vinay Kumar, Pankaj R. Dhote, S.P. Aggarwal and A. Senthil Kumar

Indian Institute of Remote Sensing, Dehradun, Uttarakhand, India

### **1. Scientific rationale and Objectives**

Remote sensing techniques had played important role in assessing quantity and quality of available water resources over recent decades. In this ever-increasing population, the availability of potable water is scares. The comprehensive sampling of a large waterbody for its quality study is usually considered as costly and time consuming. Remote sensing has been widely used for water quality assessment and a large number of documents have been published describing water quality monitoring using different multispectral sensor satellites. The spectral characteristics of the signal received from water are a function of hydrological, biological and chemical characteristics of water along with other interference factors. With the advent of new sensor technologies with improved spectral and spatial resolution namely 'hyperspectral remote sensing', there are great opportunities to assess and monitor water quality parameters. Therefore, it is essential to study spectral characteristics of water and pollutants from water quality monitoring and assessment point of view.

#### Objectives

- To collect and analyse number of water samples with regards to physical, chemical quality characteristics of water from different lakes/rivers.
- To generate spectral library of samples of different concentration of water quality parameter.
- Hyperspectral data (AVIRIS-NG & field spectroradiometer) processing and analyses with emphasis to water quality assessment and monitoring
- To generate spatio-temporal water quality maps.

## 2. Study area and data used

Chilika Lake, the largest coastal lagoon in India and the second largest lagoon in the world with width of 20 km and length of around 64 kms has been selected as study site. It is a brackish water lagoon, spread over the Puri, Khurda and Ganjam districts of Odisha state on the east coast of India, covering an area of over 1,100 km<sup>2</sup> as shown in figure 34.1.

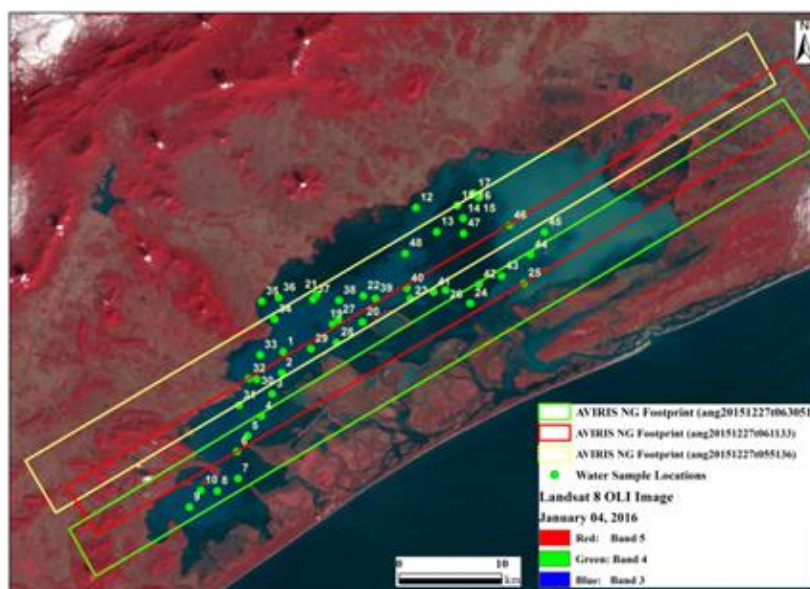


Figure 35.1. Chilika Lake as seen in Landsat 8 OLI Image along with location of sampling points and AVIRIS NG Footprints.

The frequent change in physico-chemical properties and their interaction with each other in Chilika Lake makes it a unique experimental site. In 1981, Chilika Lake was designated as the first Indian wetland of international importance under the Ramsar Convention. At the northern end, tributaries of the Mahanadi River, such as Daya, Nuna and Bhargavi join the lagoon and are responsible for the large fresh water and sediment flux to the lagoon. The lagoon is separated from the Bay of Bengal by sand bar of 60 km length. The water quality of the lagoon changes widely with onset of different seasons and exhibits different ecological characteristics in localized pockets. The Chilika Development Authority's (CDA) physico-chemical investigations indicate highly turbid water due to strong mixing of overlying water with sediments, the transparency values ranging between 8 and 117 cm. It has been also reported that the total sediment load discharged into the lagoon has increased from 1.8 M tones in 1998 to 2.94 M tones in 2001.

## AVIRIS NG Data Details

Under ISRO-NASA AVIRIS NG Airborne Hyperspectral Remote Sensing Flights Over India, the Site ID 100 was designated for Chilika Lagoon analysis. The details of each flight ID is given in table 35.1.

Table 35.1. AVIRIS-NG Imaging Schedule

Periods of imaging	Airport	Site ID	Site
24 <sup>th</sup> – 30 <sup>th</sup> Dec 15	Bhubaneswar	100 (Wetland)	Chilika lagoon

Table 35.2. Details of AVIRIS-NG Data Collected

S.No.	Site ID	Details of Radiance (L1) Data		
		Name	Date	Time (IST)
1.	100	ang20151227t055136_rdn	Dec. 27, 2015	1120 hrs
2.		ang20151227t061133_rdn		1140 hrs
3.		ang20151227t063051_rdn		1200 hrs
4.		ang20151227t085136_rdn		

The AVIRIS NG radiance data (L1) has been collected from National Remote Sensing Centre, Hyderabad for this site ID. Each dataset has 425 spectral bands ranging from 375-2500 nm wavelength with a high spatial resolution of 8 m. The flying height of the sensor was around 8 km above the ground. The details of each dataset acquired on December 27, 2015 are given in table 35.2 and their footprint are shown in figure 35.1.

### 3. Methodology

An attempt is made to map water quality of Chilika Lake using the methodology shown in Figure 35.2. Initially, turbidity has been analysed using spectral similarity approach. Turbidity is an important quality parameter of water from its optical property point of view. The change in light attenuation by water column may deteriorate aquatic life and primary productivity, as well as the growth of aquatic vegetation (Ritchie et al., 2003). It varies spatio-temporally over large waterbodies and its well distributed measurement on field is tedious and time consuming.

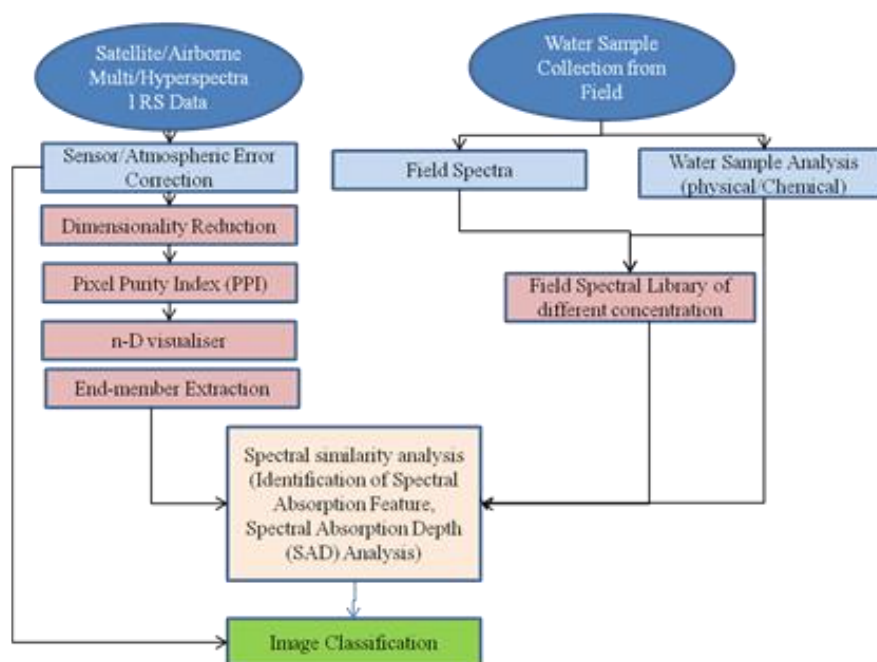


Figure 35.2. Flow chart of methodology adapted

A spectral library was generated on field for the different concentrations of turbidity using well calibrated instruments like field spectro-radiometer, turbidity meter and hand held global positioning system as shown in figure 35.3. The field spectra were classified into 7 classes of turbidity concentration as < 5, 5-10, 10-15, 15-25, 25-45, 45-100 and >100 NTU for analysis as shown in figure 35.4.

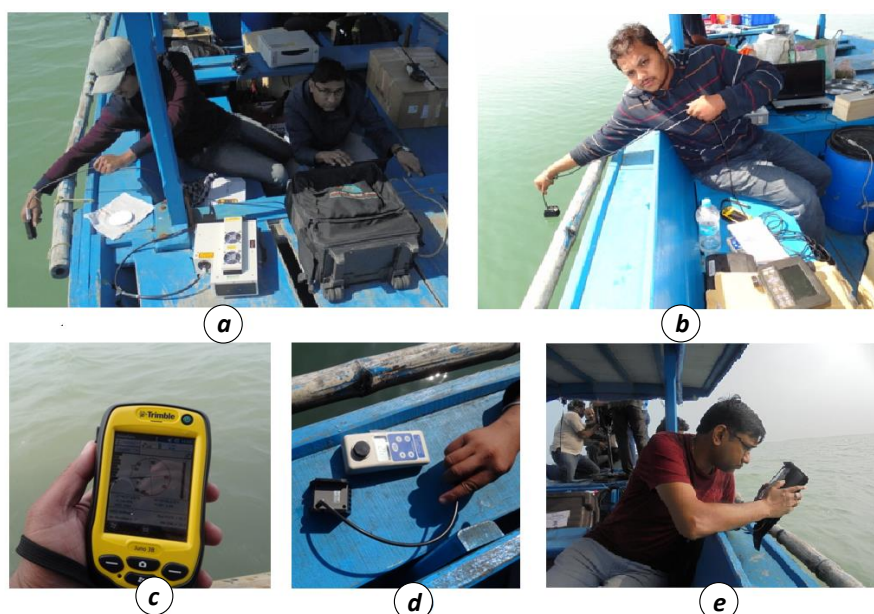


Figure 35.3. Instruments used to collect ground data, a) field spectro-radiometer, b) portable eco-sounder, c) hand held GPS, d) turbidity meter, e) sun-photometer.

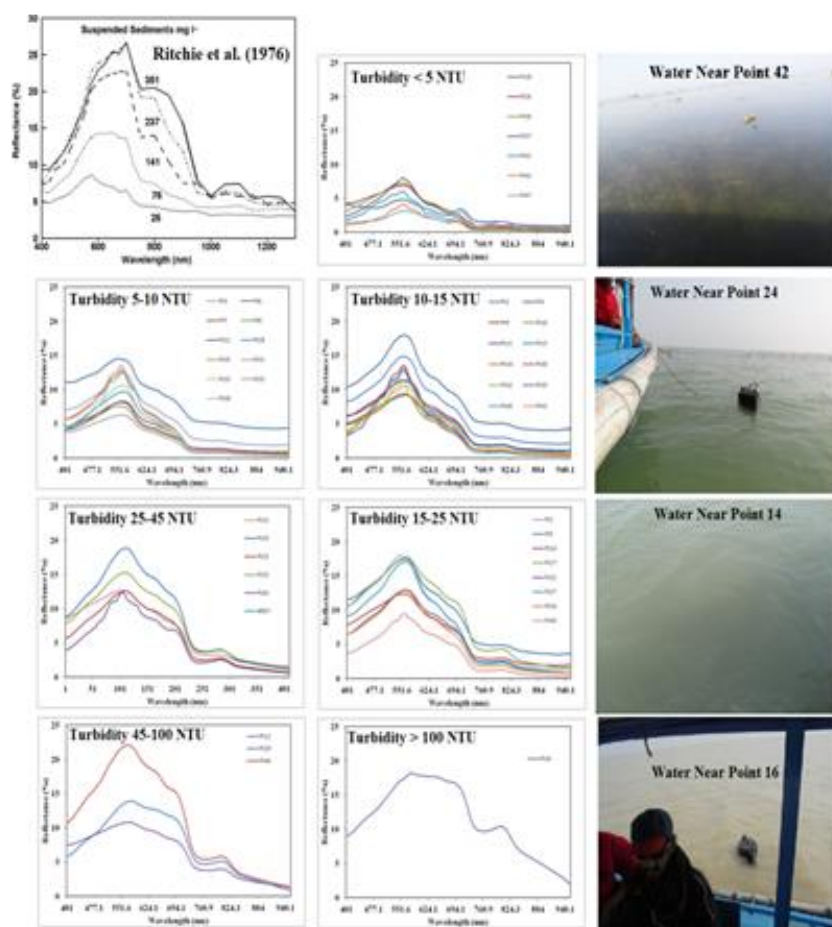


Figure 35.4. Field spectra of points fall in each turbidity concentration class and its comparison with Ritchie et al. (1976) spectra along with field photo of different water.

AVIRIS-NG image was initially pre-processed using spectral subset technique and bad bands and columns were eliminated. The values of bad columns have been replaced by average radiance value of adjacent two columns. As water is sensitive in the spectral wavelength range of 400 - 1000 nm, the bands with wavelength over 1000 nm were removed to obtain 116 bands image for further analysis. The image was further atmospherically corrected using Fast Line-of-sight Atmospheric Analysis of Hypercubes (FLAASH) which works on MODTRAN4 radiation transfer code.

In the SAM spectral similarity approach, entire spectral library of field collected spectra were matched with AVIRIS-NG image spectrum at each pixel and their spectral angle ' $\theta$ ' has been measured. Wherever, the least angle between two spectra has been measured, the turbidity class of that field spectrum has been assigned to that particular pixel. In this way, entire image has been classified according to their turbidity concentration.

## 4. Outcome

### 4.1 Salient findings

The SAM classification has been done on the reflectance image with the help of generated field spectral library using the spectral tools available in ENVI 5.0. The SAM classified image with respect to turbidity is shown in figure 35.5. After the classification, similarity of both the spectra (field and image) has been analysed at different locations. For similarity analysis, it requires continuum to be removed from both the reflectance spectra prior to analysis. Six random points representing each turbidity class were selected and their spectral similarity has been studied after removing the continuum as shown in figure 35.6.

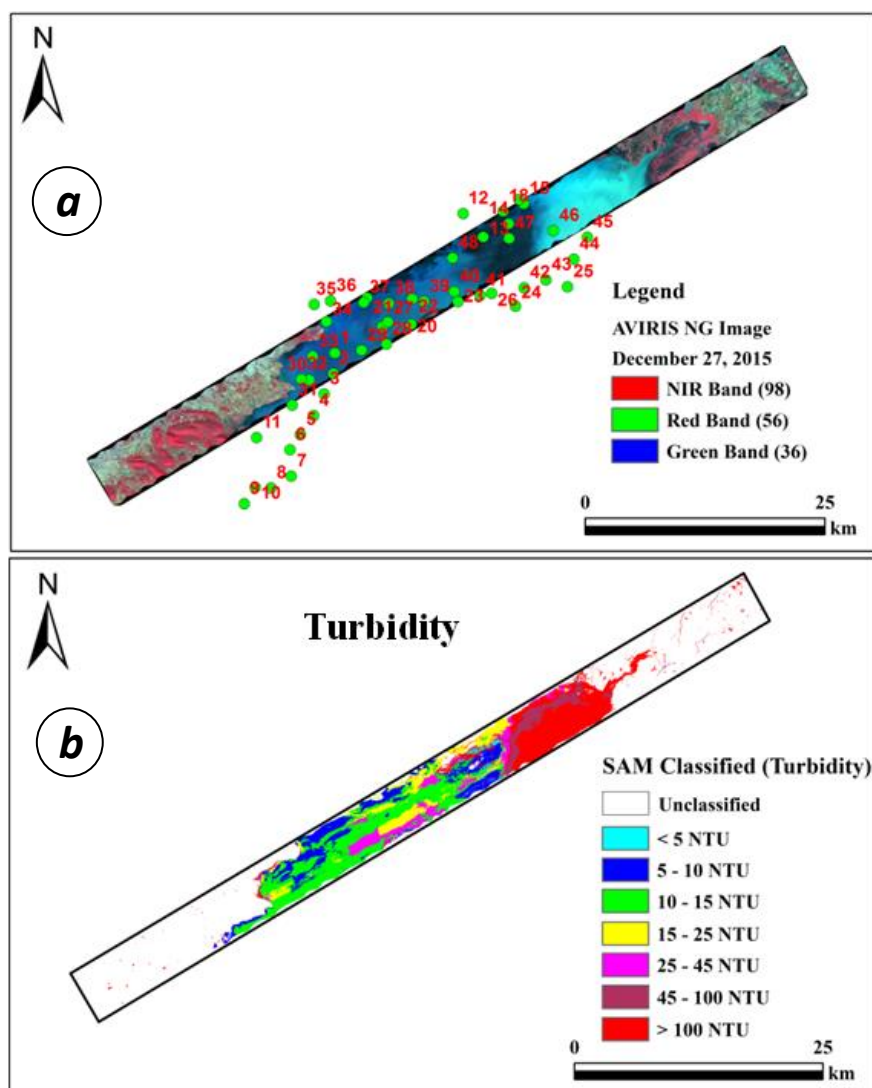


Figure 35.5. (a) FCC of AVIRIS-NG image of December 27, 2015 with location of sample collection sites (b) SAM classified image of the part of Chilika Lake.

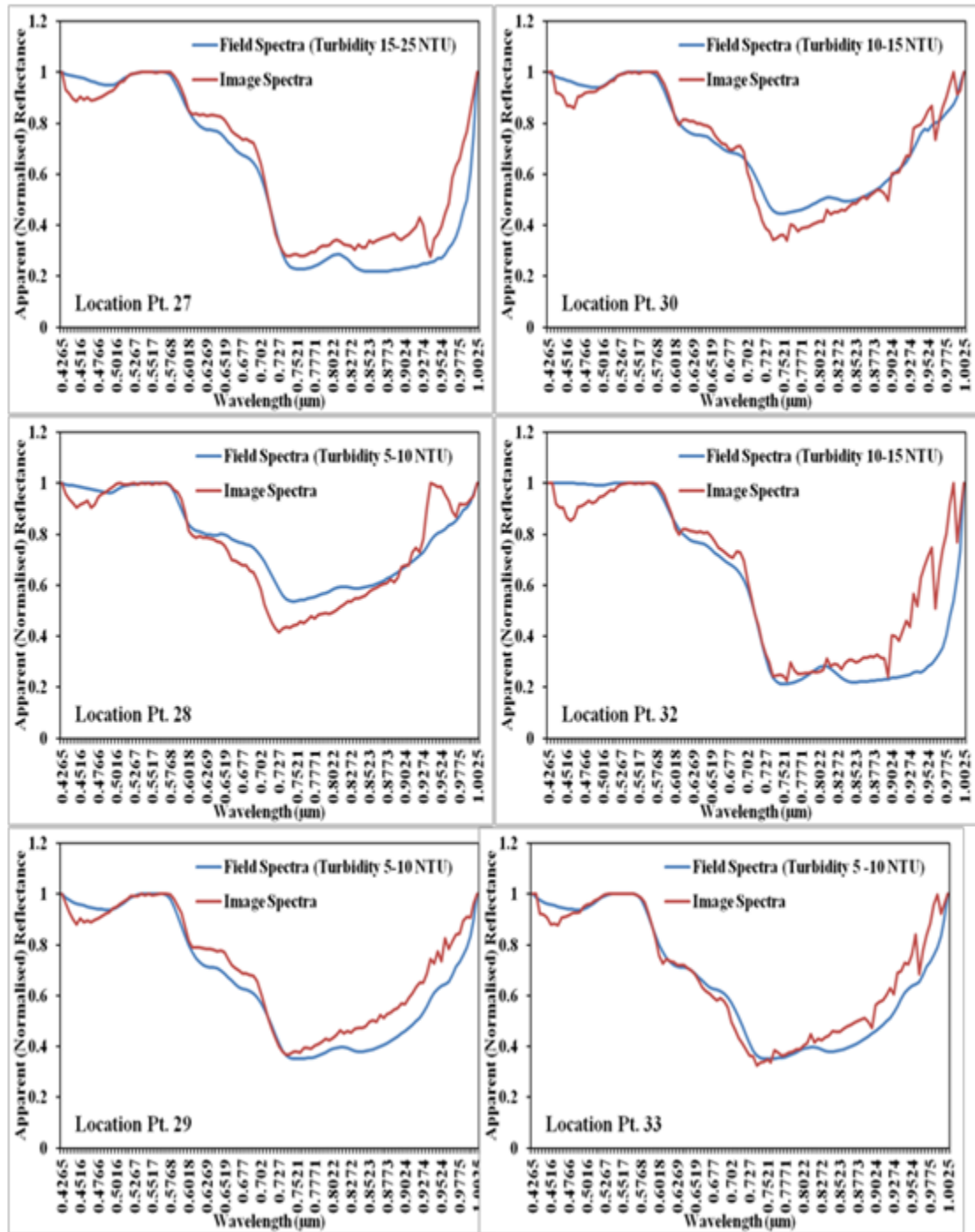


Figure 35.6. Field and AVIRIS-NG image spectra matching (continuum-removed spectra of selected locations for each class of turbidity)

The spectral similarity score of SAM spectral matching approach close to value of 1 indicates the closest match and higher confidence in the spectral similarity. At each location, the spectral similarity score found to be more than 0.9, which indicates better matching of two spectra (field and image).

## 4.2 Target vs. Achievement

Target	Achievement	Remarks
Turbidity Mapping	90%	-
TSM Mapping	75 %	-
Chl Mapping	0%	Based on sharing of underwater spectroradiometer data by SAC, Ahmadabad.
CDOM	0%	Based on sharing of underwater spectroradiometer and lab analysis data by SAC, Ahmadabad/Gujarat University.

## 4.3 Linkage to societal benefits

Chilika Lake, the highly productive ecosystem with its rich fishery resources sustains the livelihood of around 1.5 million fishermen who live in 132 villages on the shore and islands in the Lagoon (Ramesh et al., 2011). To conserve the high productivity of the lake, water quality studies are important.

## 5. Conclusions

The water quality of Chilika Lake with regard to turbidity concentration has been studied using spectral similarity approach. A spectral library, specific to Chilika Lake water quality parameters, has been generated using sophisticated instruments like field spectroradiometer, turbidity meter and hand held GPS. The field spectral library has been resampled to AVIRIS NG bandwidth and used for spectral similarity analysis adapting most widely used SAM approach. A very high similarity between the image spectrum and field spectrum was found at almost each pixel. At the selected locations the SAM similarity score was usually higher than 0.9. As, the field spectra were classified into 7 classes of turbidity concentration as < 5, 5-10, 10-15, 15-25, 25-45, 45-100 and >100 NTU, SAM classified image resulted in these 7 classes of turbidity in the selected region of the lake. The SAM classification results were quantitative in nature. Moreover, the observed turbidity concentration at different locations are well in the range of SAM classified results. The study shows usefulness of spectral library for water quality parameters and spectral similarity approach in water quality studies using imaging spectroscopy.

As the present study is an initial attempt in the direction of spectral library for water quality parameters and its application in spectral similarity analysis, a large number of recommendation needs to be followed in future research studies. The spectral library may further be improved by collecting field spectra in the different season with different

conditions. The satellite image of same date of field campaign may improve the classification accuracy. The water quality assessment is a global issue, therefore, there is a need to set the protocols to develop standard spectral library with regards to water quality parameters and their concentrations. In this way, the water quality of any region on this globe can be assessed easily through geospatial technique.

### **Acknowledgements**

The authors would like to thank the authorities of ISRO for providing financial grant for this research work. Authors would also like to extend their gratitude to Dr. Ajit Pattnaik, Chief Executive, CDA for the encouragement and permission for the collaborative study. Thanks are also due to Dr. R.N. Samal, Dr. Gurdip Rastogi, Dr. P.R. Muduli and other research staffs of CDA especially Mr. Bitu Mohanty and Mr. Abhijeet Das. They extend their gratitude to SAC, Ahmadabad team for their support during field work.

### **References**

Ritchie, J.C., Zimba, P.V., Everitt, J.H., 2003. Remote Sensing Techniques to Assess Water Quality. Photogramm. Eng. Remote Sens. 69, 695-704.

# Assessment of Water Quality by inversion of bio-optical models in inland waters using AVIRIS-NG Hyperspectral Data

Shard Chander and Ashwin Gujrati

Land Hydrology Division, GHCAG/EPISA,  
Space Applications Centre, ISRO, Ahmedabad, Gujarat, India

## ***1. Scientific rationale and Objectives***

Water quality of inland water bodies degrades due to lack of dissolved oxygen and Hazardous Algae Blooms (HAB) blooms (high Chlorophyll a concentrations). The in-situ measurements of water quality are often very scarce because of large areas to monitor. Furthermore, these measurements do not represent the actual water quality at a large scale since measurements are restricted to region specific. Consequently, one may consider measurement techniques so as to get relevant information especially at large scales and to be able to characterize water quality over a whole region.

In this context, remote sensing from space is a perfect tool to get the required information. Satellite data may be able to provide a greater amount of spatial information at an improved cost compared to spot sample grabs. The information contained in remote sensing imagery can be used to accurately quantify water quality constituents, such as fine sediment concentration (Lee and Carder 2002, Mobley et al. 2005, Albert and Gege 2006). Apparent upwelling irradiance (what the sensors effectively measure), is a function of atmospheric properties and solar inputs, as well as the upwelling irradiance at the surface (a function itself of the reflection off the bottom and constituents in the water column), and the reflection off the water surface due to both direct sunlight and diffuse skylight (Gege 2004). The potentiality of remote sensing imagery and its synergy with both local in-situ water quality measurements and radiative transfer modelling has been studied to measure the water quality parameters. Hyperspectral dataset can be used to assess physical parameters such as bathymetry and biophysical parameters such as chlorophyll, dissolved organic matter and suspended particulate matter.

The objectives of the study are:

- Develop an algorithm for deriving fine sediment, chlorophyll, and CDOM concentration for the inland water bodies from remote sensing imagery.
- Develop bio-optical model that can simulate remote sensing reflectance of water for given inputs of different aquatic optical properties.
- Provide water quality maps that can be used as a valuable information for hot-spot pollution identification.
- Derive bottom depth information by removing the effect of water column through simultaneous inversion of remote sensing reflectance.

## 2. Study area and data used

The study area comprises of Ganga River, Buxar (Site ID 150, dated February 23, 2016) and Chilika Lagoon (Site ID 54,100,92,110 dated December 27-28, 2015).

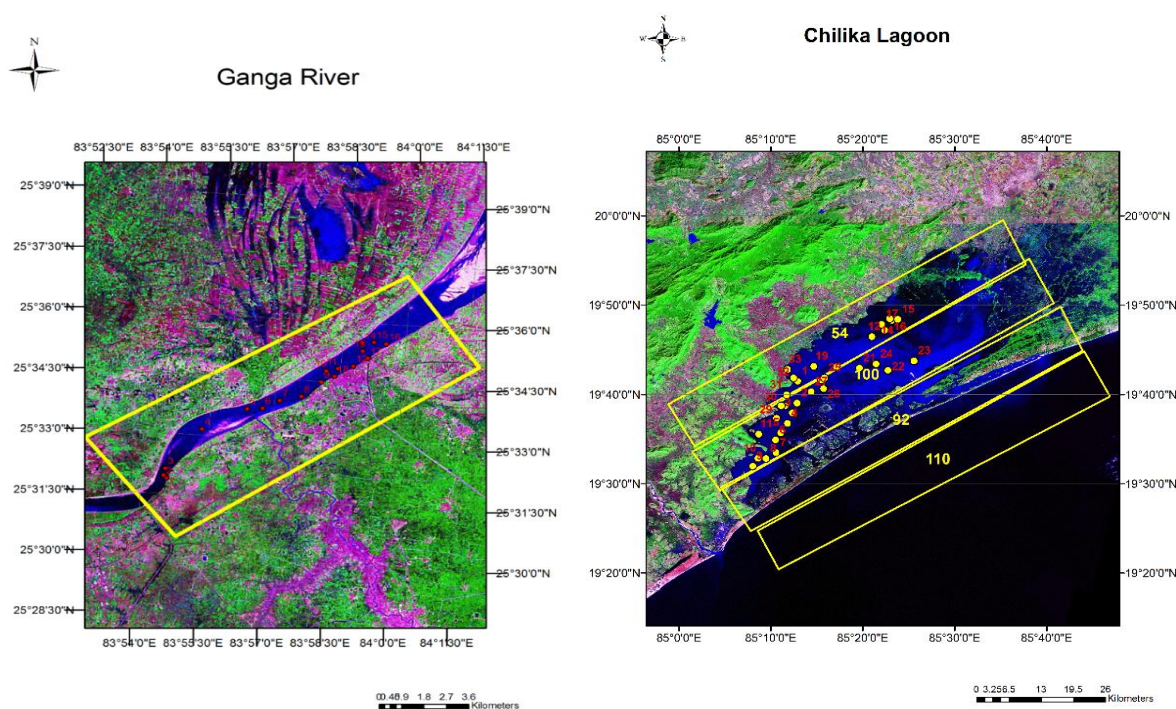


Figure 36.1. Study Area along with AVIRIS strips & locations of in-situ sampling

Data used: AVIRIS-NG data (JPL L2 product) along with in situ hyperspectral data collected with Satlantic radiometer & HR1024 spectrometer have been used for this study. Yellow strip in figure 36.1 shows the extent of AVIRIS acquired radiances, and Red dots show the location

of stations where reflectance spectra were measured. Water sample were also collected at stations for laboratory analysis.

### 3. Methodology

There are two primary methods to estimate water quality parameters. The first uses empirical models that develop statistical relations between measured field data and image data (Brando and Dekker 2003). The second approach uses physical modeling of light through the atmosphere, water column, surface and bottom to simultaneously obtain water backscatter and absorption coefficient, bottom depth, and bottom reflectance. We have investigated both empirical and model-driven methods to map fine sediment, chlorophyll, and CDOM concentrations. The methodology flow chart is shown in figure 36.2.

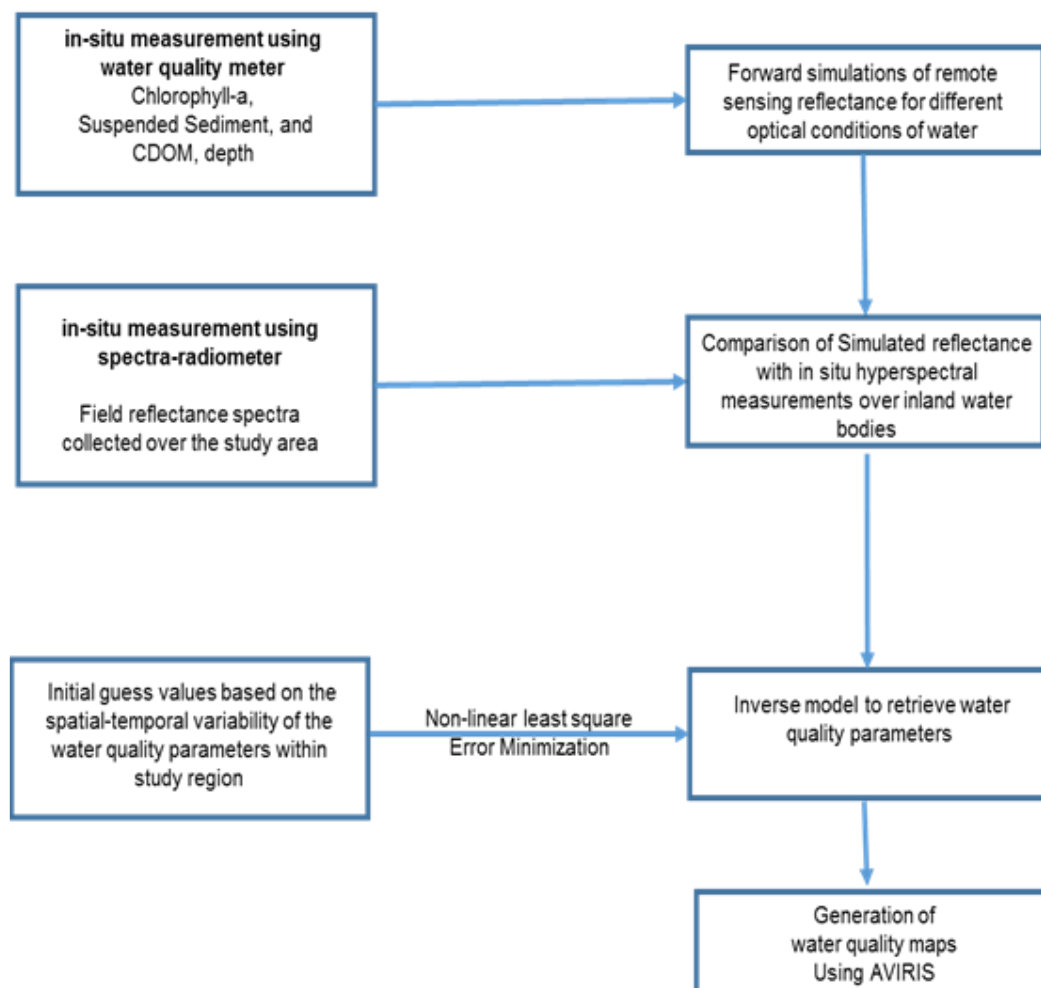


Figure 36.2. Flow chart of the methodology

## 4. Outcome

### 4.1 Salient findings

Remote Sensing reflectance was divided into optically deep water contribution and contribution of bottom type from finite depth. Forward simulations were carried out to simulate the remote sensing reflectance for all possible combinations of water quality parameter (chlorophyll, CDOM, suspended sediments) and for various depth (optically deep, 0.1m, 1m, 5m). Figure 36.3 shows one such example where remote sensing reflectance was simulated for varying chlorophyll concentrations ( $0.4 \text{ mg/m}^3$  to  $5 \text{ mg/m}^3$ ). In this case all other water optical constituents were assuming to be co-vary with the chlorophyll concentration.

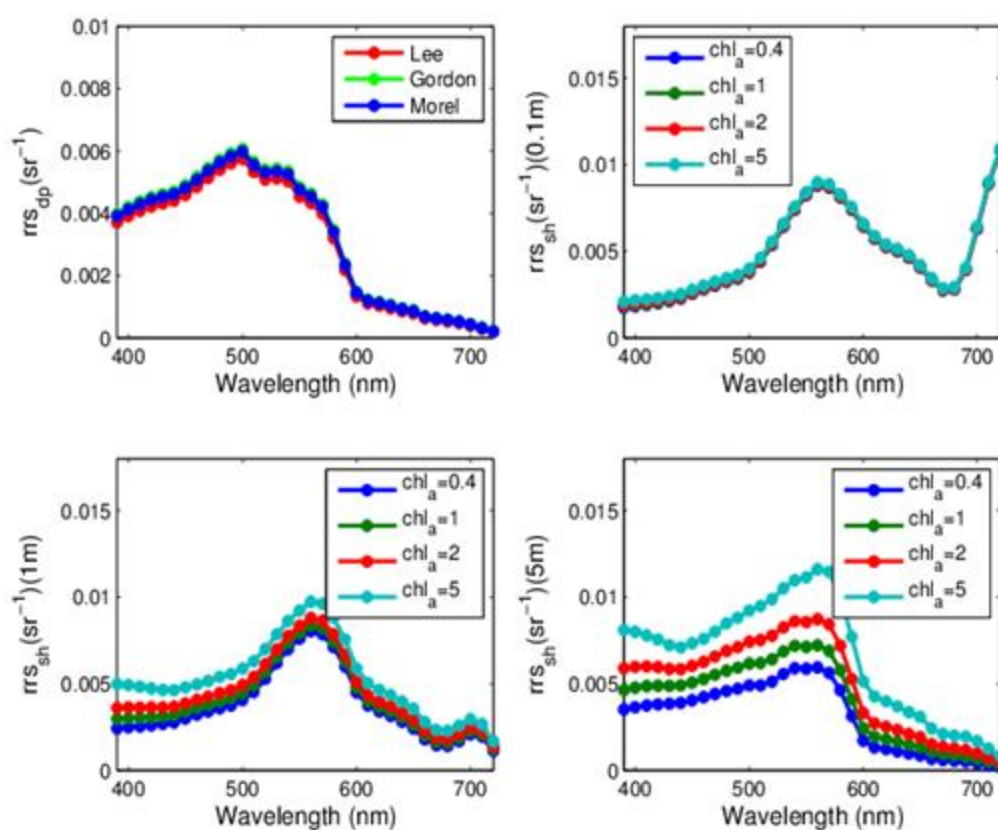


Figure 36.3. Simulated RS reflectance for varying water optical properties and various depth.

Figure 36.4 shows the results of water quality map generated using AVIRIS scene over the Ganga River, Buxar. The retrieved chlorophyll values were found to be  $20\text{-}40 \text{ mg/m}^3$  and suspended sediments were found to be in the range  $0\text{-}20 \text{ g/m}^3$ . It can be clearly inferring that

some of the sewerage drainage are entering into the main stream that cause a drastic rise in the water turbidity.

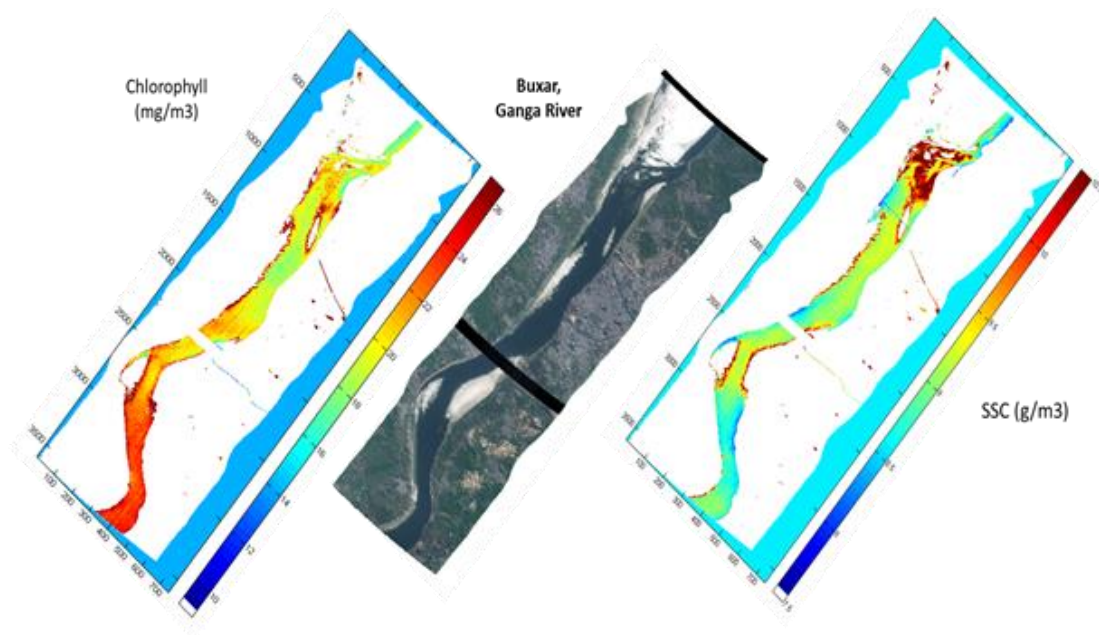


Figure 36.4. Water quality maps over Ganga River, Buxar

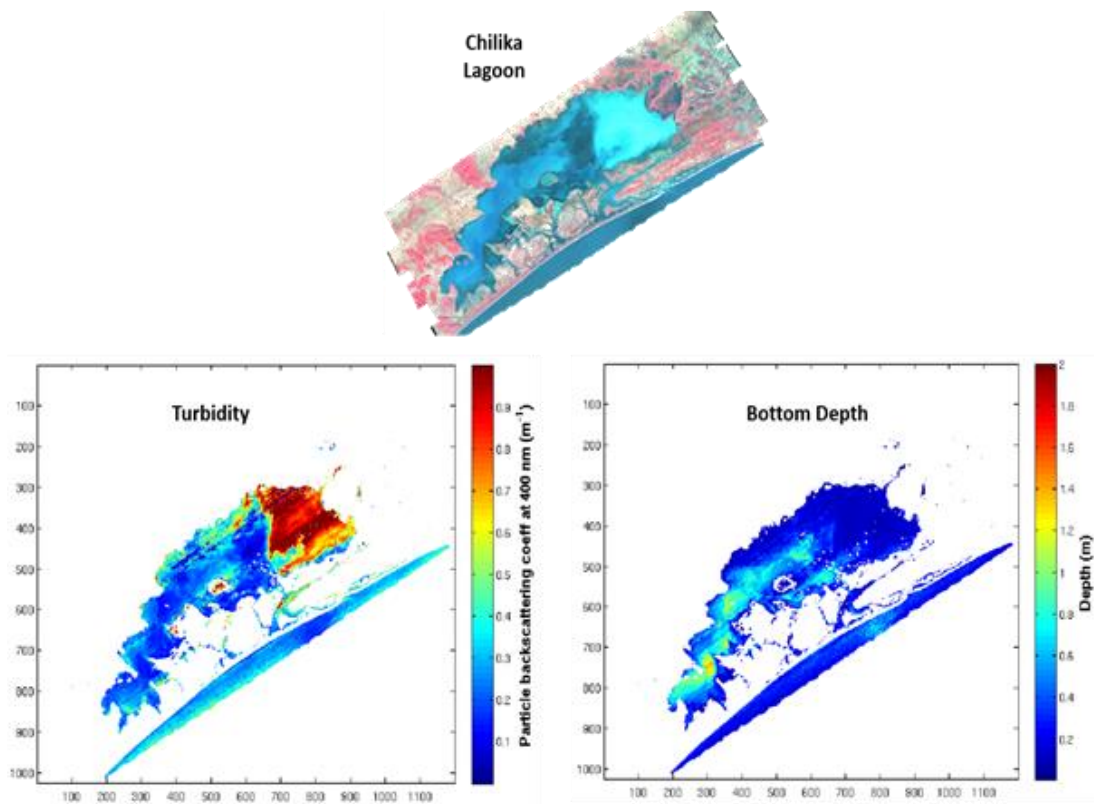


Figure 36.5. Turbidity and bathymetry maps over Chilika Lagoon

Figure 36.5 shows the result obtained over Chilika lagoon of turbidity and bottom depth using AVIRIS scenes. Water was found to be more turbid in the northern sector that may be due to the river input and resuspension from shallow bathymetry. The overall variability in the depth in the north sector (0.1 m) and southern sector (2.6 m) was found to be matched with the literature values. Retrieved bottom depth was validated with the in-situ echo sounder measured bottom depth and found to be matched with R2 0.80 and RMSE of 0.67 m.

### **4.3 Linkage to societal benefits**

The study will be used to generate water quality maps over inland water bodies, especially over the Ganga river basin. The hot-spots of point source pollution due to sewerage discharges from drainage can also be identified using hyperspectral meter level spatial resolution imagery. This will provide very useful information to pollution control agencies for finding out potential location of water quality contamination.

## **5. Conclusions**

Semi analytical based algorithms were implemented to generate water quality maps from AVIRIS-NG images of Chilika Lagoon, and Ganga river. The algorithms consist of inversion of remote sensing reflectance using bio-optical modelling without using any ground truth dataset. Results were validated with the echo sounder measured depth. More ground-truth dataset is required to further strengthen the study and develop global inland water quality retrieval algorithms.

## **Acknowledgements**

We express our sincere gratitude to Shri Tapan Misra, Director and Dr Raj Kumar, Deputy Director EPSA for providing overall support. The guidance and encouragement received from Dr. R. P. Singh, Head, LHD are acknowledged with thanks. We also extend our gratitude to Dr Arvind Sahay for facilitating in collecting the radiometer dataset and NRSC & IIRS team for their support during field work.

## References

Albert, A. and Gege, P., 2006, "Inversion of irradiances and remote sensing reflectances in shallow water between 400 and 800 nm for calculation of water and bottom properties". *Applied Optics*, 45 (10):2331-2343.

Brando et al., 2009, "A physics based retrieval and quality assessment of bathymetry from suboptimal hyperspectral data", *Remote Sensing of Environment*, 113: 755-770.

Gege, P., 2004, "The water color simulator WASI: An integrating software tool for analysis and simulation of in-situ spectra". *Computer & Geosciences*, 30:523-532.

Lee et al., 2002, "Derived Inherent optical properties from water color: a multiband quasi-analytical algorithm for optically deep waters". *Applied Optics*, 41(27): 5755-5772.

Mobley, C. D., L. K. Sundman, C. O. Davis, J. H. Bowles, T. V. Downes, R. A. Leathers, M. J. Montes, W. P. Bissett, D. D. R. Kohler, R. P. Reid, E. M. Louchard, and A. Gleason. 2005. Interpretation of hyperspectral remote-sensing imagery by spectrum matching and look-up tables. *Appl. Opt.* 44:3576-3592.



**Land Use Land Cover and  
Urban Applications**

### Summary

Finer level land use land cover classes are essential, especially to formulate urban policies in terms of flood risk management, drainage network, waste management, heat action plans, roof-top solar etc. The imaging hyperspectral data from AVIRIS-NG were found to generate greater number of land use classes as compared to multi-spectral imaging data of LISS-IV equivalent resolution as exemplified over Mangalore, Karnataka. Visual observations have shown that AVIRIS NG data gave an improved classified map as compared to LISS IV data. The LISS-IV Classified map had much confusion within the considered 15 classes - burnt area and river water, costal sand and roads, fallow land and scrub land etc. Coastal sand delineation was observed to be accurate in AVIRIS classified map. It can be depicted that urban features like roads, buildings and scrubland and fallowland were well extracted from AVIRIS-NG data as compared to LISS IV data. A spectral library for different roof-top materials, pervious and impervious surfaces has been built using the ground-based data collection with spectroradiometer over cities of Ahmedabad, Gujarat and Gulbarga, Karnataka. The fraction of impervious surfaces could be identified using the spectra in the VNIR region based on high and low albedo while different major roof types such as Concrete, China Mosaic and Metallic surfaces could be identified using spectral differences in VNIR and SWIR band regions. Hyperion data were also utilized for Ahmedabad city to discriminate concrete, tar, soil where accuracy was found be the highest for concrete detection.

# AVIRIS - NG Data Utilization for Land Use/ Land Cover Applications

V. Satya Sahithi, Mohit Modi, Rajiv Kumar and G. Ravi Shankar

Land Use and Cover Monitoring Division,  
National Remote Sensing Centre, ISRO, Hyderabad, India

## ***1. Scientific rationale and Objectives***

Although land use land cover is a vast and generalized field for Hyperspectral data utilization, a step forward was made for utilizing the AVIRIS - NG data to examine the uniqueness of HS data over the multispectral data in identifying various LULC classes. The spectral information available from broadband optical datasets is barely enough to distinguish certain closely resembling classes like plantation and tree clad areas, riverine sand and urban structures, salt affected land and dry sand, grass lands and croplands, scrub land and fallow land etc. Discerning these classes require an image with high spectral, spatial and radiometric resolutions. The current study was taken up to identify the significance of airborne AVIRIS - NG hyperspectral data with respect to multispectral data (of high spatial and radiometric resolution) in extraction of LULC classes. The high dimensionality/huge volume of the HS data cause redundancy in the information and bear a limitation in terms of high processing time and storage. Hence, identifying the optimum wavelength regions for various LULC classes attains significance in terms of reducing the processing time during the course of the current study for individual land cover features.

### **a. Short term goals**

- Pre - processing of data: atmospheric & geometric corrections, dimensionality reduction
- Comparison of FLAASH reflectance, ATREM reflectance (JPL reflectance), and instrument reflectance spectra.
- Understanding the distinctiveness of hyperspectral data over high resolution multispectral data for LULC applications.
- Field spectra collection for various LULC classes using ASD spectro radiometer.
- LULC classification based on image and field spectra. Discussing the merits and demerits.

## b. Long term goals

- Optimum band or wavelength region for LULC classes.
- Spectral library development for various LULC classes of the considered study area.

## 2. Study area and data used

The study area constitutes a part of coastal region of Mangalore, Karnataka, India (Acquisition number-ang20151231t074114). The data was acquired on December 30, 2015 at 7.50 AM. It is a mixed built up region with various land use and cover features. The important LULC features in the area include - different urban roof tops, crop land, fallow, agriculture plantation (mango, banana, coconut, palm), water bodies (river, sea), coastal sand, mangroves etc. The LISS IV multispectral data for the same area and same time was also used for a comparative analysis. ASD field spectro radiometer was used for ground data collection.

## 3. Methodology

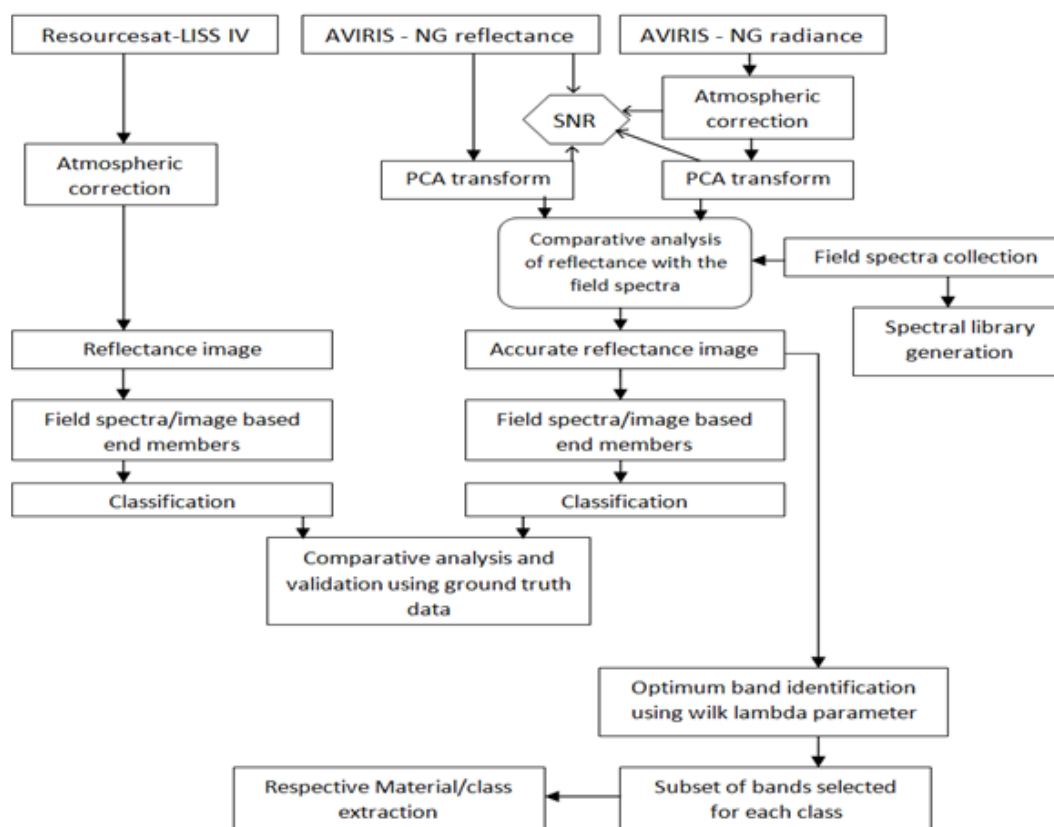


Figure 37.1. Flow chart of the methodology

## 4. Outcome

### 4.1 Salient findings

#### a. Comparison of reflectance from FLAASH, ATREM, ASD spectroradiometer.

During the ground data collection, spectra of various LULC categories like built up, agriculture, vegetation, waste lands etc were picked up. Comparison of Ground, ATREM derived and FLAASH derived reflectances of various LULC features (mango being a semi evergreen species, it shown taken as an example) have shown that, FLAASH derived spectra has comparatively better correlation than the ATREM derived spectra. The noise/no data regions between 1300-1400nm and 1800-1950nm remained the same in all three profiles.

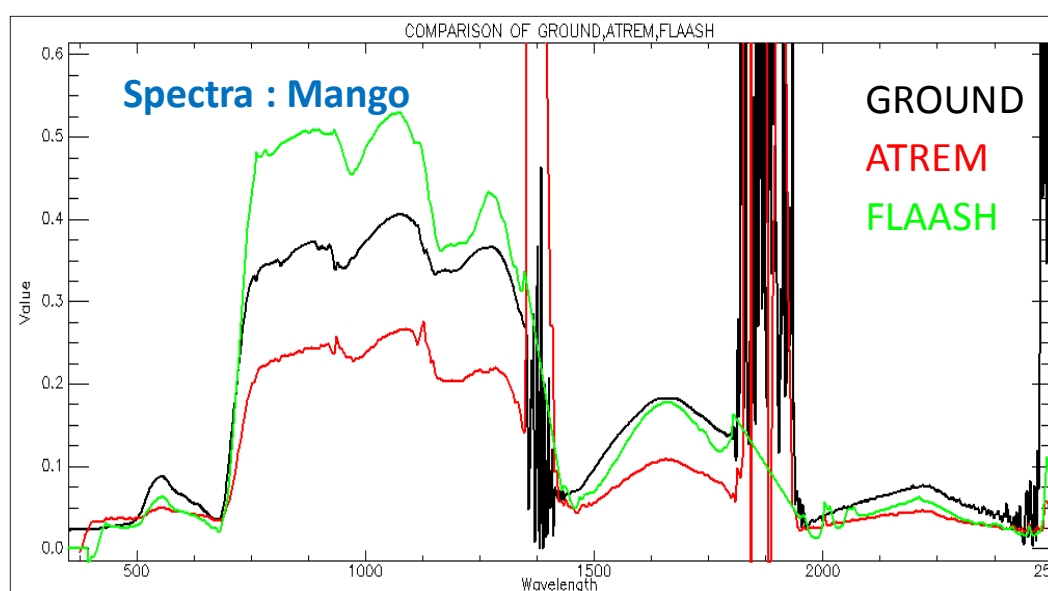


Figure 37.2. Comparison of ground, ATREM and FLAASH

#### b. Some observations between reflectance images from FLAASH and ATREM (L-2)

Out of the 425 bands of L-2 data 75 bands were observed to be noisy leading to poor SNR ratio and classification results. As can be seen from the table, a negative SNR was noted (due to -ve mean values) for ATREM data of considered site. The FLAASH corrected reflectance image gave good SNR of 1.1097. It was observed that the SNR of the PCA transformed image has reduced from 1.109728 to 0.494252. Hence the same FLAASH corrected image (without PCA transformation) was used for further processing. The SNR of LISS IV was observed to be 2.6044 due to its high radiometric resolution.

<i>Parameter</i>	<i>JPL_ATREM reflectance data</i>	<i>FLAASH reflectance data</i>
Total number of bands	425(processed)/432(radiance)	387/432
Number of noisy/no data bands observed	75 noisy bands (in L-2 image)	45 no data bands
Missing/noisy wave length regions	0.3466-0.3763, 1.3481-1.478, 1.7938-1.9842, 2.465-2.500 $\mu\text{m}$	0.3466-0.3917, 1.3534-1.4235, 1.8092-1.9444, 2.5054 $\mu\text{m}$
PCA result	Not successful/noisy results obtained	Good results obtained (but with low SNR-0.494)
SNR (avg mean/ avg std. dev)	-3.32664	1.109728

### c. Classification of AVIRIS and LISS IV images

15 different end member spectra (a combination of ground and image derived) were used for classifying the LISS IV and AVIRIS - NG images. Spectral Angle Mapper classifier with an angle of 0.35 for AVIRIS and 0.4 for LISS IV were used. Classification results showcased the importance of spectral resolution in delineating the closely resembling classes. The classes riverine water and burnt area, two mangrove types and vegetation, fallow lands and scrub land, fallow and concrete were confused in LISS IV classified image while a clear distinction between these classes was evident in the AVIRIS classified map.

- Visual observations have shown that AVIRIS NG data gave an improved classified map compared to LISS IV data. The LISS-IV Classified map had much confusion within the considered 15 classes - burnt area and river water, coastal sand and roads, fallow land and scrub land etc.
- Coastal sand delineation is observed to be accurate in AVIRIS classified map (figure 37.3 (1)).
- It can be depicted from figure 37.3 (2) that urban features like roads, buildings and scrub land and fallow land were well extracted from AVIRIS-NG data as compared to LISS IV data.
- Figure 37.3 (3) indicates the confusion in river and burnt area classes and wetland and vegetation classes in LISS IV map which is absent in AVIRIS – NG classified map.

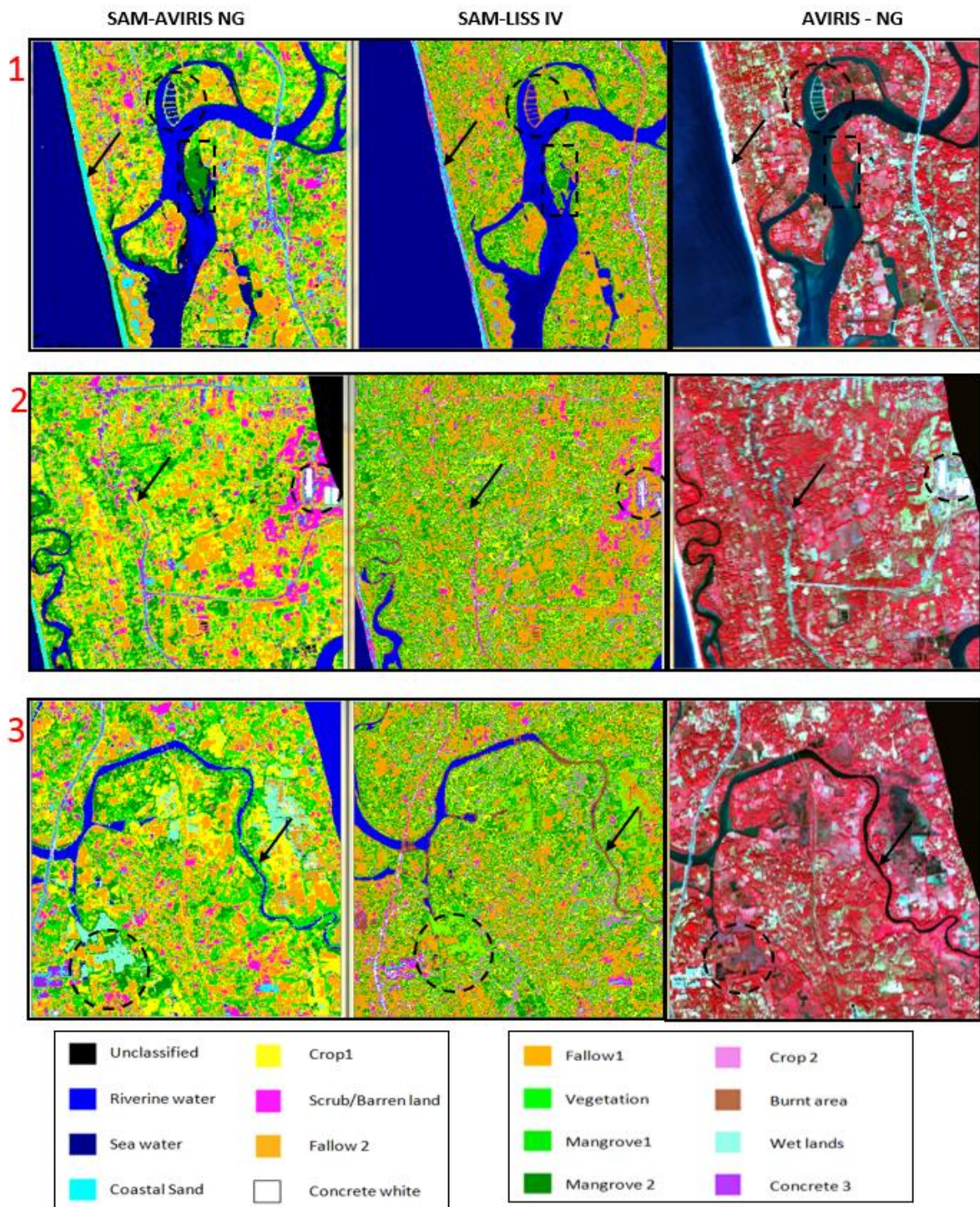


Figure 37.3. Classified land use map

## 4.2 Target vs. Achievement

S.No	Activity	Nov	Dec	Jan	Feb	Mar	Apr	May	Jun	Jul	
		2016			2017						
1.	Gathering the datasets	Completed									
2.	Subsetting and pre-processing		Completed	Completed							
3.	Field work - Ground spectra collection					50%					
4.	End member spectra collection				Completed						
5.	Classification						70%				
6.	Accuracy Assessment and comparative analysis						50%				
7.	Spectral library generation							40%			
7.	Optimum band identification								10%		
8.	Extraction of classes from the identified bands- validation								Future targets		

■ Completed  
■ In progress  
■ Future targets

## 4.3 Linkage to societal benefits

As stated earlier, there are certain confusing LULC classes that are difficult to be distinguished using the broad band multispectral images. High resolution hyperspectral datasets can be highly beneficial in extracting the LULC classes with less confusion (thus reducing the manual efforts as well). Identifying the optimum bands for LULC classes can help in reducing the redundancy and minimize the number of bands to be processed for feature extraction (in case of specific applications).

## 5. Conclusions

- The airborne AVIRIS - NG data is found to have enough utility in improved extraction of LULC classes as compared to the high resolution multispectral data.
- Many LULC classes found to be confusing in the LISS IV data were well distinguished in AVIRIS - NG data.
- Optimum band identification can help in reducing the processing time and redundancy of information and is yet to be explored.

## Acknowledgements

We would like to thank GD LRUMG, DD RSA and Director, NRSC for the constant support, guidance and encouragement for taking up this study.

## References

Kruse, F. A. "Comparison of ATREM, ACORN, and FLAASH atmospheric corrections using low-altitude AVIRIS data of Boulder, CO." Summaries of 13th JPL Airborne Geoscience Workshop, Jet Propulsion Lab, Pasadena, CA. 2004.

George Rajee, HitendraPadalia, and S. P. S. Kushwaha. "Forest tree species discrimination in western Himalaya using EO-1 Hyperion." *International Journal of Applied Earth Observation and Geoinformation* 28 (2014): 140-149.

# Hyper-spectral Remote Sensing of Urban and Peri-Urban Areas

Gaurav V. Jain and Shashikant Sharma

Space Applications Centre, ISRO, Ahmedabad, Gujarat, India

## ***1. Scientific rationale and Objectives***

Urban land cover is characterized by heterogeneous mix of both anthropogenic and naturally occurring materials. Hyper-spectral imaging enables detection of narrow band absorption features that aid in separation of different material classes. Harold et al. (2004) examined the spectral profiles of typical land cover types and materials found in urban areas. Weng et al. (2007) demonstrated application of EO-1 ALI imagery and Hyperion imagery in extraction of impervious surfaces such as roads, building roofs, side walk and parking lots, in Indiana (USA). Sugumaran et al. (2007) attempted extraction of transportation infrastructure using 4.0 m, 380-2500 nm AVIRIS data in Shelton Nebraska and concluded that while quarry, highway, brick road, railroad, roof tops and fitness tracks can be separated with high accuracy, city streets and concrete streets give low accuracy. Harold and Roberts (2010) utilized high-resolution AVIRIS data in extracting red tile roofs, wood shingle roofs and asphalt roads. It is therefore evident that hyper-spectral data offers several advantages in urban land cover classification. While most of the studies are carried out in developed world, the application of hyper-spectral data in densely populated, unplanned cities of India dominated by slums and shanties with stressed housing conditions, narrow streets, and haphazard development, poses several challenges. This study therefore attempts to analyze hyperspectral images in cities and their peripheral urban zones, while attempting to characterize roof-types and land cover types in cities. Roof-type classification on the basis of materials has significant potential in terms of assessment of disaster risk and socio-economic studies linked with housing stress condition. Hyper-spectral data can be used for detailed classification of pervious and impervious surfaces which may be useful for storm water runoff modeling, landscape fragmentation analysis, urban planning and urban heat island studies. Following are the major objectives of this study:

- To characterize urban land cover material composition and building roof types using air-borne hyper-spectral data.
- To estimate pervious and impervious land cover types in urban areas using air-borne hyper-spectral images in conjunction with very high spatial resolution satellite images.

## 2. Study area and data used

The study area covers part of Ahmedabad city that includes the densely populated inner city, eastern Ahmedabad (predominance of industrial sheds), western Ahmedabad (relatively newer residential and commercial establishments), rural settlements and slums. H-series tables published by Census of India (2011) show that 72.9% of buildings in Ahmedabad city have concrete roof, whereas 21.9% of the buildings roofs comprise G.I., Metal or Asbestos sheets. Figure 38.1 shows the extent of study area covered in Ahmedabad city. The natural color composite overlaid on the false color composite is the mosaic of all three scenes acquired by AVIRIS-NG sensor over Ahmedabad city and the yellow line indicates the proposed study area boundary.

Table 38.1. List of Data Used

<b>Sr. No.</b>	<b>Data Product</b>	<b>Date</b>	<b>Time (IST)</b>	<b>Spatial Resolution</b>	<b>Image Dimensions</b>	<b>No. of Bands</b>
1	Level-1	11-Feb-2016	13:20:04	8.0 m	826 x 4151	425 (0.3764 to 2.5001)
2	Level-1	11-Feb-2016	13:31:29	8.0 m	839 x 4152	
3	Level-1	14-Feb-2016	10:40:14	8.0 m	792 x 4110	

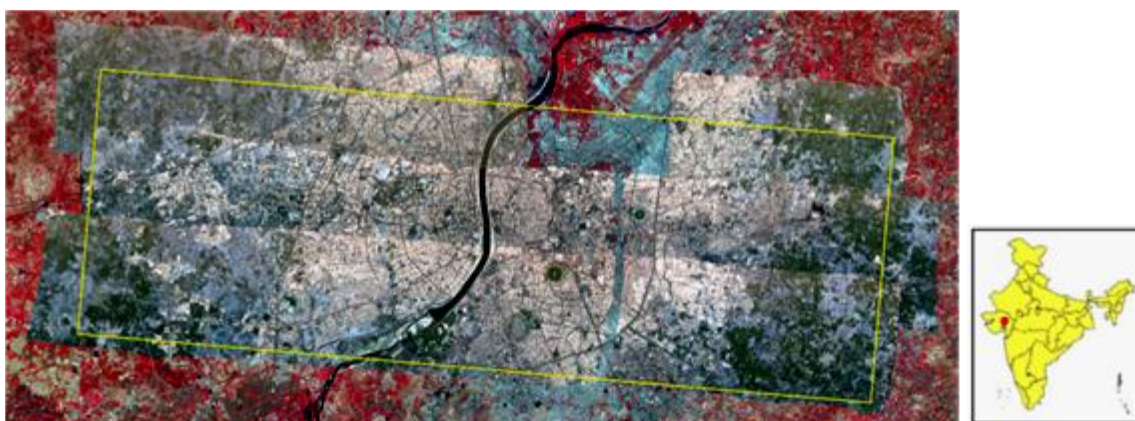


Figure 38.1. Study Area - Part of Ahmedabad city

### ***3. Methodology***

The in-situ measurements of spectral profile of several urban materials were collected in Kalaburgi city during December 7, 2015 to December 10, 2015 (4 days). The ground campaign for Ahmedabad city in Gujarat was carried out during February 8, 2016 to February 12, 2016 (5 days). HR-1024 spectro-radiometer was used to collect field spectral profiles at different types of materials observed in urban areas, including building roofs, roads, parks and playgrounds, water bodies, etc.

The Level-1 data with calibrated radiance values was used in this study. The data was first corrected for atmospheric attenuations using ENVI's FLAASH module. The reflectance thus obtained were compared with the field spectra at selected locations along with the reflectance image (Level-2 product) provided by NASA-JPL. The Minimum Noise Fraction (MNF) transformation approach was used to reduce the dimensionality of the AVIRIS data and simplify further processing. The Linear Spectral Mixture Analysis was applied to estimate the proportion of pervious and impervious surfaces in each pixel. Initially, four major end members, viz. vegetation, soil, impervious surface with high albedo, and low albedo impervious surface were considered for LSMA. However, as the urban area has more heterogeneity and complexity in terms of material composition and geometric structure, ten different materials for which end members could be obtained from the image comparable to field spectral profiles, were considered. The proportion of different pervious and impervious surface covers were combined to estimate the corresponding distribution at plot level in one town planning scheme of Ahmedabad. Spectral Angle Mapper (SAM) was used to classify the reflectance image into fourteen urban land cover categories including different types of roofs. Furthermore, average proportion of roof-cover types in selected municipal-wards of Ahmedabad city as well as on all plots of Town Planning Scheme No. 2 (Kankaria) were estimated. The selected end members were also used for supervised classification of LISS-4 image to understand the utility of increased bands and reduced band-widths in urban areas.

## 4. Outcome

### 4.1 Salient findings

This study developed a spectral library of urban land cover materials for India cities, viz. Kalaburgi and Ahmedabad. AVIRIS-NG data was used to estimate the pervious and impervious surfaces in part of Ahmedabad city up to individual plot-level. Furthermore, the data was used to estimate the distribution of roof-type materials in study area. The results are discussed in the subsequent sections.

#### a. Spectral Library of Urban Materials.

Spectral libraries provide detailed knowledge about spectral material characteristics in the form of spectra. Spectral libraries serve as an important input information for pre-processing and classification of hyper-spectral data. The diversity of urban materials is one of the foremost reasons for limited information availability on spectra of urban materials. Figure 38.2 shows the spectral profiles of selected materials collected in Ahmedabad city during AVIRIS-NG ground campaign.

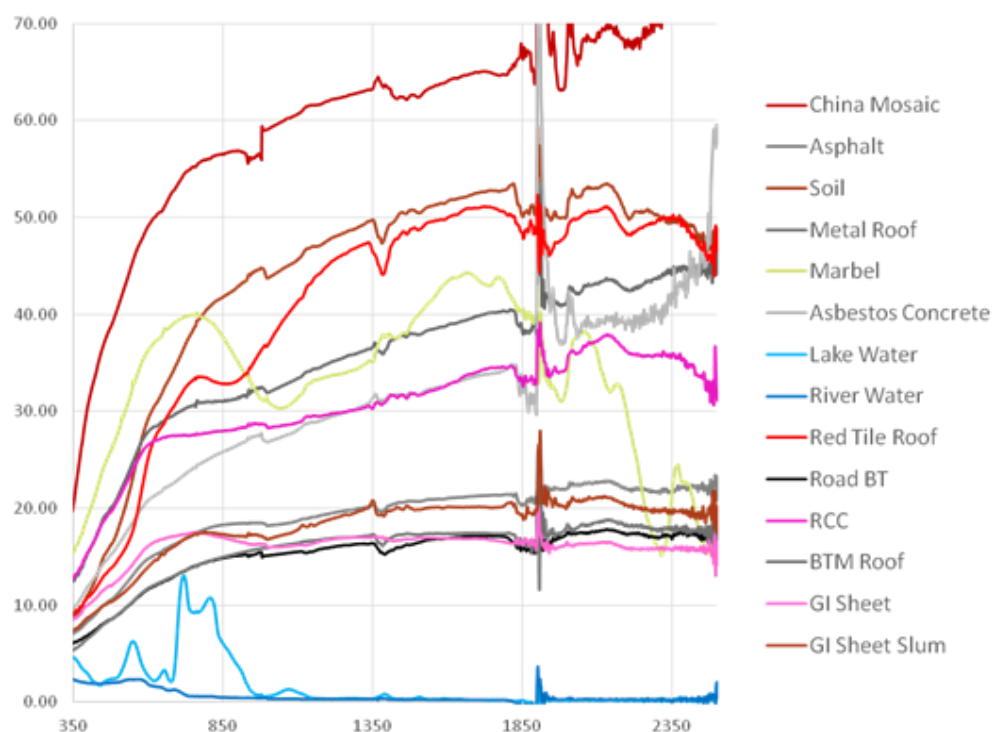


Figure 38.2. Field Spectra Collection in Ahmedabad City

The spectral profile of urban materials was collected in different types of land use categories including residential, commercial, industrial, public and semi-public, educational, recreational and transportation. The sites for residential land use covered different types of houses such as apartments, slums, old city houses and hostels. Similarly, the commercial land use sites covered cold storage, warehouse, malls and hotels. Several different types of building roof covers were considered such as concrete, GI sheets, red clay tiles, bitumen sheets, asbestos pitched roofs, fiber, tarpaulin sheets, china mosaic etc. The spectra of selected urban features were compared with the corrected reflectance image of AVIRIS-NG image (figure 38.3).

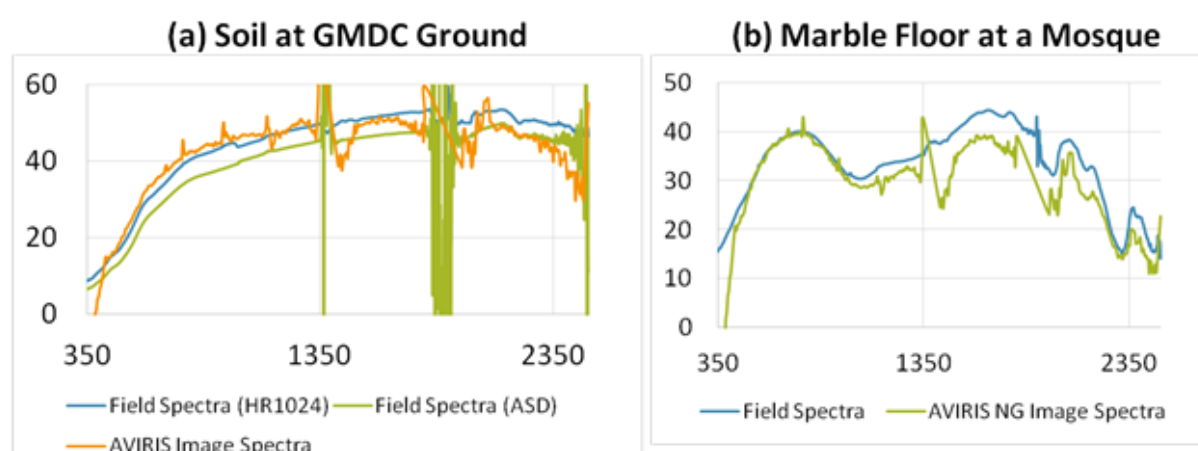


Figure 38.3. Comparison of Field Spectra with Image Spectra

## b. Estimation of Pervious and Impervious Land Cover

Linear Spectral Mixture Analysis was used to estimate the fraction of various urban materials in each pixel. The end-members for linear spectral mixture model for estimation of impervious surface can be selected by three methods: (1) extraction of impervious surface as one of the end-members; (2) estimation by the addition of high-albedo and low-albedo fraction images; and (3) the combination of several impervious surface endmembers from a multiple end member model. Initially, the endmembers corresponding to low and high albedo regions, defining the impervious surfaces were used. This resulted into very large root-mean-square (RMS) error, which was reduced by increasing the end members. Subsequently, ten endmembers were selected for LSMA in this study, viz. soil, metal roof, marble floor, china mosaic, asbestos concrete, lake water, lawn, vegetation, asphalt and river water. These endmembers were corresponded to large homogenous areas visible on the image. The

pervious and impervious surfaces were thereafter aggregated and total proportion of impervious surface in each pixel was thus estimated. This was further used to estimate the fraction of impervious surface on each plot of one town planning scheme area as shown in figure 38.4.

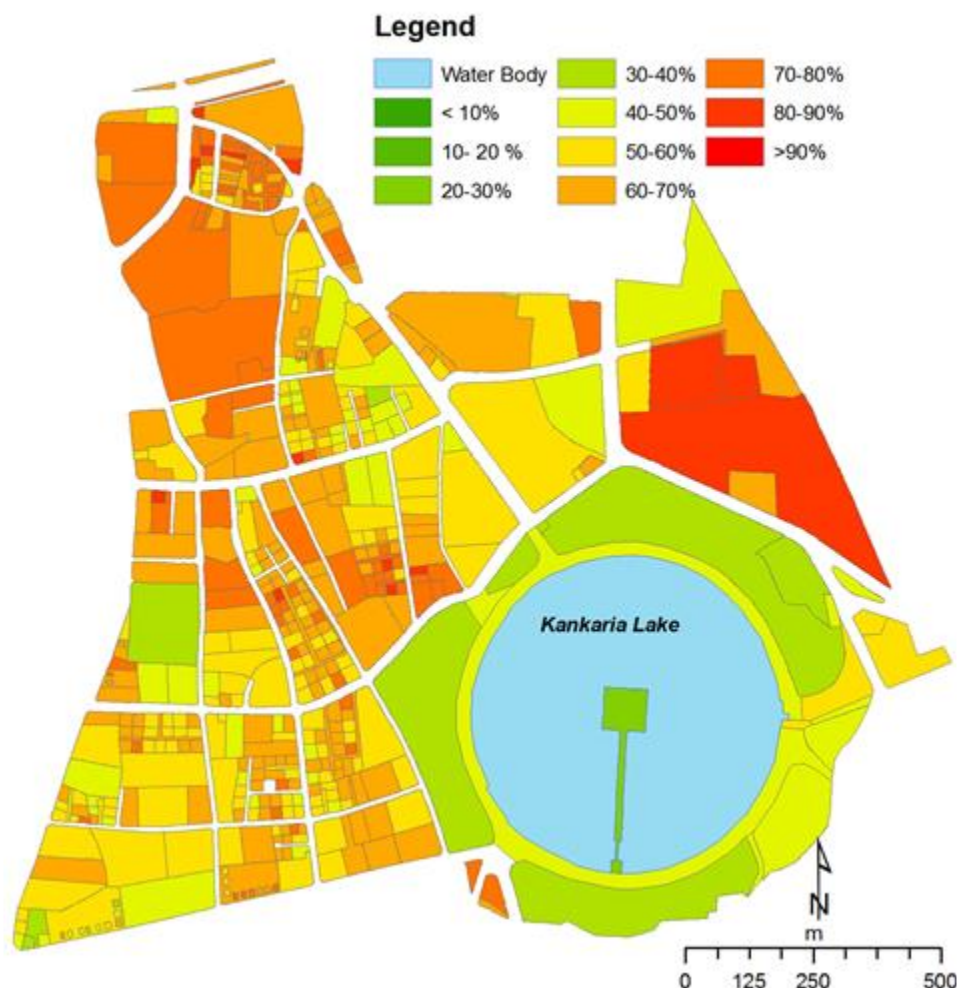


Figure 38.4. Plot-level Estimation of Fraction of Impervious Surface

### c. Determination of Roof Type

Spectral Angle Mapper (SAM) method was used for classification of various roof-top materials in Ahmedabad city. The endmember spectra used for SAM are shown in figure 38.5. In addition to the spectra used for LSMA, few other materials such as red Mangalore tiles, blue painted G. I. sheet, waterproof tarpaulin, and swimming pools were also included. These features were selected on the basis of field spectral profiles and very high resolution satellite images of corresponding areas.

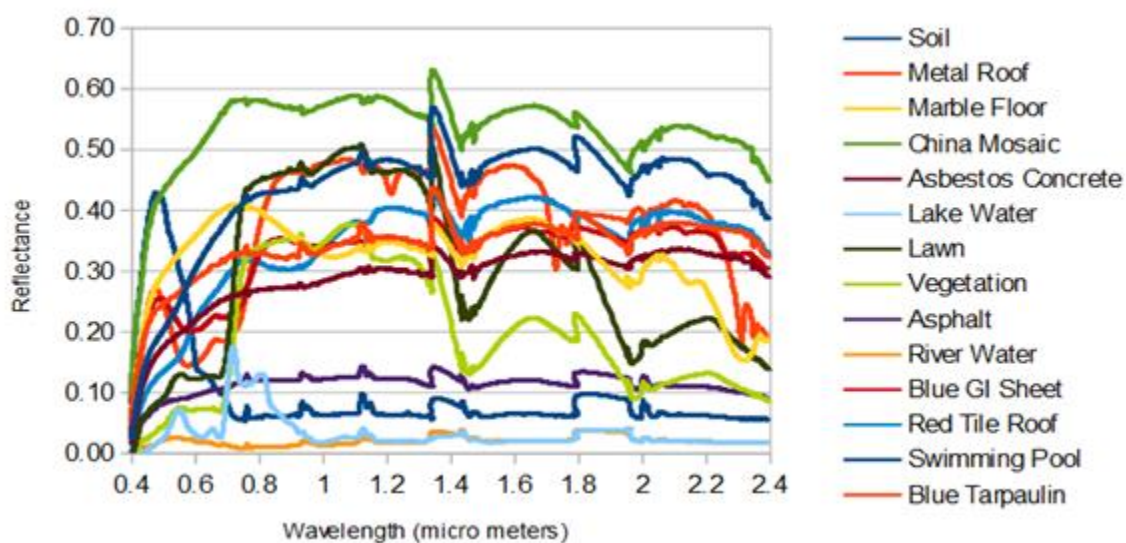


Figure 38.5. Spectral End Members for SAM

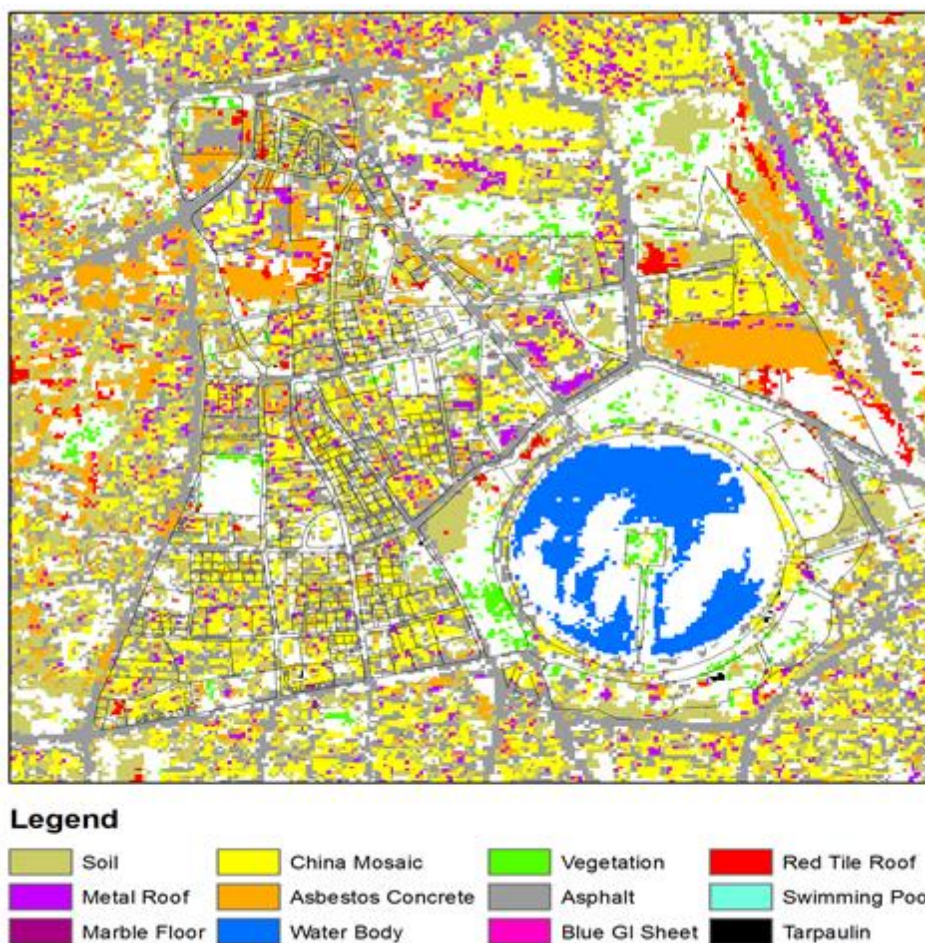


Figure 38.6. Urban Land Cover Classification using SAM

The Spectral Angle Mapping method was able to discriminate between major roof types such as China Mosaic, Metal Roof and Concrete. Figure 38.6 shows the urban land cover classification using SAM over part of Ahmedabad city. The ward boundaries were further used to estimate the proportion of buildings of different types of roof for comparison with H-Series data of Census of India. AVIRIS NG data is able to identify some of the materials such as red tile roof, marble floor, metal roof and asbestos concrete, which can otherwise not be detected even in very high resolution images. It was observed that inner city areas and parts of eastern Ahmedabad are showing high proportion of metal roof surfaces, whereas the western part of the city have greater concentration of china mosaic and concrete roof material.

#### **4.2 Target vs. Achievement**

The study attempted to retrieve roof-type material from AVIRIS NG data. However, as the resolution of data is coarse, it is resulting into mixed-pixel problem for urban areas. Preliminary results indicate broad categorisation of roof material into Concrete, China Mosaic and Metallic surfaces. Comparison of VIS classification from LISS-4 and AVIRIS-NG needs to be done to assess the improvement in estimation of impervious surfaces. Object-based Image Analysis (OBIA) technique is being evaluated for AVIRIS-NG data. Combining Hyperspectral data with other high-resolution data for OBIA may improve the results. Results are to be compared with H-Series data of Census (2011). Ground / Field Validation of Results also needs to be completed.

#### **4.3 Linkage to societal benefits**

The estimation of pervious and impervious surface cover is important for several studies such as urban hydrology, urban heat island, urban growth modeling, etc. Similarly, information on roof-cover types is important for understanding the socio-economic profile, modeling urban hydrology, and assessing disaster risk and climate resilience of a city.

### **5. Conclusions**

This study demonstrated the application of AVIRIS-NG data for urban land cover classification. The spatial resolution of 8.0 meters is, however, not sufficient for urban areas as the scale of urban objects is much smaller and the material composition in urban areas is heterogeneous. Furthermore, the roof-type and urban material composition are likely to vary across cities

situated in different climatic zones. Jodhpur city, for example, due to its arid climate has over 82% houses with stone \ slate clad roofs (Census of India 2011). Similarly, Srinagar city, situated in Kashmir Valley, has a humid subtropical climate receiving moderate to heavy snowfall in winter. The city therefore comprises over 85% houses with G.I./Metal/Asbestos sheet roofs. This study therefore proposes to cover such cities situated in different climatic zones, to be imaged at higher spatial resolution.

### **Acknowledgements**

We sincerely thank the support of Shri Rajendra Gaikwad, Shri Deepak Maaroo, Dr. SulochanaShekhar, Ms. Asfa Siddique, Shri Aniruddha, Shri Shashikant Patel, Shri Parag Sanjay Khopkar, Shri Piyush Patel, students from Central University of Karnataka, Kalaburgi, for all the valuable support during ground campaign.

### **References**

Harold, M. and Roberts, D. A. (2010). The Spectral Dimension in Urban Remote Sensing. In Rashed, T. and Jürgens, C. (Eds.) Remote Sensing of Urban and Suburban Areas. Remote Sensing and Digital Image Processing 10, Springer Science+Business Media B.V.

Harold, M. et al. (2004). Spectrometry for urban area remote sensing—Development and analysis of a spectral library from 350 to 2400 nm. Remote Sensing of Environment, 91, pp 304-319.

Sugumaran, R., Gerjevic, J., and Voss, M. (2007). Transportation Infrastructure Extraction Using Hyperspectral Remote Sensing. In Weng Q. (Ed.) Remote Sensing of Impervious Surfaces, CRC Press, Taylor and Francis Group, Boca Raton.

Weng, Q., Hu, X. and Lu, D. (2007). Extracting Impervious Surface from Hyperspectral Imagery with Linear Spectral Mixture Analysis. In Weng Q. (Ed.) Remote Sensing of Impervious Surfaces, CRC Press, Taylor and Francis Group, Boca Raton.

# Hyper-spectral Remote Sensing of Urban Areas

Asfa Siddiqui, Vinay Kumar, Aniruddha Deshmukh, Pramod Kumar  
and A. Senthil Kumar

Indian Institute of Remote Sensing, Dehradun, Uttarakhand, India

## ***1. Scientific rationale and Objectives***

The study of light as a function of emitted, reflected or scattered wavelength from various materials is called spectroscopy. The photons which are reflected from the material surface or the photons which get refracted in order to encounter another grain and get scattered away from the surface may be detected and measured. All natural surfaces emit photons when they are above absolute zero which may also be measured as well (Clark, et al., 1990). (Hunt, 1977) studied the reflectance spectra of minerals and rocks in visible and NIR region and developed the theory of interpreting this spectrum in terms of quantum mechanics and chemistry of the substance.

The similarity among the collected field spectra can be matched using Spectral similarity measures. So far these measures have been effectively used to distinguish between vegetation and background soil spectra (Chang, 2000), mineral spectra (Meer, 2006) and crop spectra (Chauhan, et al., 2014). Three spectral similarity measures selected in such a way that they reveal the complete information for spectral similarity are used in the study. The study uses two spectral distance based and one spectral angle based measures. Spectral similarity values among same material spectra are computed by the three measures and the spectra having abnormal values are considered as outlier and therefore rejected. Conventionally the spectra were selected by averaging collected field spectra after rejecting outlier based on spectral shape.

Outlier rejection addressed in this study uses the same statistics which is used by classification algorithm. Spectral distance based measures use the first order statistics hence if spectral distance based measures predict high separability among the classes in which image is to be classified spectral distance based classifier such as Euclidian distance can be used. Spectral angle based measures uses the second order statistics. Hence if spectral angle based

measures predict high separability among the classes in which image is to be classified spectral angle based classifier such as Spectral Angle Mapper (SAM) can be used.

## ***2. Study area and data used***

Field observations were carried out using SVC HR 1024 spectro-radiometer with GPS locations in Ahmedabad covering all major urban material types viz. bitumen, china mosaic, concrete, granite, iron, marble, soil, tar, terracotta, tin, and water. The field observations were taken over at a total of 71 sites, number varying for each material. The spectro-radiometer has 1024 channels within the range of 348 to 2502.6 nm.

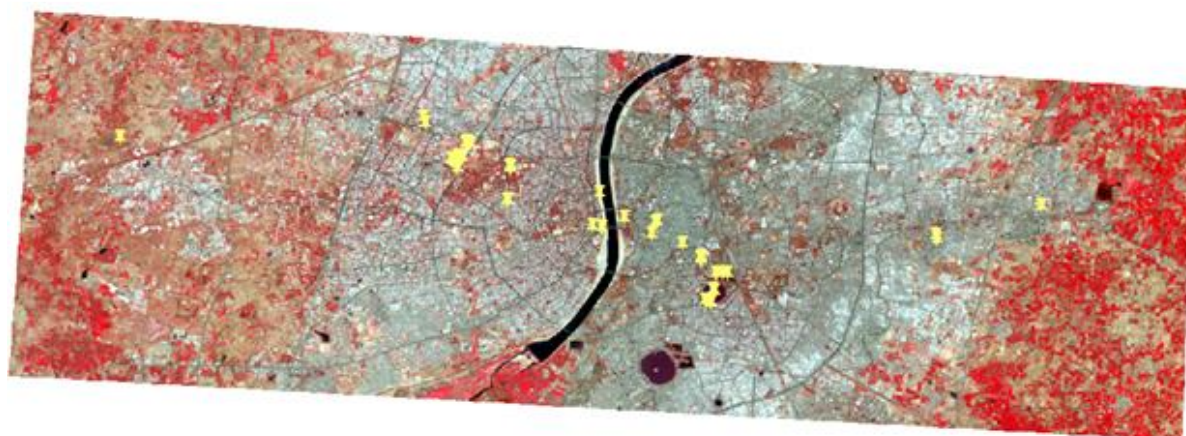


Figure 39.1. GPS location showing different locations for field spectra collection/LISS III

Spectra at a given location was gathered (figure 39.1) after optimizing the integration time which provides fore-optic information, recording dark current and collecting white reference reflectance. The target reflectance is the ratio of reflected energy to incident energy on the target. The measurements were acquired from one meter above the material with the sensor facing the target and oriented normal to the surface. Explicit care was taken so as not to cast shadows over the area being scanned by the instrument.

## ***3. Methodology***

The intent of the exercise was to do spectral similarity analysis for field corrected spectra using spectral similarity measures like City Block Distance, Spectral Angle Mapper and Euclidian Distance. The outlier spectra can be rejected and a precise spectral library can be built avoiding the library with outliers. Later, the precise spectra were used for classification in Ahmedabad city using Hyperspectral data for Ahmedabad.

## 4. Outcome

### 4.1 Salient findings

#### a. Conventional method for rejection of outlier spectra

The spectra gathered amid field study were prepared utilizing ENVI. Conventionally collected field spectra were averaged after rejecting outlier based on spectral shape (Rao et al., 2007). For the present review, we initially built up the field spectra routinely by dismissing the exception spectra in light of otherworldly shape. The spectra after regular dismissal and averaging are shown in figure 39.2.

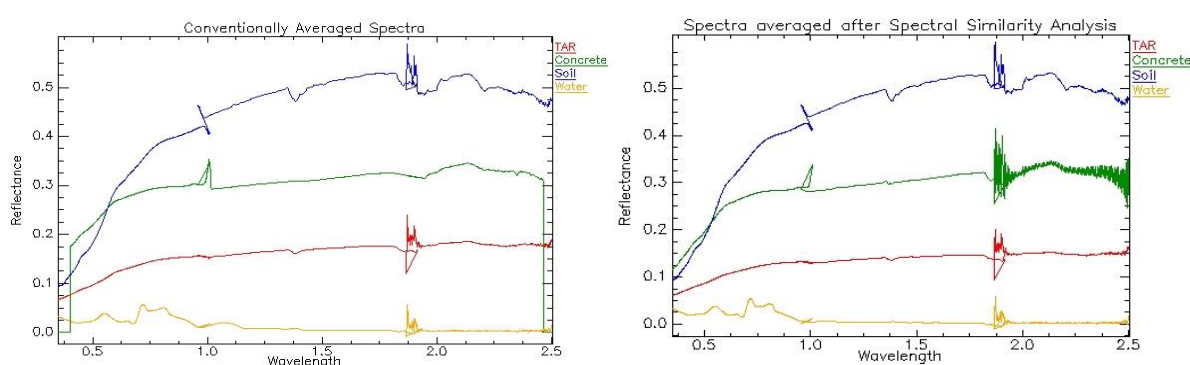


Figure 39.2. Spectra averaged using conventional method and spectral similarity analysis

#### b. Analysis of Spectral Similarity to develop Precise Spectra

To develop precise spectra based on spectral similarity CBD, SAM and SDS similarity values were computed among same material spectra. The spectra having larger values with other spectra of same material class were considered as outlier and rejected. The matrices showing CBD, SAM and SDS(Ed) values of all the materials are shown in tables.

The spectral similarity measure estimations of CBD, SAM and SDS were examined keeping in mind the end goal to dismiss spectra with anomalous qualities. After rejecting all the spectra with abnormal values for each of the material, the remaining spectra were averaged in order to create spectral library. The averaged spectra after spectral similarity analysis are shown in figure 39.2.

Upper triangle demonstrates the CBD, SAM and SDS estimations of four materials in particular concrete, tar, soil and water (table 39.1 for CBD over concrete). Altogether there were 18

gathered spectra for concrete, 27 for soil, 14 for tar and 12 spectra for water, out of which spectra of with unusual CBD, SAM and SDS values, were rejected to figure exact spectra.

Table 39.1. CBD analysis for Concrete

SAM	Spectra	a	b	c	d	e	f	g	h	i	j	k	l	m	n	o	p	q	r
a		0	0.0746	0.00826	0.04345	0.10653	0.13969	0.09261	0.07335	0.06147	0.07361	0.10395	0.09843	0.12254	0.10018	0.17638	0.11419	0.10303	0.15402
b			0	0.07999	0.03265	0.04169	0.09351	0.07721	0.03162	0.05013	0.04235	0.16616	0.12545	0.06183	0.03398	0.10791	0.0595	0.15737	0.0891
c				0	0.04773	0.11162	0.14088	0.09194	0.07664	0.06328	0.07607	0.0982	0.09632	0.12742	0.10535	0.18054	0.11895	0.09895	0.15765
d					0	0.0677	0.10854	0.04982	0.03975	0.04369	0.13727	0.1064	0.08527	0.05969	0.13648	0.07917	0.13942	0.11546	
e						0	0.09684	0.10752	0.05566	0.08217	0.0683	0.19592	0.16046	0.05392	0.03677	0.09175	0.05553	0.18038	0.07189
f							0	0.12441	0.07338	0.08226	0.06889	0.1913	0.14178	0.10407	0.09256	0.09327	0.11011	0.19182	0.07962
g								0	0.0638	0.04702	0.0603	0.09121	0.08792	0.12164	0.10045	0.16908	0.11455	0.09005	0.14673
h									0	0.02852	0.0144	0.14956	0.11275	0.07309	0.0494	0.10998	0.0713	0.14295	0.0884
i										0	0.019	0.12682	0.08615	0.0923	0.0691	0.12972	0.08908	0.12698	0.10976
j											0	0.14219	0.10273	0.08165	0.05867	0.1147	0.0803	0.13898	0.09405
k												0	0.10041	0.20639	0.18701	0.25031	0.19855	0.0705	0.22794
l													0	0.15839	0.13868	0.19357	0.15384	0.12464	0.17891
m														0	0.03876	0.06769	0.01619	0.1812	0.05316
n															0	0.08592	0.041	0.17244	0.07054
o																0	0.08011	0.23042	0.03235
p																	0	0.1713	0.06906
q																		0	0.20664
r																			0

As for the comparison of individual spectra of material is shown in figure 38.4, 38.5, 38.6 and 38.7 for tar, soil, concrete and water respectively. It is observed that concrete has maximum deviation in between conventionally and precisely averaged spectra. While for soil has almost no deviation in the two spectra. Further for calculating exact quantitative effectiveness of these spectral similarity measures, a supervised calculation was carried out on a Hyperspectral image of Ahemdabad City.

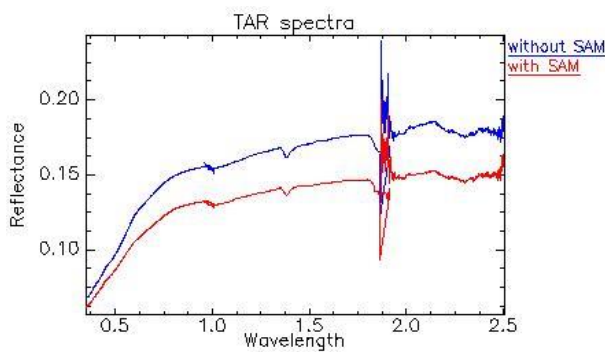


Figure 39.3. Comparison of TAR spectra

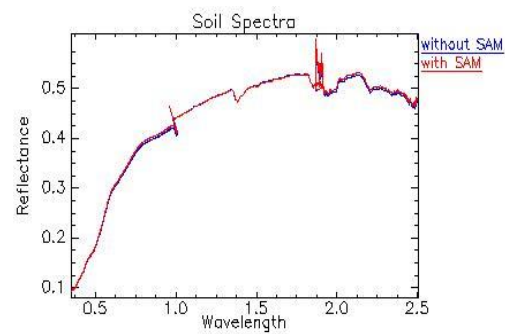


Figure 39.4. Comparison of Soil spectra

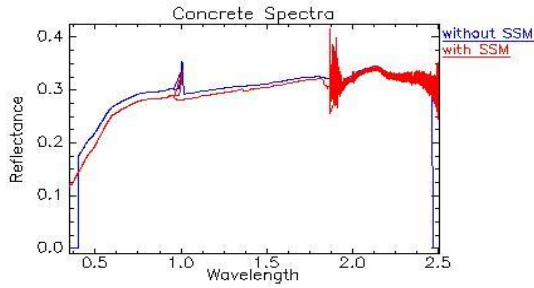


Figure 39.5. Comparison of Concrete spectra

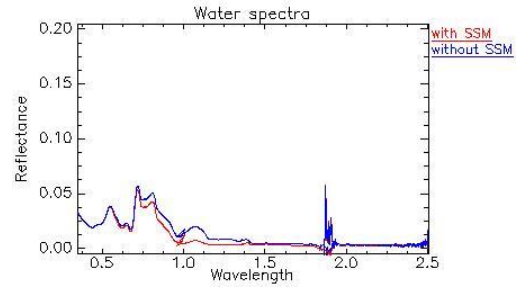


Figure 39.6. Comparison of Water spectra

### c. Supervised Classification

Hyperion’s atmospherically corrected image is used as an input data for classification. The definitive point of the image analysis and pre-processing was classification. To carry out classification for built-up area only, pixels having NDVI value more than 0.4 are masked. Classification was performed as input spectra from two spectra i.e. field spectra developed routinely and exact field spectra created in light of spectral similarity. Image was classified into real four yield classes, viz. concrete, tar, soil and water. The pixels not have a place within these four classes were classified as unclassified. Accuracy assessment of the classified image was done for both the cases by cross validating classified pixels against testing pixels gathered from Google Earth in order to generated error matrix to test accuracy.

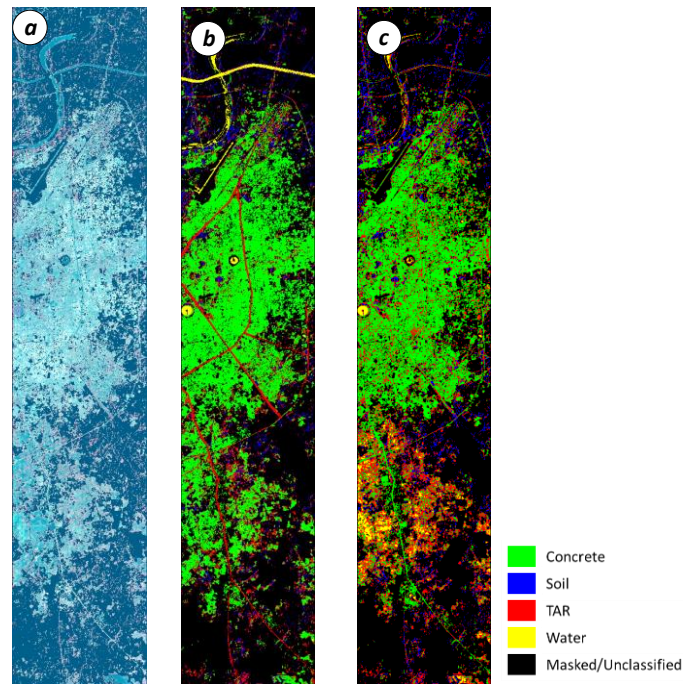


Figure 39.7. (a) Hyperion image; (b) classified image using spectra developed precisely; (c) classified image using spectra developed conventionally.

A sensibly higher overall accuracy demonstrates less class predisposition that shows exact spectra created in view of spectral similarity is more effective to recognize one class among different classes. After Kappa analysis for the individual error matrices of the two classified images, Kappa for classified image using conventionally developed spectra is 0.5588 with an overall accuracy of 64.71%, while for the classified image using precisely developed spectra is 87.06% with kappa equal to 0.7695. Consequently, image classified using exact spectra demonstrates considerable change in classified image approved by kappa measurements

Table 39.2. Accuracy assesment of image classified using conventionally developed spectra

	<i>Producer's Accuracy (%)</i>	<i>User's Accuracy (%)</i>	<i>Kappa</i>
Tar	38.89	38.89	0.3425
Concrete	96.67	73.42	0.6524
Soil	5.56	100.00	1.0000
Water	80.00	80.00	0.7960

Table 39.3. Accuracy assesment of image classified using precisely developed spectra

	<i>Producer's Accuracy (%)</i>	<i>User's Accuracy (%)</i>	<i>Kappa</i>
Tar	64.71	43.14	0.3439
Concrete	55.56	68.63	0.5833
Soil	53.33	62.75	0.5128
Water	78.13	49.02	0.4170

## 4.2 Target vs. Achievement

<i>S.No.</i>	<i>Target</i>	<i>Achievement</i>	<i>Remarks</i>
1.	Spectral similarity analysis for all collected spectra	Completed	The task was completed using technical spectral similarity measures
2.	Performance evaluation of spectral library through sample type spectra on Hyperion imagery classification	Completed	It was done using Tar, Concrete, Soil and Water spectra
3.	Impervious surface extraction	Ongoing	Twenty percent completed
4.	Land use classification (material specific)	Ongoing	Twenty percent completed

## 4.3 Linkage to societal benefits

The following exercise is important for material specific land use classification. It can be useful in linking the urban climate with the sprawling cities and the role of construction (material

architecture) in contributing to urban heating/cooling. It has direct impact to the surroundings and hence, for the urban purview, the study of hyperspectral data can be of great usage.

## **5. Conclusions**

The AVIRIS-NG campaign was an effort in the direction of using high resolution satellite imagery in the various dimensions of the environment around us. Better resolution of hyperspectral imagery can be extremely useful for further narrowing down our research in absence of stereo data, LIDAR data and otherwise.

## **Acknowledgements**

We are extremely grateful to our Chairman, Shri A.S. Kiran Kumar for his sightful vision in the application of hyperspectral imagery for the various domains of the environmental set up. We are also extremely thankful to Director, IIRS, Dr. A. Senthil Kumar for his constant motivation in utilizing the campaign for the benefit to research fraternity. I express my heartfelt gratitude to Group Head, PPEG and Head URSD, Shri Pramod Kumar for his support in materializing the field visits and continuing the research in the right direction. I am very much thankful to SAC, Ahmedabad and the team members for urban area analysis, Dr. Gaurav V. Jain and Shri Deepak Maroo, for their immense support and guidance throughout the field at Ahmedabad. I am also thankful to Justin George for his support and efforts in conceptualizing the research.

## **References**

Chang Chein I, An Information-Theoretic Approach to Spectral Variability, Similarity, and Discrimination for Hyperspectral Image [Journal] // IEEE transactions on information theory. - August 2000. - 5 : Vol. 46. - pp. 1927-1932.

Chauhan Hasmukh and Mohan B. Krishna, Effectiveness of spectral similarity measures to develop precise crop spectra for hyperspectral data analysis [Conference] // ISPRS Annals of the Photogrammetry, Remote Sensing and Spatial Information Sciences. - Hyderabad, India : [s.n.], 2014. - Vol. 2.

Clark R. N. [et al.], High spectral resolution reflectance spectroscopy of minerals [Journal] // Journal of Geophysical Research. - 1990. - B8 : Vol. 95.

Hunt Graham R., Spectral Signatures of Particulate Minerals in visible and near infrared [Journal] // Geophysics. - April 1977. - 3 : Vol. 42. - pp. 501-513.

Meer Freek van der, Effectiveness of spectral similarity measures for the analysis of hyperspectral imagery [Journal] // International Journal of Applied Earth Observation and Geoinformation. - 2006. - Vol. 8. - pp. 3-17.

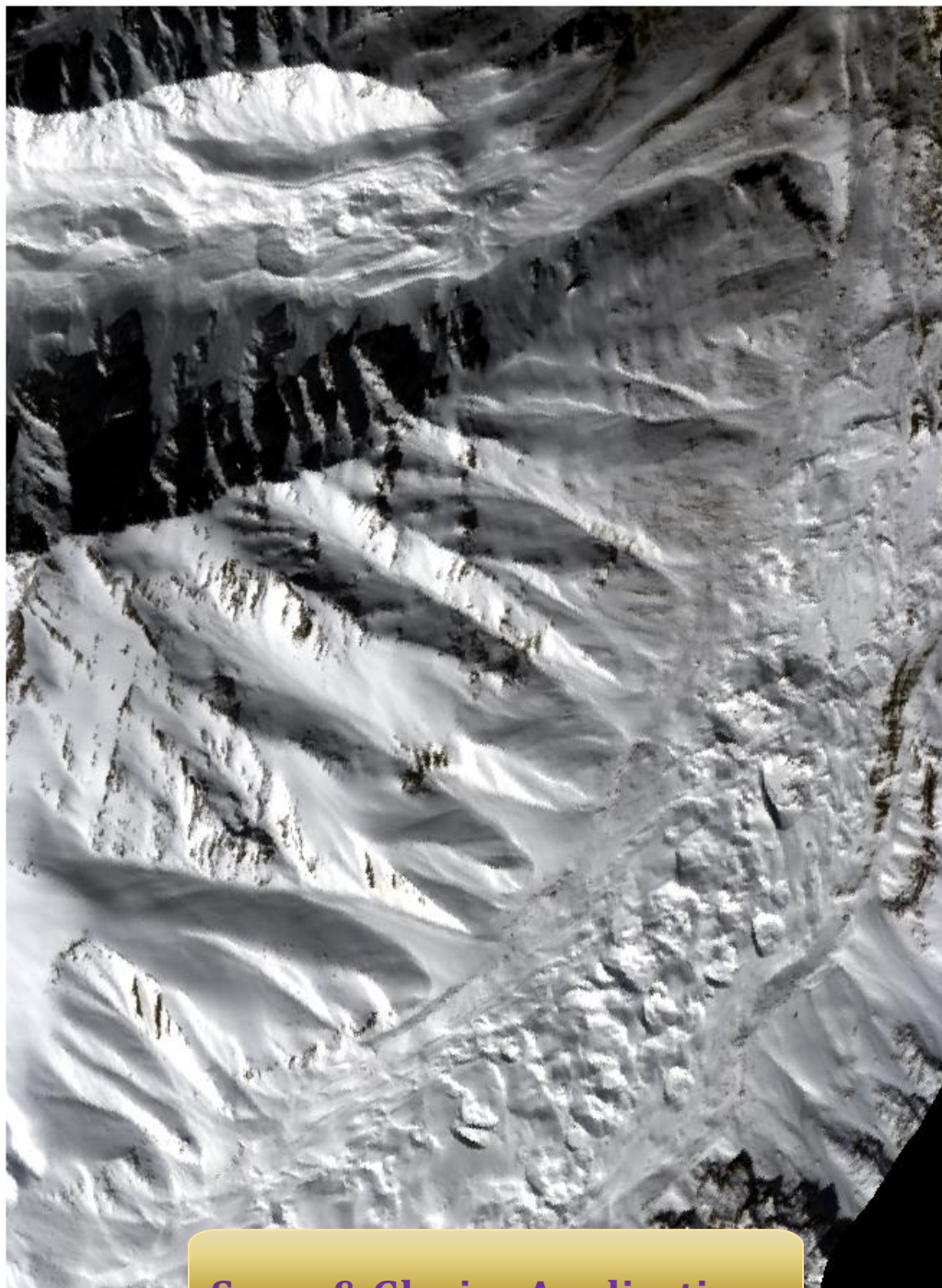
Rao N. Rama, Garg P. K. and Ghosh S. K., Development of an agricultural crops spectral library and classification of crops at cultivar level using hyperspectral data [Journal] // Precision Agriculture. - 2007. - 4 : Vol. 8. - pp. 173-185.

S Rashmi [et al.], Spectral Angle Mapper Algorithm for Remote Sensing Image Classification [Journal] // International Journal of Innovative Science, Engineering & Technology. - June 2014. - 2 : Vol. 1.

Sharma Subhash, Applied multivariate techniques [Book]. - [s.l.] : John Wiley & Sons, Inc, 1996.

Sweet James Norman, The Spectral Similarity Scale and its Application to the Classification of Hyperspectral Remote Sensing Data [Journal] // IEEE Explore. - 2004. - pp. 92-99.

Sweet James, Granahan James and Sharp Mary, An objective standard for hyperspectral image quality [Conference] // Proceedings: AVIRIS Workshop. - February, 2000.



**Snow & Glacier Applications**

### Summary

Snow cover is an important component of Earth Science System which controls the Hydrological and Climatological applications at regional and global scale. Snow cover is very dynamic in nature. The major river basins of Himalayan region, viz. Indus, Ganga and Brahmaputra, showed a seasonal variation in snow cover from 92%, 77% and 84% in accumulation months to 10%, 11% and 8% in ablation months, respectively. Snow and glacier melt runoff contributes almost 30-50 % melt runoff to the rivers originating in Northern Indian Himalayas, which are crucial for agricultural, industrial and domestic purposes. Once deposited and redistributed on Earth surface, atmospheric variation in temperature and amount and type of contamination influences the snow physical properties in different part of spectrum. Reflectance substantially reduces in visible region due to contamination whereas grain size variability affects the NIR part of spectrum. AVIRIS-NG hyperspectral airborne data was collected in parts of Himalaya to understand the variability in reflectance with respect to varying snow physical properties. Synchronous *in-situ* data was collected using spectroradiometer and collateral instruments for measuring radiometric and physical properties of snow. Variation in snow grain size affects the absorption peak centered at 1025 nm. Radiative transfer model was used to understand the grain size variability and its effect on absorption peak. Continuum removal was performed of absorption peak and band depth was estimated for ground observations and airborne data. Normalized difference snow index was estimated using visible and SWIR band and a threshold of 0.70 was used to identify pure snow pixels. Other pixels were masked out from the image. Grain size variability was observed to vary from 100  $\mu\text{m}$  to 500  $\mu\text{m}$  with altitude using AVIRIS-NG data. This exercise shows the capability and potential to retrieve snow physical parameters using Hyperspectral data in Himalayan region. More such data covering seasonality in Himalayan region will be important for retrieving snow and glacier ice properties which can improve the input requirement for hydrological and climatological studies.

# Snowpack Characterization using Hyperspectral airborne data

S.K. Singh, B.P. Rathore, Snehmani and I.M. Bahuguna

Space Applications Centre, ISRO, Ahmedabad, Gujarat, India

## ***1. Scientific rationale and Objectives***

Snow is a mixture of air and ice crystal that forms in the air under suitable conditions and descends through atmosphere and gets deposited and redistributed on the Earth surface. Snow becomes a three phase material when temperature rises and water appears between ice crystals. Snow appears as a bright target on the Earth surface as it strongly reflects (more than 80%) in visible region and looks dark in SWIR due to strong absorption. This distinct behavior has been exploited to map and monitor snow pixel on ground using Normalized Difference Snow Index (NDSI) approach for multi-spectral optical channels (Kulkarni et al., 2006, Hall et al., 1995, Hall et al., 2002; Singh et al., 2014).

Reflectance of snow is sensitive to various varying snow physical properties in different part of VNIR region of EM spectra. Minute concentration of impurities can lower down the reflectance by 5-15% in visible region (Warren and Wiscombe, 1980; Negi et al., 2010). Contamination added in snow due to triggering of avalanche (on Solang-Dhundi route) severely influences the visible region. Reflectance substantially drops by 65% from clean to heavily contaminated snow along with a shift of peak from visible to NIR region. However, strength, position and shape of curve may provide details on amount and type of contamination (Singh et al., 2010). Reflectance in NIR and SWIR region decreases by approximately 29% and 8% respectively with increased grain size from <0.5 mm to 1.0-2.0 mm. Asymptotic radiative transfer (ART) theory has been used previously to retrieve the grain size and albedo of snow in the Himalayan region (Negi and Kokhanovsky, 2011). Snow grain size influences the band depth in NIR region and can provide an information on retrieval of grain size (Nolin, 2010; Painter et al., 2003). An algorithm was developed for quantitative retrieval of snow properties using AVIRIS data over US region (Painter et al., 2013). In present

study, preliminary study was carried out to retrieve snow grain size using AVIRIS-NG airborne and field data over Himalayan region.

## 2. Study area and data used

In this exercise, Airborne AVIRIS-NG data over Patsio region in Bhaga basin was used along with ground observations in Beas basin. Patsio observatory is located in Bhaga basin and Dhundi observatory falls in Beas basin. Bhaga basin falls in Greater Himalayas with elevation ranging from 2900 m to 6400 m. This region experiences cold and dry climate, and is mainly fed by Western disturbances. Snow remains dry during winter with low density.

ASD spectroradiometer was used to collect the radiometric measurements covering a range of 350-2500 nm wavelength region. ASD Field Spectroradiometer belongs to Model Field Pro FR which covers a range of 350 nm to 2500 nm of wavelength in optical region. The available field of view with instrument used, was 25° (bare fibre). Crystal gauge was used for providing grain size of different types of snow particles while thermometer was used get information about temperature of the snow surface. Density meter was used to provide the density of snow in the snow bound areas. Figure 40.1 shows the locations of observatories and set up of the instruments for measurements made during the field investigations. Experiments have been conducted on 17-18 February 2015.

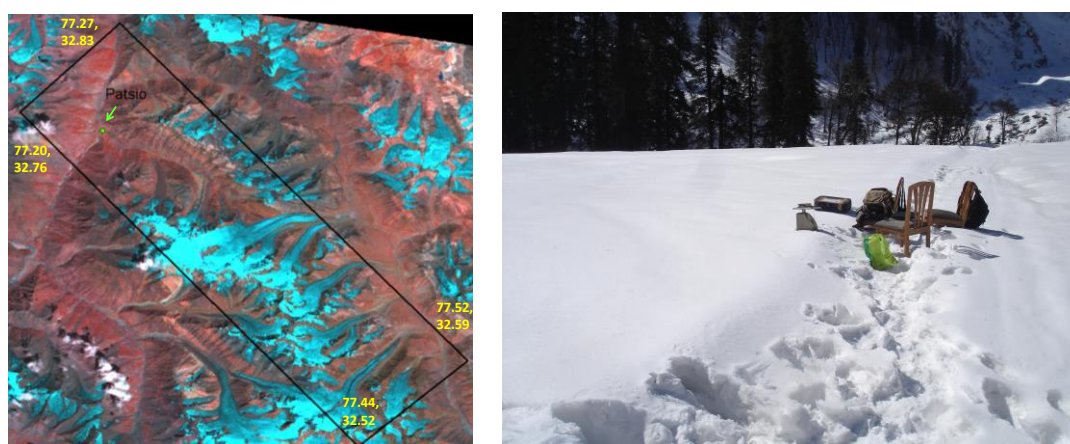


Figure 40.1. Location map of Patsio region and ground measurement at Dhundi Observatory

## 3. Methodology

AVIRIS-NG airborne reflectance data over one sample region of study area was used to retrieve the grain size information. Radiative transfer model was used to generate snow

reflectance spectra for various grain size and band depth at 1025 nm to estimate grain size spectra for each reference. Continuum removal and band depth of absorption peak at 1030 nm was also estimated for field reflectance measurement. The similar approach was implemented over AVIRIS-NG airborne data of patsio region. Normalized difference snow index was estimated using visible and SWIR band and a threshold of 0.7 was used to identify pure snow pixels. Other pixels were masked out from the image.

## 4. Outcome

### 4.1 Salient findings

Figure 40.2 shows the continuum removed spectra of model derived grain size and field based measurement. It is clearly evident that as the snow grain size increases, band depth also increases.

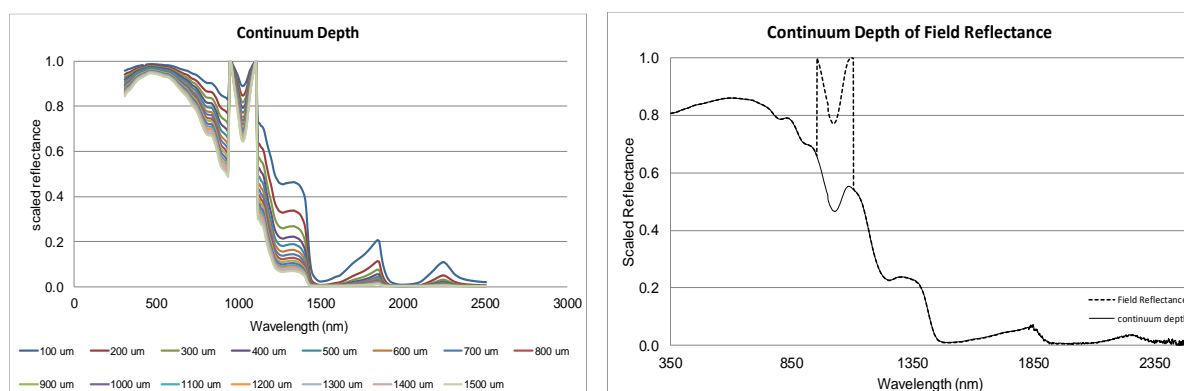


Figure 40.2. Continuum removed spectra of model derived and field derived snow reflectance

Figure 40.3 shows the grain size variability of AVIRIS-NG data where the snow grain size was varying from 100  $\mu\text{m}$  to 500  $\mu\text{m}$ . It was also observed from the variation in absorption peak depth that grain size was coarser for valley region and fine at high altitude region.

### 4.2 Target vs. Achievement

- Approach for retrieval of snow grain size has been worked out which has to improve to cover a wide range of grain size further using model and ground based measurements in Himalayan region.
- Retrieval of albedo using Hyperspectral data and studying the variability of different type of snow.

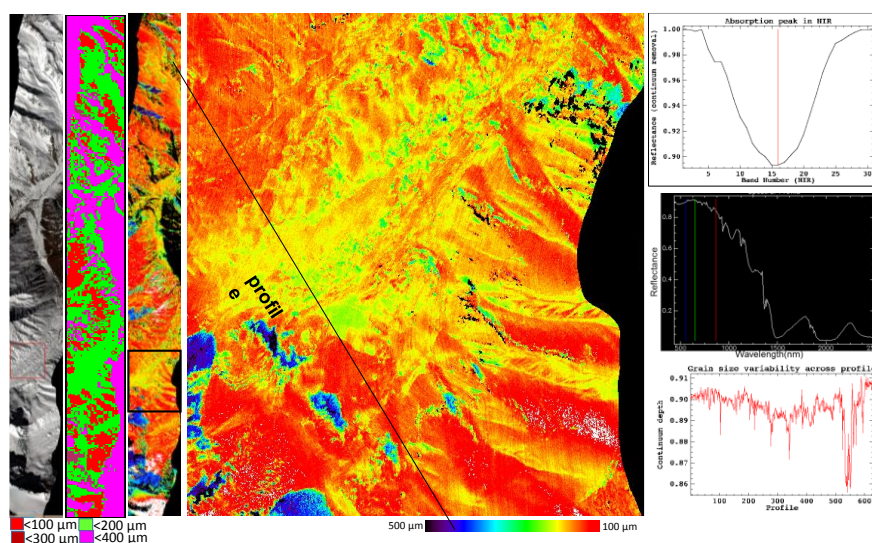


Figure 40.3. Snow grain size variability over AVIRIS-NG data in Patsio region.

### 4.3 Linkage to societal benefits

Snow grain size is important for understanding the variability in albedo and snow melt runoff studies.

## 5. Conclusions

- AVIRIS-NG airborne data was found useful in deriving snow physical properties and requires to cover seasonality over the Himalayan region.
- Apart from covering monthly data over snow covered region, it will also be crucial to collect hyperspectral data for different glacier features in synchronous with field observations for developing algorithm to retrieve glacier targets.

## Acknowledgements

Authors are thankful to Director, Space Applications Centre, ISRO, Ahmedabad and Director, Snow and Avalanche Study Establishment, DRDO, Chandigarh to support this study under AVIRIS-NG airborne campaign programme. Authors are also thankful to SAC and JPL team members for perfectly coordinating in collecting wonderful and unique AVIRIS-NG dataset over Himalayan region.

## References

Hall, D.K, Riggs, G.A., Salomonson, V.V., DiGirolamo, N. and Bayr, K.J., 2002. MODIS snow cover products. *Remote Sensing of Environment*, 83, pp 181–194.

Kulkarni, A.V., Singh, S.K., Mathur, P., and Mishra, V.D., 2006. Algorithm to monitor snow cover using AWiFS data of RESOURCESAT-1 for the Himalayan region. *International J. Remote Sensing*, 27, pp 2449–2457.

Negi, H.S. and Kokhanovsky, A., 2011b. Retrieval of snow grain size and albedo of western Himalayan snow cover using satellite data. *The Cryosphere Discuss.*, 5, doi:10.5194/tc-5-831-2011, pp 203-217.

Negi, H. S., Singh, S. K., Kulkarni, A. V. and Semwal, B. S., 2010. Field based spectral reflectance measurements of seasonal snow cover in Indian Himalaya. *International Journal of Remote Sensing*, 31(9), pp 2393-2417.

Nolin, A.W., 2010. Recent advances in remote sensing of seasonal snow. *J. of Glaciology*, 56(200), pp 1141-1150.

Painter T.H., Seidel F.C., Bryant A.C., Skiles S.M. and Rittger K., 2013, Imaging spectroscopy of albedo and radiative forcing by light absorbing impurities in mountain snow, *J. Geophysical Research, Atmospheres*, 118, doi:10.1002/jgrd.50520, 2013, pp 1-13.

Painter, T.H., Dozier, J., Roberts, D.A., Davis, R.R. and Green, R.O., 2003. Retrieval of subpixel snow covered area and grain size from imaging spectrometer data. *Remote sensing of Environment*, 85, pp 64-77.

Singh, S. K., Kulkarni, A. V. and Chaudhary, B. S., 2010. Hyperspectral analysis of snow reflectance to understand the effects of contamination and grain size. *Annals of Glaciology*, 54(44), pp 83-88.

Singh, S.K., Rathore, B.P., Bahuguna, I.M. and Ajai, 2014, Snow cover variability in the Himalayan-Tibetan region, *International Journal of Climatology*, 34, pp 446-452. Wiscombe, W.J. and Warren, S.G., 1980. A model for the spectral albedo of snow I: pure snow. *J. of Atmospheric Sciences*, 37, pp. 2712–2733.

## Author Index

---

### A

A. Hakeem · 239  
A. K. Mathur · 16  
A. Senthil Kumar · 110, 115, 254, 288  
A.S. Rajawat · 225  
Abha Chhabra · 38  
Abhishek Chakraborty · 135  
Abhishek Danodia · 115  
Abhra Chanda · 239  
Aditya K. Dagar · 181  
Anil Kumar · 110  
Anirban Akhand · 239  
Aniruddha Deshmukh · 288  
Annie Maria Issac · 250  
Anup Das · 73  
Anurag Gupta · 59  
Arindam Guha · 210  
Arundhati Misra · 1, 73, 158  
Arunkumar SVV · 225  
Arvind Sahay · 59  
Asfa Siddiqui · 288  
Ashwin Gujrati · 234, 263  
Ashwini Muddaliar · 104  
Ateeth Shetty · 225

---

### B

B.P. Rathore · 298  
Bimal K Bhattacharya · 1, 81, 95, 121, 129, 143  
Bipasha Paul Shukla · 33, 49  
Biswadip.G · 44

---

### C

C. P. Singh · 171  
C. Patnaik · 73  
C.S. Jha · 153  
C.S. Reddy · 153  
Ch. V. Jayaram · 239  
Chandrasekar K · 135

---

### D

David R. Thompson · 21  
Debojyoti Dhar · 1  
Devanshi Joshi · 234

---

### G

G. Rajashekar · 153  
G. Ravi Shankar · 272  
G. Srinivasulu · 1  
Gaurav V. Jain · 279

---

### H

Harshad Patel · 234  
Hrshikesh Kumar · 192

---

### I

I.M. Bahuguna · 298

---

### J

J. Singhal · 153  
Jakesh Mohapatra · 171  
Jinya John · 33, 49  
Justin George K · 110, 115

---

### K

K N Chaudhari · 129  
K. Abdul Hakeem · 250  
K. N. Babu · 16  
K. Vinod Kumar · 210, 219  
K.S. Jayappa · 225  
K.V. George · 38  
Karthik Reddy · 250  
Karunkumar Choudary · 135  
Komal Pasricha · 210

---

**M**

Maresh P · 44  
Mallikarjun.K · 44  
Manish Saxena · 1  
Manoj K Mishra · 27  
Meenakshi Sarkar · 54  
Mehul Pandya · 38, 129  
Michael L. Eastwood · 21  
Mohit Arora · 234  
Mohit Modi · 272  
Muktipada Panda · 163

---

**N**

Nandini Ray Chaudhury · 234  
Neetu Chakov · 239  
Nikhil Lele · 163  
Nilima Rani Chaube · 158  
Nirmala Jain · 219  
Nitesh Kaushik · 54

---

**P**

P. N. Patel · 16  
P. V. Nagamani · 239  
Pankaj R. Dhote · 254  
Prakash Chauhan · 38  
Pramod Kumar · 288  
Preeti Rajput · 225  
Priyom Roy · 219

---

**R**

R. P. Prajapati · 16  
R.N. Samal · 163, 225  
Rahul Nigam · 81, 95, 121  
Rajiv Kumar · 272  
Rajsi Kot · 81, 95  
Rakesh · 153  
Rakesh Baral · 225  
Rakesh Patel · 234  
Rao P.V.N. · 44  
Ratheesh R · 225

Rekha Kashyap · 38  
Robert O. Green · 1, 21  
Rohit Nagori · 67, 89  
Rojalin Tripathy · 129

---

**S**

S.K. Singh · 298  
S.P. Aggarwal · 254  
Sadasiva Rao · 1  
Saroj Maity · 73  
Satadru Bhattacharya · 181  
Sesha Sai M.V.R. · 44  
Shailendra S. Srivastava · 54  
Shard Chander · 263  
Shashikant Sharma · 1, 279  
Snehmani · 298  
Somnath Paramanik · 104, 143  
Sreenivas. G · 44  
Srikanth P · 135  
Subhendu Modal · 210  
Subin Jose · 44  
Sujay Dutta · 104, 143  
Sumit Pathak · 181  
Suresh Kumar · 115  
Sushanta Das · 163  
Syed Moosa Ali · 59

---

**T**

Tapas Martha · 219  
TVR Murthy · 163

---

**U**

Umamaharswara Rao · 239

---

**V**

V. M. Chawdary · 239  
V. Satya Sahithi · 272  
Vaibhav Garg · 254  
Vinay Kumar · 115, 254, 288

